General Disclaimer

One or more of the Following Statements may affect this Document

- This document has been reproduced from the best copy furnished by the organizational source. It is being released in the interest of making available as much information as possible.

- This document may contain data, which exceeds the sheet parameters. It was furnished in this condition by the organizational source and is the best copy available.

- This document may contain tone-on-tone or color graphs, charts and/or pictures, which have been reproduced in black and white.

- This document is paginated as submitted by the original source.

- Portions of this document are not fully legible due to the historical nature of some of the material. However, it is the best reproduction available from the original submission.

Produced by the NASA Center for Aerospace Information (CASI)

DRD Line Item No. SE-7 DOE/JPL-954929-79/4

INVESTIGATION OF RELIABILITY ATTRIBUTES AND ACCELERATED STRESS FACTORS ON TERRESTRIAL SOLAR CELLS

(NASA-CR-158854) INVESTIGATION OF RELIABILITY ATTRIBUTES AND ACCELERATED STRESS FACTORS ON TERRESTRIAL SOLAR CELLS (Clemson Univ.) 276 p HC A13/MF A01 CSCL 10A G3/44 N79-28724 Unclas 31612

FIRST ANNUAL REPORT

J.L. Prince and J.W. Lathrop
Department of Electrical and Computer Engineering
Clemson University
Clemson, SC, 29631

MAY 1979

AUG 1979
RECEIVED
NASA STI FACILITY
ACCESS DEPT.

PREPARED FOR
JET PROPULSION LABORATORY

PREPARED BY
CLEMSON UNIVERSITY, CLEMSON, SOUTH CAROLINA 29631

DRD Line Item No. SE-7 DOE/JPL - 954929-79/4

ENGINEERING AREA

INVESTIGATION OF RELIABILITY ATTRIBUTES AND ACCELERATED STRESS FACTORS OF TERRESTRIAL SOLAR CELLS

FIRST ANNUAL REPORT

J.L. Prince and J.W. Lathrop

Department of Electrical and Computer Engineering

Clemson University

Clemson, SC 29631

May 1979

The JPL Low-Cost Silicon Solar Array Project is sponsored by the U.S. Department of Energy and forms part of the Solar Photovoltaic Conversion Program to initiate a major effort toward the development of low-cost solar arrays. This work was performed for the Jet Propulsion Laboratory California, Institute of Technology by agreement between NASA and DoE.

ACKNOWLEDGEMENTS

The authors acknowledge the contributions of the following Clemson University research workers in the conduct of this program: Dr. L.T. Fitch, Dr. J.N. Thurston, Mr. K. Labib, Mr. C. Saylor, Mr. T.B. DuBose, Mr. R.C. Eng, Mr. D. Hawkins, Ms. D. Eggers, and Mr. D. Martins, all of the Department of Electrical and Computer Engineering. Special acknowledgement is made of the contributions of Dr. F.W. Morgan, Department of Mathematical Sciences, and Mr. R.A. Hartman, Department of Electrical and Computer Engineering. Acknowledgement is also made of the contributions of Mr. G.W. Witter, Optical Coating Laboratory, Inc., to the work on contact integrity testing.

Mr. E.L. Royal was the Jet Propulsion Laboratory Technical Manager for this work.

ABSTRACT

The results of accelerated stress testing of four different types of silicon terrestrial solar cells are discussed. The accelerated stress tests used included bias-temperature tests, bias-temperature-humidity tests, thermal cycle and thermal shock tests, and power cycle tests. Characterization of the cells was performed before stress testing and at periodic down-times, using electrical measurement, visual inspection, and metal adherence pull tests. Electrical parameters measured included short-circuit current, I_{sc}, open circuit voltage, V_{oc}, and output power, voltage, and current at the maximum power point, P_m, V_m, and I_m respectively. Incorporated in the report are the distributions of the prestress electrical data for all cell types. Data was also obtained on cell series and shunt resistance. Significant differences in the response to the various stress tests was observed between cell types. On the basis of the experience gained in this research work, a suggested Reliability Qualification Test Schedule was developed.

SUMMARY

At the end of the first year of the accelerated reliability testing program of silicon solar poststress electrical parameter data showed significant degradation for some cell types and some stress tests, while other combinations of cell types and stress tests resulted in virtually no degradation. For example:

1. Bias-temperature stress testing showed significant degradation, consistent in time, for one cell type and somewhat less significant degradation for two other cell types. However, for this same stress the remaining cell type showed absolutely no degradation at all.
2. Substantial differences in electrical parameter degradation rate between cell types was also observed for bias-temperature-humidity stress testing.
3. Sensitivity to thermal cycle and thermal shock stress varied widely between cell types.
4. Power cycle, uniformly showed no effect on cell electrical parameters. Cells subjected to this stress test also showed no metal adherence strength degradation, while all of the other stress tests resulted in degraded metal adherence for some or all of the cell types.

Analysis of electrical parameters and visually observable effects resulted in some understanding of the mechanisms responsible for the results observed. However, the degree of this understanding is small. This fact, and the difficulty in extrapolating the results obtained in the course of the research to use conditions despite the large volume of data obtained, point up the need for further work in this area.

Need for further work is especially evident in the areas of physical analysis of stressed cells, further stress testing using longer times and more varied degrees of stress, and in the critical area of actual field degradation modes and rates.

Finally, a Reliability Qualification Test Schedule was drawn up based on stress testing results for the four cell types investigated, and based on a physics of failure foundation. Of necessity, this test schedule is tentative at this point.

TABLE OF CONTENTS

Section	Page
ACKNOWLEDGEMENTS	
ABSTRACT	
SUMMARY	
1.0 INTRODUCTION	1
1.1 Test Considerations	3
1.2 Reliability Considerations	13
2.0 ACCELERATED STRESS TEST PROCEDURES	21
3.0 ELECTRICAL MEASUREMENT TECHNIQUES	33
3.1 General Considerations	35
3.2 Maximum Power Determination	45
3.3 Reliability Considerations	49
4.0 STRESS TEST RESULTS AND DATA ANALYSIS	63
4.1 Stress Test Population Characteristics	65
4.2 Thermal Cycle/Thermal Shock Stress Testing	69
4.3 Bias-Temperature Stress Testing	109
4.4 Bias-Temperature-Humidity Stress Testing	153
4.5 Power Cycle Stress Testing	175
4.6 Contact Integrity of Stress-Tested Cells	187
5.0 RELIABILITY QUALIFICATION TEST SCHEDULES - PRELIMINARY RECOMMENDATIONS	207
6.0 CONCLUSIONS	213
7.0 RECOMMENDATIONS	221
8.0 NEW TECHNOLOGY	225
APPENDICES	
A - Data Management and Analysis	A 1
B - Prestress Paramenter Distribution of Stress Test Cell Populations	B 1
C - Method 1010.1, MIL-STD-883A, "Thermal Cycling"	C 1
D - Method 1011.1, MIL-STD-883A, "Thermal Shock"	D 1
E - Contact Integrity Test Procedure for Terrestrial Solar Cells	E 1

LIST OF FIGURES

Figures	Title	Page
1.1.1	Reliability Methodology	8
1.1.2	Relationship of Phase I and Phase II Testing	10
2.1	Example Visual Inspection Form	24
2.2	Enlarged Photo of Cell	25
2.3	Cell Contacting Method Used in B-T Tests	29
2.4	Oven Loaded With 150 Cells Ready for Stress Testing	30
3.1.1	Electrical Measurement Schematic	39
3.1.2	Electrical Measurement Facility	40
3.1.3.a	Electrical Measurement Jig	41
3.1.3.b	Measurement Jig, Loaded with E Slice	41
3.1.4	Typical Cell Output I-V Characteristic, With Constant-Power Hyperbolas Superimposed, and a Far-Forward Diode I-V Characteristic	42
3.3.1	Temperature Dependence of V_{oc} and I_{sc} for Type B Cell, Irradiance 1000 W/m^2, ELH Lamp Source	53
3.3.2	Temperature Dependence of Type B Cell Power Output at Maximum Power Point. Irradiance 1000 W/m^2, ELH Lamp Source	54
3.3.3	Temperature Dependence of V_{oc} and I_{sc} for Type E Cell, Irradiance 1000 W/m^2, ELH Lamp Source	55
3.3.4	Temperature Dependence of Type E Cell Power Output At Maximum Power Point. Irradiance 1000 W/m^2, ELH Lamp Source	56
3.3.5	Reference Cell in Use in Conjunction with Irradiance Profiling Table	57
3.3.6	Typical Light Source Irradiance Profile	59
3.3.7	Variation of P_m For a B-Cell Over a Three Month Period	61

Figures	Title	Page
4.2.1	Temperature of Type A Cell During Thermal Cycle Stress	73
4.2.2	Temperature of Type A Cell During Thermal Shock Stress. A: High Temperature-Low Temperature Transient. B: Low Temperature-High Temperature Transient	74
4.2.3	Type A Cell with Conchoidal Silicon Fracture at Tab Attachment Point	77
4.2.4	Type E Cell with Conchoidal Silicon Fracture at Tab Attachment Point	78
4.2.5	Type B Cell with Conchoidal Silicon Fracture at Tab Attachment Point	79
4.2.6	Type A Cell with Collector and Grid Delamination (Type Y Break)	80
4.2.7	Type C Cell with Delamination of Back Metal (Type Y Break)	81
4.2.8	Type A Cell with Long Silicon Fracture (Type Z Break)	83
4.2.9	Type A Cell with Long Silicon Fracture (Type Z Break)	84
4.2.10	Behavior of P_m Distribution and Lot Mean P_m with Thermal Cycle Stress Type A Cells	92
4.2.11	Behavior of P_m Distribution and Lot Mean P_m with Thermal Cycle Stress, Type B Cells	93
4.2.12	Behavior of P_m Distribution and Lot Mean P_m with Thermal Cycle Stress, Type C Cells	94
4.2.13	Behavior of P_m Distribution and Lot Mean P_m with Thermal Cycle Stress, Type E Cells	95
4.2.14	Behavior of P_m Distribution and Lot Mean P_m with Thermal Cycle Stress, Type A Cells	103
4.2.15	Behavior of P_m Distribution and Lot Mean P_m with Thermal Cycle Stress, Type B Cells	104
4.2.16	Behavior of P_m Distribution and Lot Mean P_m with Thermal Shock Stress, Type C Cells	105
4.2.17	Behavior of P_m Distribution and Lot Mean P_m with Thermal Shock Stress, Type E Cells	106

Figures	Title	Page
4.3.1	Behavior of P_m Distribution and Lot Mean P_m with 75°C Bias-Temperature Stress, Type A Cells	118
4.3.2	Behavior of P_m Distribution and Lot Mean P_m with 135°C Bias-Temperature Stress, Type A Cells	119
4.3.3	Behavior of P_m Distribution and Lot Mean P_m with 150°C Bias-Temperature Stress, Type A Cells	120
4.3.4	Behavior of P_m Distribution and Lot Mean P_m with 165°C Bias-Temperature Stress, Type A Cells	121
4.3.5	Behavior of P_m Distribution and Lot Mean P_m with 75°C Bias-Temperature Stress, Type B Cells	122
4.3.6	Behavior of P_m Distribution and Lot Mean P_m with 135°C Bias-Temperature Stress, Type B Cells	123
4.3.7	Behavior of P_m Distribution and Lot Mean P_m with 150°C Bias-Temperature Stress, Type B Cells	124
4.3.8	Behavior of P_m Distribution and Lot Mean P_m with 165°C Bias-Temperature Stress, Type B Cells	125
4.3.9	Behavior of P_m Distribution and Lot Mean P_m with 75°C Bias-Temperature Stress, Type C Cells	126
4.3.10	Behavior of P_m Distribution and Lot Mean P_m with 135°C Bias-Temperature Stress, Type C Cells	127
4.3.11	Behavior of P_m Distribution and Lot Mean P_m with 150°C Bias-Temperature Stress, Type C Cells	128
4.3.12	Behavior of P_m Distribution and Lot Mean P_m with 165°C Bias-Temperature Stress, Type C Cells	129
4.3.13	Behavior of P_m Distribution and Lot Mean P_m with 75°C Bias-Temperature Stress, Type E Cells	130

Figures	Title	Page
4.3.14	Behavior of P_m Distribution and Lot Mean P_m with 135°C Bias-Temperature Stress, Type E Cells	131
4.3.15	Behavior of P_m Distribution and Lot Mean P_m with 150°C Bias-Temperature Stress, Type E Cells	132
4.3.16	Behavior of P_m Distribution and Lot Mean P_m with 165°C Bias-Temperature Stress, Type E Cells	133
4.3.17	Mean Percent Decrease in P_m for 75°C Bias-Temperature Stress Test, All Cell Types	135
4.3.18	Mean Percent Decrease in P_m for 135°C Bias-Temperature Stress Test, All Cell Types	136
4.3.19	Mean Percent Decrease in P_m for 150°C Bias-Temperature Stress Test, All Cell Types	137
4.3.20	Mean Percent Decrease in P_m for 165°C Bias-Temperature Stress Test, All Cell Types	138
4.3.21	Mean Percent Decrease in P_m for Bias-Temperature Stress Test, Type A Cells	139
4.3.22	Mean Percent Decrease in P_m for Bias-Temperature Stress Test, Type B Cells	140
4.3.23	Mean Percent Decrease in P_m for Bias-Temperature Stress Test, Type C Cells	141
4.3.24	Mean Percent decrease in P_m for Bias-Temperature Stress Test, Type E Cells	142
4.3.25	Type A Cell I-V Characteristics After 165°C B-T Stress, Typical Case	144
4.3.26	Type A Cell I-V Characteristics After 165°C B-T Stress, Best Case	145
4.3.27	Type A Cell I-V Characteristics After 165°C B-T Stress, Worst Case	146
4.3.28	Behavior of R_s with B-T Stress Time, Typical Type A Cells	147

Figures	Title	Page
4.3.29	Cummulative Mean Percent P_m Degradation Versus Bias-Temperature Stress Time, Lognormal Scale	148
4.3.30	Behavior of Time to 10% Degradation versus Inverse Temperature, Type A Bias-Temperature Stress Test Lots	150
4.4.1	Behavior of P_m Distribution and Lot Mean P_m with Biased 85°C/85% R.H. Stress, Type A Cells	161
4.4.2	Behavior of P_m Distribution and Lot Mean P_m with Biased 121°C/15 Psig Steam Stress, Type A Cells	162
4.4.3	Behavior of P_m Distribution and Lot Mean P_m with Biased 85°C/85% R.H. Stress, Type B Cells	163
4.4.4	Behavior of P_m Distribution and Lot Mean P_m with Biased 121°C/15 Psig Steam Stress, Type B Cells	164
4.4.5	Behavior of P_m Distribution and Lot Mean P_m with Biased 85°C/85% R.H. Stress, Type C Cells	165
4.4.6	Behavior of P_m Distribution and Lot Mean P_m with Biased 121°C/15 Psig Steam Stress, Type C Cells	166
4.4.7	Behavior of P_m Distribution and Lot Mean P_m Biased 85°C/85% R.H. Stress, Type E Cells	167
4.4.8	Behavior of P_m Distribution and Lot Mean P_m with Biased 121°C/15 Psig Steam Stress, Type E Cells	168
4.4.9	Mean Percent Decrease in P_m versus Stress Time, 85°C/85% R.H. Test	170
4.4.10	Mean Percent Decrease in P_m versus Stress Time, 121°C/15 Psig Steam Test	171
4.5.1	Behavior of P_m Distribution and Lot Mean P_m with Power Cycle Stress, Type A Cells	180
4.5.2	Behavior of P_m Distribution and Lot Mean P_m with Power Cycle Stress, Type B Cells	181

Figures	Title	Page
4.5.3	Behavior of P_m Distribution and Lot Mean P_m with Power Cycle Stress, Type C Cells	182
4.5.4	Behavior of P_m Distribution and Lot Mean P_m with Power Cycle Stress, Type E Cells	183
4.5.5	Behavior of Lot Mean P_m with Power Cycle Stress, All Cell Types	184
4.6.1	Cell A Test Lead Placement	198
4.6.2	Cell B Test Lead Placement	198
4.6.3	Cell C Test Lead Placement	199
4.6.4	Cell E Test Lead Placement	199
6.1	Relative Effects of Accelerated Stress Tests on P_m	216
6.2	Relative Effects of Accelerated Stress Tests on Contact Integrity	217
A-1	Data Printout from SAS Program	A 5
A-2	Histogram of P_m Distribution for Type B Cells, Lot 10, Prestress. Lot Size = 60 Cells	A 6
A-3	Scatter Plot of I_{sc} vs. I_m, Type A Cells, Prestress	A 7
A-4	Printout Showing Results of Analysis of Variance and Duncan's Multiple Range Test	A 8
B-1	Prestress Distribution of V_{oc}, Type A	B 6
B-2	Prestress Distribution of I_{sc}, Type A	B 7
B-3	Prestress Distribution of V_m, Type A	B 8
B-4	Prestress Distribution of I_m, Type A	B 9
B-5	Prestress Distribution of P_m, Type A	B 10
B-6	Prestress Distribution of V_{oc}, Type B	B 11
B-7	Prestress Distribution of I_{sc}, Type B	B 12
B-8	Prestress Distribution of V_m, Type B	B 13
B-9	Prestress Distribution of I_m, Type B	B 14

Figures	Title	Page
B-10	Prestress Distribution of P_m, Type B	B 15
B-11	Prestress Distribution of V_{oc}, Type C	B 16
B-12	Prestress Distribution of I_{sc}, Type C	B 17
B-13	Prestress Distribution of V_m, Type C	B 18
B-14	Prestress Distribution of I_m, Type C	B 19
B-15	Prestress Distribution of P_m, Type C	B 20
B-16	Prestress Distribution of V_{oc}, Type E	B 21
B-17	Prestress Distribution of I_{sc}, Type E	B 22
B-18	Prestress Distribution of V_m, Type E	B 23
B-19	Prestress Distribution of I_m, Type E	B 24
B-20	Prestress Distribution of P_m, Type E	B 25
E-1	Test Lead Bend	E 4
E-2	Solder Cream Placement	E 5
E-3	Test Lead Placement	E 5
E-4	Test Lead Solder	E 6
E-5	Test Lead Bend For Epoxy Method	E 7
E-6	Test Lead Placement, Epoxy Method	E 7

LIST OF TABLES

Tables	Title	Page
2.1	Stress Test and Lot Identification	27
3.3.1	Reference Cell Output at 100 mW/cm^2	58
4.1.1	Cell Purchase Lots and Date of Receipt at Clemson University	68
4.1.2	Physical Characteristics of Four Cell Types Subjected to Stress Testing	68
4.2.1	Results of -65°C to 150°C Thermal Cycling, Phase I Experiments	85
4.2.2	Results of Thermal Cycling Experiments, Phase II Cells	85
4.2.3	Thermal Cycle Stress Test Schedule	87
4.2.4	Summary of Results of Thermal Cycle Stressing, Type A Cells	88
4.2.5	Summary of Results of Thermal Cycle Stressing, Type B Cells	89
4.2.6	Summary of Results of Thermal Cycle Stressing, Type C Cells	90
4.2.7	Summary of Results of Thermal Cycle Stressing, Type E Cells	91
4.2.8	Physical Effects Observed During Thermal Cycle Stress Testing, Type A Cells	97
4.2.9	Physical Effects Observed During Thermal Cycle Stress Testing, Type B Cells	97
4.2.10	Physical Effects Observed During Thermal Cycle Stress Testing, Type C Cells	98
4.2.11	Physical Effects Observed During Thermal Cycle Stress Testing, Type E Cells	98
4.2.12	Thermal Shock Stress Test Schedule	100
4.2.13	Thermal Shock Response of Type A Cells	101
4.2.14	Thermal Shock Response of Type B Cells	101
4.2.15	Thermal Shock Response of Type C Cells	102

Tables	Title	Page
4.2.16	Thermal Shock Response of Type E Cells	102
4.3.1	Forward Current Used in Bias-Temperature Stress Tests	114
4.3.2	Bias-Temperature Stress Test Schedule	116
4.3.3	Down-times for Bias-Temperature Stress Tests	117
4.4.1	Sample Size and Down-Time for Phase I Experiments, B-T-H Stress	158
4.4.2	Sample Size and Test Duration, Large-Quantity Tests, B-T-H Stress	158
4.4.3	Mean Values of P_m (W) for Biased Pressure Cooker Experiments	159
4.4.4	Mean Values of P_m (W) for Biased 85°C/85% Relative Humidity Experiments	159
4.4.5	Down-Times for Bias-Temperature-Humidity Stress Tests	160
4.4.6	Mean Percent Decrease in P_m and I_{sc}, versus B-T-H Stress Test Time, Type C Cells	173
4.5.1	Thermal Time Constant of Type A and Type B Cells, Ambient Temperature 35°C	178
4.5.2	ON Current for Power Cycle Stress Test	178
4.6.1	Number of Cells from Stress Test Lots and Control Cell Population Subjected to Contact Integrity Testing	197
4.6.2	Pull-Tests Performed During Contact Integrity Testing	200
4.6.3	Mean Pull Force and Predominant Failure Mode, Contact Integrity Test Control Units	200
4.6.4	Contact Adherence Strength of Stressed Cells Relative to Virgin Cells, Manufacturer-Attached Tab (MAT)	204
4.6.5	Contact Adherence Strength of Stressed Cells Relative to Virgin Cells, Solder-Attached Tab (SAT)	204

Tables	Title	Page
5.1	Reliability Qualification Test Schedule for Cell Technology Qualification	210
5.2	Reliability Qualification Test Schedule for Reliability Monitoring	210
B-1	Mean P_m and Standard Deviation, Phase II Cell Population Prestress	B 4
B-2	Mean I_{sc} and Standard Deviation, Phase II Cell Population Prestress	B 4
B-3	Mean V_{oc} and Standard Deviation, Phase II Cell Population Prestress	B 4
B-4	Mean I_m and Standard Deviation, Phase II Cell Population Prestress	B 5
B-5	Mean V_m and Standard Deviation, Phase II Cell Population Prestress	B 5
B-6	Results of Application of Duncan's Multiple Range Test to Phase II Lot Mean P_m, Type A Cells. Means With the Same Letter are not Significantly Different	B 27
B-7	Results of Application of Duncan's Multiple Range Test to Phase II Lot Mean P_m, Type B Cells. Means With the Same Letter are not Significantly Different	B 27
B-8	Results of Application of Duncan's Multiple Range Test to Phase II Lot Mean P_m, Type C Cells. Means With the Same Letter are not Significantly Different	B 29
B-9	Results of Application of Duncan's Multiple Range Test to Phase II Lot Mean P_m, Type E Cells. Means With the Same Letter are not Significantly Different	B 29
E-1	Pull Test Failure Mode Codes	E 8

1.0 INTRODUCTION

1.1 Test Considerations

PRECEDING PAGE BLANK NOT FILMED

This report describes the first year activities of a combined technical development study and reliability test program on silicon terrestrial solar cells being performed by Clemson University as part of DOE's Low Cost Solar Array (LSA) Project under contract to the Jet Propulsion Laboratory. The reliability test program being performed by Clemson University was started in December 1977 and represented the first known systematic attempt by independent investigators to define the basic reliability attributes of terrestrial solar cells. Goals of the program were to accumulate baseline reliability data and develop test methodologies for use in solar cell evaluations. The test program was designed to include several different cell types, sizes and configurations - all unencapsulated and representative of commercial, state-of-the-art cells used in JPL/LSA Block II and III solar cell module procurements.

Quantification of reliability was not a prime objective. Instead, this program was designed to be a precursor to future reliability testing of solar cells - by first obtaining a better understanding of failure mechanisms, failure modes and accelerated stress testing techniques.

Experience in the field-use applications of photovoltaic modules and array subsystems will be the ultimate verification of reliability. However, for a number of reasons, it is reasonable to attempt to assess reliability of the solar cell as a module component from accelerated test data. With non-accelerated testing the times required are often too great to obtain a statistically significant number of failures and also technology may, in the meantime, have completely changed; or the number of devices required to test become prohibitively large. Therefore, one prime objective was to develop methodology and to recommend an accelerated stress test schedule that could be used in the future reliability testing of terrestrial solar cells.

It was anticipated, before the program was started, that the most likely failure modes would be those involving the metalization system. A solar cell is after all merely a large diode and should be fairly immune to many types of the more esoteric failure modes which plague the more sophisticated integrated circuits, such as channel formation, surface state phenomenon, and oxide step effects. Consequently, a preliminary accelerated stress schedule was formulated, based on portions of the military reliability specifications for semiconductor devices (MIL-M-38510 and MIL-STD-883) which were associated with the metal-semiconductor contact and interconnection system.

Four state-of-the-art, commercially available cell types involving different metalization systems were obtained from four different manufacturers. The cell types were identified as A,B, C, and E (originally a fifth manufacturer, D, was to have been included). Approximately 500 cells of each type were included in the test program.

The primary test schedule was first applied to small quantities of the four different solar cell types in an effort to determine appropriate stress levels and observe any unexpected effects. It was anticipated that the results of accelerated stress would be seen as either a gradual degradation of a cell's electrical characteristics, notably its maximum power output, or as a catastrophic failure due to loss of electrical connection (open circuit).

It was expected that these two types of failure characteristics, gradual degradation and catastrophic, might be manifestations of the same effect, i.e., the metal-semiconductor contact becoming poorer electrically resulting in increased series resistance and a gradual decline in power output, and at the same time becoming poorer mechanically giving rise to eventual catastrophic separation. Metalization pull tests, which act in

reality as accelerated mechanical tests, were therefore instituted as an additional measurement procedure. The true significance of these pull tests appeared when they were used in conjunction with other accelerated stresses. This type of testing may eventually answer a question such as: Is the adherence of the cell metalization significantly weakened by the application of stresses such as temperature-humidity-bias?

Based on physics of failure reasoning and likely use-condition stresses, the schedule of accelerated stress test that was synthesized for use in the investigation included bias-temperature tests, bias-temperature-humidity tests, thermal cycle and thermal shock tests, and a power cycle (intermittent life) test. Fixturing was developed for large-quantity solar cell stress testing. A procedure for visual inspection of cells was developed. An electrical measurement facility capable of accurate, repeatable measurements of ($\pm$ 1%) of V_{oc}, I_{sc}, and P_m, and slightly less accurate measurements of I_m, V_m, R_s, and R_{sh} was established.

The program utilized the conventional reliability methodology illustrated in Figure 1.1.1. The cells were intially electrically measured, visually inspected, and the metalization adherence determined. Quantities of cells were then subjected to various stresses for various lengths of times and remeasured. This sequence of measure-stress-measure was repeated many times for each stress test. The measurement repeatability insured that electrical degradation due to stress as small as $\pm$ 2% could be detected.

A system was established for management and analysis of the large volume of electrical parameter data generated in the work. All electrical data, a total of 24,445 parameter values including both prestress and poststress data, currently is stored on disk and is available for further

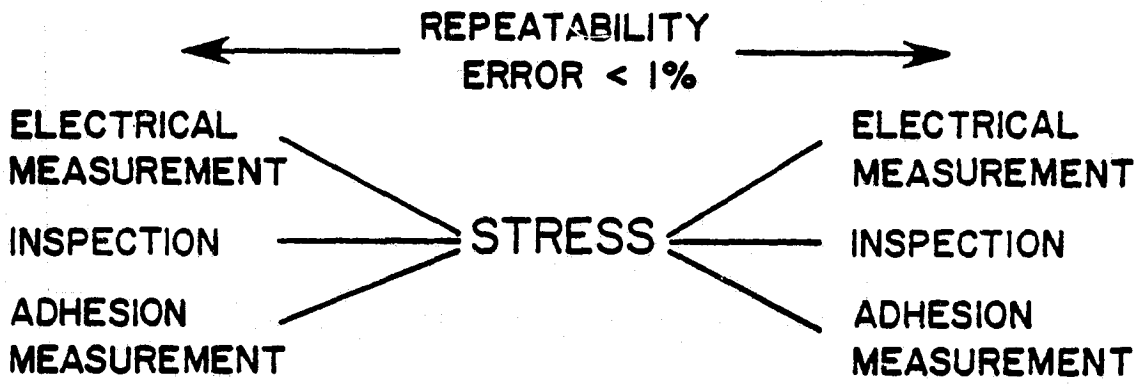

ELECTRICAL PARAMETERS

V_{oc} I_{sc} R_s V_m I_m P_m

INSPECTION

LOW POWER MAGNIFICATION

PHOTOGRAPHY

ADHESION

PULL STRENGTH DETERMINATION

Figure 1.1.1 Reliability Methodology

analysis. A procedure for determining the metal adherence strength of terrestrial solar cells was developed and applied to both stress tested cells and control populations.

By submitting small quantities of cells to somewhat arbitrarily selected preliminary stress levels and times, knowledge could be gained by which to define more statistically significant, large scale tests. The small quantity "quick look" tests were called Phase I tests, while the large quantity tests were designated as Phase II tests. Figure 1.1.2 illustrates the relationship between the two test plans. In most cases the initial "guesses" concerning stress levels and times were found to be reasonable and could be used directly in Phase II. In some instances, however, such as the thermal cycle and BTH tests, it was determined that the Phase I plan was overly conservative and the Phase II schedule was modified accordingly.

In addition to selecting appropriate stress levels and times the two phase approach allowed measurement methods and handling techniques to be developed and refined. Thus there were no significant errors introduced in obtaining the large quantity of Phase II data.

Phase I test data was thus only used to determine the Phase II schedule. The accelerated test data referred to in the remainder of the report is therefore, only Phase II data involving the following stresses:

Bias-Temperature (B-T) at 75°C, 135°C, 150°C, and 165°C

Bias-Temperature-Humidity (B-T-H)

121°C, 15 Psig steam

85°C/85% R.H.

Power Cycle, intermittent forward bias, ambient temperature 50°C

Thermal Cycle

Thermal Shock.

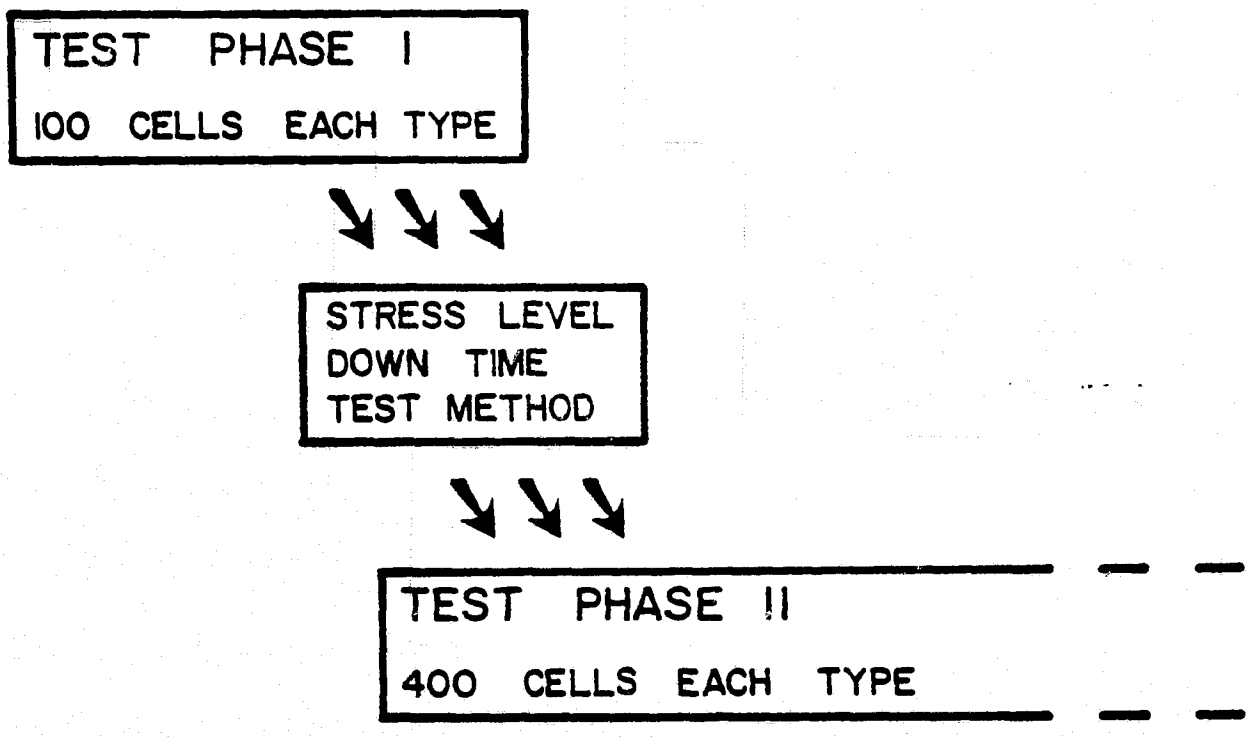

Figure 1.1.2 Relationship of Phase I and Phase II Testing.

Some experimentation was done with a reverse bias, but all "serious" testing involved only the application of a forward bias. The temperatures for the B-T tests were selected to span the range from operating conditions to the solder melting point (175°C). The conditions for the B-T-H tests are those historically used in integrated circuit corrosion susceptibility testing.

1.2 Reliability Considerations

PRECEDING PAGE BLANK NOT FILMED

Very little is found in the open literature concerning the nature of the time-to-failure (TTF) distributions of solar cells in terrestrial ambient conditions, the failure modes and failure mechanisms which control the TTF distributions, the appropriate methods for accelerated stress testing for reliability verification, or the process modifications which might be required to upgrade reliability performance.

It has repeatedly been observed that the most common TTF distribution of semiconductor devices (diodes, transistors, and integrated circuits) under use stress and accelerated stress is the lognormal distribution. In this distribution the logarithms (to the base 10) of the times-to-failure of a large population of devices are normally distributed about a median-time-to-failure (MTTF) t_m, with dispersion σ. This distribution thus does not give a constant failure rate. Other TTF distributions, such as the Weibull, have sometimes been found to best characterize mechanical-type failures of semiconductor devices. These other TTF distributions are also characterized by a non-constant failure rate. Twenty years is approximately 1.7×10^5 hours. Simple, commercial, plastic encapsulated circuits used by Bell Telephone Laboratories have t_m in the neighborhood of 10^7 hours (1142 years) under relatively benign, telephone installation conditions. Assuming that $t_m = 1.8 \times 10^7$ hours (2050 years) for terrestrial solar cells in the field environment, then for $\sigma = .87$ approximately 1% of the cells will fail in 20 years. On the other hand, if $t_m = 1.8 \times 10^6$ hours (205 years) and $\sigma = .87$, then 12.1% of the cells would fail on the average during a 20 year useful life. This implies a relatively large number of electrically inactive cells at the end of 20 years, and possibly frequent field replacements. Thus, even though the median time to failure for solar cells may be quite long, of the order of hundreds of thousands of hours,

system reliability may be unsatisfactory because of the large number of cells which are incorporated in a system. The above example ignored infant mortality failures which increase the failure fraction of units in early system life. Neither t_m, nor σ, nor the contributing mechanisms which go toward determining t_m and σ, have been determined for terrestrial cells.

Accelerated Stress Testing approach to determining reliability is to attempt to accelerate device failure by overstressing the device, i.e., subjecting it to greater stresses than it would encounter in the field. However, the failures which are obtained under these conditions must be similar to the failures observed in the field, i.e., the failure mechanisms must be the same. A key factor in the use of accelerated test methods is the recognition that it is the failure mechanism which must be the same and not necessarily the stress. For example, if an integrated circuit is known to fail because of the formation of an oxygen rich metallic compound then baking the device in an atmosphere of pure oxygen would be a legitimate and effective accelerated stress even though the device would never see a pure oxygen ambient in the field.

The danger in attempting to accelerate failure, of course, is that the applied overstress may introduce new failure modes which would not appear in the field. An example would be the acceleration of a metalization failure caused by solid state diffusion. Raising the temperature will accelerate the diffusion process provided the temperature is kept below the melting point. If melting occurs a new failure mode, not normally seen in the field, is introduced.

Establishing reliability by accelerated testing should therefore be an iterative phenomenon. First, tests are run, statistics analyzed and failure modes identified. Then more tests are run at a higher stress

level and the statistics again analyzed and the failure modes again identified. Ideally, the failure modes should be the same, with more devices failing in a given time at the higher stress level. Unfortunately, it is seldom this simple because of appearance of additional failure modes, some of which may be legitimate and some of which may not. In this fashion, over a period of time, it is possible to build up a vast background of reliability knowledge which will provide confidence that device manufactured by method A will last longer in the field than those made by method B. It is even possible to determine acceleration factors and to estimate how long the two types of devices can be expected to last. An understanding of device performance under accelerated stress will either permit manufacturer B to modify his processes for improved reliability or permit manufacturer A to sacrifice some reliability for a lower cost.

Conventional reliability testing of semiconductor devices involves the sequence of stress followed by electrical measurement. Failure can then be defined in reference to the electrical specifications set by the manufacturer. Statistics are gathered on the number of failures which occur as a function of stress level and time. A device is considered a failure whether one particular parameter gradually "drifts" outside a specification or whether it suddenly becomes inoperative. In other words, no distinction is usually made between catastrophic and degradation failures - both are considered equally severe. In addition, no distinction is made between the "borderline good" device which needs to change only slightly to become a bad device, and the superior device which must degrade appreciably before becoming a failure. Also, it is considered that once a failure always a failure, and a failed device is removed from further testing.

This same philosophy of device reliability testing cannot be used in the accelerated reliabilty testing of present day solar cells primarily because no firm electrical specifications exist at the cell level. Consequently, the approach considered for this program was to electrically test each cell before and after stressing and to note any changes which took place in the absolute values of the measured parameters rather than attempting to characterize the devices as "good" or "bad". This approach effectively sidesteps the question of failures for devices which degrade with stress testing. Catastrophic changes which occur when the cells crack or when the leads come off can be considered failures, of course, but these are relatively rare in most tests. One could argue that a cell whose maximum power output decreases by 10% or 20% or some other number should be considered a failure. This type of reasoning, however, ignores the initial distribution factor and could result in "failures" with greater power output than "good" units. Consequently, in this initial reliability test program, despite the fact that severe degradation was observed under different test conditions, no conventional failure statistics involving mean time to failure, etc., are quoted. Instead, statistics are presented in terms of changes from the initial prestress values. This difference in philosophy need not be a cause for concern, however, since the program was still able to identify the stress tests and levels effective in inducing degradation modes even though the exact definition of a failure was not made. Because electrical test limits have not been established for solar cells, the distribution of initial parameter values will be of great interest in themselves to cell manufacturers and others who eventually will be concerned with setting specifications. For this reason they are presented in the report in their entirety in Appendix B.

In many respects, interpreting tests in terms of changes from initial values puts additional emphasis on both electrical measurements and data analysis. The rather elaborate electrical test facility which was established is discussed in Section 3.2, while the approach to the complication and statistical manipulation of the data is discussed in Appendix A. A summary of the stress test data, arranged by test type, add its analysis and interpretation is presented in Section 4. Based on the results of these tests a proposed Qualification Test Schedule was prepared and is published in Section 5. This schedule is based on the response of the four types of cells in the program to the accelerated stress test applied and in many respects represents the program's "bottom line".

2.0 ACCELERATED STRESS TEST PROCEDURES

Cells received from the manufacturers were numbered serially by lightly scratching an identification number in the back-side metalization. Each cell was then placed in a separate plastic petri dish and the dish was labeled. Because each cell was permanently marked there was no chance of getting the cells mixed in the dishes. Each cell was examined visually under low power magnification and any peculiarities noted on an inspection form. Each cell type had its own inspection form with an outline drawing which could be marked to show irregularities or imperfections. A sample form for one type of cell is shown in Figure 2.1. The inspection process was complicated by two factors initially - the inspector was not sure of how much detail to record nor exactly what he was looking for. The units of Phase I therefore were examined quite closely and in considerable detail. With experience during the Phase I experiments it became more clear what effects were taking place, and a less detailed examination was possible on the Phase II units.

In addition to visual inspection each cell was photographed using high resolution black and white film. Here again, it was not clear exactly what characteristics it was desired to record, but it was felt that a photographic record could supply valuable information concerning structural changes which might occur. Therefore, initial prestress photographs were taken of every cell and the negatives developed, but not printed. If any peculiar poststress effects were noted, poststress photographs could then be taken and an enlarged print made of both the before and after negatives for comparison. In general, however, unless changes were noted, poststress photographs were not taken. Information concerning the cell was included in the photograph for identification. An example of a typical prestress photograph is shown in Figure 2.2.

PRECEDING PAGE BLANK NOT FILMED

22

CELL # A-

DATE: _____

INSPECTOR: _____

HISTORY: _____

FRONT

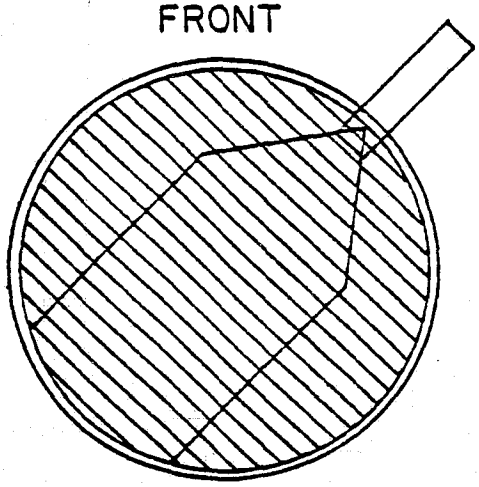

BACK

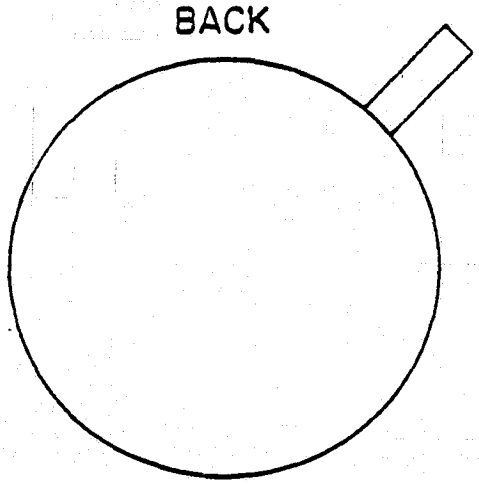

VISUAL INSPECTION SHEET

Figure 2.1. Example Visual Inspection Form

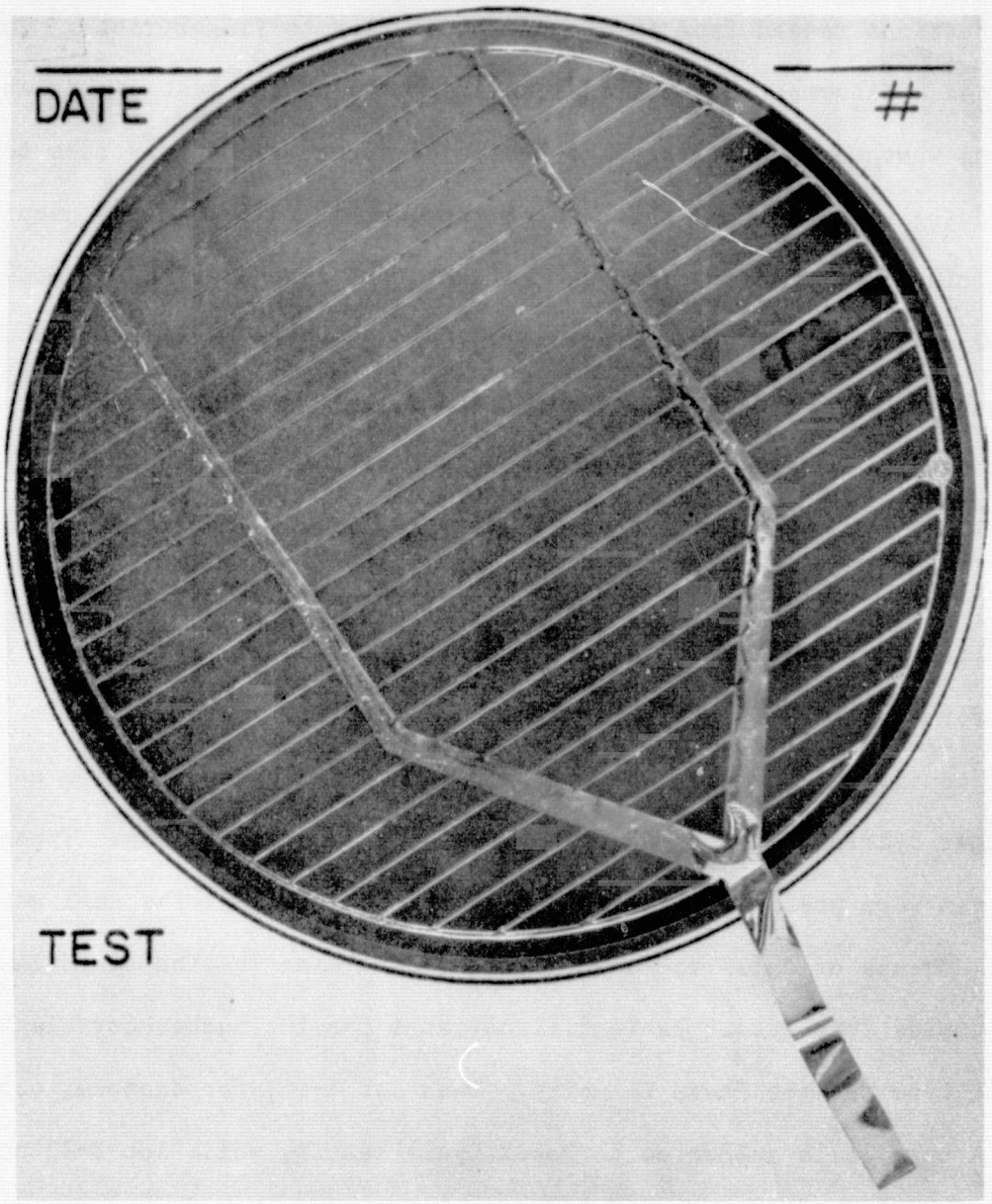

Figure 2.2. Enlarged Photo of Cell

Manufacturing history was not available on the cells. It was intended that they be supplied in their normal state prior to assembly into modules, but this could not be verified. Cells as received from the manufacturers were often quite dirty by semiconductor device standards. Imperfections ranged from traces of solder flux to fingerprints. This presented a dilemma. One could clean the cells to the best of his ability, using what were apparently the best procedures, prior to stress testing. In doing this one runs the risk of introducing failure modes peculiar to his cleaning techniques and at the same time removing failure modes that show up in modules due to improper cleaning by the manufacturer. On the other hand, if the cells are not cleaned, one runs the risk of observing contamination induced defects that might be removed by a proprietary process prior to assembly into modules. The limited amount of information available from the manufacturers indicated that further cleaning would probably not ordinarily be performed. Therefore all stress testing was performed on cells in the as-received condition. Care was taken, however, not to introduce additional contamination. Cells were handled using either Delrin^R tweezers, cotton gloves, or a vacuum pickup. Tweezers or gloves were preferable since contact was made only at the cell edge.

Groups of cells to be subjected to the same testing schedule were assembled into lots. Table 2.1 indicates the lot number correlation with test type for the Phase II units. Thus lot A-16, for example, consisted of A type cells subjected to Power Cycle testing while lot B-12 consisted of B type cells subjected to 150°C Bias-Temperature testing. Initially, and during each down time between stresses, the cells were electrically measured and visually inspected. Lot travelers accompanied each lot indicating the sequence of these operations. As each operation was

LOT #	STRESS TEST
10	75°C Bias-Temperature
11	135°C Bias-Temperature
12	150°C Bias-Temperature
13	165°C Bias-Temperature
14	121°C, 15 Psig Steam Bias-Temperature-Humidity
15	85°C/85% R.H. Bias-Temperature-Humidity
16	Power Cycle
17	Thermal Cycle
18	Thermal Shock

Table 2.1. Stress Test and Lot Identification

completed it was signed off and dated. In this way a glance at the traveler told the status of the lot and it was not possible to become confused and, for example, subject the lot to a stress without first electrically measuring the lot. As a further check, a log book was kept by each oven or test apparatus and a record maintained in it of the lots processed through that equipment, together with appropriate observations concerning settings, temperature, times, etc.

With the exception of thermal cycle and thermal shock, all the stress tests involved the application of voltage to the cells. It was thus necessary to find an inexpensive and simple method of making electrical connection to the cells which also would not introduce extraneous failure modes. The expedient solution was to use miniature cadmium plated steel alligator clips (Mueller #34C). One clip was attached to the front side lead and another to the back-side metal by gripping the slice, but with the jaw which contacts the front of the slice being insulated by a Teflon^{R} sleeve. A photograph of the contacting is shown in Figure 2.3.

This system worked reasonably well for the small quantities of Phase I, but in the process of scaling up to Phase II size lots (an increase of about a factor of five) problems inherent in the present jig design were uncovered. A stress test oven loaded with 150 cells is shown in Figure 2.4 and illustrates the crowding that occurs in actual use. Jigging problems were mainly of two types: (1) stress applied to the cell tabs and tab attachment points due to the electrical connections which are made to the hanging cells by means of the flexibly connected alligator chips, and (2) handling problems in loading and unloading the jigs. Loading such

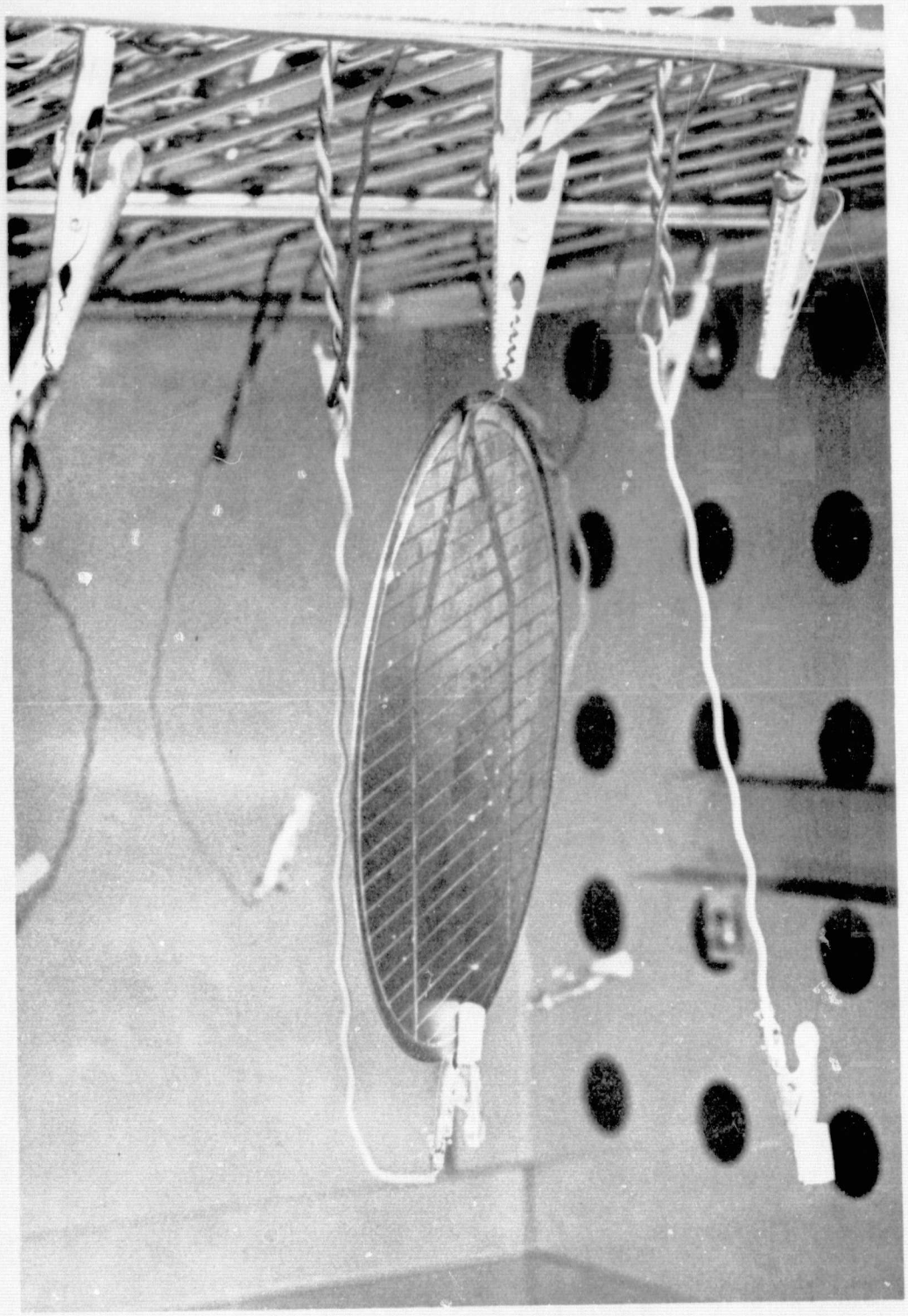

Figure 2.3. Cell Contacting Method Used in B-T Tests.

REPRODUCIBILITY OF THE
ORIGINAL PAGE IS POOR

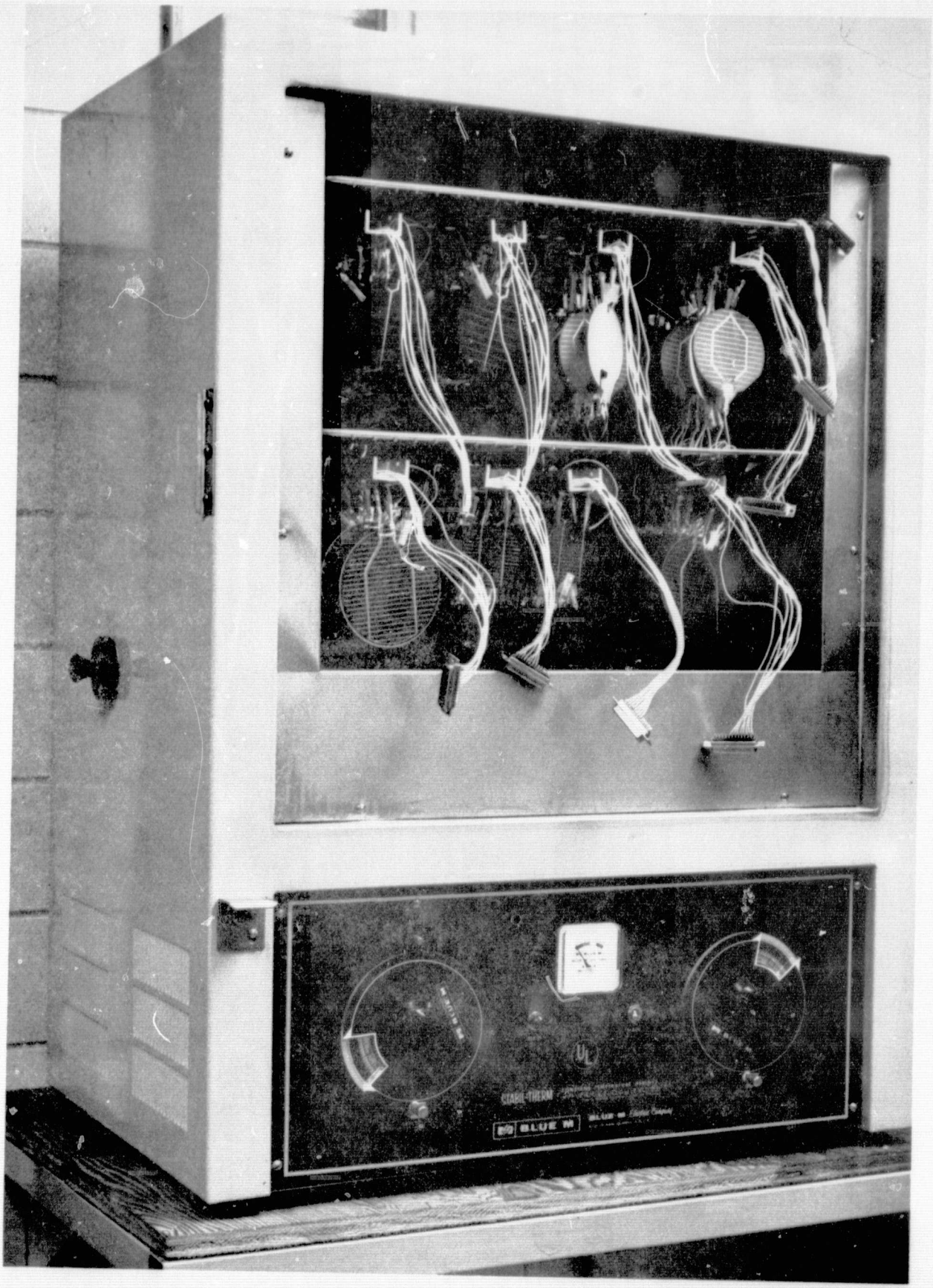

Figure 2.4. Oven Loaded With 150 Cells Ready For Stress Testing.

REPRODUCIBILITY OF THE
ORIGINAL PAGE IS POOR

a large quantity of cells in a confined space can result in dynamically stressing tabs and attachment points. In addition, unless extreme care is taken, electrical shorting of the cells can result. This causes very long cell loading times. It is evident from this scaling-up experience that the present stress test jig design is not an optimum one. While the present jig design evolved as an expedient solution to a pressing problem, it is not the best solution for the long term.

3.0 ELECTRICAL MEASUREMENT TECHNIQUES

3.1 General Considerations

As has been pointed out, reliability testing involves repeated sequences of electrical measurement followed by stress followed by electrical measurement. Comparison of before and after measurements are used to detect irreversible changes brought about by the stressing. Since these changes may be small, an accurate and highly reproducible measurement system is required in order to distinguish between random errors and effects brought about by stress. Since the "after" measurements may be taken weeks or even months after the "before" measurements, the repeatability requirement is particularly severe. Consequently, considerable effort was devoted during the course of the program to establishing an electrical measurement capability.

It is possible, of course, to completely characterize the power quadrant of a solar cell by measuring its I-V characteristic under one sun illumination at 28°C. Such a curve, while technically interesting, is of little use in accelerated reliability testing of the type performed on this program because it essentially contains too much information. One can visualize overlaying the before and after curves and noting qualitative changes, but to quantitatively compare the two cases, as might be done in a digital computer using a statistical analysis program, requires the measurement of a few significant parameters which reflect the cells performance. The single most significant parameter which characterizes a cell's performance is its maximum power. Thus prestress and poststress measurements of each cell's open circuit voltage, V_{oc}, short circuit current, I_{sc}, and series resistance, R_s, were made but it was the maximum power output, P_m, which was primarily examined for degradation (or improvement) before and after stressing.

PRECEDING PAGE BLANK NOT FILMED

PAGE 36 INTENTIONALLY BLANK

The approach to measuring P_m (and the other parameters) is shown in the schematic of Figure 3.1.1. The cell was mounted in a test jig with Kelvin probes such that one pair of probes carried the current while the other pair was used for voltage sensing. Digital meters and an x-y plotter read the current and voltage. Bucking variable power supplies permitted the entire power quadrant to be drawn out as the rheostat was varied. A photograph of the equipment is shown in Figure 3.1.2.

Figure 3.1.3 shows the Kelvin-type cell electrical test jig. The cell is held down by vacuum to the water cooled jig. Current is passed through the entire back surface of the cell which is in contact with the jig, while voltage is sensed by a single probe located in the center of the jig. This probe is a spring loaded, quick-response thermocouple so that it senses temperature as well as voltage. The front voltage sending probe is a clip-on contact made to the soldered lead. Since no current is carried by the voltage sensing circuit, this connection may be made anywhere along the lead beyond the current carrying connection with identical results. The front current connection is a clamp to the soldered lead. The clamp is planar with the cell's surface to avoid mechanically stressing the lead during measurement. Each different diameter cell has its separate jig. The jigs are adaptable only to cells having a metalized back surface and one or more top surface leads.

Reversing switches not shown in the schematic of Figure 3.1.1 permit the far forward characteristic ($V > V_{oc}$ and reverse current) to be plotted. Figure 3.1.4 shows an I-V and far-forward characteristic typical of traces obtained from the equipment. The series resistance, R_s, can be determined (approximately) from the slope of the far-forward characteristic. This technique results in a lower limit value of R_s. The exact values of forward current involved are not critical so long as the I-V

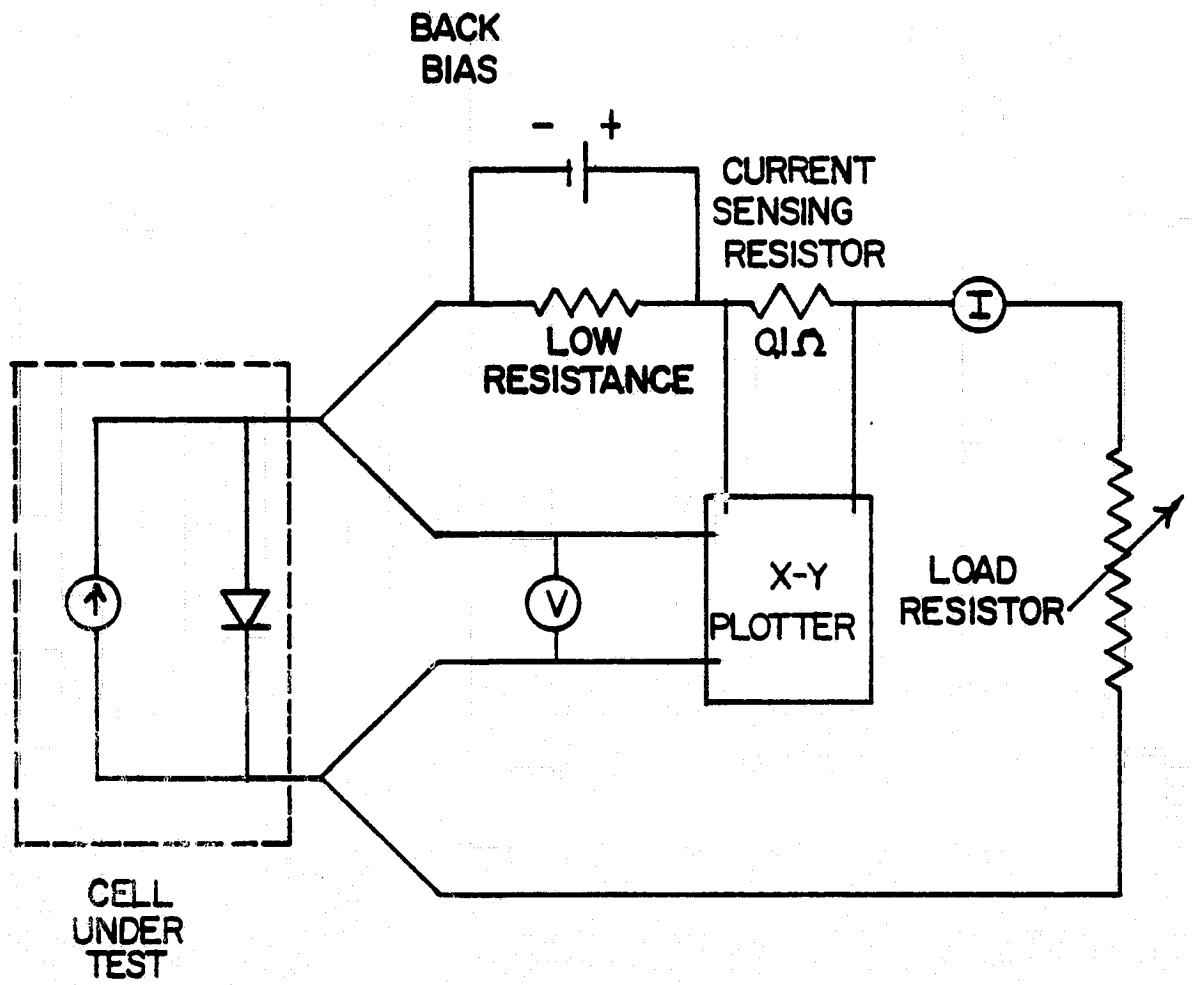

Figure 3.1.1. Electrical Measurement Schematic.

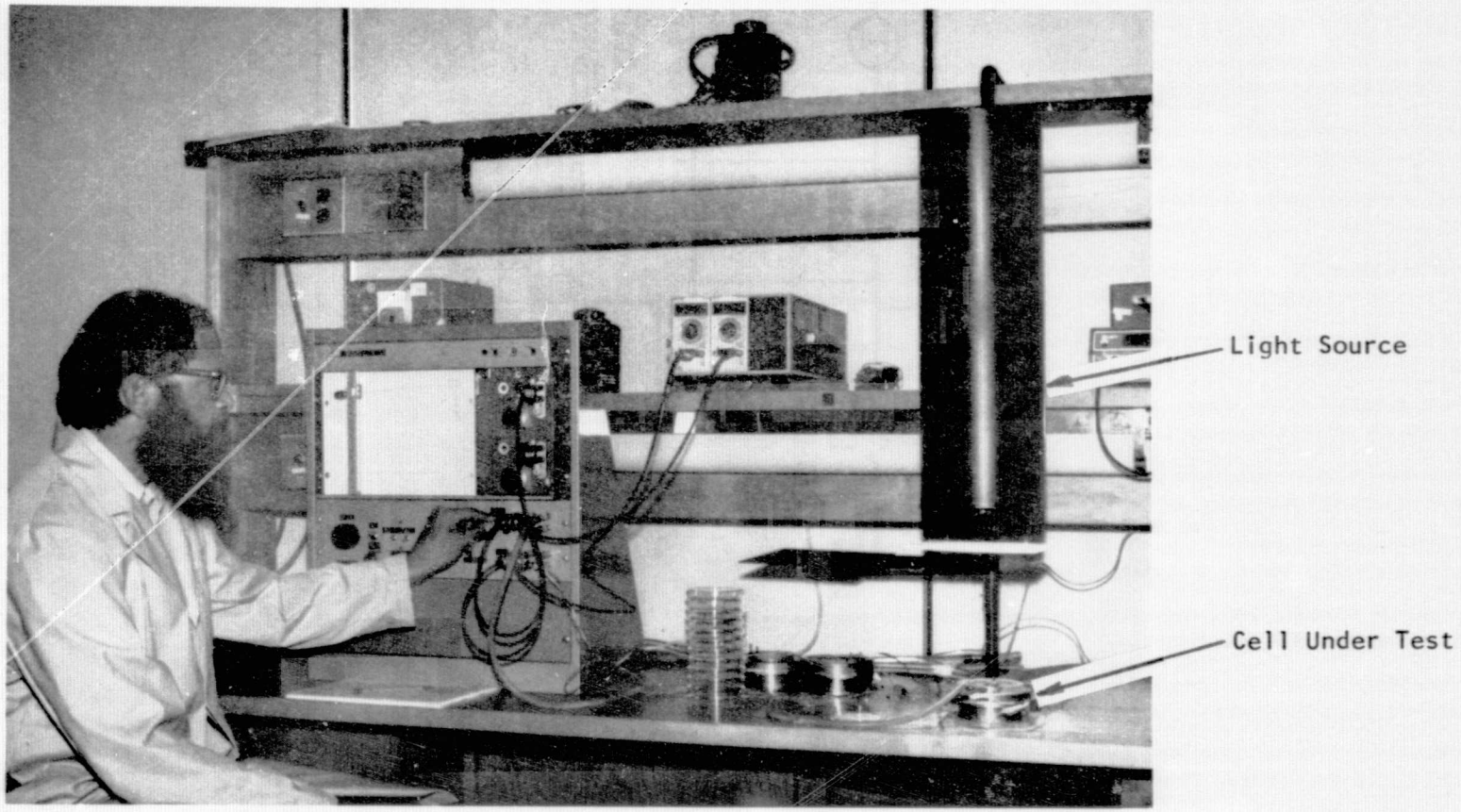

Figure 1. Electrical Measurement Facility

REPRODUCIBILITY OF THE
ORIGINAL PAGE IS POOR

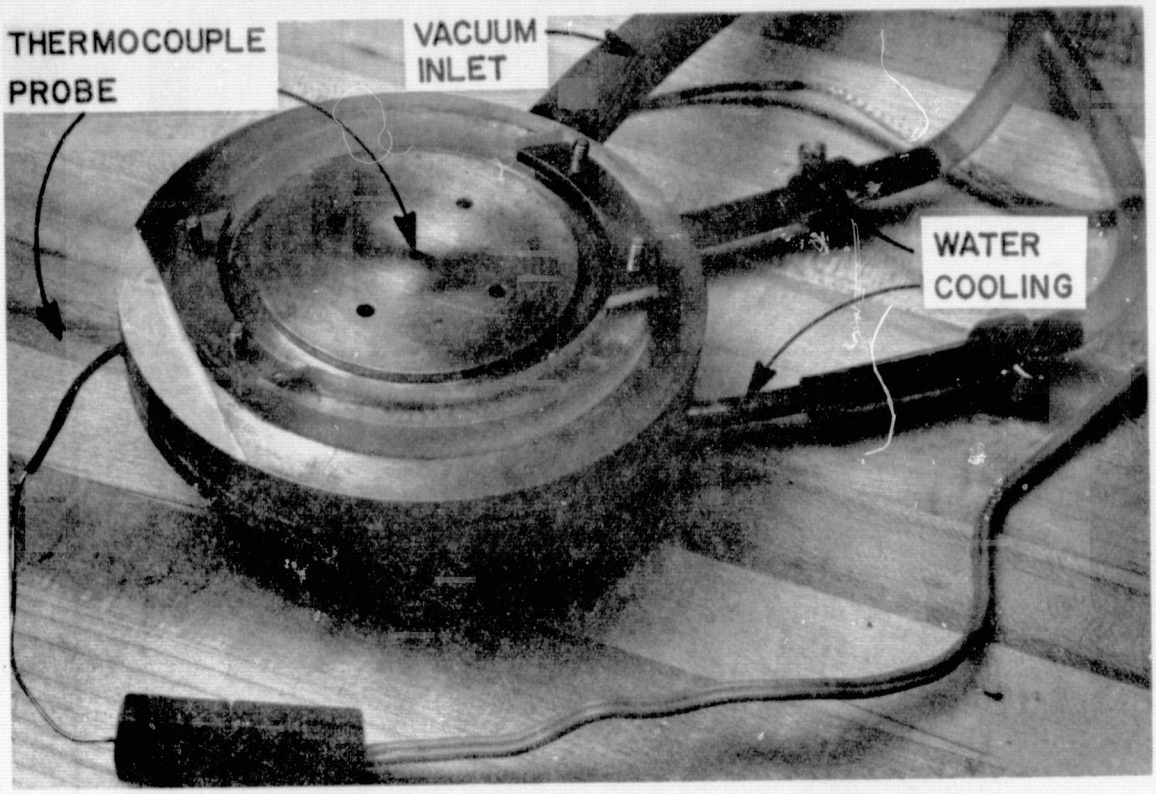

Figure 3.1.3.a. Electrical Measurement Jig.

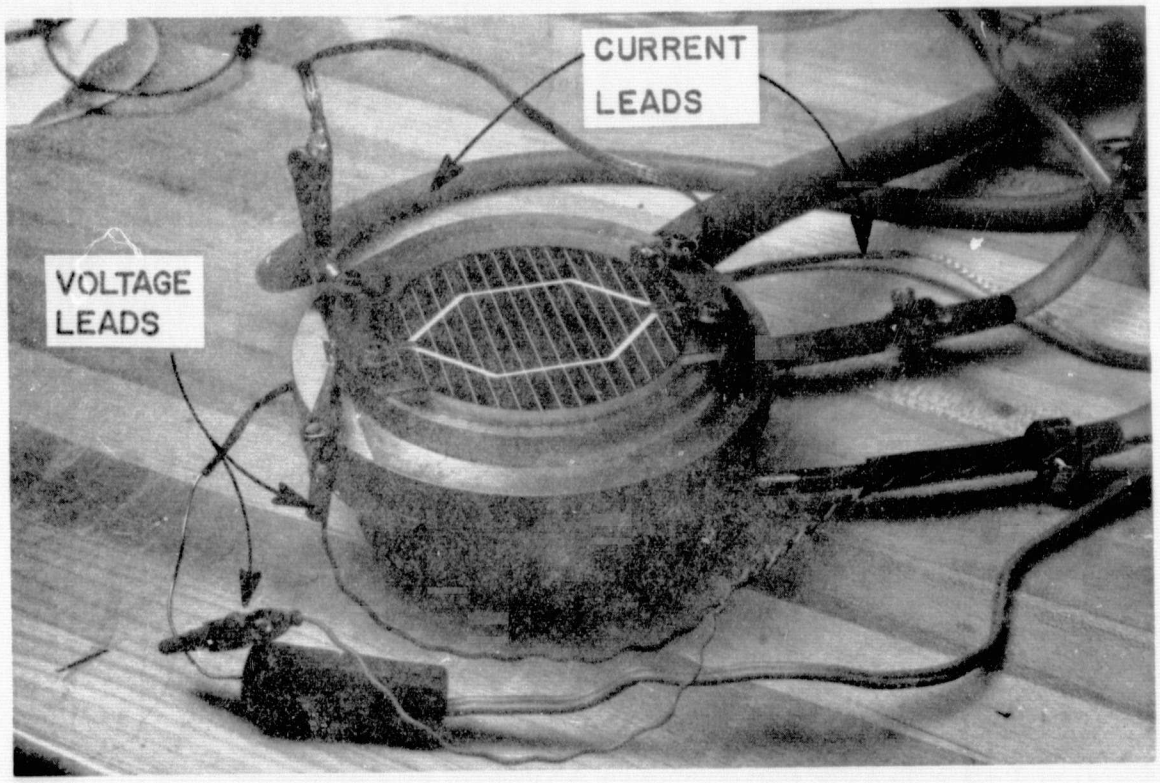

Figure 3.1.3.b. Measurement Jig, Loaded with E Slice.

REPRODUCIBILITY OF THE
ORIGINAL PAGE IS POOR

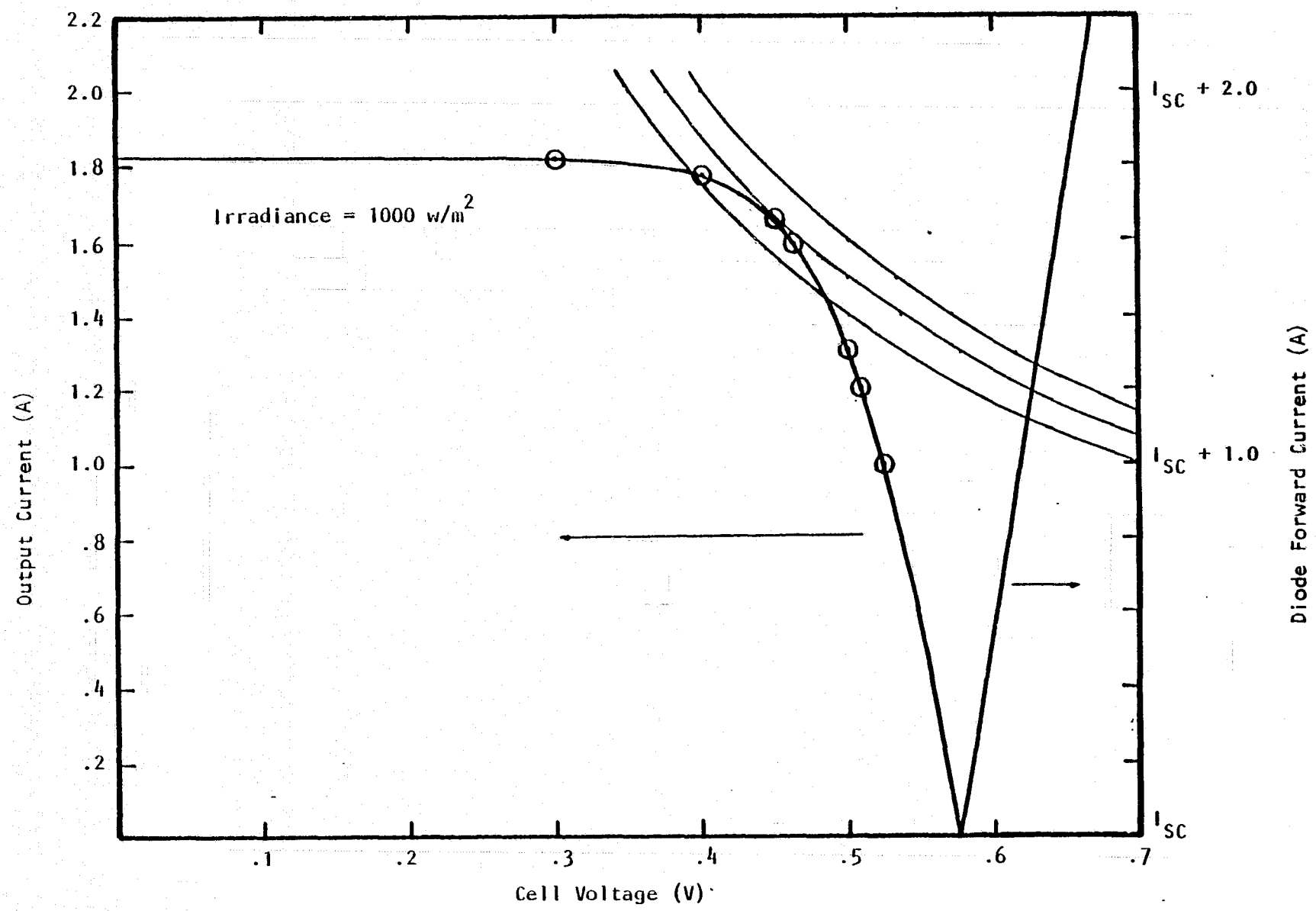

Figure 3.1.4. Typical Cell Output I-V Characteristic, With Constant-Power Hyperbolas Superimposed, and a Far-Forward Diode I-V Characteristic.

curve is linear. In practice this often means a minimum current of 3 to 6 times the short circuit current. The maximum far forward current through the diode in the actual down-time measurements ranged only from 1 to 2 times the short circuit current. However, for the majority of cells this part of the I-V curve has been found to be linear. Where a slight curvature in the far forward characteristic exists, changes in R_s can still be detected although absolute values can not be determined with a high degree of accuracy. Thus the measured R_s parameter represents a consistent, repeatable lower limit value for the series resistance, but not necessarily an accurate measurement of the actual series resistance. A more accurate determination of R_s can be done, but would require an inordinate amount of time for the quantities of units entailed.

The shunt resistance, R_{sh}, can in theory be determined for the slope of the I-V characteristic at V=0. Unfortuantely, the scale factors of the illuminate V-I trace are such that only R_{sh} values of the order of V_{oc}/I_{sc} can be determined accurately. Since R_{sh} is normally much greater than this, the V-I characteristic is of little use in determining R_{sh} unless it is abnormally low initially or decreases to a low value during stress testing.

V_{oc} is read from the continuously monitoring digital voltmeter when I=0, and I_{sc} is read from the continuously monitoring digital ammeter when V=0. By reading the data directly from meters, rather than from the V-I tracing, accuracy can be maintained to 3 significant figures. Thus, V_{oc} was read to the nearest millivolt and I_{sc} to the nearest milliamp.

Cell measurement thus consisted of recording the V-I characteristic on a plain piece of tracing paper. Information also entered on this paper

was the cell number, date of measurement, V_{oc} and I_{sc} values as read from the meters, and the thermocouple reading. The maximum power point was then obtained by overlaying the V-I trace on a sheet of graph paper on which a family of constant power hyperbolas had been drawn. Figure 3.1.4 shows the projection of such hyperbolas on an I-V plot. The maximum power point occurs where the V-I characteristic is tangent to the highest valued hyperbola. In general, because of the limited number of hyperbolas drawn, an exact tangential match could not be found and some interpolation was required. It is, of course, necessary to very accurately align the V-I trace to the master hyperbola graph. This is accomplished by placing marker points on the trace at "even" values of voltage and current, e.g., V = .3, .4, .5V, etc., and I = .8, 1.0, 1.2A, etc. Marker points are shown schematically in Figure 3.1.4 as circles, but actually show up as dots of the same diameter as the trace line width, but darker. These marker points, which are placed on the trace by "dotting" the pen at appropriate digital voltmeter readings after the characteristic has been drawn, permit very accurate alignment with the underlying graph. In addition, they serve as a constant check on the stability of the X-Y recorder. In addition to the marker points a base line is also drawn to help in alignment.

3.2 Maximum Power Determination

The maximum power, P_m, was calculated by multiplying V_m by I_m rather than attempting to determine the interpolated hyperbolic curve from the graph. Determination of both V_m and I_m graphically was rather inaccurate even if interpolation were not a factor, because the two curves usually appeared to be tangential over an extended range of values. Selection of a single tangential point became a "judgement call" on the part of the observer. However, while V_m and I_m were individually subject to errors their product was relatively accurate. If, for example, the value of V_m determined from the graph were too low, then I_m would be too high; but the product would be nearly correct. Thus V_m and I_m values could not be determined to better than 2 significant figures - V_m to the nearest 10 millivolts and I_m to the nearest 10 milliamps - an order of magnitude worse than V_{oc} and I_{sc}. The product, P_m, on the other hand, probably had 3 significant figure accuracy in most cases.

The 8 1/2" x 11" sheet of tracing paper containing the V-I characteristic and test information was filed by lot in a filing cabinet. Included in each lot folder was a lot summary sheet containing the data on each cell's V_{oc}, I_{sc}, V_m, T, and R_s. The T values were recorded for reference, but no use was made of them since readings were only taken within $\pm$ 0.5°C of 28°C and this small amount of variation had a negligible effect on the parameters (see below). R_s was not recorded on the summary sheet unless significant changes appeared. R_s values could always be obtained from the tracings if needed. A glance at the summary sheet could tell qualitatively changes that had occurred to a lot upon stressing. A statistical analysis of the parameters involved key punching the data on cards and entering this information into the computer (see Appendix A).

PRECEDING PAGE BLANK NOT FILMED

3.3 Repeatability Considerations

Two factors in addition to the electronic instrumentation which significantly affected measurement accuracy and repeatability were the incident illumination and the cell temperature. Both were required to be accurately determined and maintained constant. The Kelvin type vacuum hold down jigs were constructed with a water jacket for temperature control. Water from a constant temperature bath circulated through the jacket. The standard junction temperature for cell measurements is specified as 28^{+1}_{-0} °C. A copper-constantan spring-loaded thermocouple contacted the back side of the cell in the jig and also served as the Kelvin voltage probe. Temperature was constantly monitored using a DVM in conjunction with an Omega Model LXVJ reference junction. V-I characteristics were only made at thermocouple readings of 28 ± 0.5°C. By allowing the temperature to vary $\pm$ 0.5°C rather than $^{+1}_{-0}$ °C notice was taken that the top surface of the illuminated cell was slightly hotter than the bottom surface.

It was found that irregularities such as solder bumps on a cell's back surface could present difficulty in maintaining constant temperature during measurement. The jigs employed a gasketed vacuum hold down and a large irregularity on the back surface would cause the cell to crack when vacuum was applied. If the gasket were removed, or the amount of vacuum reduced so that the force was not large enough to crack the cell, the cell would not be in intimate thermal contact with the heat sink over a large area and the temperature would rise. In theory the temperature of the heat sink could then be reduced until the cell temperature came within acceptable limits. However, because of the thermal inertia of the water bath this would have required an unacceptably long time. Irregularities

sufficiently severe to preclude normal testing procedure were noted in approximately 15% of the type A cells. Since in order to have sufficient cells for the Phase II testing it was not possible to discard these cells, some were measured at a higher than normal temperature with the hope that it would be possible to relate any changes observed during accelerated stress tesing to a 28°C equivalent value, while on others the solder was mechanically removed by scraping.

To examine the sensitivity of measured parameters to temperature, a B-cell and an E-cell were measured over a temperature range of approximately ± 30°C about room temperature. Curves of V_{oc}, I_{sc}, and P_m for the two types of cells are shown as Figures 3.3.1 through 3.3.4. These curves show that if the temperature is held to within ± 0.5°C during measurement the maximum error that will result is 0.5% in V_{oc}, 0.06% in I_{sc}, and 0.5% in P_m.

The light source used for measurement was a 4-lamp ELH light source housed in the 7 inch diameter metal tube shown in Figure 3.1.2. A cooling fan is also housed in the tube. Each lamp could be individually adjusted by means of separate variable transformers and then all lamps simultaneously turned up or down by means of a common variable transformer. It was observed that the lamps drifted upward in intensity after being turned on, but leveled out after about an hour. Consequently, the light source was allowed to warm up for an hour before measurements were made and was only shut down at night.

A small profiling table, shown in Figure 3.3.5 was constructed for use in calibrating the light source. This table fitted over the cell holder retaining ring (cell holder removed) and could be accurately referenced to the measurement bench by means of detent pins. The table height was such that when a reference cell was placed on it, its surface

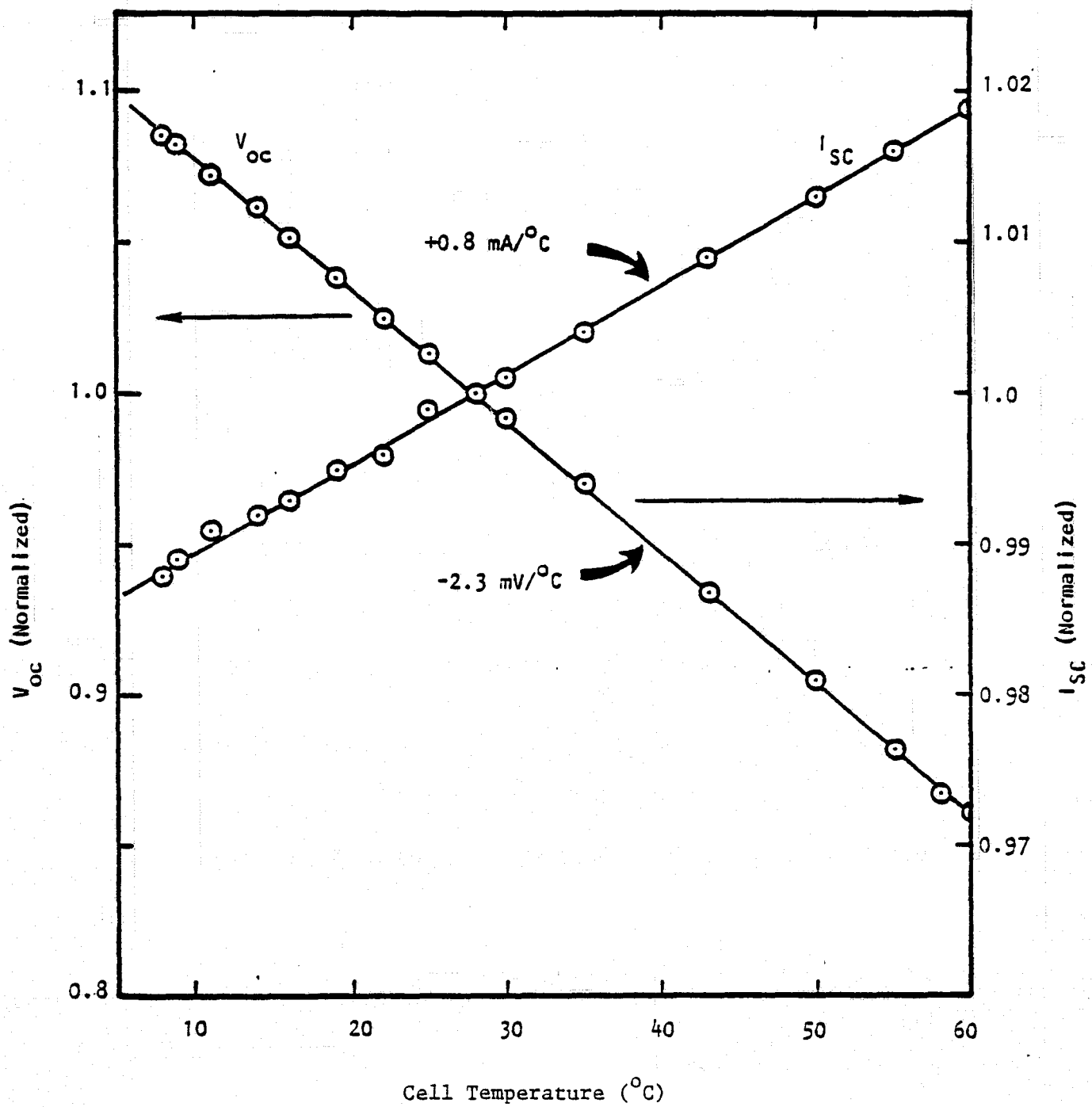

Figure 3.3.1 Temperature Dependence of V_{oc} and I_{sc} for Type B Cell, Irradiance 1000 W/m^2, ELH Lamp Source.

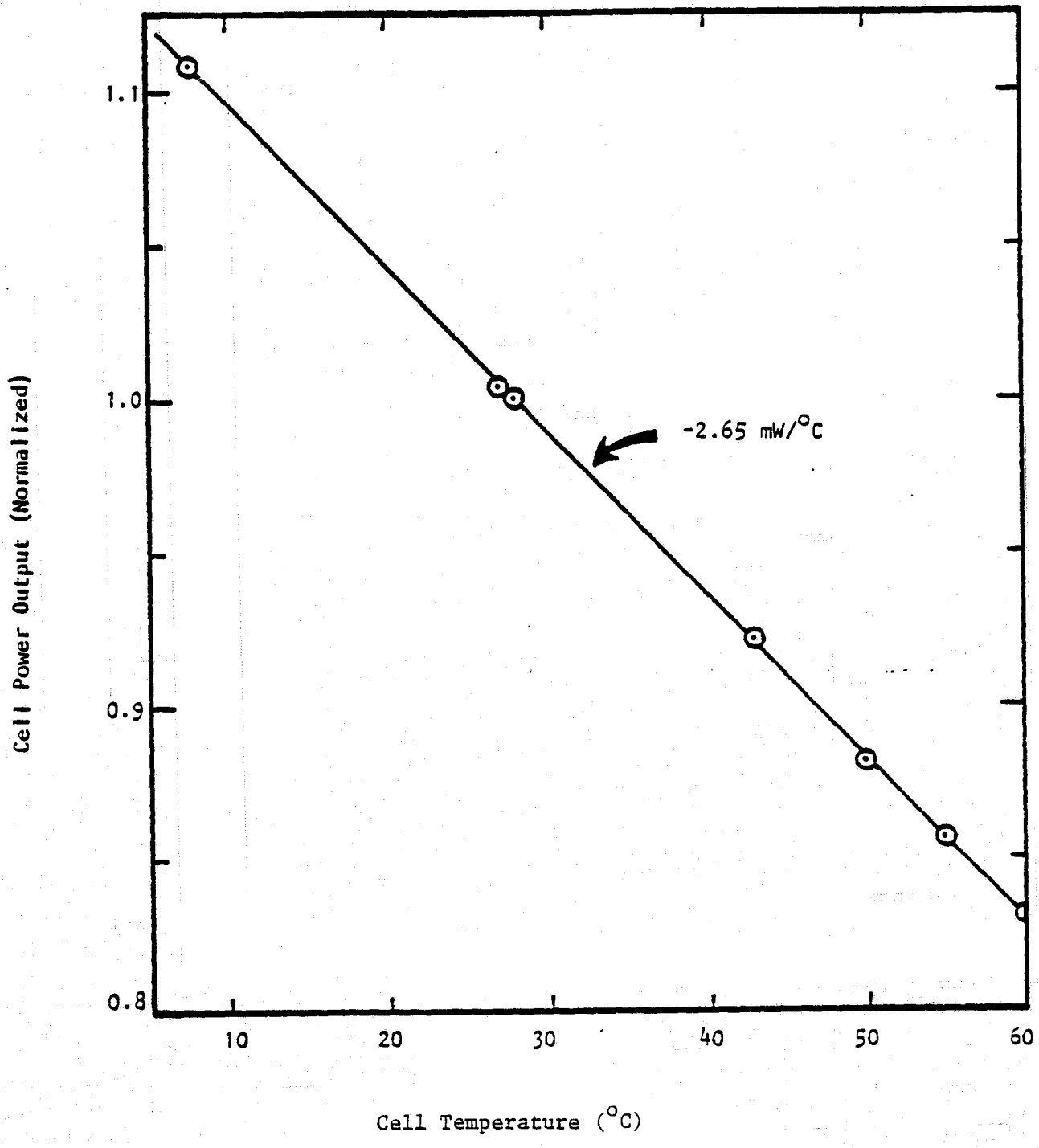

Figure 3.3.2 Temperature Dependence of Type B Cell Power Output at Maximum Power Point. Irradiance 1000 W/m^2, ELH Lamp Source.

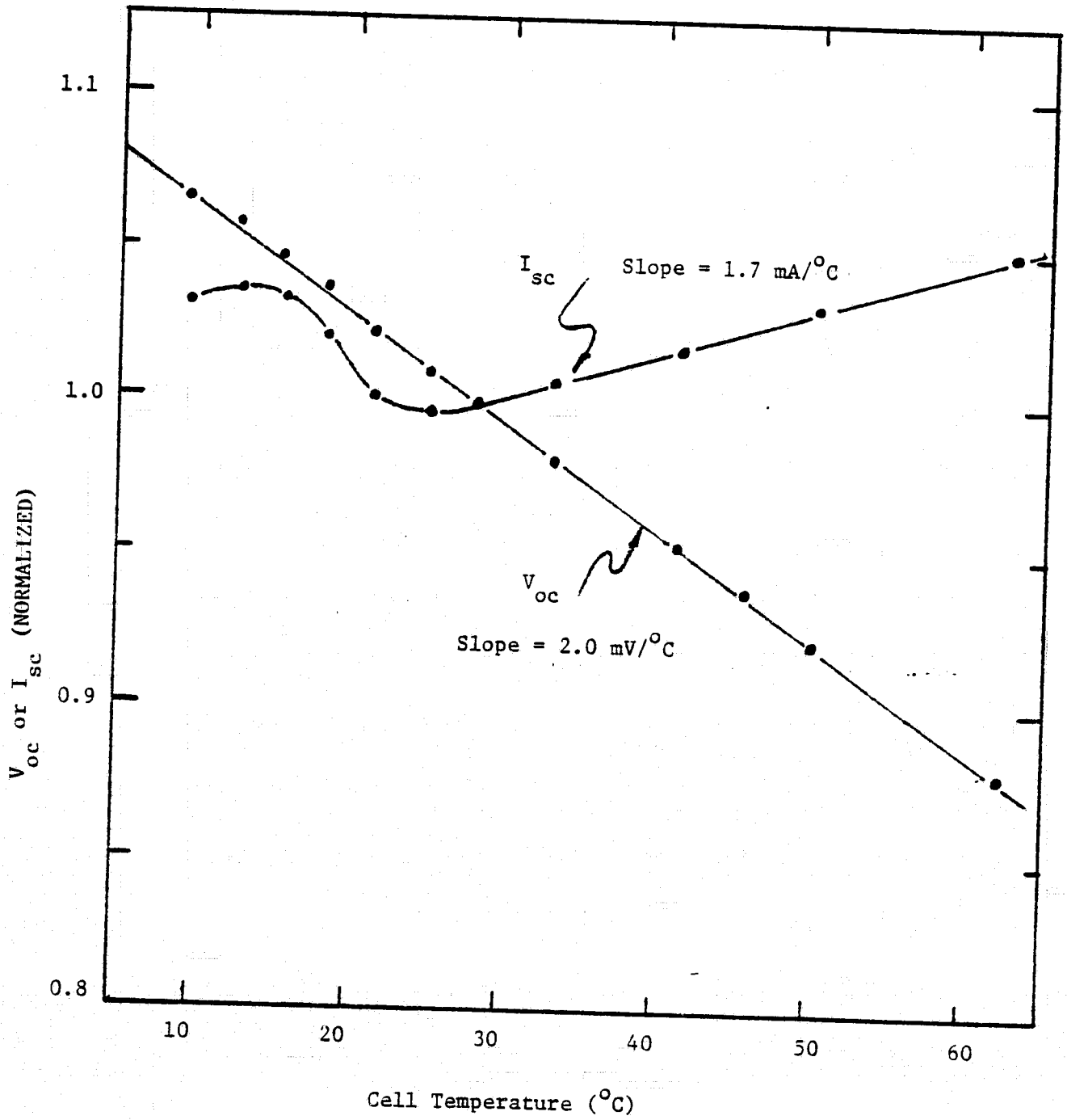

Figure 3.3.3 Temperature Dependence of V_{oc} and I_{sc} for Type E Cell, Irradiance 1000 W/m^2, ELH Lamp Source.

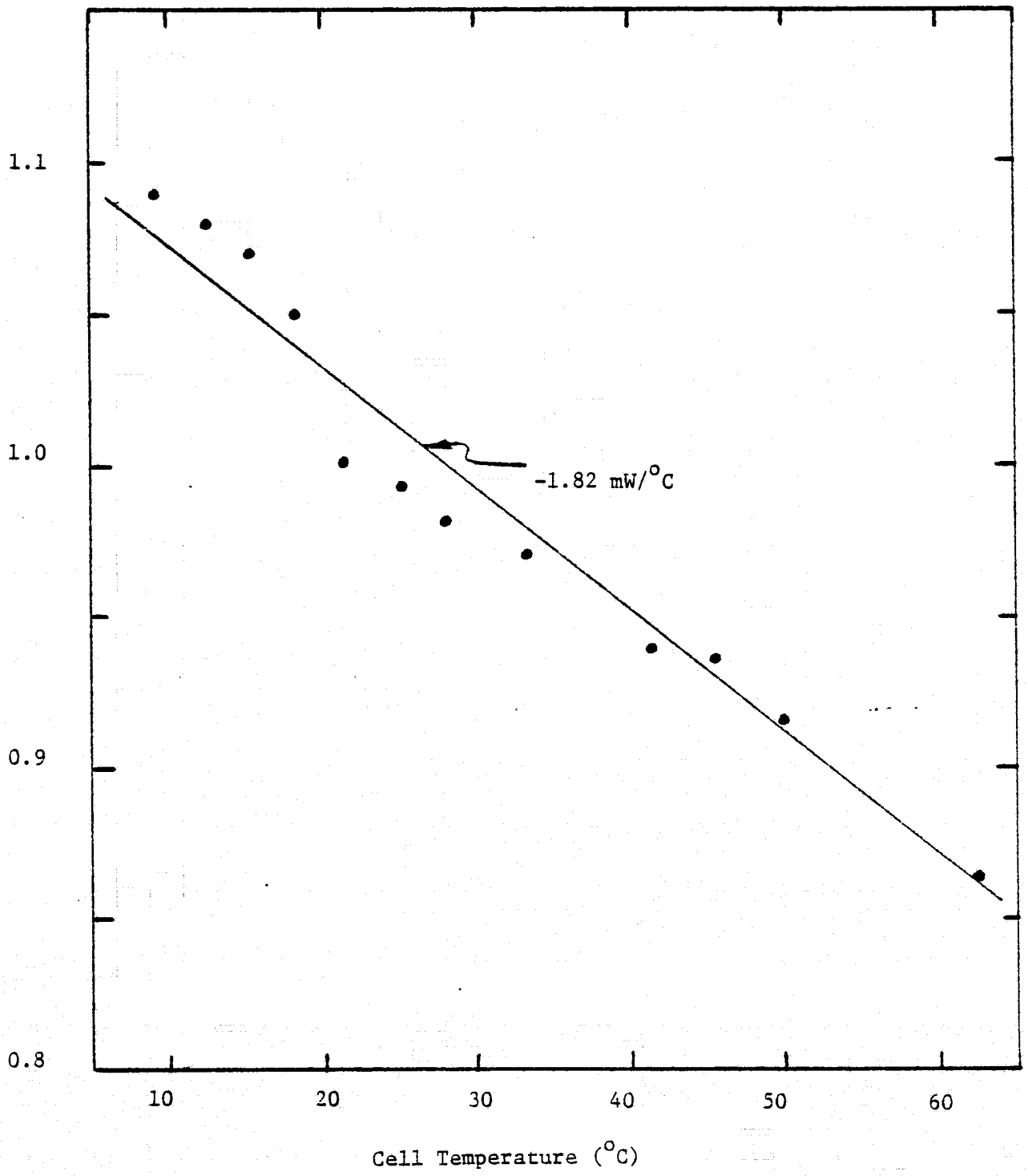

Figure 3.3.4 Temperature Dependence of Type E Cell Power Output At Maximum Power Point. Irradiance 1000 W/m^2, ELH Lamp Source.

REPRODUCIBILITY OF THE
ORIGINAL PAGE IS POOR

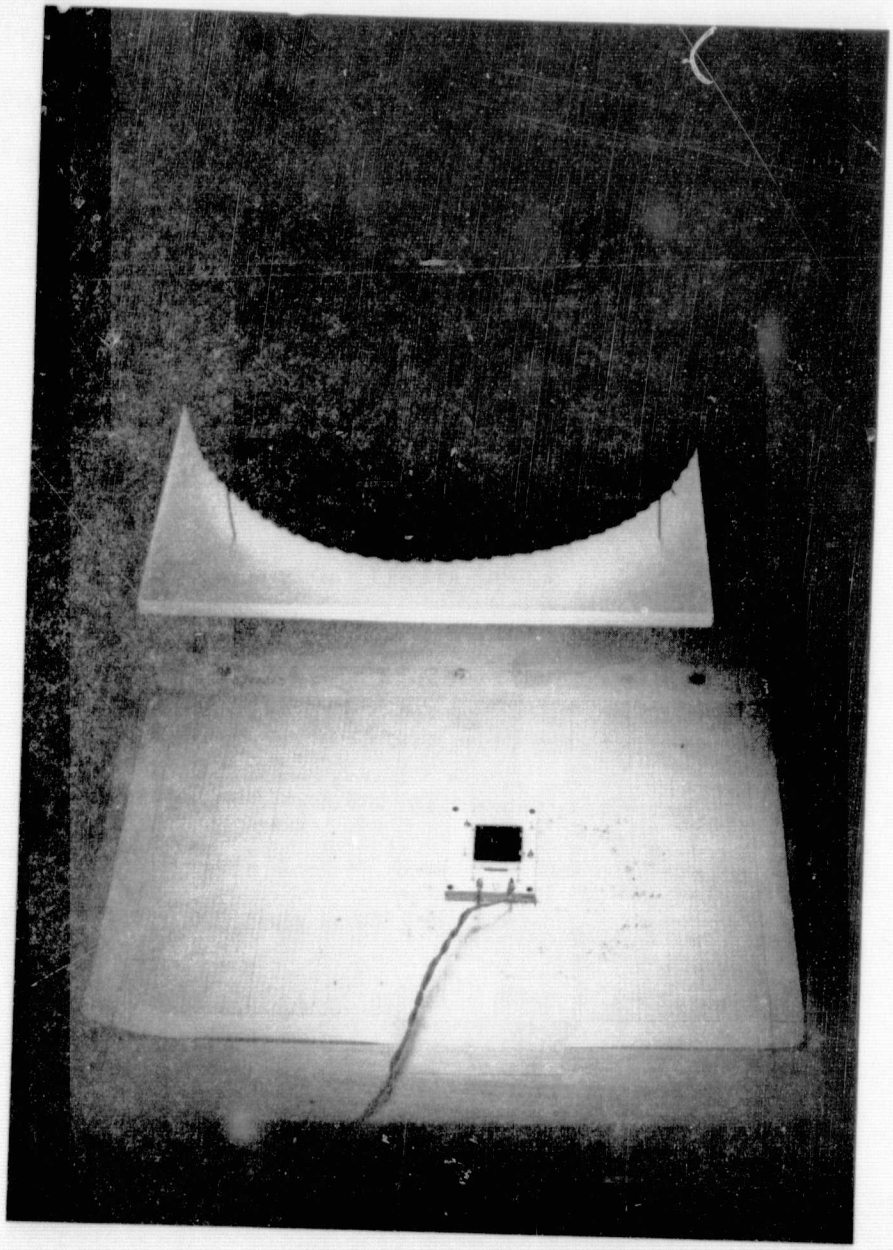

Figure 3.3.5 Reference Cell in Use in Conjunction with Irradiance Profiling Table.

would be at the same height as the surface of a cell under test. Graph paper was accurately positioned on the table thereby giving a coordinate system in the cell test plane that was precisely referenced to the cell holder. A JPL-supplied reference cell was moved over this coordinate system and readings recorded on the graph paper. A separate reference cell was used for each cell type. Table 3.3.1 shows the voltage output for each reference cell type at an illumination level of 100 mW/cm^2.

Cell Type	Output (mV)
A	45.0
B	62.3
C	53.2
E	62.8

Table 3.3.1. Reference Cell Output at 100 mW/cm^2

The light source calibration procedure was to first profile each lamp separately using similar variable transformer settings. These profiles tended to show slight differences in the maximum intensity of each lamp, caused primarily by bulb aging. Next each variable transformer was adjusted so that the maximum intensity from each lamp was the same. Then with all lamps set to the same intensity, a complete 4-lamp profile was made with the common variable transformer set to give a maximum reading of approximately 100 mW/cm^2. A typical profile is shown in Figure 3.3.6. It can be seen that over the largest area of interest, corresponding to a 100mm diameter cell, the variation from maximum (center) to minimum (edge) is 10%. For a cell of 3 inch diameter the variation is 3%. The contours of constant intensity were used to locate the cell holder retaining ring. Finally, with the reference cell located at the average contour center (the position marked with the cross in Figure 3.3.6 and not necessarily

Outline of
100 mm cell

				46.8	48.3	46.0	48.7	47.6				
		46.8	49.2	51.0	52.6	53.5	53.1	51.8	49.8			
	47.6	50.4	52.8	54.7	56.4	57.0	56.4	55.0	52.8	49.6	45.8	
46.6	50.4	53.5	55.9	57.9	59.2	59.5	59.0	57.5	55.2	51.9	48.0	
48.2	52.3	55.4	58.1	60.0	60.8	60.9	60.4	59.1	56.9	53.6	49.4	
49.1	53.4	57.1	59.7	61.0	66.2	61.1	60.9	60.3	57.9	54.5	50.5	45.2
48.9	53.8	57.9	60.3	61.2	61.2	60.8	60.7	60.1	58.5	55.0	50.5	45.3
48.2	53.0	56.7	59.2	60.3	60.3	59.8	59.6	59.1	57.4	54.4	49.8	
46.8	51.2	54.9	57.3	58.2	58.8	58.6	58.1	57.1	55.3	52.3	48.4	
	48.6	51.9	54.0	55.6	56.4	56.6	56.1	54.7	52.6	49.9		
		48.4	50.7	52.3	53.3	53.3	52.9	51.7	49.8	47.1		
			47.1	48.5	49.2	49.4	49.0	48.2				

Figure 3.3.6 Typical Light Source Irradiance Profile.

the position of maximum intensity) the common variable transformer was adjusted to give a 100 mW/cm^2 reading per the values listed in Table 3.3.1.

The procedure just described is rather tedious and was only performed when a bulb had to be replaced or after extended periods without profiling. The daily start-up procedure involved only the adjustment of the common variable transformer with the reference cell positioned at the average countour center. Then, periodically during the day this value was rechecked. In a test with B-cells it was found that I_{sc} varied by 19 mA for each mV change in reference cell readings. The maximum observed variation in reference cell readings over 1 day's span has been 0.4 mV (upward drift). This is equivalent to 7.6 mA variation in I_{sc} or 0.6% for the B-cell.

The variation in intensity across a cell is undoubtably the weakest point in the measurement method. Small non-uniform cell changes could conceivably go undetected because of this variation. On the other hand overall reproducibility was quite good. As a check on this, one cell of each type was set aside as an "unofficial" reference cell. Before measuring cells of a given type the reference cell was always measured. Figure 3.3.7 shows the variation of the maximum power for the "unofficial" B-reference cell obtained over a three month period. This figure indicates that P_m measurements were reproducible to within $\pm$ 1% including all measurement errors, calculation errors, temperature variations, and light source changes.

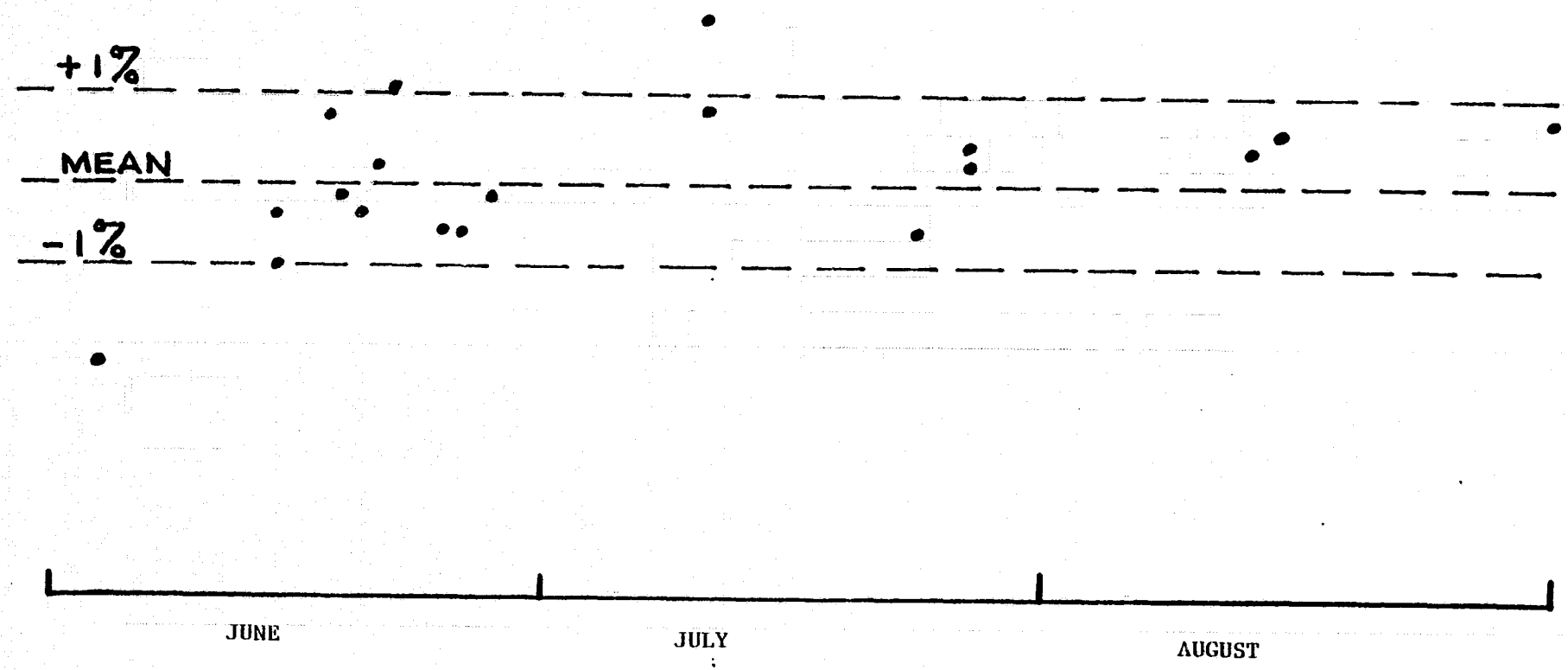

Figure 3.3.7. Variation of P_m For a B-Cell Over a Three Month Period.

4.0 TEST RESULTS AND DATA ANALYSIS

PAGE 62 INTENTIONALLY BLANK

4.1 Stress Test Population Characteristics

Cells to be stress tested were procured from four manufacturers, covering nearly the entire cell technology spectrum represented in the Jet Propulsion Laboratory Block II procurement. The cells were obtained in two procurements, occurring six months apart, except for the type E cells. The earlier quantity procurement was for 100 cells each of A, B, and C types to be used in Phase I, small quantity stress testing. The later procurement was for 400 cells of all four types to be used in Phase II, large quantity stress testing, plus 100 additional type E cells for Phase I testing. Table 4.1.1 gives quantities and date of receipt of the various cell shipments. Table 4.1.2 gives some of the physical characteristics of the four cell types. Considerable variability was observed in the incoming condition of the cells. That is, the cells from some manufacturers were at least superficially clean, while the cells from other manufacturers arrived with obvious surface contamination. The nature of the contamination ranged from fingerprints to what was apparently soldering flux residue. As discussed earlier the decision was made not to clean the cells. They were, however, handled in such a manner as to not increase the surface contamination already present, and they were stress tested with the incoming surface contamination present.

Prestress cell electrical data was analyzed for statistical bias using techniques described in Appendix A. Results of the analysis, and prestress data distributions, are contained in Appendix B.

PRECEDING PAGE BLANK NOT FILMED

66 INTENTIONALLY BLANK

Cell Type	Quantity Purchased	Date of Receipt at Clemson University
A	100 (Phase I)	December 1977
A	400 (Phase II)	May 1978
B	100 (Phase I)	December 1977
B	400 (Phase II)	May 1978
C	100 (Phase I)	December 1977
C	400 (Phase II)	May 1978
E	500 (Phase I & II)	July 1978

Table 4.1.1. Cell Purchase Lots and Date of Receipt at Clemson University.

Cell Type	Cell Dia. (inch)	Cell Thickness (mils)	Antireflective Coating	Primary Metalization	Cell Technology
A	4	24	No	Solder	P/N
B	3	19	Yes	Ti/Pd/Ag	N/P
C	2	20	Yes	Solder	N/P
E	3	15	No	Thick-Film Ag	N/P

Table 4.1.2. Physical Characteristics of Four Silicon Cell Types Subjected to Stress Testing.

4.2 Thermal Cycle and Thermal Shock Stress Testing.

4.2.1 Stress Test Conditions and Experiment Design

Thermal Shock and Thermal Cycle Stress tests were performed in order to determine the sensitivity of stress tested cells to rapid, thermally induced expansion and contraction. The two stress tests are very similar in nature, the only difference being the rate of change of temperature and thus the rate of change of thermally induced stress and strain. They are intended to bring out thermal mismatch problems (weaknesses) such as metal delamination, fracture or fatiguing, and silicon fracture caused by process-induced silicon defects or by metal-silicon thermal expansion mismatch. Establishment of a relationship between results observed in these highly accelerated stress tests, and cell behavior under long-term use conditions, is difficult. Derivation of such an acceleration factor must be deferred until more data from field usage is available, or until further experiments are performed using lower stress levels. However, the ability of these tests to establish relative technological weaknesses, such as the propensity for massively solder-coated cells to exhibit silicon fracture at tab attachment points, was clearly established during the course of the tests.

The Thermal Cycle stress test was modeled after Method 1010-1 of MIL-STD-883A (Appendix C). The equipment used was a Blue M Electric Company Model WSP-109B-3 Dual Thermal Shock Test Cabinet. This Shock Test Cabinet has two separate chambers, high temperature (air ambient) and low temperature (nitrogen ambient), with a movable work chamber which transfers the stress test samples between them at a programmable rate and holds the samples at high and low temperatures for predetermined (and adjustable) periods. The stress test units thus did not dwell at 25°C, as

they would have if two separate ovens with manual work transfer had been used, but instead cycled directly from high to low temperature. Note that in Method 1010.1 the maximum dwell time at 25°C is specified as 5 minutes; no minimum dwell time is specified.

During Phase I experiments, the cells were simply placed flat on a wire rack in the movable chamber. For the larger quantity Phase II tests, holding fixtures were fabricated which allowed the cells to stand on edge, without application of any mechanical force. The effect of these fixtures on the thermal response of the cells was quite negligible. Figure 4.2.1 shows the transient thermal response of a type A cell during several thermal cycles. Note that this cell type was the most massive of the four cell types stressed. The data shown in this figure was obtained by soldering a thermocouple directly into the collector metalization of the cell. From the information in this figure, it became clear that the thermal response of the cells was of the order of 1 minute, and that 10 minute dwell times at the high and low temperature extremes were sufficient for temperature equilibration. Details of the combinations of high and low temperatures used in the experiments and rationale for the sequences of temperature combinations used in the large scale testing are discussed in Section 4.2.2.

The Thermal Shock stress test was modeled after Method 1011.1 of MIL-STD-883A (Appendix D). For the specific test a slight modification of Condition C of Method 1011.1 was used. Thermal Shock stress differs from Thermal Cycle stress in that the unit to be stress tested is transferred from a hot liquid to a cold liquid, and then back to the hot liquid to complete one cycle. The resulting cell thermal transient can be seen in Figure 4.2.2, which shows both the high temperature-low temperature

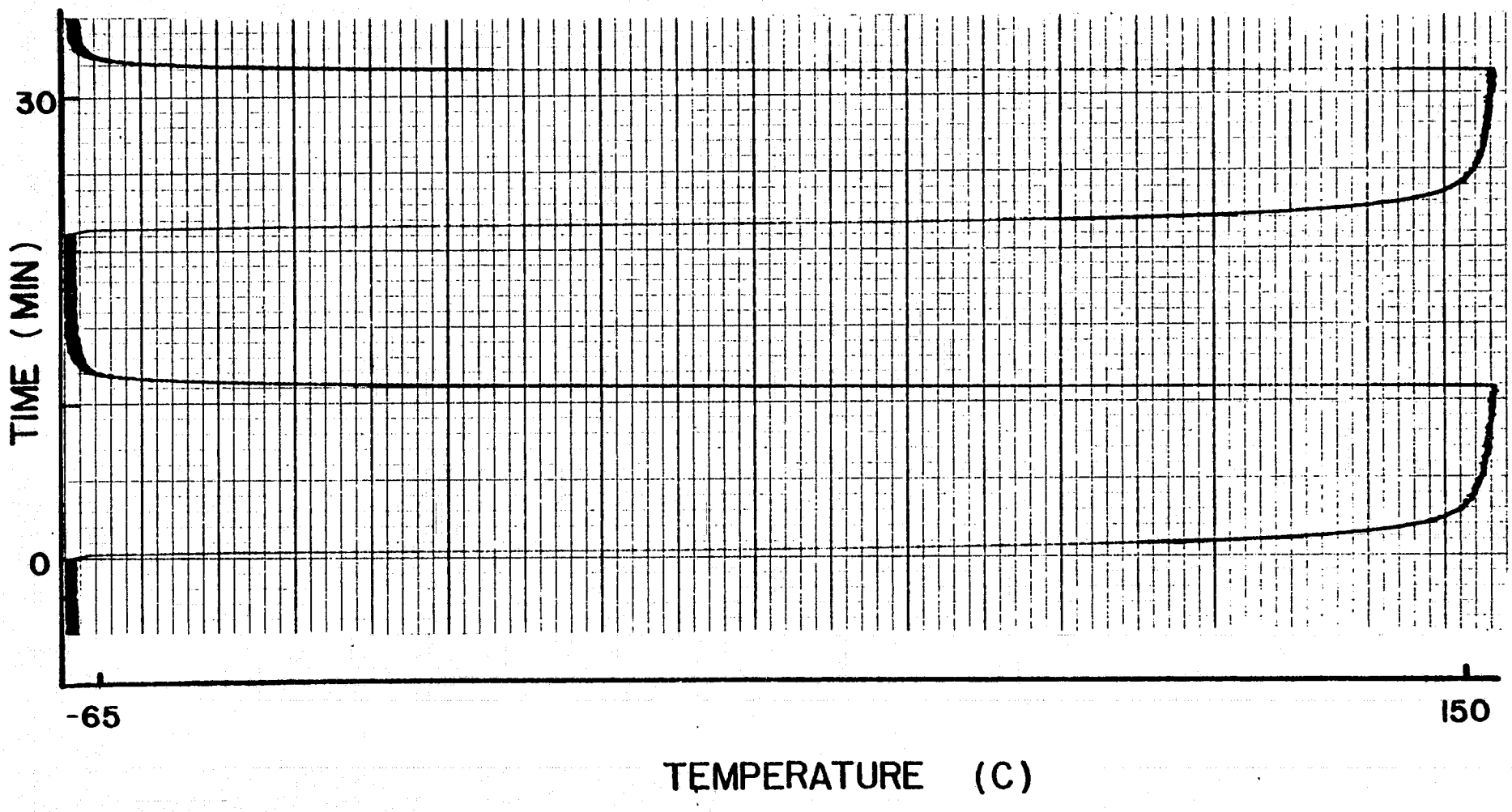

Figure 4.2.1. Temperature of Type A Cell During Thermal Cycle Stress.

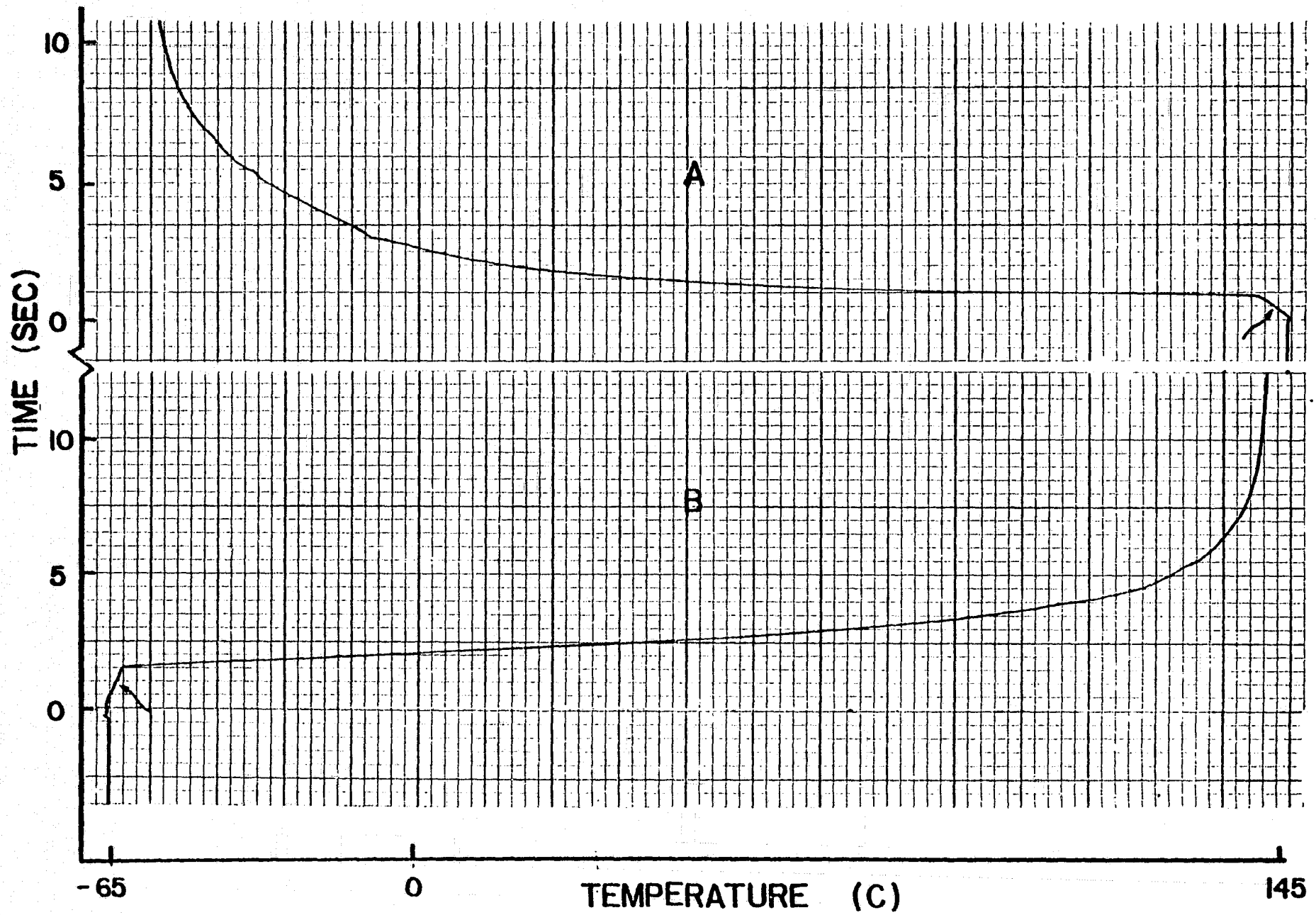

Figure 4.2.2. Temperature of Type A Cell During Thermal Shock Stress.

A: High Temperature-Low Temperature Transient. B: Low Temperature-High Temperature Transient.

transient (Figure 4.2.2A) and the low temperature-high temperature transient (Figure 4.2.2B) for a type A cell. Note that in both cases the thermal response of the cell was approximately 10 seconds.

For the actual thermal cycle stress tests a high and low temperature dwell time of five minutes was used. The high temperature was approximately 140°C, set by the boiling point of the FC 40 Fluorinert™ test fluid. The low temperature was approximately -65°C. FC77 Fluorinert™ test fluid was used for the low temperature bath, and the low temperature was achieved by partially submerging a stainless steel beaker (filled with FC77) in a dewar flask which was filled with a mixture of methanol and dry ice. This mixture has a stable phase at -78°C. Thermal transfer to the beaker resulted in the -65°C FC77 temperature. The physical transfer of cells from hot to cold and vice versa took less than 2 seconds. The heating and cooling of the cells during the transfer can be seen in Figure 4.2.2 as the linear rise and fall in temperature indicated by the arrows; from this the transfer time can be accurately determined.

During the Phase I experiments the cells were suspended by clips on the tabs during stress testing. Further experimentation showed that no apparent damage occurred by clipping directly to the cells with small alligator clips, and all large quantity thermal shock tests used this technique.

4.2.2 Thermal Cycle Stress Test Results

Initial experimentation and subsequent larger quantity stress testing showed that physical results of thermal cycle stress fell into three general categories:

Type X Breaks. Type X breaks involved conchoidal silicon fractures, under metalization generally at the tab attachment point. Some units of all four cell types exhibited this effect at some point in the thermal cycling schedule, including both Phase I experiments and Phase II stress testing. Examples of the most common types of type X break are shown in Figures 4.2.3 through 4.2.5. In some of these figures the overlying metal has been peeled back to exhibit the conchoidal fracture. Although the fractures shown in the last three figures were the most common Type X breaks observed, some conchoidal fractures occurred in other areas of the Type A cells. These other areas were under the collector metal, some distance away from the tab attachment area.

Type Y Breaks. Type Y breaks involved delamination of metal over unfractured silicon. In some cases the metal delamination occurred in conjunction with conchoidal silicon fractures. Two distinct types of type Y breaks were observed. One type involved delamination of front-side metal, both collectors and grids in some cases, and occurred only with type A cells. Figure 4.2.6 shows this delamination for a type A cell which had been subjected to 10 thermal cycles 0°C to +150°C to 0°C and 10 thermal cycles -25°C to +150°C to -25°C. The other type of Y break involved peeling of backside metal, and was observed only for type C cells. An example of this result is seen in Figure 4.2.7. The cell in this figure had been subjected to 10 thermal cycles 0°C to +150°C to 0°C, 10 thermal cycles -25°C to +150°C to -25°C, and 10 thermal cycles -45°C to +150°C to -45°C. The backside solder was manually peeled back to better demonstrate the effect in the photograph. A notable point in connection with this type of metal delamination was that during the act of manually peeling the metal, a gas was released from under the

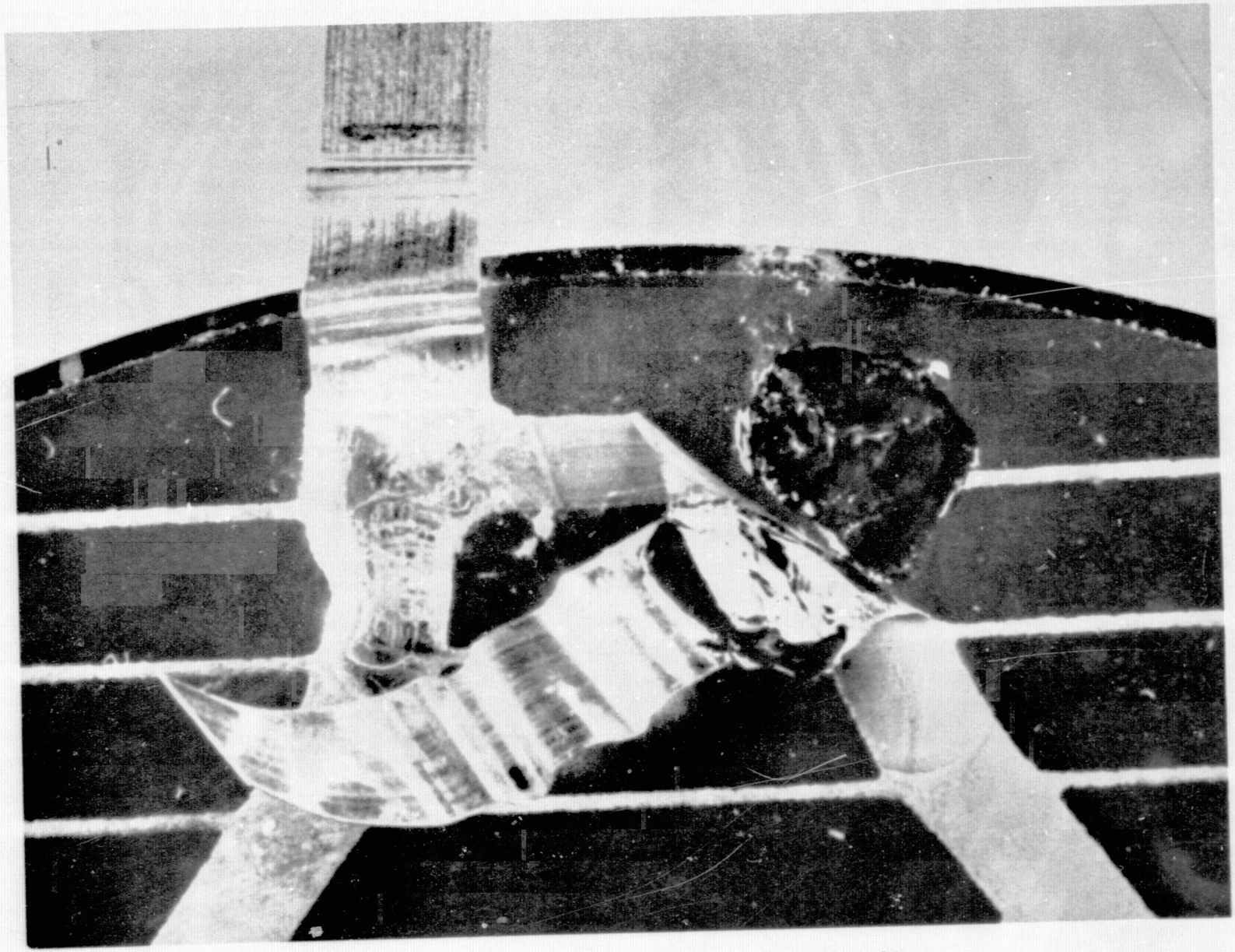

Figure 4.2.3. Type A Cell with Conchoidal Silicon Fracture at Tab Attachment Point.

REPRODUCIBILITY OF THE ORIGINAL PAGE IS POOR

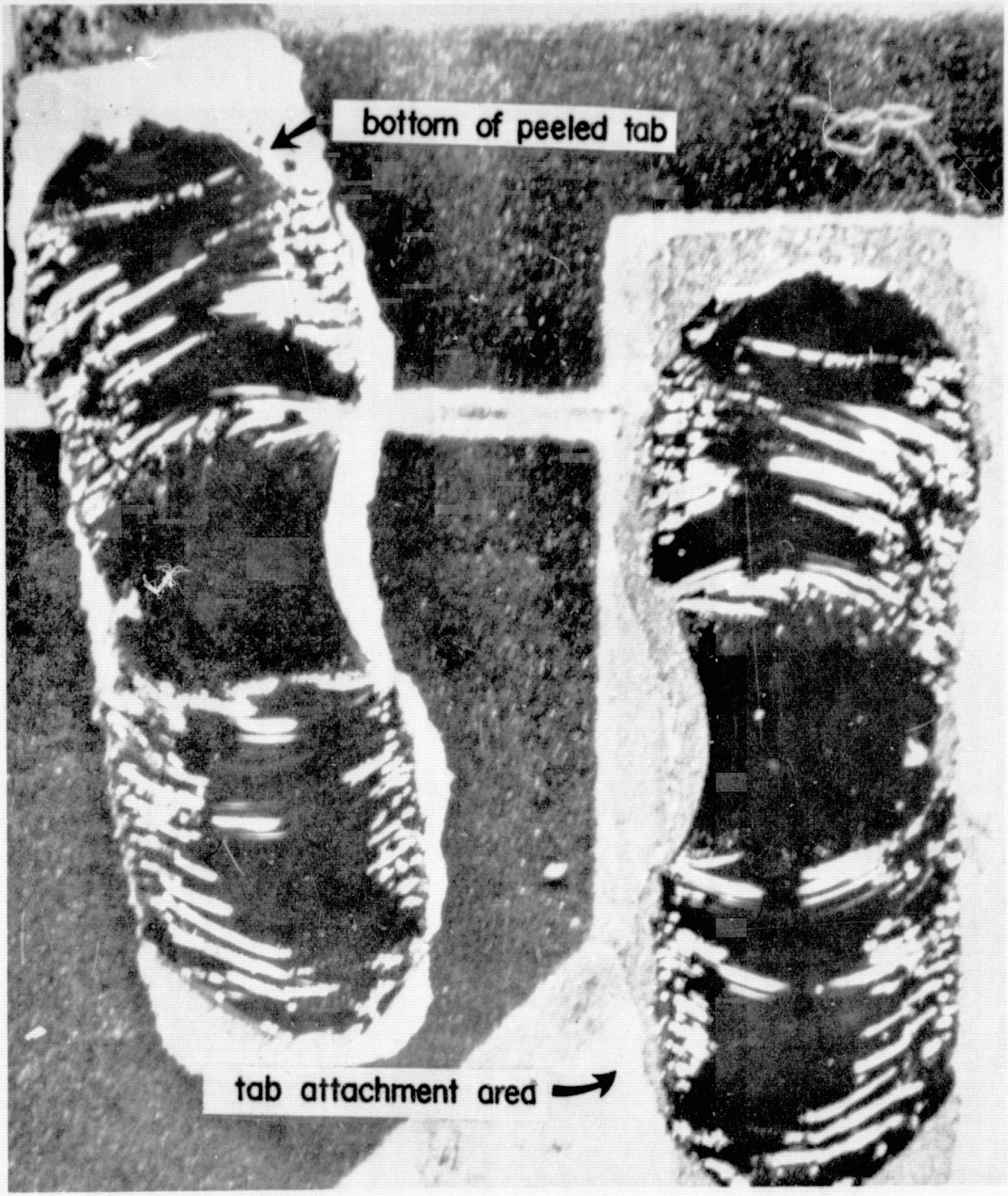

Figure 4.2.4. Type E Cell with Conchoidal Silicon Fracture at Tab Attachment Point.

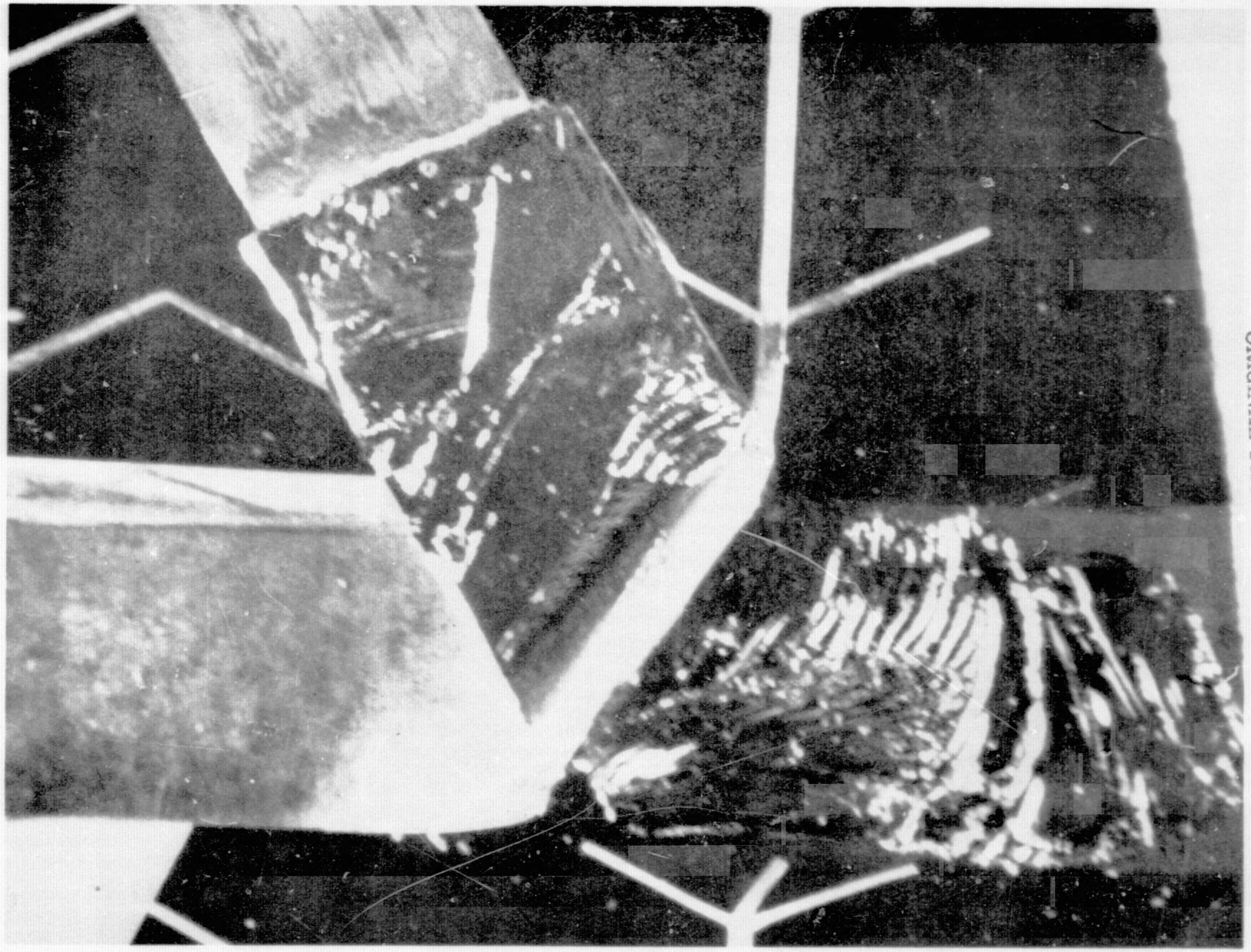

Figure 4.2.5. Type B cell with Conchoidal Silicon Fracture at Tab Attachment Point.

REPRODUCIBILITY OF THE
ORIGINAL PAGE IS POOR

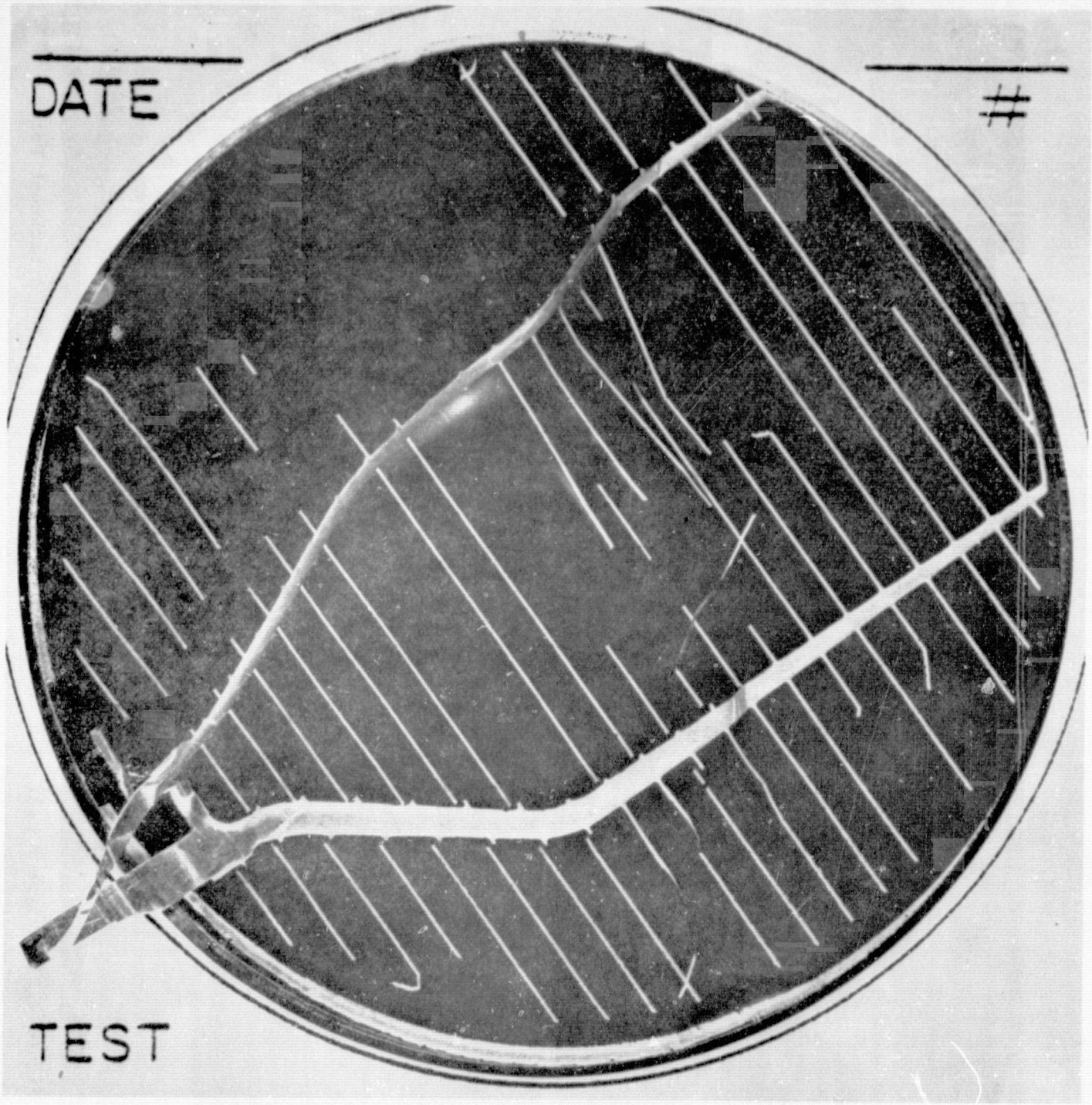

Figure 4.2.6. Type A Cell with Collector and Grid Delamination (Type Y Break).

REPRODUCIBILITY OF THE
ORIGINAL PAGE IS POOR

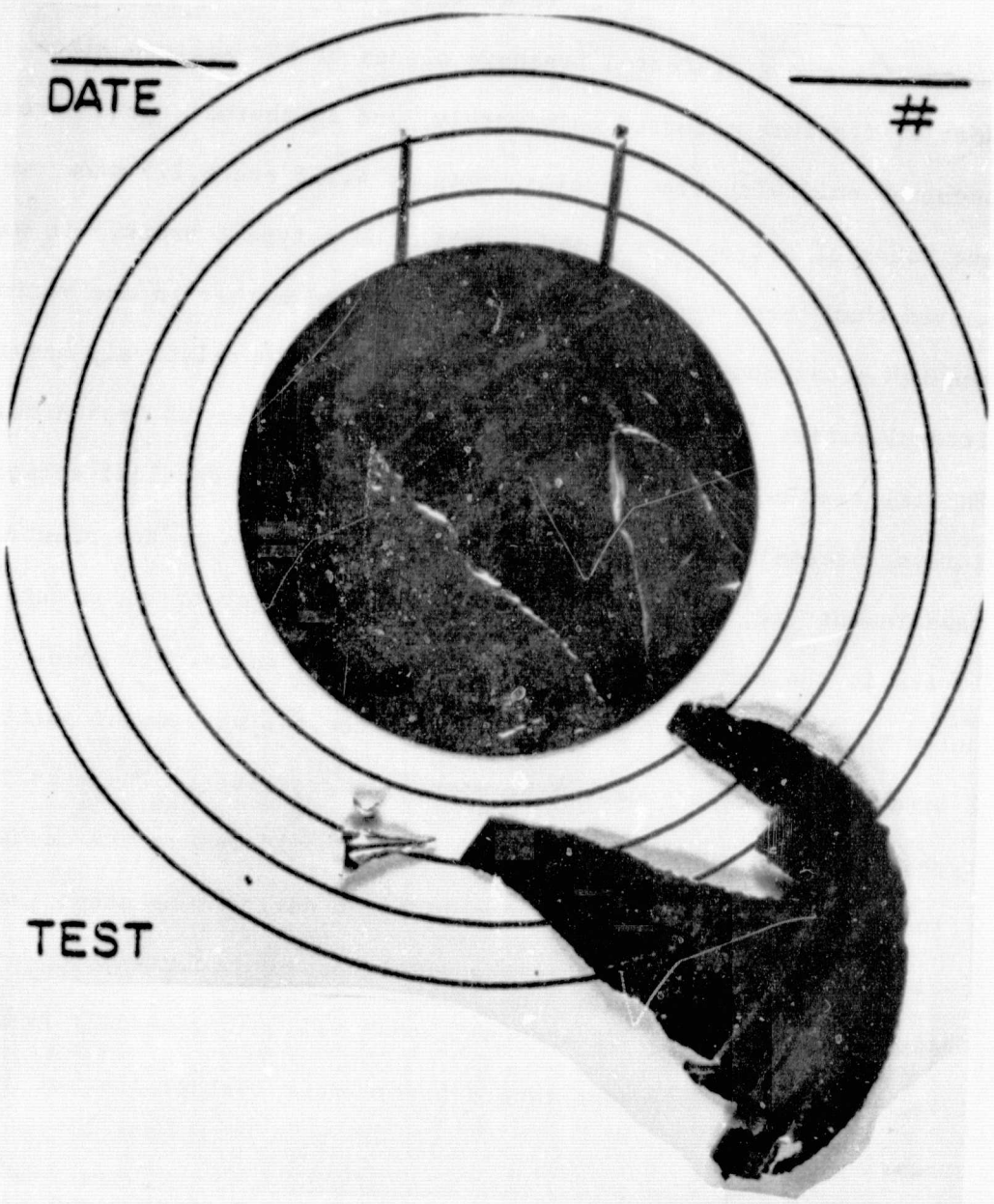

Figure 4.2.7. Type C Cell with Delamination of Back Metal (Type Y Break).

solder. The gas had an acetic acid-like smell, and was evident in all type C cells which showed delamination.

Type Z Breaks. Type Z breaks were relatively long silicon fractures, apparently along preferred breakage planes of the silicon slice. This sort of fracture occurred only rarely, and in thermal cycle stress testing occurred only with type A cells. Figure 4.2.8 and 4.2.9 show two different views of a type A cell which exhibited a type Z break. It was observed that these type breaks always occurred either in the vicinity of the tab attachment points or in association with relatively massive solder irregularities ("lumps") in the rear-surface solder of type A cells. Partial removal of any existing solder lumps by mechanical scraping before stress, necessitated by the planarity requirements of the electrical measurement jig, undoubtedly lowered the frequency of occurrence of type Z breaks in the subsequent thermal cycle stress tests. It should also be noted that to a degree type X breaks at the tab attachment point and type Z breaks are probably caused by competing processes. The occurrence of a type X break at the tab attachment point should reduce the mechanical stress level in the vicinity of this point during subsequent thermal cycles and thus should reduce the likelihood of occurrence of a type Z break. The occurrence of a type Z break will not generally reduce the likelihood of a subsequent type X break under further thermal cycle stressing.

Initial thermal cycle experimentation was performed according to Condition C of Method 1010.1, MIL-STD-883A, using Phase I cells. Physical results of these experiments are shown in Table 4.2.1. Curiosity about the influence of rear-surface solder-lumps (type A cells), changes in type A front-surface metalization geometry between Phase I and Phase II cell

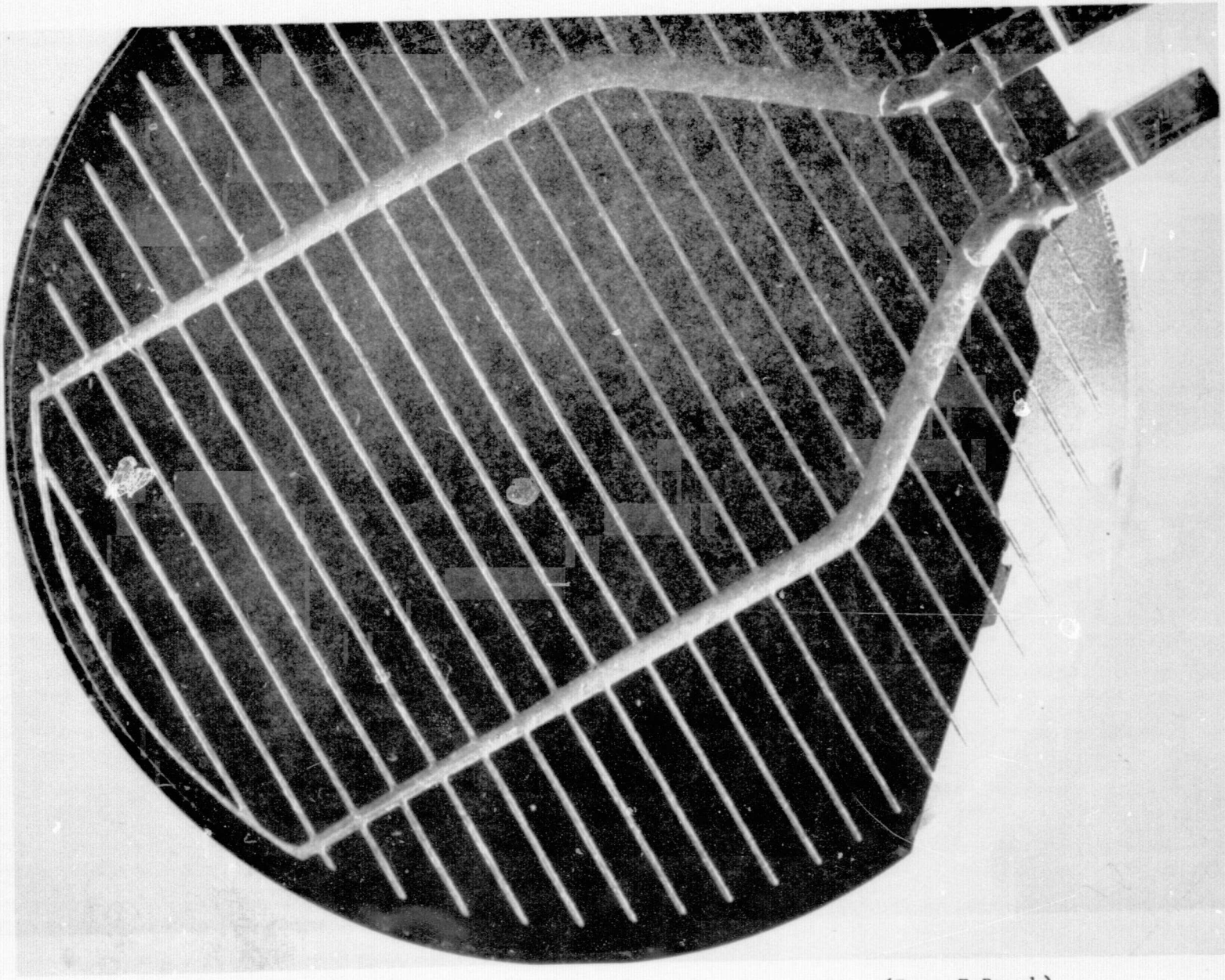

Figure 4.2.8. Type A Cell with Long Silicon Fracture (Type Z Break).

REPRODUCIBILITY OF THE
ORIGINAL PAGE IS POOR

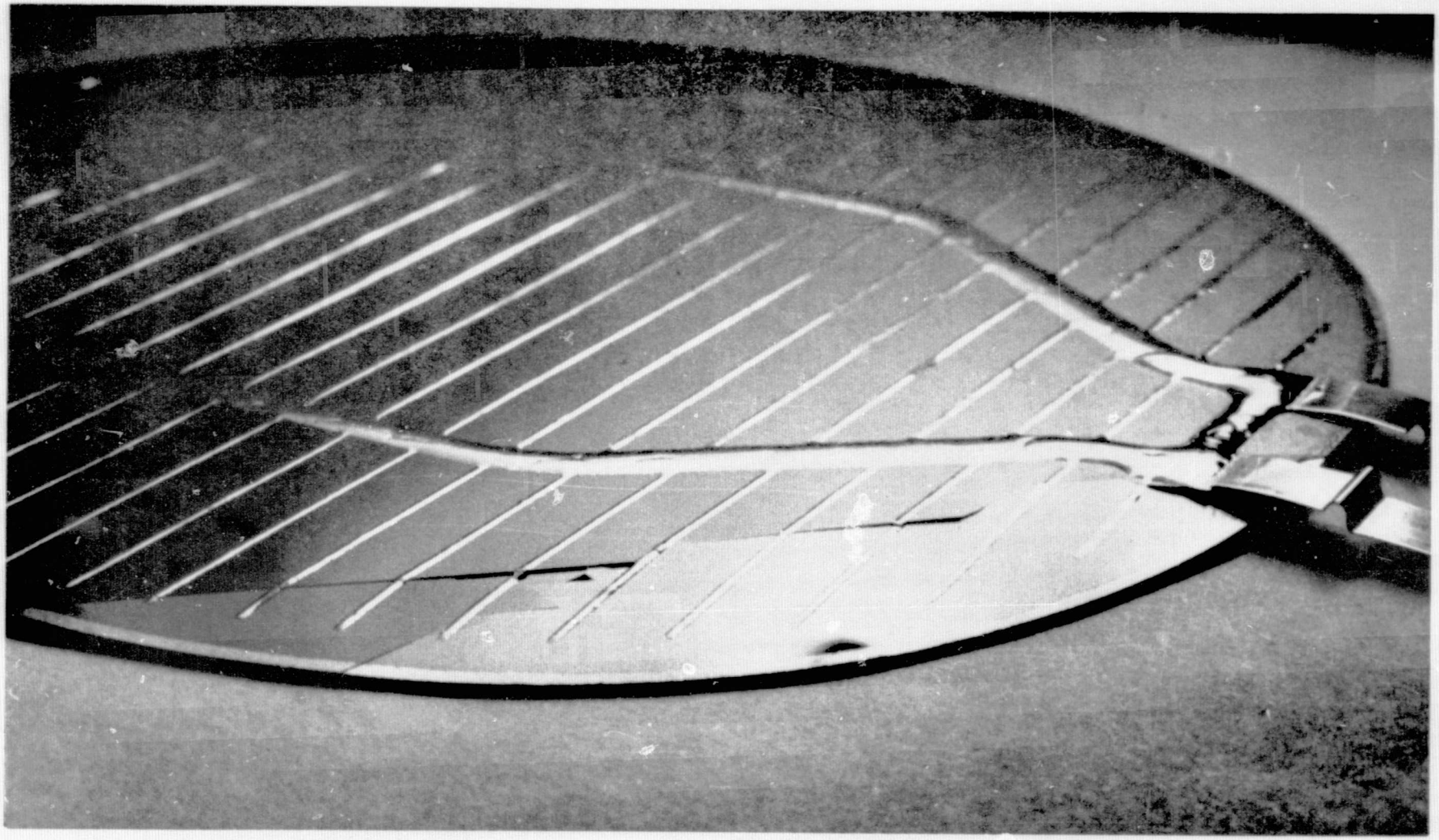

Figure 4.2.9. Type A Cell with Long Silicon Fracture (Type Z Break).

Cell Type	1 Cycle	5 Cycles	10 Cycles
A (3 cells)	No Effect	1 Type X Break 1 Type Y Break	1 Type X Break 2 Type Y Breaks
B (4 cells)	No Effect	No Effect	No Effect
C (4 cells)	No Effect	No Effect	2 Type X Breaks
E (4 cells)	No Effect	No Effect	No Effect

Table 4.2.1. Results of -65°C to 150°C Thermal Cycling, Phase I Experiments.

Cell Type	Upper Temperature/ Lower Temperature	Observation
A (4 cells, solder bumps)	+150°/-65°C	All Type Z Breaks After 1 Cycle
A (3 cells, no solder bumps)	+150°/-65°C	All Type X Breaks After 1 to 5 Cycles, All Type Z Breaks After 5 to 7 Cycles.
A (3 cells, solder bumps)	+150°C/-25°C	One Type Z Break After 5 Cycles; No Further Effect to 20 Cycles.
C (3 cells)	+150°C/-25°C	No Effect to 20 Cycles

Table 4.2.2. Results of Thermal Cycling Experiments, Phase II Cells.

populations, and the sensitivity of both type A and type C cells to reduced amplitude thermal cycling led to further experimentation. Physical results of this experimentation are shown in Table 4.2.2. Electrical results of all the Phase I experiments showed fairly small effects. However the cells were in a relatively aseptic environment during the thermal cycling and electrical measurement operations; the field environment of a module would be quite different and electrical effects of the various "breaks" may show up in real time. Also, the tab pull strength was clearly degraded for several of the cells.

In light of the results of the thermal cycling experiments, the step stress schedule shown in Table 4.2.3 was designed for use in the large-quantity stress testing. Summaries of the results of thermal cycle stressing using this schedule are given in Tables 4.2.4 through 4.2.7. Figures 4.2.10 through 4.2.13 show the behavior of the P_m distribution and the behavior of the lot mean P_m with increasing stress, for the four cell types. In these figures the P_m data was normalized to the prestress mean P_m, and the normalized P_m is shown as "Standardized P_m."

The electrical data shown in these tables and figures can be misleading because catastrophic failures were removed and not counted in the mean P_m calculation. This is especially true for the type A cells since by the final measurement down-time, half of the cells had been removed from the test population as catastrophic failures. These were cells which were so badly broken that obtaining meaningful electrical measurements was problematical if not impossible. Thus the apparent improvement in P_m between the last two measurement down-times for the type A cells was surely an artifact caused by removal of the two "worst" cells due to catastrophic failure.

Stress Level/ Down-Time No.	No. of Cycles	Test Population*	Electrical Measurement
0°C - + 150°C/(1)	10	12	yes
+			
-25°C - + 150°C/(2)	10	12	yes
+			
-45°C - + 150°C/(3)	10	12	no
+			
-65°C - + 150°C/(4)	10	12	yes
+			
-65°C - + 150°C/(5)	10	12	no
+			
-65°C - + 150°C/(6)	15	12	yes

*Test population does not count eight cells removed for contact integrity testing after three down-times.

Table 4.2.3. Thermal Cycle Stress Test Schedule.

TYPE A THERMAL CYCLE

Stress Level (Cumulative)	No. Cells Surviving	No. Cells Catastrophic cumulative	Mean Percent Decrease in P_m surviving cells ONLY
INITIAL	20	0	
10 cycles 0° to +150°	20	0	2.86
10 cycles 0° to +150° +10 cycles −25° to +150°	20*	0	6.55
10 cycles 0° to +150° +10 cycles −25° to +150° +10 cycles −45° to +150° +10 cycles −65° to +150°	8	4	10.53
10 cycles 0° to +150° +10 cycles −25° to +150° +10 cycles −45° to +150° +35 cycles −65° to +150°	6	6	4.00

*8 CELLS REMOVED FOR CONTACT INTEGRITY TESTING

Table 4.2.4. Summary of Results of Thermal Cycle Stressing, Type A Cells.

TYPE B THERMAL CYCLE

Stress Level (Cumulative)	No. Cells Surviving	No. Cells Catastrophic cumulative	Mean Percent Decrease in P_m surviving cells ONLY
INITIAL	20	0	
10 cycles 0° to +150°	20	0	-3.12
10 cycles 0° to +150° +10 cycles −25° to +150°	20*	0	-1.72
10 cycles 0° to +150° +10 cycles −25° to +150° +10 cycles −45° to +150° +10 cycles −65° to +150°	11	1	-1.59
10 cycles 0° to +150° +10 cycles −25° to +150° +10 cycles −45° to +150° +35 cycles −65° to +150°	11	1	-1.02

*8 CELLS REMOVED FOR CONTACT INTEGRITY TESTING

Table 4.2.5. Summary of Results of Thermal Cycle Stressing, Type B Cells.

TYPE C THERMAL CYCLE

Stress Level (Cumulative)	No. Cells Surviving	No. Cells Catastrophic cumulative	Mean Percent Decrease in P_m surviving cells ONLY
INITIAL	20	0	
10 cycles 0° to +150°	20	0	.50
10 cycles 0° to +150° +10 cycles −25° to +150°	20*	0	1.69
10 cycles 0° to +150° +10 cycles −25° to +150° +10 cycles −45° to +150° +10 cycles −65° to +150°	10	2	1.65
10 cycles 0° to +150° +10 cycles −25° to +150° +10 cycles −45° to +150° +35 cycles −65° to +150°	10	2	3.72

* 8 CELLS REMOVED FOR CONTACT INTEGRITY TESTING

Table 4.2.6. Summary of Results of Thermal Cycle Stressing, Type C Cells.

TYPE E THERMAL CYCLE

Stress Level (Cumulative)	No. Cells Surviving	No. Cells Catastrophic cumulative	Mean Percent Decrease in P_m surviving cells ONLY
INITIAL	20	0	
10 cycles 0° to +150°	20	0	-1.75
10 cycles 0° to +150° +10 cycles −25° to +150°	20*	0	- .64
10 cycles 0° to +150° +10 cycles −25° to +150° +10 cycles −45° to +150° +10 cycles −65° to +150°	9	3	2.85
10 cycles 0° to +150° +10 cycles −25° to +150° +10 cycles −45° to +150° +35 cycles −65° to +150°	0	12	

*8 CELL REMOVED FOR CONTACT INTEGRITY TESTING

Table 4.2.7. Summary of Results of Thermal Cycle Stressing, Type E Cells.

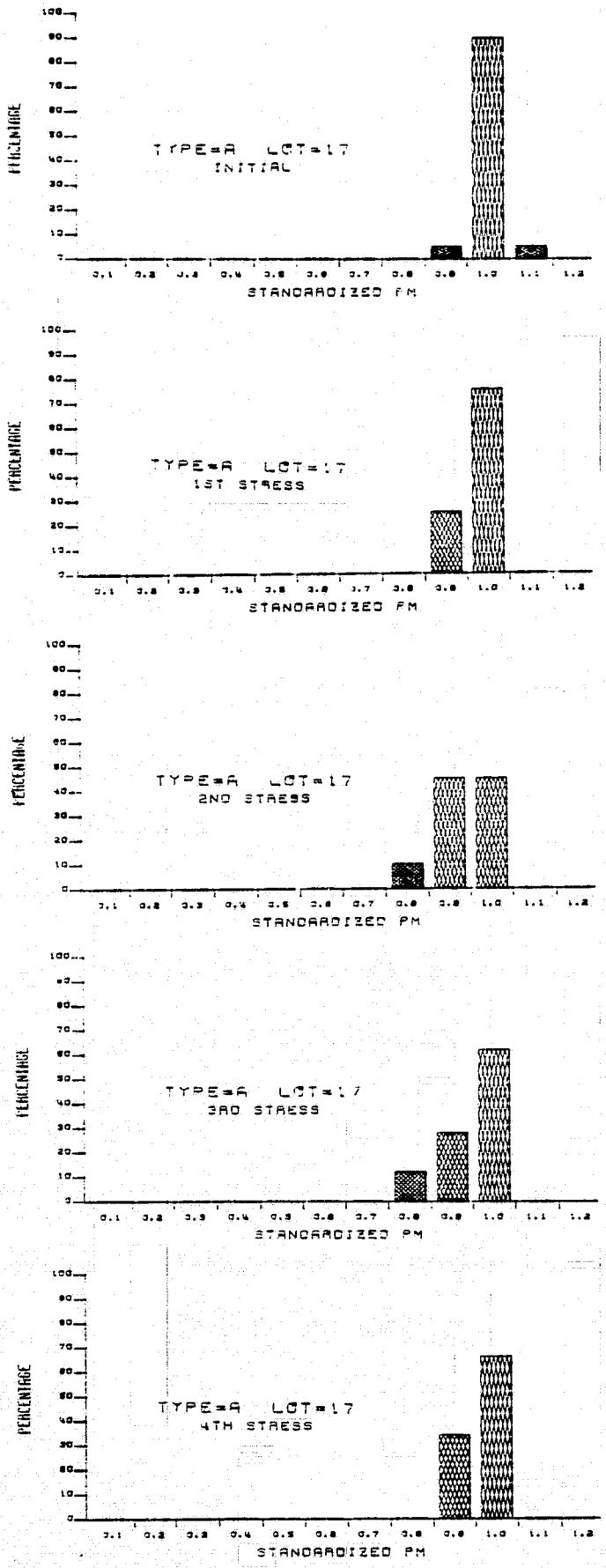

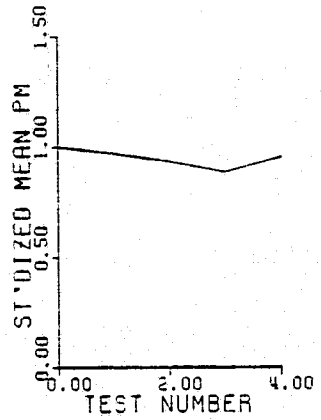

REPRODUCIBILITY OF THE
ORIGINAL PAGE IS POOR

CELL TYPE A	
STRESS THERMAL CYCLE	
MEASUREMENT DOWN-TIME (CUMULATIVE)	
INITIAL	0 cycles
1	10 cycles 0° to +150°
2	10 cycles 0° to +50° +10 cycles −25° to +150°
3	10 cycles 0° to +150° +10 cycles −25° to +150° +10 cycles −45° to +150° +10 cycles −65° to +150°
4	10 cycles 0° to +150° +10 cycles −25° to +150° +10 cycles −45° to +150° +35 cycles −65° to +150°

Figure 4.2.10. Behavior of P_m Distribution and Lot Mean P_m with Thermal Cycle Stress Type A Cells.

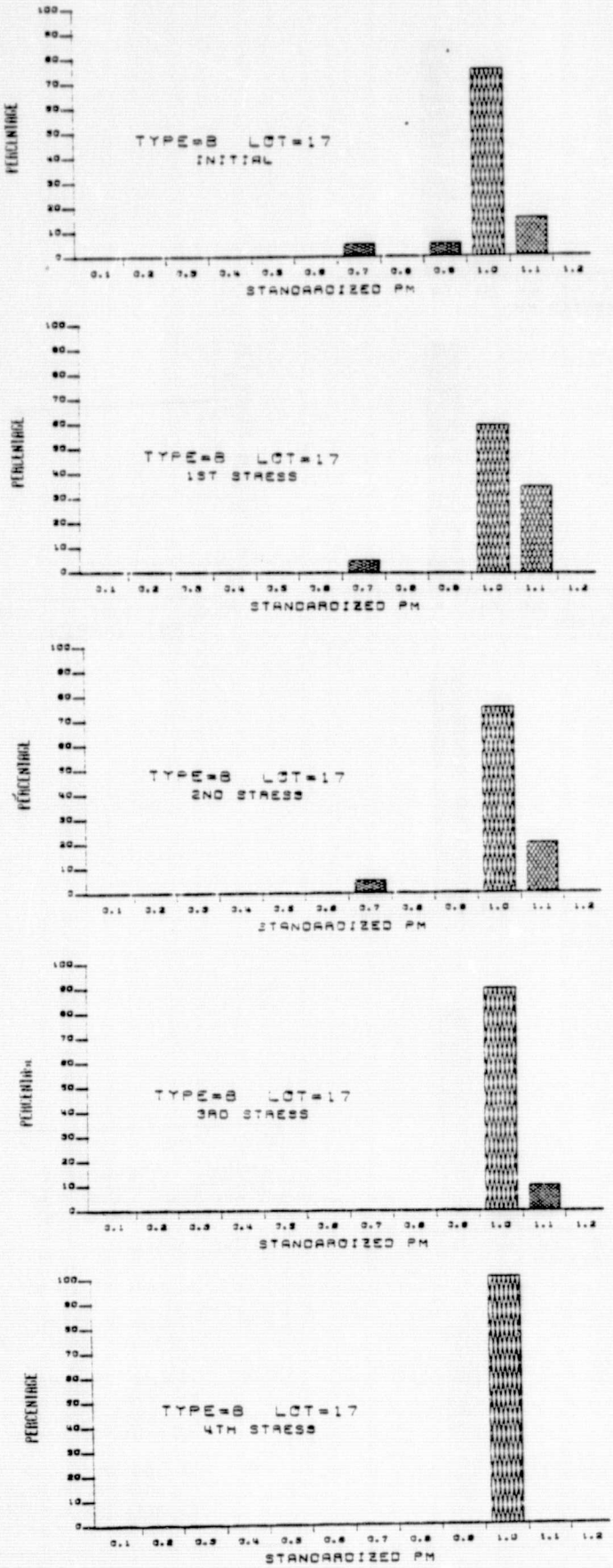

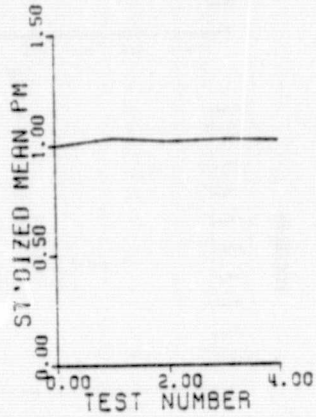

REPRODUCIBILITY OF THE
ORIGINAL PAGE IS POOR

CELL TYPE	B
STRESS	THERMAL CYCLE
MEASUREMENT DOWN-TIME (CUMULATIVE)	
INITIAL	0 cycles
1	10 cycles 0° to +150°
2	10 cycles 0° to +50° +10 cycles −25° to +150°
3	10 cycles 0° to +150° +10 cycles −25° to +150° +10 cycles −45° to +150° +10 cycles −65° to +150°
4	10 cycles 0° to +150° +10 cycles −25° to +150° +10 cycles −45° to +150° +35 cycles −65° to +150°

Figure 4.2.11. Behavior of P_m Distribution and Lot Mean P_m with Thermal Cycle Stress, Type B Cells.

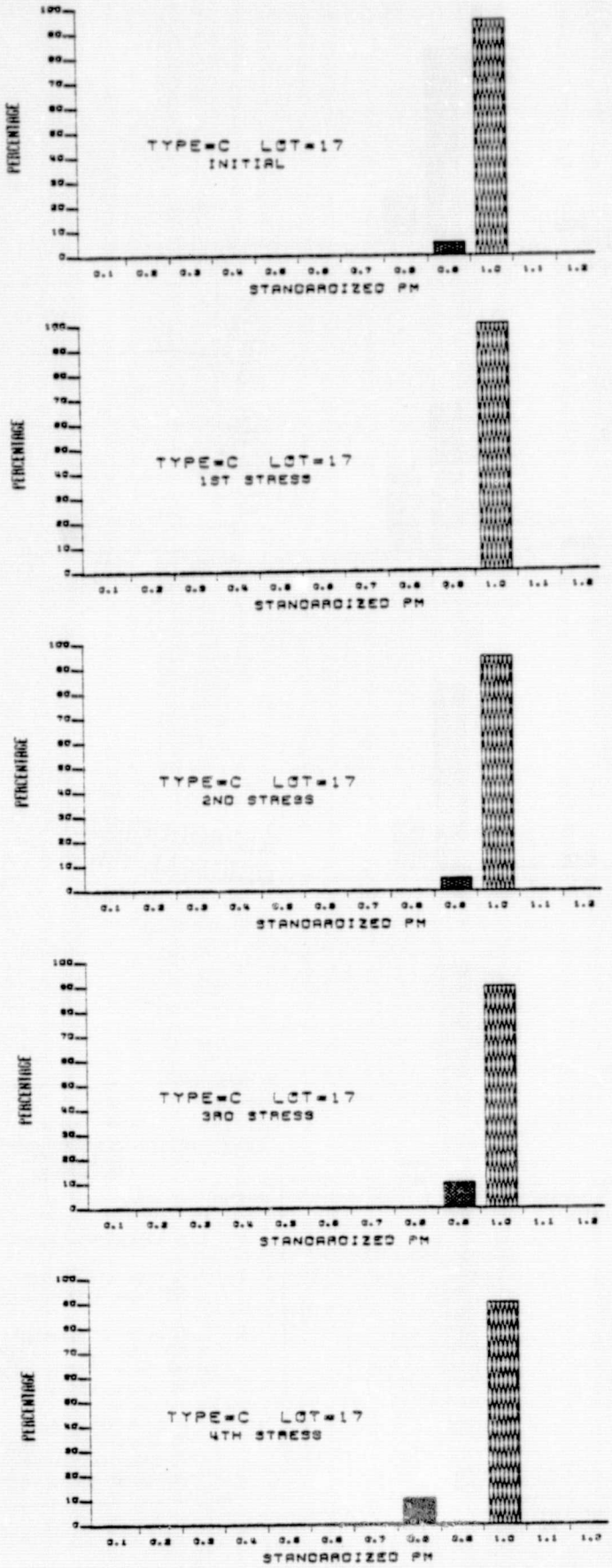

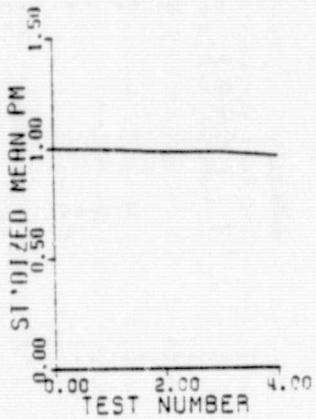

CELL TYPE	C
STRESS	THERMAL CYCLE
MEASUREMENT DOWN-TIME (CUMULATIVE)	
INITIAL	0 cycles
1	10 cycles 0° to +150°
2	10 cycles 0° to +150° +10 cycles −25° to +150°
3	10 cycles 0° to +150° +10 cycles −25° to +150° +10 cycles −45° to +150° +10 cycles −65° to +150°
4	10 cycles 0° to +150° +10 cycles −25° to +150° +10 cycles −45° to +150° +35 cycles −65° to +150°

Figure 4.2.12. Behavior of P_m Distribution and Lot Mean P_m with Thermal Cycle Stress, Type C Cells.

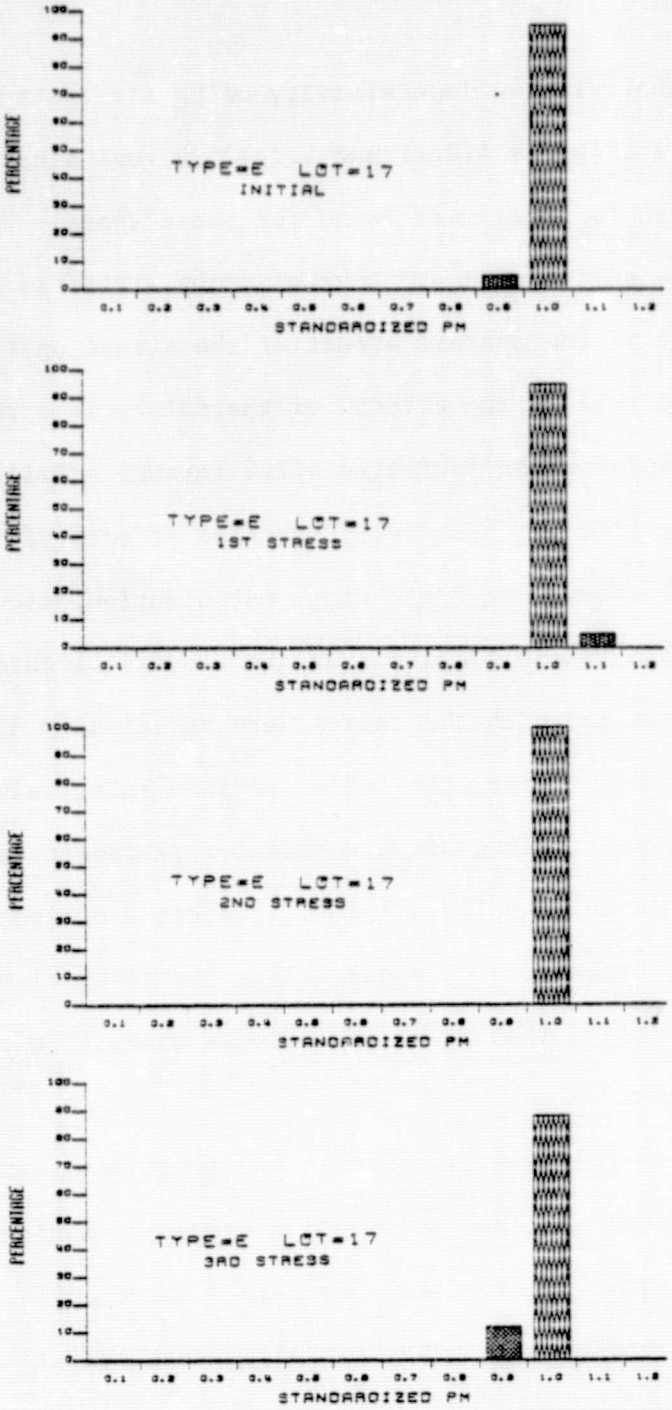

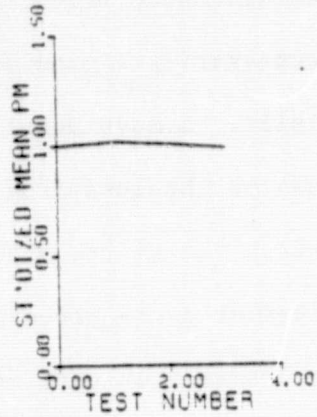

REPRODUCIBILITY OF THE ORIGINAL PAGE IS POOR.

CELL TYPE	E
STRESS	THERMAL CYCLE
MEASUREMENT DOWN-TIME (CUMULATIVE)	
INITIAL	0 cycles
1	10 cycles 0° to +150°
2	10 cycles 0° to +150° +10 cycles −25° to +150°
3	10 cycles 0° to +150° +10 cycles −25° to +150° +10 cycles −45° to +150° +10 cycles −65° to +150°
4	10 cycles 0° to +150° +10 cycles −25° to +150° +10 cycles −45° to +150° +35 cycles −65° to +150°

Figure 4.2.13. Behavior of P_m Distribution and Lot Mean P_m with Thermal Cycle Stress, Type E Cells.

On the other hand, the relative insensitivity of P_m for the type B and C cells demonstrated in Figures 4.2.11 and 4.2.12 is real since essentially no catastrophic failures were found for these types. However, as discussed below, insensitivity of P_m to thermal cycle stress is not necessarily a good measure of the overall effect of the stress on the cells. A more detailed picture of the effects of thermal cycle stressing can be obtained from the information in Tables 4.2.8 through 4.2.11. In these tables are shown the visually observable physical effects of the thermal cycle stress. They show that fracturing, delamination, etc., occurred much earlier in the stress testing than the electrical data would indicate. The Type X breaks shown in the tables were essentially all located under the tabs. As discussed earlier, the cells are in a relatively aseptic environment during the thermal cycling and electrical measurement operations; the field environment of a module would be quite different and electrical effects of the fracture may show up much sooner. Thus the physical effects observed are probably more significant than the effects shown by measurement of the electrical parameters.

From the information in Tables 4.2.4 through 4.2.11 it is clear that the tab attachment area is a likely failure point under thermo-mechanical stress for all but type C cells. This is true even for type B and E cells, which had very small amounts of solder used in the tab attachment operation. Strangely, the worst-performing cell under thermal cycle stress was the heavily solder-metalized type A cell, and the best performing cell was the heavily solder-metalized type C cell. Without details of the substrate silicon characteristics and the lead attachment process it is not possible to determine the source of this performance difference, although several possibilities exist. The subject of tab related, thermal cycle-induced type X

Down-Time No.	Cells in Test*	Cells Exhibiting Type X Breaks (cumulative)	Cells Exhibiting Type Y Breaks (cumulative)	Cells Exhibiting Type Z Breaks (cumulative)
1	12	0	0	0
2	11(one accidental breakage)	5	0	0
3	11	9	5	0
4	11	10	5	1
5	8	10	9	1
6	8	10	10	2

*Cells eventually removed for contact integrity testing not counted in totals.

Table 4.2.8. Physical Effects Observed During Thermal Cycle Stress Testing, Type A Cells.

Down-Time No.	Cells in Test*	Cells Exhibiting Type X Breaks (cumulative)
1	12	0
2	11(one accidental breakage)	2
3	11	6
4	11	6
5	11	6
6	11	6

*Cells eventually removed for contact integrity testing not counted in totals.

Table 4.2.9. Physical Effects Observed During Thermal Cycle Stress Testing, Type B Cells.

Down-Time No.	Cells in Test*	Cells Exhibiting Type Y Breaks (cumulative)
1	12	0
2	12	0
3	12	4
4	12	6
5	12	7
6	12	7

*Cells eventually removed for contact integrity testing not counted in totals.

Table 4.2.10. Physical Effects Observed During Thermal Cycle Stress Testing, Type C Cells.

Down-Time No.	Cells in Test*	Cells Exhibiting Type X Breaks (cumulative)
1	12	0
2	12	0
3	12	2
4	12	11
5	12	12
6	12	12

*Cells eventually removed for contact integrity testing not counted in totals.

Table 4.2.11. Physical Effects Observed During Thermal Cycle Stress Testing, Type E Cells.

breaks certainly deserves further investigation since some of the observed fractures occurred strangely early, under stress conditions which would be considered benign for other semiconductor devices.

4.2.3 Thermal Shock Stress Test Results

Initial thermal shock experimentation was performed according to Condition C of Method 1011.1, MIL-STD-883A, using Phase I cells. Physical effects observed in the experiments were similar to the results found in thermal cycle experiments. For the large-scale thermal shock stress testing it was decided to use the stress test schedule shown in Table 4.2.12, which is based on Condition C of Method 1011.1. Physical results of thermal shock stress testing are shown below in Tables 4.2.13 through 4.2.16. Parameter distribution and lot mean P_m behavior is shown in Figure 4.2.14 through 4.2.17 for the various down-times in the thermal shock stress testing. As discussed for the thermal cycle results, the electrical data shown in these figures must be considered in the light of the relatively clean stress test and electrical measurement environment. Although only very minor electrical effects are manifested in the above figures, it is clear that the cells themselves were damaged during stressing. In many individual cases only the metal itself held tabs on, or held parts of cells together, after cells were subjected to thermal shock.

The physical and electrical results of thermal shock stress testing generally agreed with results from thermal cycle stress testing. For example, the type A cells performed worst and the type C cells performed best under thermal shock stress. Also, delamination of back-side metal of type C cells was accompanied by the same acetic acid-like smell noticed

Stress Level	No. of Cycles (cumulative)	Test Population*	Electrical Measurement
-65°C - + 150°C	5	8	yes
-65°C - + 150°C	15	8	yes
-65°C - + 150°C	35	8	yes

*Test population does not show seven cells removed for contact integrity testing after one down-time.

Table 4.2.12. Thermal Shock Stress Test Schedule.

No. of Shock Cycles (cumulative)	No. of Cells in Test	No. of Type X Breaks (cumulative)	No. of Type Y Breaks (cumulative)	No. of Type Z Breaks (cumulative)
8	8	8	0	5
15	8	8	1	6
35	8	8	3	8

Table 4.2.13. Thermal Shock Response of Type A Cells.

No. of Shock Cycles (cumulative)	No. of Cells in Test	No. of Type X Breaks (cumulative)	No. of Type Y Breaks (cumulative)	No. of Type Z Breaks (cumulative)
5	8	2	0	0
15	8	2	1	0
35	8	2	4	1(18 cycles)

Table 4.2.14. Thermal Shock Response of Type B Cells.

No. of Shock Cycles (cumulative)	No. of Cells in Test	No. of Type X Breaks (cumulative)	No. of Type Y Breaks (cumulative)	No. of Type Z Breaks (cumulative)
5	8	0	0	0
15	8	0	1	0
35	8	0	1	0

Table 4.2.15. Thermal Shock Response of Type C Cells.

No. of Shock Cycles (cumulative)	No. of Cells in Test	No. of Type X Breaks (cumulative)	No. of Type Y Breaks (cumulative)	No. of Type Z Breaks (cumulative)
5	8	1	0	0
15	8	1	0	0
35	8	4	0	1(17 cycles)

Table 4.2.16. Thermal Shock Response of Type E Cells.

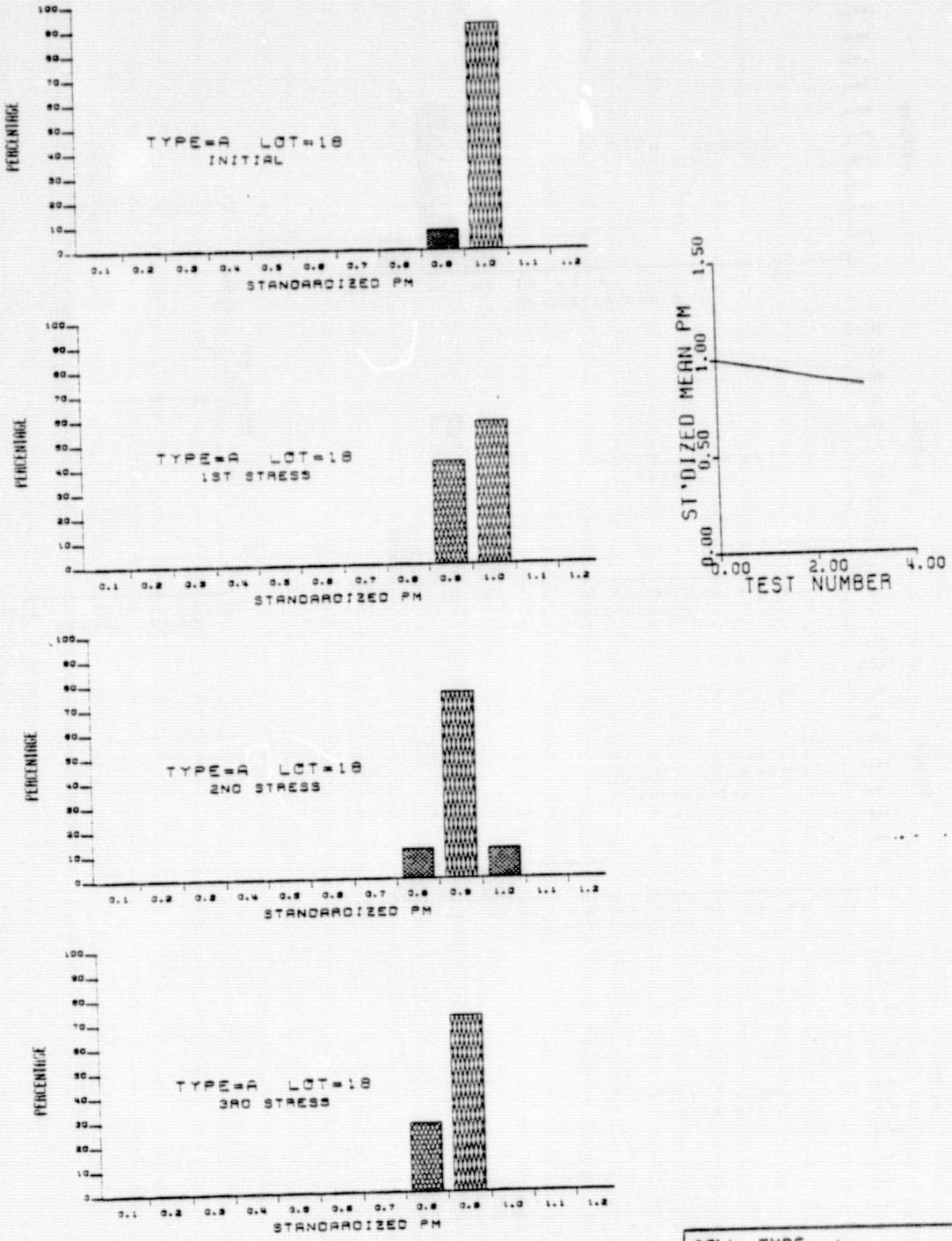

CELL TYPE	A	
STRESS	THERMAL SHOCK	
MEASUREMENT	DOWN-TIME (CUMULATIVE)	
INITIAL	0	
1	5	SHOCKS
2	15	SHOCKS
3	35	SHOCKS

Figure 4.2.14. Behavior of P_m Distribution and Lot Mean P_m with Thermal Shock Stress, Type A Cells.

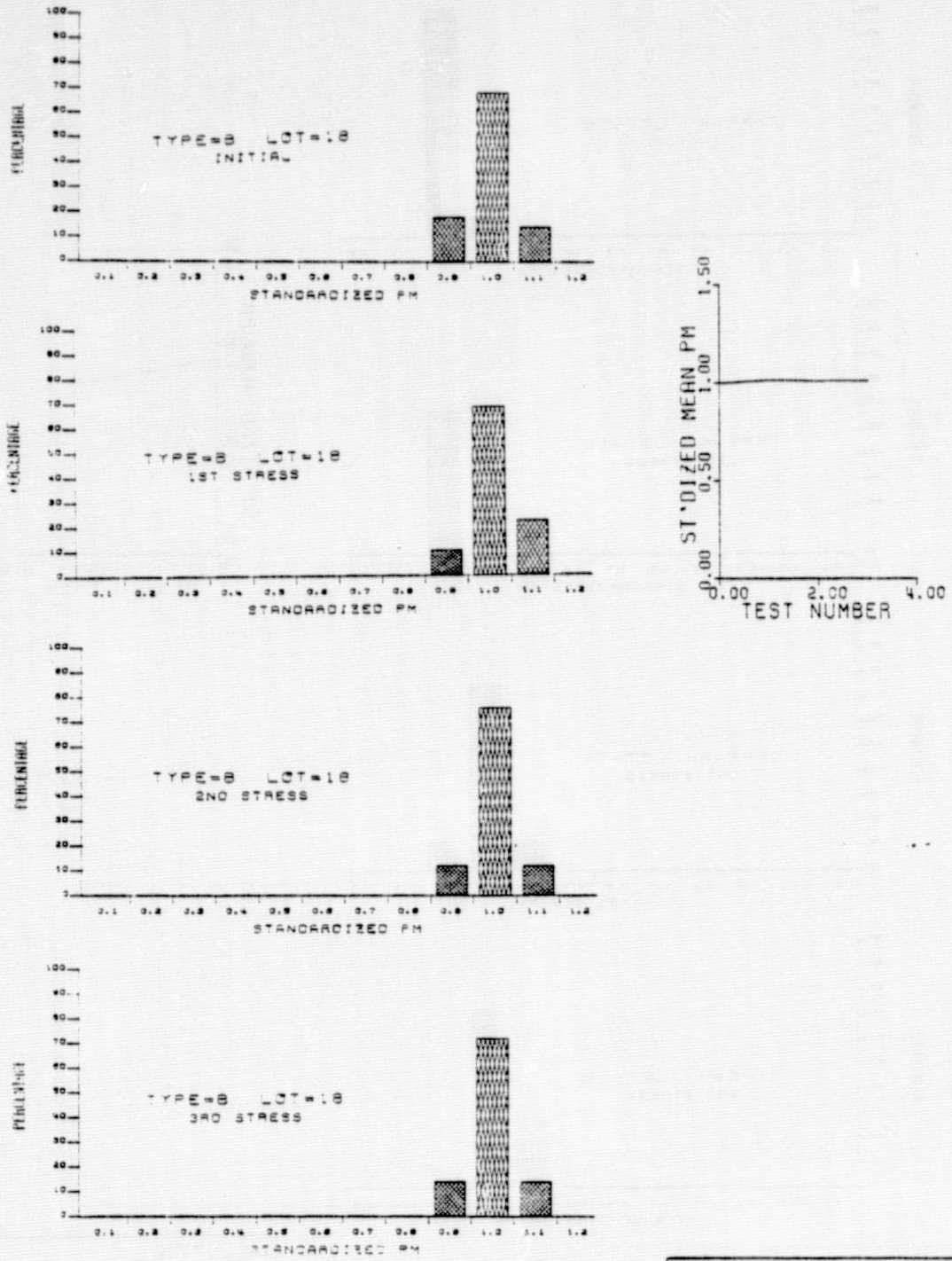

CELL TYPE	B	
STRESS	THERMAL SHOCK	
MEASUREMENT	DOWN-TIME (CUMULATIVE)	
INITIAL	0	
1	5	SHOCKS
2	15	SHOCKS
3	35	SHOCKS

Figure 4.2.15. Behavior of P_m Distribution and Lot Mean P_m with Thermal Shock Stress, Type B Cells.

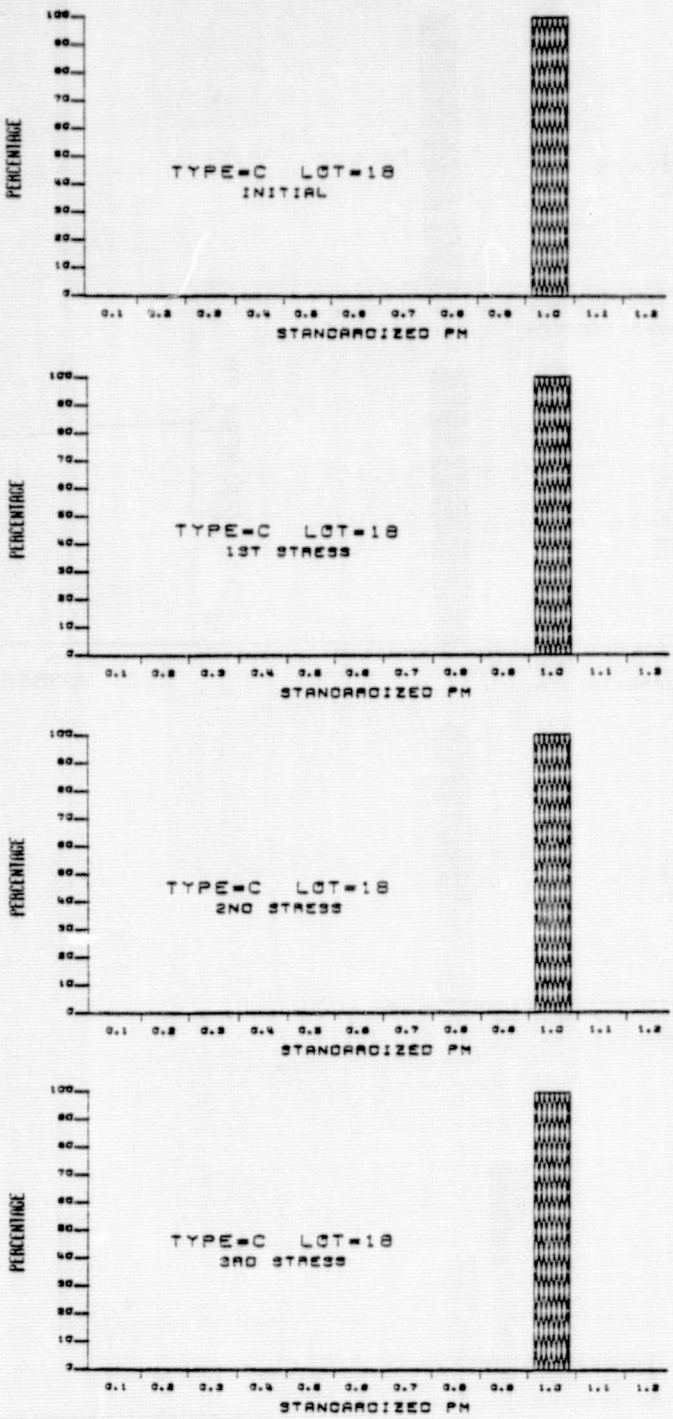

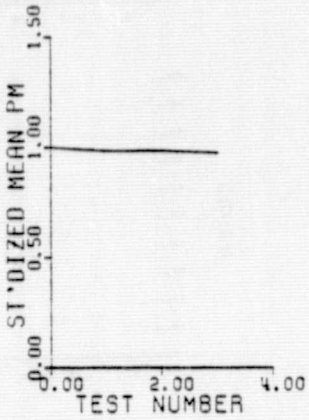

CELL TYPE	C	
STRESS	THERMAL SHOCK	
MEASUREMENT	DOWN-TIME (CUMULATIVE)	
INITIAL	0	
1	5	SHOCKS
2	15	SHOCKS
3	35	SHOCKS

Figure 4.2.16. Behavior of P_m Distribution and Lot Mean P_m with Thermal Shock Stress, Type C Cells.

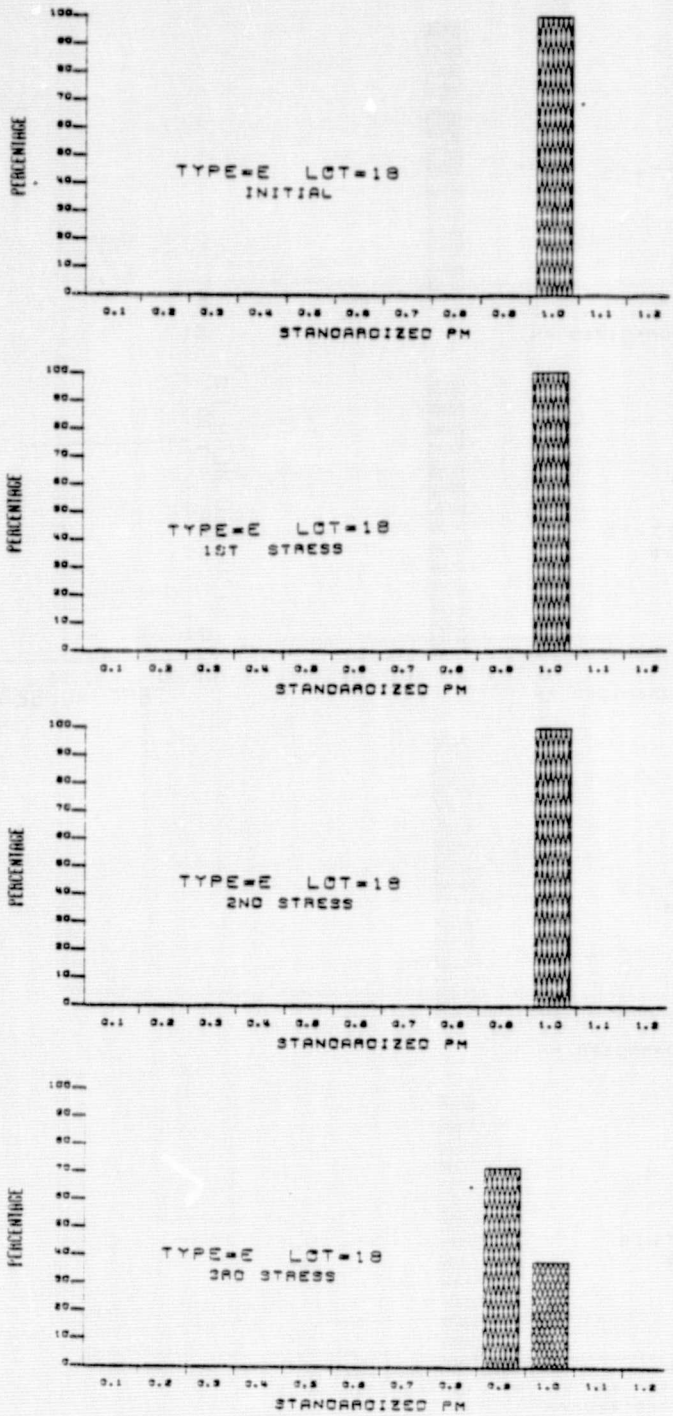

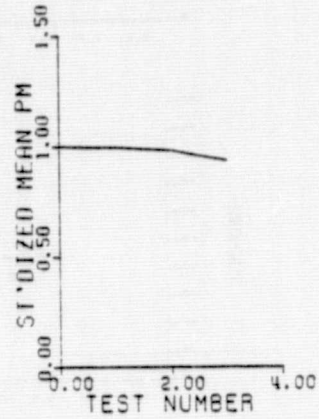

CELL TYPE	E	
STRESS	THERMAL SHOCK	
MEASUREMENT	DOWN-TIME (CUMULATIVE)	
INITIAL	0	
1	5	SHOCKS
2	15	SHOCKS
3	35	SHOCKS

Figure 4.2.17. Behavior of P_m Distribution and Lot Mean P_m with Thermal Shock Stress, Type E Cells.

during thermal cycle stress testing. Interestingly, fewer conchoidal fractures under tabs were observed under thermal shock than under thermal cycle, for all but the type A cells. Why this would be so is not clear since the thermal shock stress testing is a more rigorous regimen than the thermal cycle stress, at least as conducted in this research. The previously noted relative insensitivity, in the laboratory environment, of cell electrical parameters to gross physical damage was also found to hold for thermal shock stress.

4.3 Bias Temperature Stress Testing

PRECEDING PAGE BLANK NOT FILMED

4.3.1 Stress Test Conditions and Experiment Design

Bias-Temperature stress testing was performed in order to determine the sensitivity of solar cells to degradation which is accelerated by current flow, or high temperature, or both. Degradation mechanisms which could be accelerated by these factors include junction penetration by metalization, electromigration, segregation effects or voiding in the metalization system which in turn could lead to high series resistance or poor metal or tab adherence, and other metal-related phenomena. Considering the spectrum of mechanisms that could be accelerated by the stress conditions, this stress test was considered a key test which, if done right and if the laws of physics permit, would allow a use-condition degradation rate to be obtained by extrapolation. This degradation rate ("failure" rate) would of course be that due only to current and temperature and the additional degradation due to any other use-condition stress would be additive. A standard test which is similar in intent and implementation is "Steady State Life," Method 1005.1, MIL-STD-883A.

In order to properly conduct the stress test(s) three conditions had to be determined: test temperature, the amount of current flow and its direction (forward or reverse), and the number of units to be used in the test(s). A fourth condition, the number of hours of test duration, is not independent of the number of units on test, and to some extent a direct tradeoff of test duration and test population size can be done. Of course, the final choice of all of the conditions was heavily weighted by practical considerations. For example, the maximum stress test temperature was determined by the melting temperature of the solder which was used to attach tabs to the cells. The solder melting temperature was found to be in the range 171° to 175°C for all four cell types.

110 INTENTIONALLY BLANK

Considering heating due to applied bias, and possible test chamber temperature variations, the upper temperature limit for stress testing was chosen to be 165°C. The lower limit for the stress testing was chosen keeping in mind the possible upper temperature limit in normal operation, which could be somewhat in excess of 50°C. It was decided that a stress test temperature of 75°C was sufficiently close to 50°C to insure that anomalous degradation mechanisms would not be activated, but high enough that some useful acceleration of degradation mechanisms would occur. Thus, for example, mechanisms which proceed according to an Arrhenius relationship with an activation energy of 1 eV would be accelerated at 75°C by a factor of 12 relative to their rate of 50°C, and by a factor of 144 relative to their rate of 27°C. Knowing the upper and lower temperature limits, it remained to decide how many temperatures should be used, i.e., how many separate, parallel bias-temperature stress tests should be conducted at what temperatures. It was decided to perform one stress test at 75°C primarily as a control test. Since 75°C was so close to use conditions little degradation was expected in the amount of time available for testing (significantly less than one year), but as a matter of good engineering practice this test temperature was included. A stress test at 165°C was included because degradation should occur most rapidly at the highest feasible temperature. It was decided to perform two other stress tests, at 150°C and 135°C. These temperatures are also high enough to give considerable acceleration to most possible degradation mechanisms. Taken with the 165°C test, results from these high temperature tests should define three points in the degradation rate-inverse temperature quadrant; ideally, degradation rate at room temperature could be obtained by extrapolation from these points even if no significant data were

obtained from the 75°C stress test. Practically, four bias-temperature stress tests were the maximum which could be performed under the existing limits of time and money.

The amount of current flow, and the direction, were determined by compromise from practical considerations. There is a fundamental compromise to be made between bias polarity and direction of current flow, since without insolation, if the bias polarity is the same as that under generating conditions, the direction of current flow is opposite to that under generating conditions, and vice versa. For terrestrial solar cells surface instabilities such as occur in integrated circuits are not expected, thus the polarity of the bias voltage would appear to be immaterial and the proper choice would seem to be that which allows current flow in the "proper" direction. However, this would result in reverse bias being applied to the p-n junction, and in order to achieve appreciable current flow (e.g., of the order of I_{sc}) most of the cell types would have to be operated in reverse breakdown. The reverse breakdown voltage ranged between 5 and more than 20 volts for the cells investigated, except for one type that showed resistive reverse characteristics and for which breakdown was not observed. Thus for stress test conditions using reverse bias the cells would have been under conditions of large and variable power dissipation, and without heat-sinking the cell temperatures would have varied widely. It was thus decided for practical reasons (e.g., the inability to provide temperature chamber space and fixturing for large numbers of heat-sunk cells) to stress the cells with forward voltage (the "proper" polarity) and diode forward current (the "opposite" polarity). Current levels were chosen as roughly equal to 1.7 times I_{sc}. Table 4.3.1 shows values of cell current used in the stress tests. Experiments showed that single cells operated under these conditions in the stress

test temperature chambers had temperatures approximately 1°C to 2°C above ambient.

Cell Diameter (in.)	Forward Current (A)
2	1
3	2
4	3

Table 4.3.1. Forward Current Used in Bias-Temperature Stress Tests.

Determination of the test population size and the total stress time for each bias-temperature stress test was difficult in view of the almost complete lack of pertinent prior degradation rate data. The test populations were required to be large enough that infant mortalities could be identified as such, and large enough that real, but seemingly minor changes in electrical parameters could be discriminated. On the other hand, they were required to be small enough to be accommodated with available stress test facilities, and small enough for meaningful electrical and physical data acquisition. Note that the considerations of population size and test duration interact with the number of stress test temperatures when stress test facility and electrical measurement capacity limits are under examination. A simplistic technique was used in order to scope the experiment design problem. First simulations were performed which indicated that if the "failure rate" (to some undefined criterion) were constant, observation of 15 "failures" would permit satisfactory definiton of the "failure rate" and the reasonable assurance that it was in fact constant. Then it was assumed that under conditions of 55°C cell temperature, the cells would exhibit a "failure rate" of 1%/20 years, again to an undefined criterion. It might be said that if the

failure rate was non-interacting and was in fact 1%/20 years, then the whole question of cell reliability would be unimportant. However, for purposes of experiment design it is far better to assume a too low degradation or "failure" rate than it is to assume a too high value. It was further assumed that the temperature dependence of the degrading mechanism was describable by an Arrenhius relationship with activation energy of 1 eV. Under these assumptions, the test population sizes required to observe at least one failure in 5,000 hours of test, at the 90% confidence level, were calculated as 1850 at 75°C, 14 at 135°C, 5 at 150°C, and 2 at 165°C. Thus test populations of fairly reasonable size, and stress tests of reasonable duration (e.g., 30 units at 165°C and 75 units at 150°C, for 5,000 hours), appeared to have a good chance of producing significant results from the high temperature tests under the experiment design assumptions. On the other hand, the above scenario predicted that no usable results would proceed from the 75°C stress test even for inordinately large test populations, in 5,000 test hours.

From results of the analysis described above, and in light of capacity and absolute time limitations, the stress test schedule of Table 4.3.2 was designed. Actual test duration during the first year's effort is also shown in the table.

In order to provide preliminary information on degradation rates, Phase I experiments were performed using step-stress testing. Quantities of 5 units per type, temperatures of 75°C, 105°C, 150°C, and 165°C, and time per step of 150 hours, were used in these experiments. Results from these experiments were intended to allow the proper choice of initial down-time for the larger quantity tests and to insure that anomalously rapid degradation would not be encountered.

Stress Test Temperature (°C)	Initial Test Population	Planned Test Duration (hr)	Actual Test Duration (hr)
75	50	3,000	2,800
135	50	3,000	2,300
150	40	2,000	1,380
165	40	2,000	1,180

Table 4.3.2. Bias-Temperature Stress Test Schedule.

4.3.2 Bias-Temperature Stress Test Results

Initial bias-temperature stress test experimentation was performed using the step-stress schedule discussed in Section 4.3.1. From results of this experimentation initial electrical measurement and inspection down times were chosen. Subsequent down-times were selected considering both the results obtained at earlier down-times and electrical measurement capacity. Table 4.3.3 shows actual down-times for the four bias-temperature stress tests. Results of these stress tests are shown in Figures 4.3.1 through 4.3.16. These figures show the behavior of the P_m distribution and the mean P_m at each of the four bias-temperature stress levels. The distribution plots shown in these figures coupled with the lot mean P_m graphs allow estimates of the behavior of both the P_m mean and dispersion with bias-temperature stress.

Stress Test Temperature (°C)	First Down-Time (hr)	Second Down-Time (hr)	Third Down-Time (hr)	Fourth Down-Time (hr)
75	968	1481	2000	2800
135	600	958	1500	2300
150	282	538	800	1380
165	148	362	600	1180

Table 4.3.3. Down-times for Bias-Temperature Stress Tests.

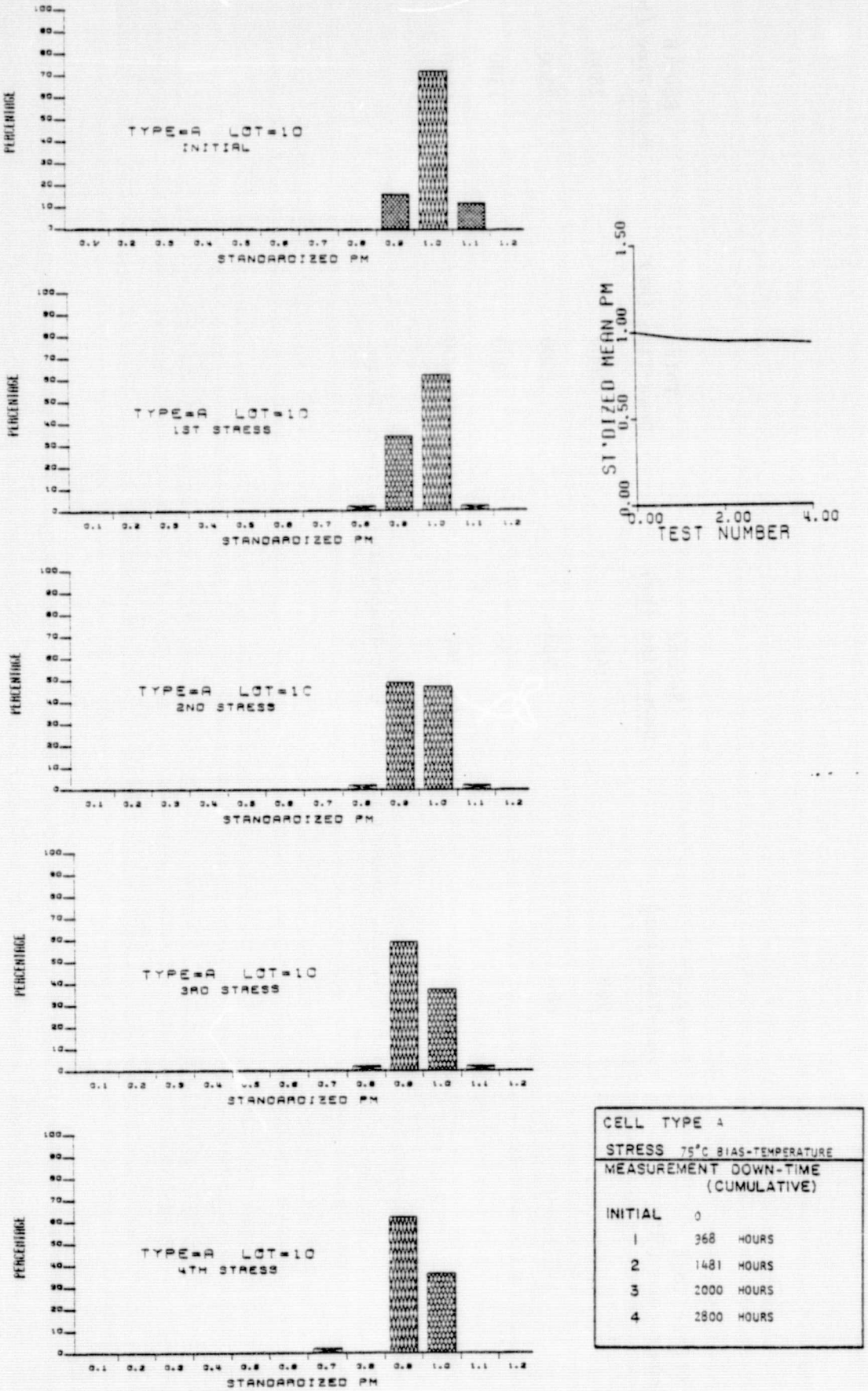

Figure 4.3.1. Behavior of P_m Distribution and Lot Mean P_m with 75°C Bias-Temperature Stress, Type A Cells.

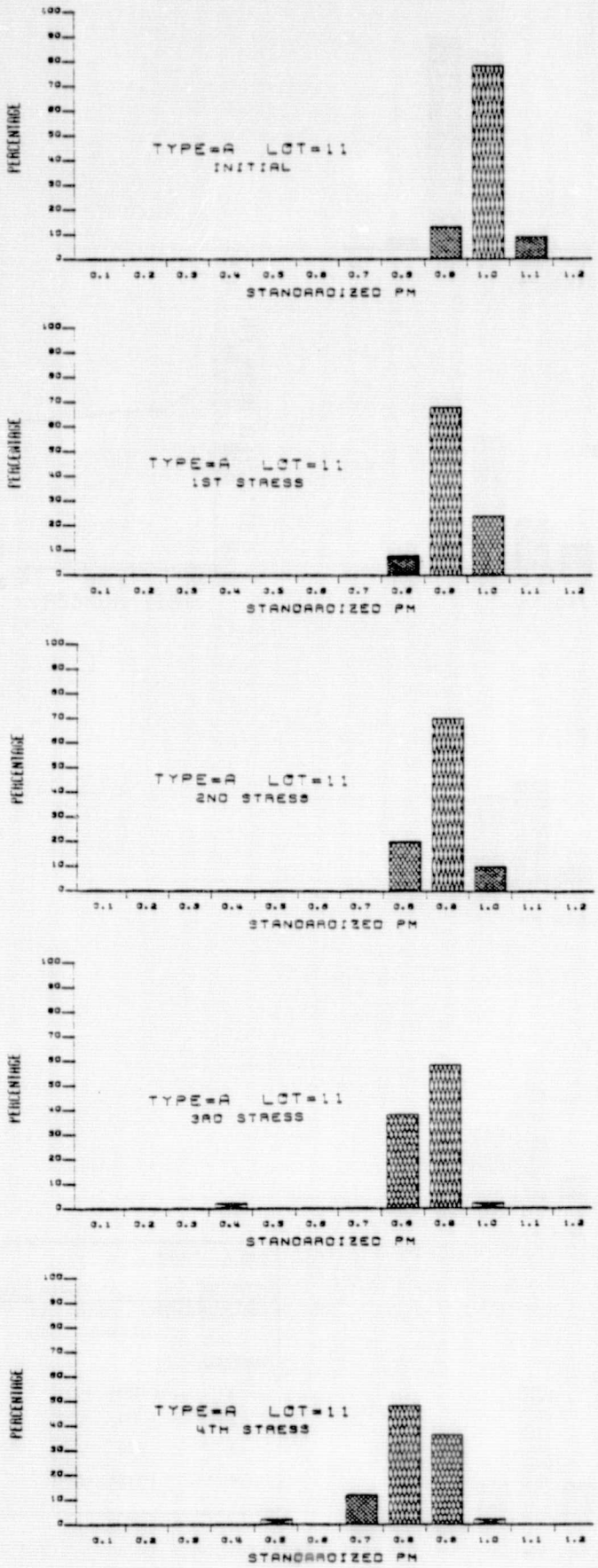

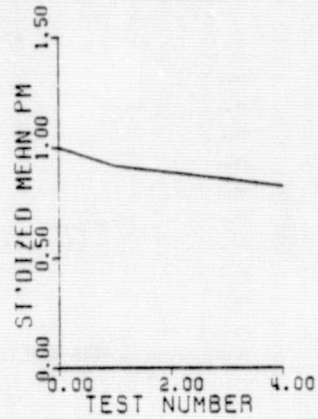

REPRODUCIBILITY OF THE
ORIGINAL PAGE IS POOR

CELL TYPE A	
STRESS 135°C BIAS-TEMPERATURE	
MEASUREMENT	DOWN-TIME (CUMULATIVE)
INITIAL	0
1	600 HOURS
2	958 HOURS
3	1500 HOURS
4	2300 HOURS

Figure 4.3.2. Behavior of P_m Distribution and Lot Mean P_m with 135°C Bias-Temperature Stress, Type A Cells.

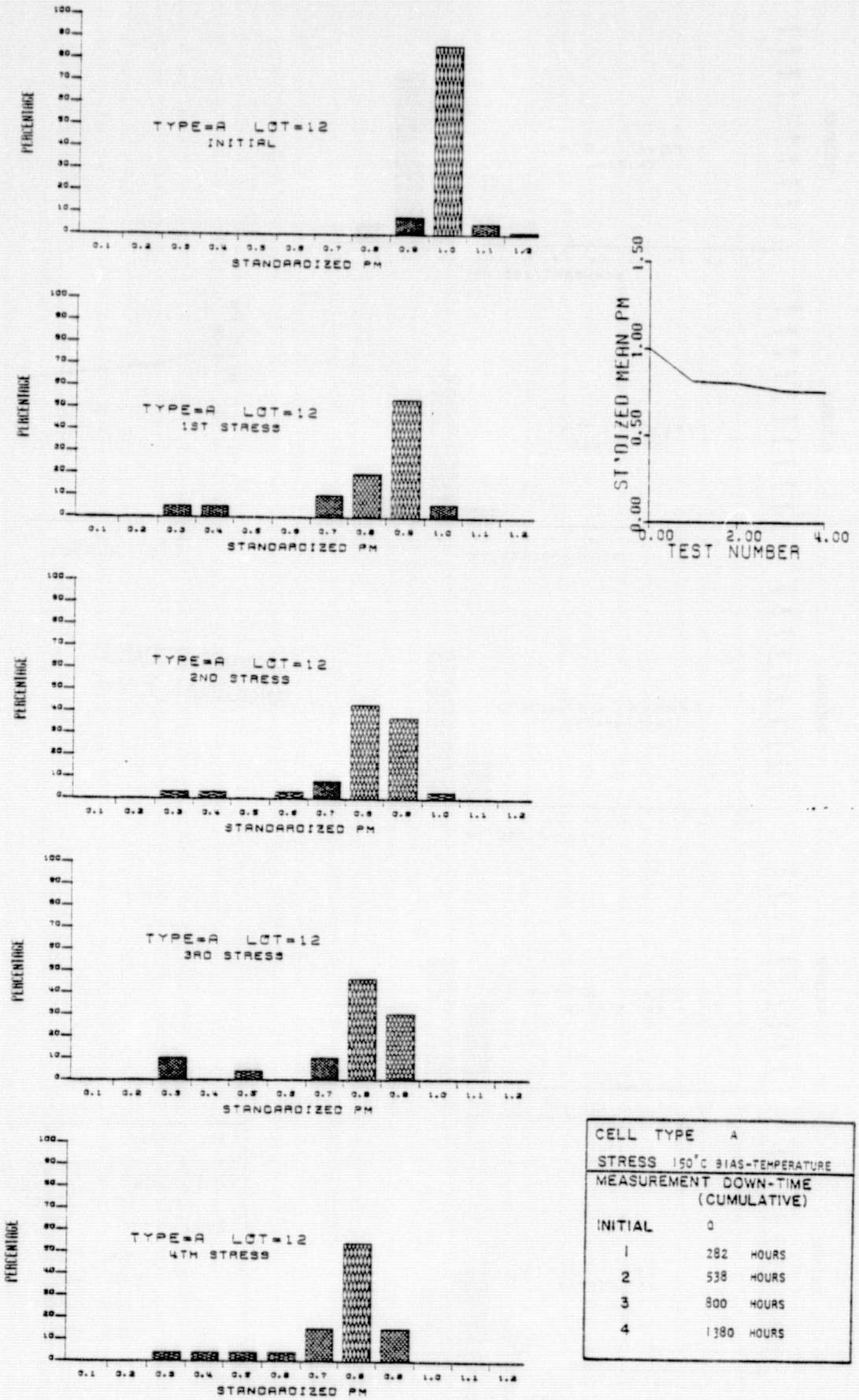

Figure 4.3.3. Behavior of P_m Distribution and Lot Mean P_m with 150°C Bias-Temperature Stress, Type A Cells.

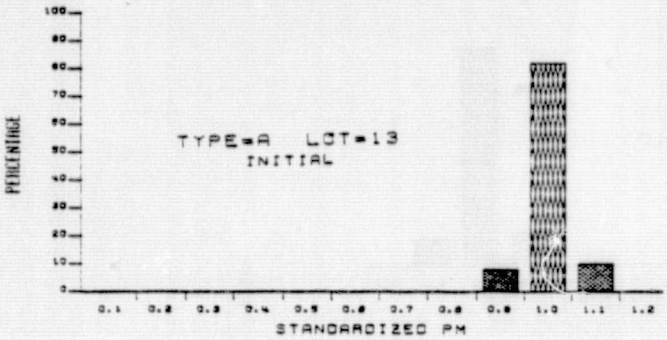

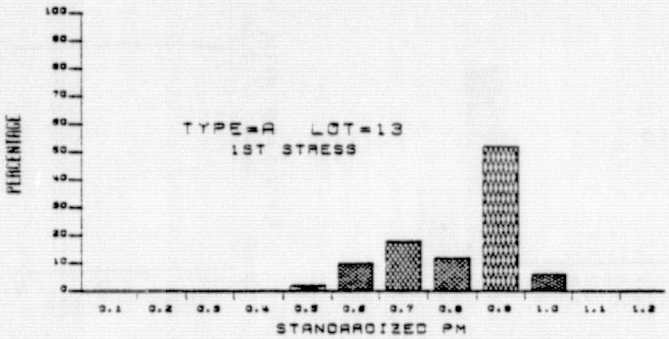

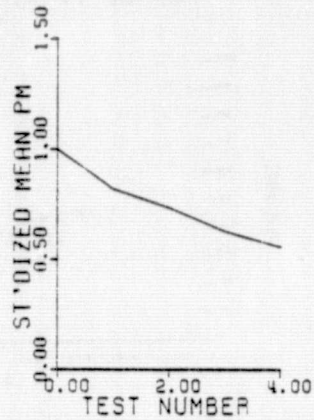

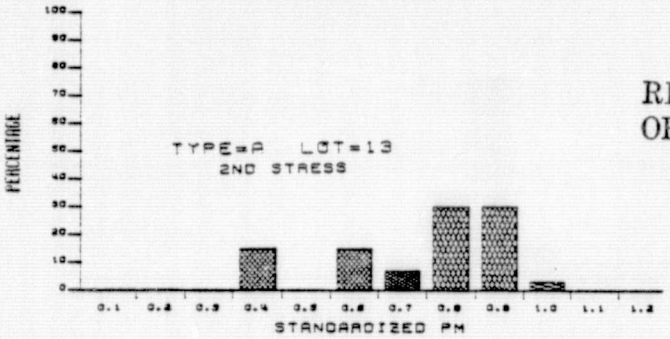

REPRODUCIBILITY OF THE
ORIGINAL PAGE IS POOR

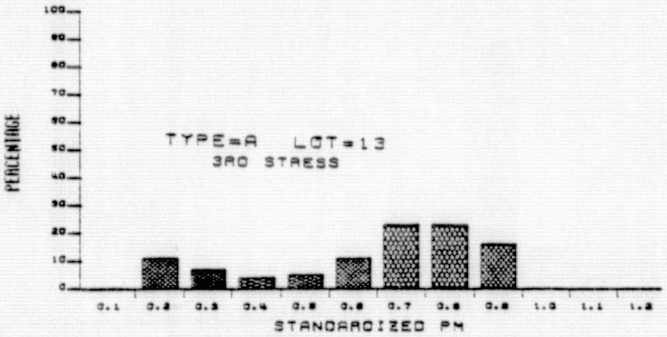

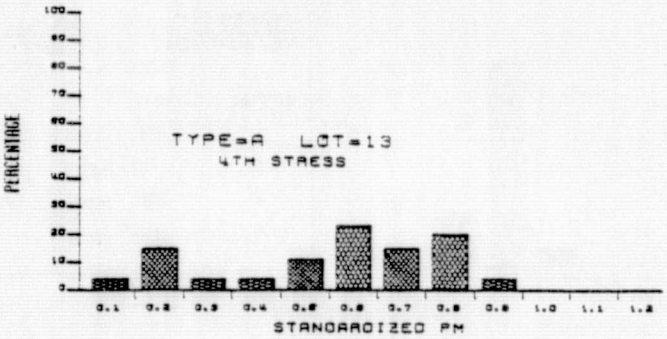

CELL TYPE	A	
STRESS	165°C BIAS-TEMPERATURE	
MEASUREMENT	DOWN-TIME (CUMULATIVE)	
INITIAL	0	
1	148	HOURS
2	362	HOURS
3	600	HOURS
4	1180	HOURS

Figure 4.3.4. Behavior of P_m Distribution and Lot Mean P_m with 165°C Bias-Temperature Stress, Type A Cells.

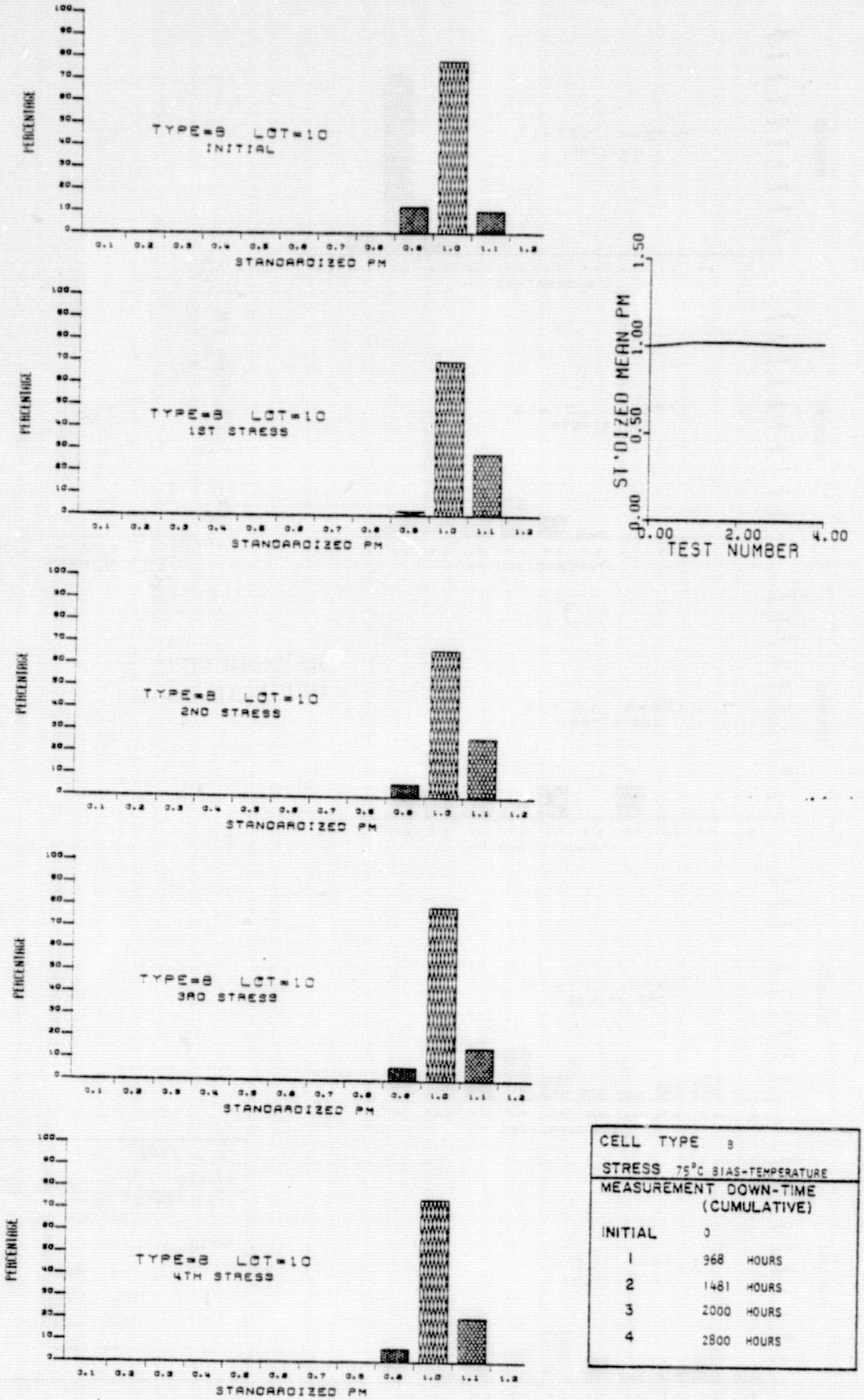

Figure 4.3.5. Behavior of P_m Distribution and Lot Mean P_m with 75°C Bias-Temperature Stress, Type B Cells.

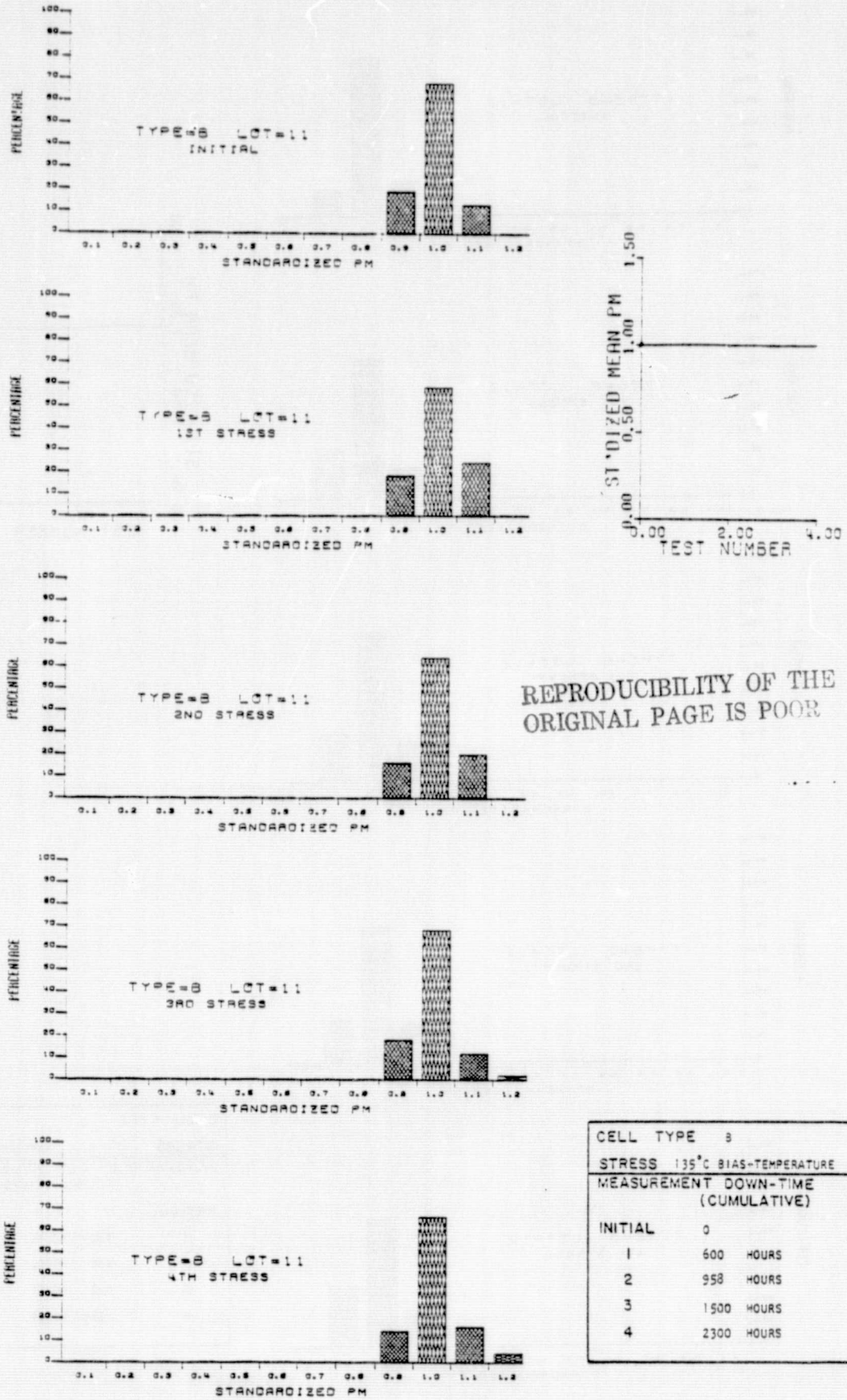

REPRODUCIBILITY OF THE
ORIGINAL PAGE IS POOR

CELL TYPE	B
STRESS	135°C BIAS-TEMPERATURE
MEASUREMENT DOWN-TIME (CUMULATIVE)	
INITIAL	0
1	600 HOURS
2	958 HOURS
3	1500 HOURS
4	2300 HOURS

Figure 4.3.6. Behavior of P_m Distribution and Lot Mean P_m with 135°C Bias-Temperature Stress, Type B Cells.

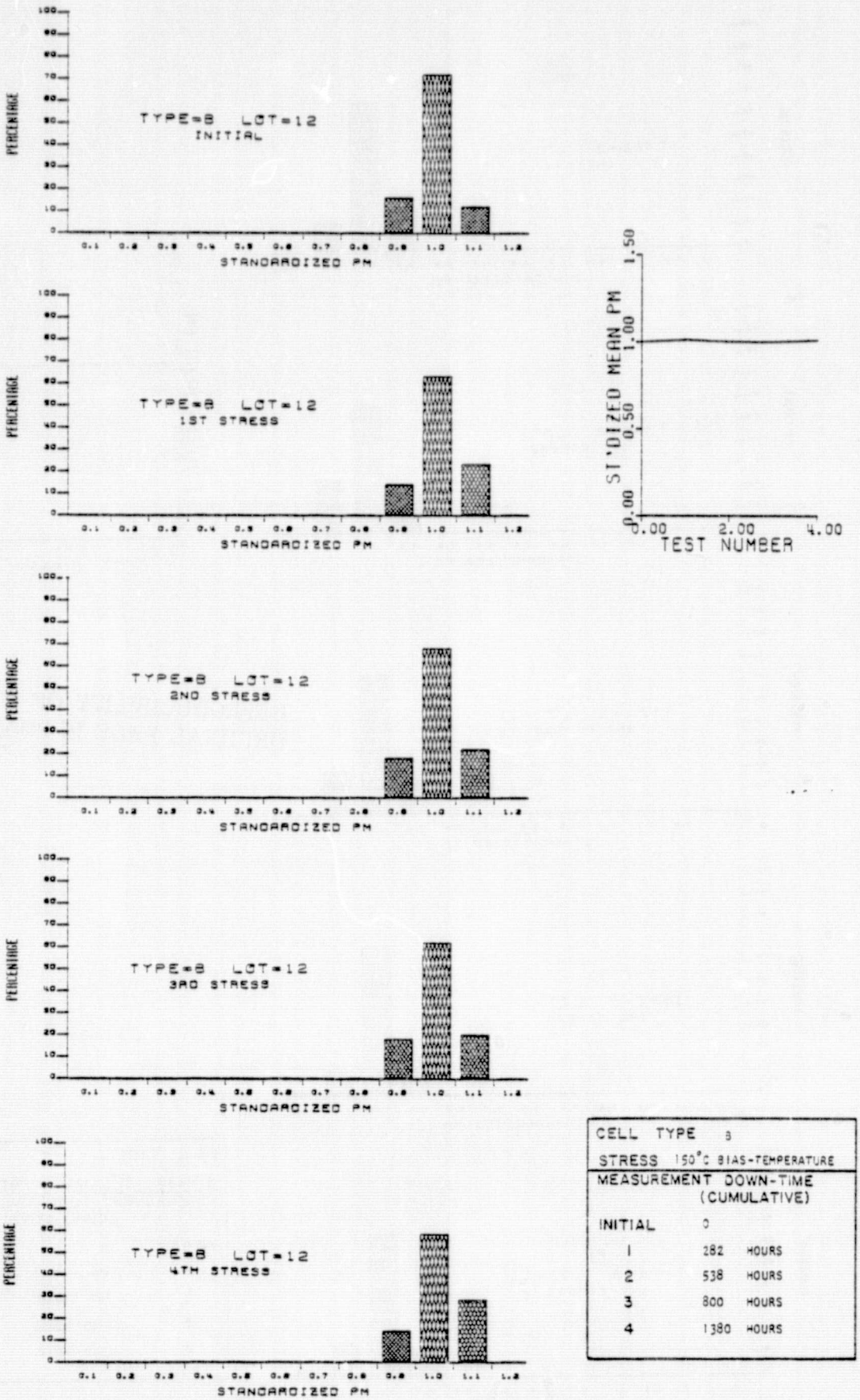

Figure 4.3.7. Behavior of P_m Distribution and Lot Mean P_m with 150°C Bias-Temperature Stress, Type B Cells.

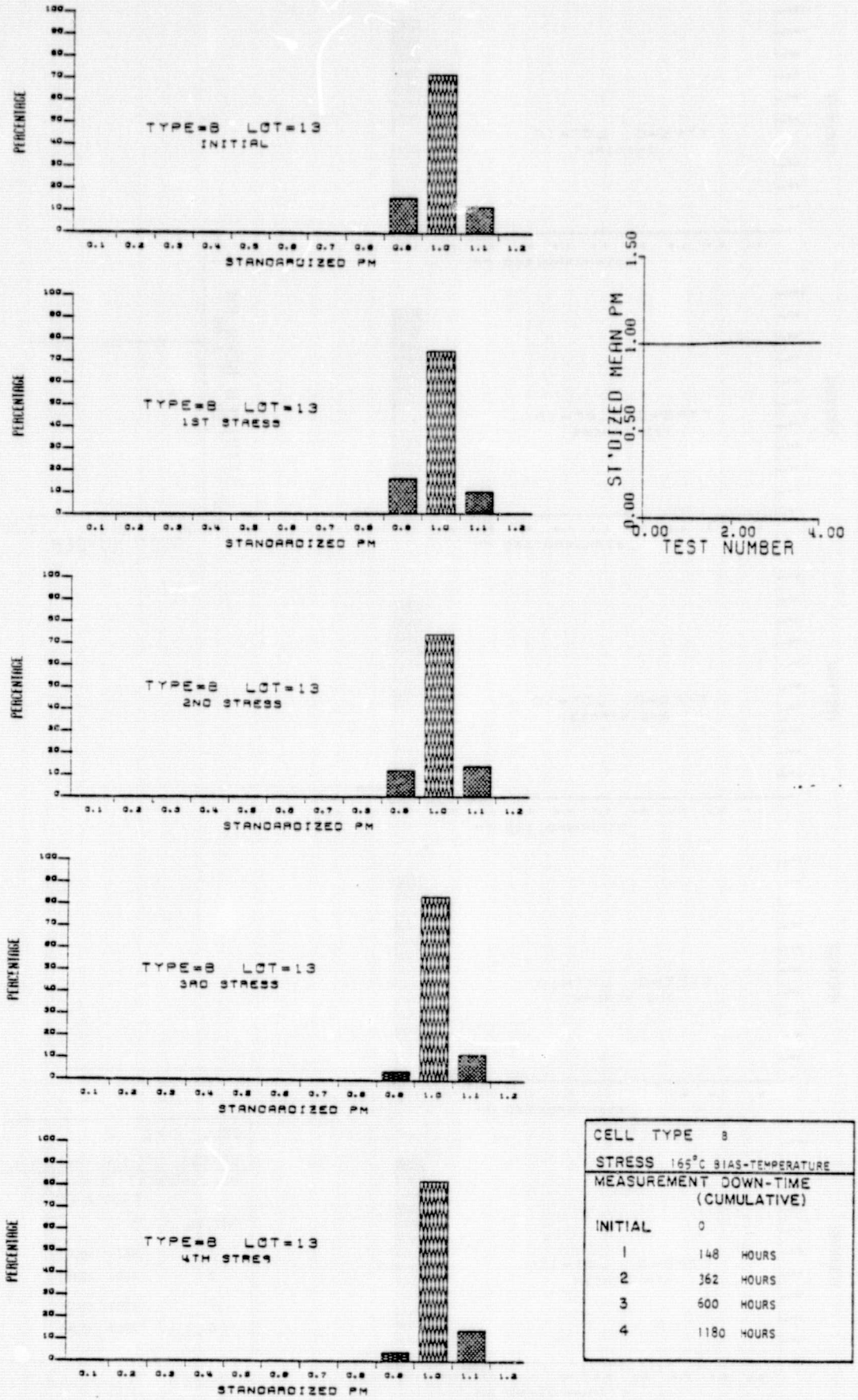

Figure 4.3.8. Behavior of P_m Distribution and Lot Mean P_m with 165°C Bias-Temperature Stress, Type B Cells.

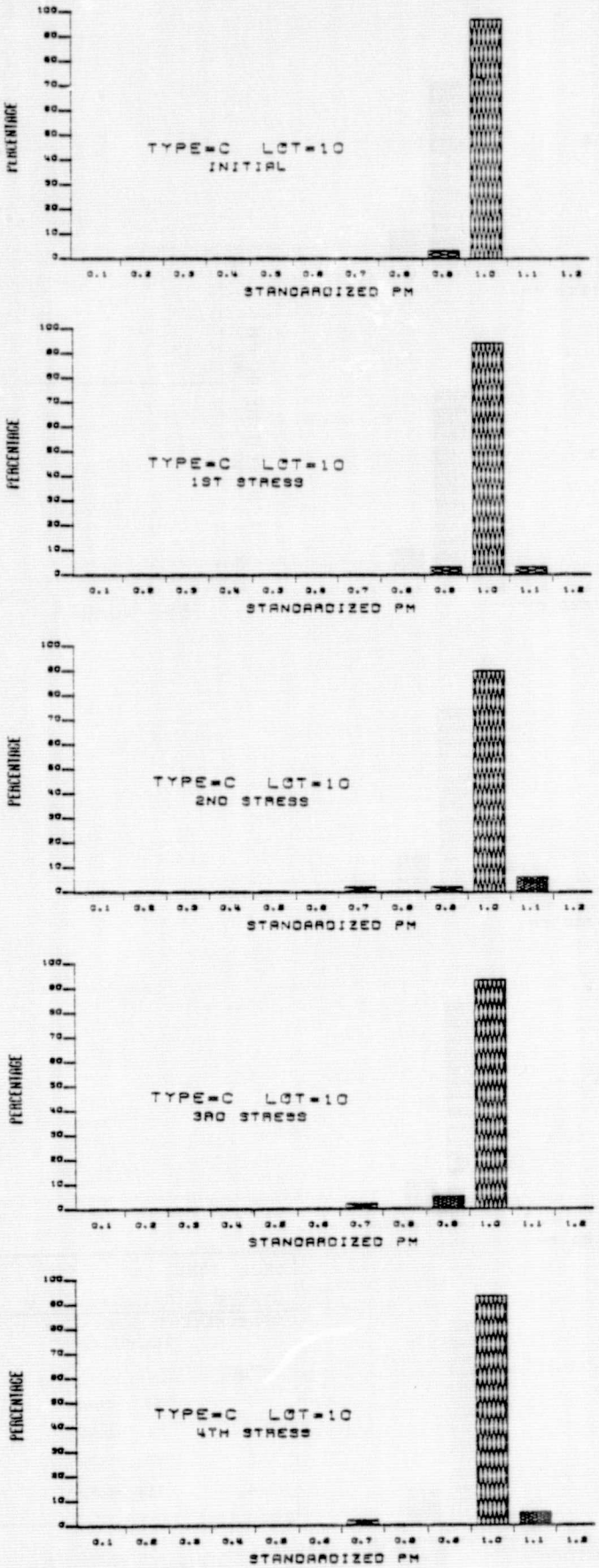

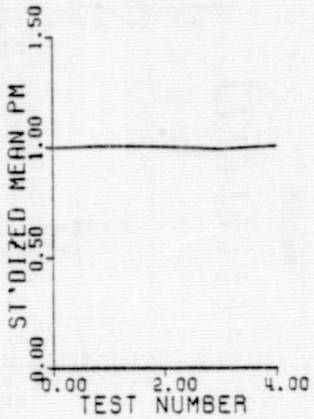

CELL TYPE C	
STRESS 75°C BIAS-TEMPERATURE	
MEASUREMENT	DOWN-TIME (CUMULATIVE)
INITIAL	0
1	968 HOURS
2	1481 HOURS
3	2000 HOURS
4	2800 HOURS

Figure 4.3.9. Behavior of P_m Distribution and Lot Mean P_m with 75°C Bias-Temperature Stress, Type C Cells.

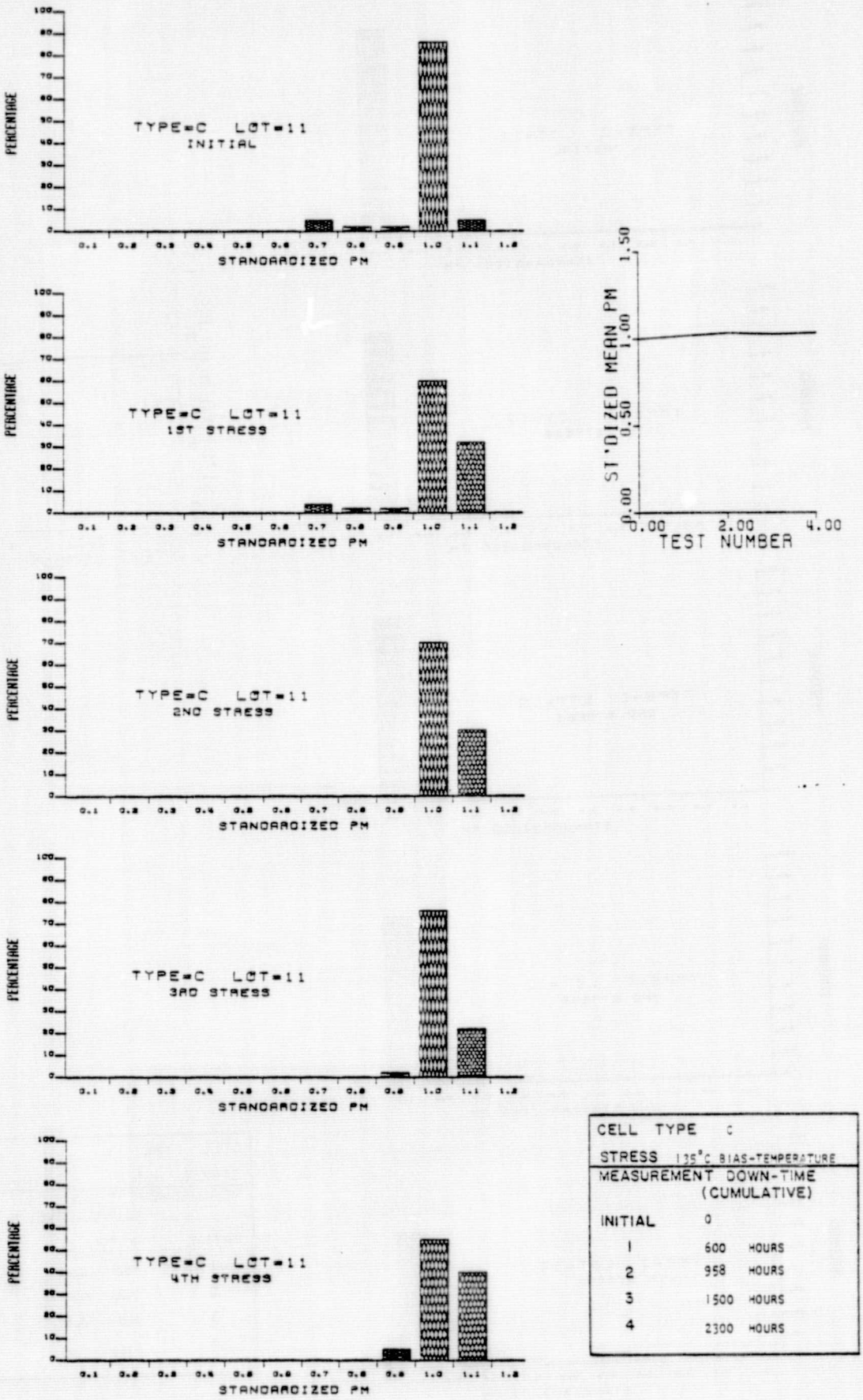

Figure 4.3.10. Behavior of P_m Distribution and Lot Mean P_m with 135°C Bias-Temperature Stress, Type C Cells.

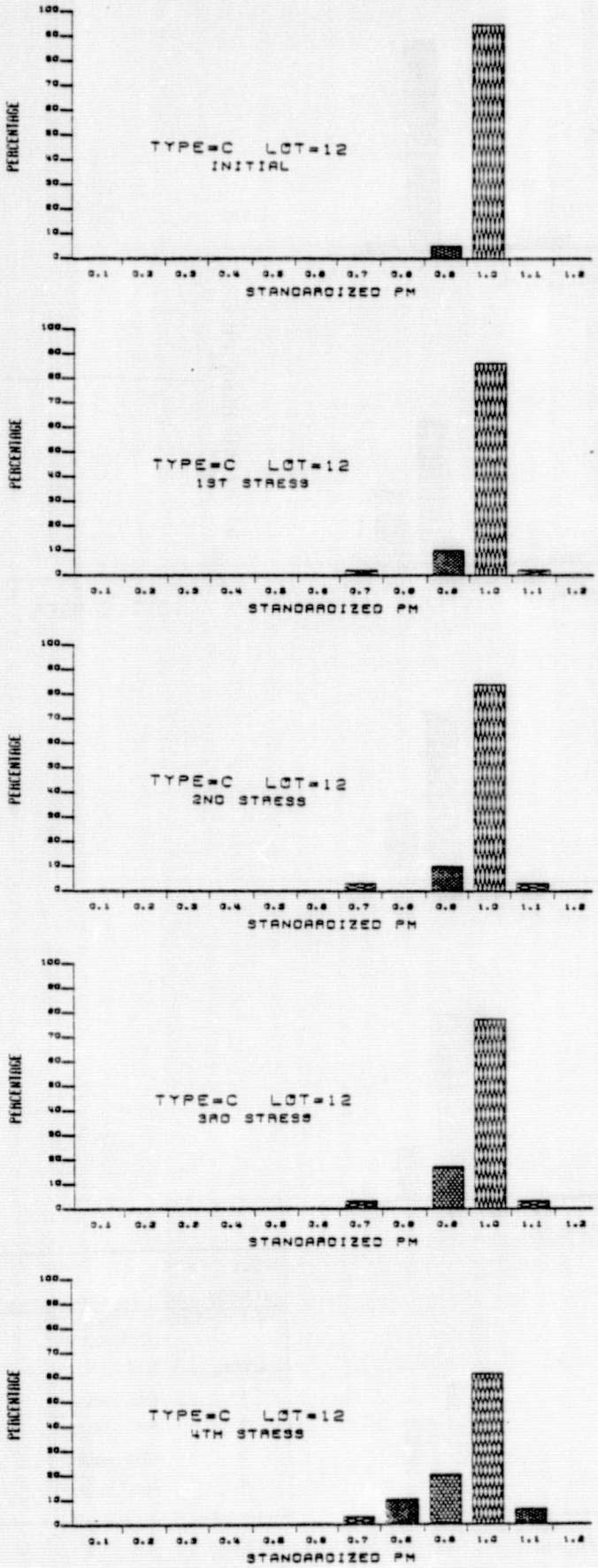

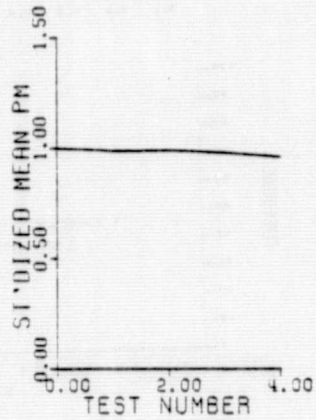

CELL TYPE C		
STRESS 150°C BIAS-TEMPERATURE		
MEASUREMENT	DOWN-TIME (CUMULATIVE)	
INITIAL	0	
1	282	HOURS
2	538	HOURS
3	800	HOURS
4	1380	HOURS

Figure 4.3.11. Behavior of P_m Distribution and Lot Mean P_m with 150°C Bias-Temperature Stress, Type C Cells.

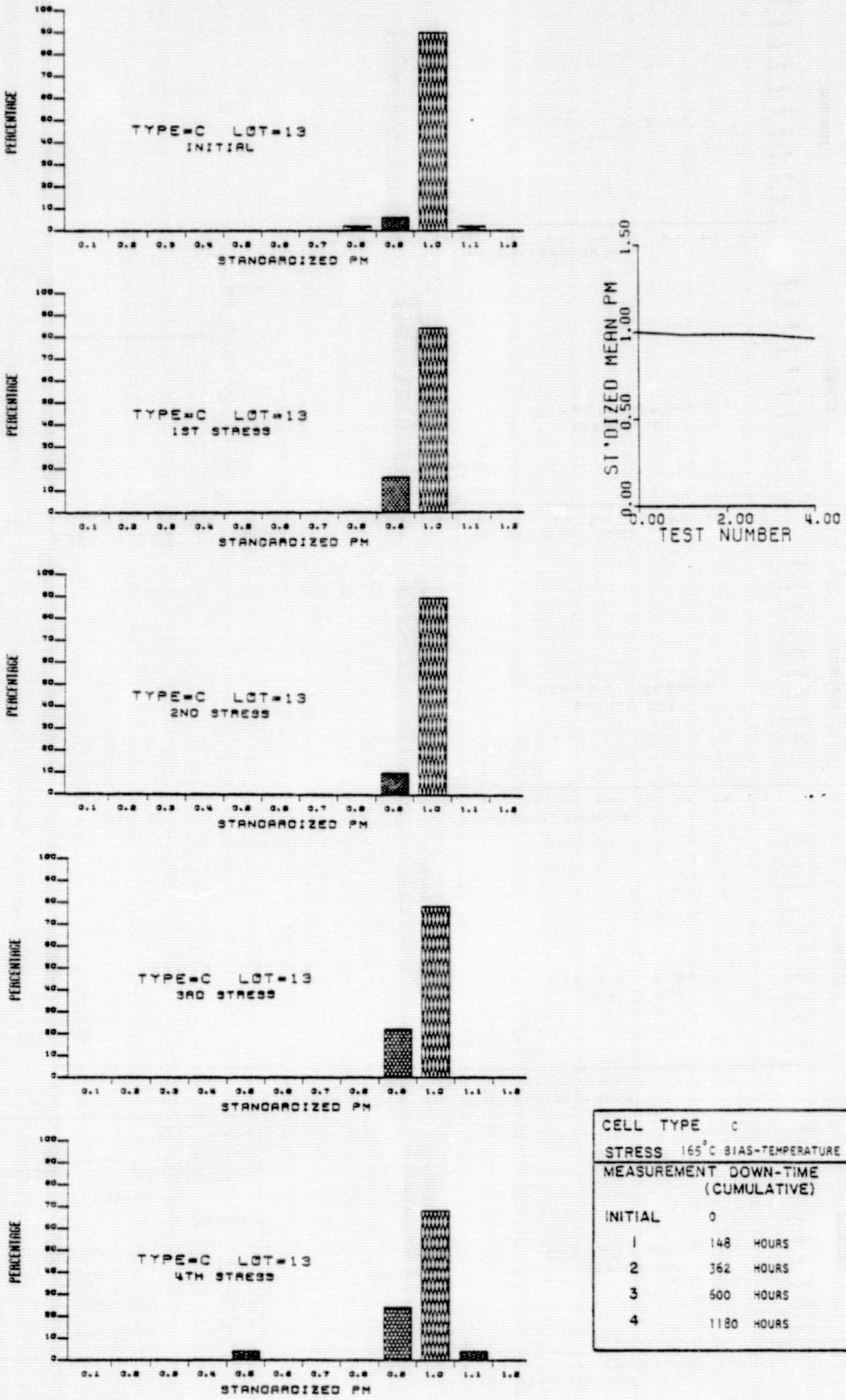

Figure 4.3.12. Behavior of P_m Distribution and Lot Mean P_m with 165°C Bias-Temperature Stress, Type C Cells.

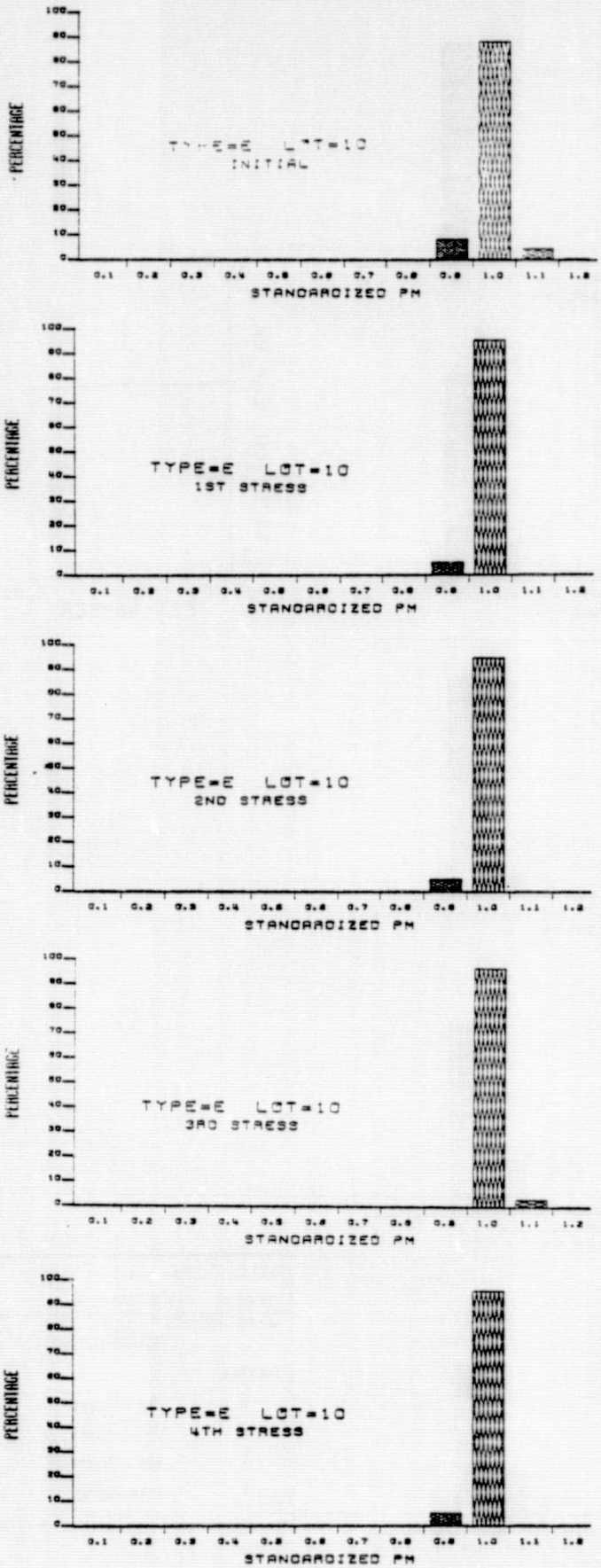

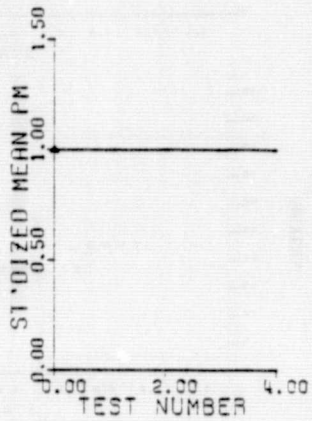

CELL TYPE E	
STRESS 75°C BIAS-TEMPERATURE	
MEASUREMENT	DOWN-TIME (CUMULATIVE)
INITIAL	0
1	968 HOURS
2	1481 HOURS
3	2000 HOURS
4	2800 HOURS

Figure 4.3.13. Behavior of P_m Distribution and Lot Mean P_m with 75°C Bias-Temperature Stress, Type E Cells.

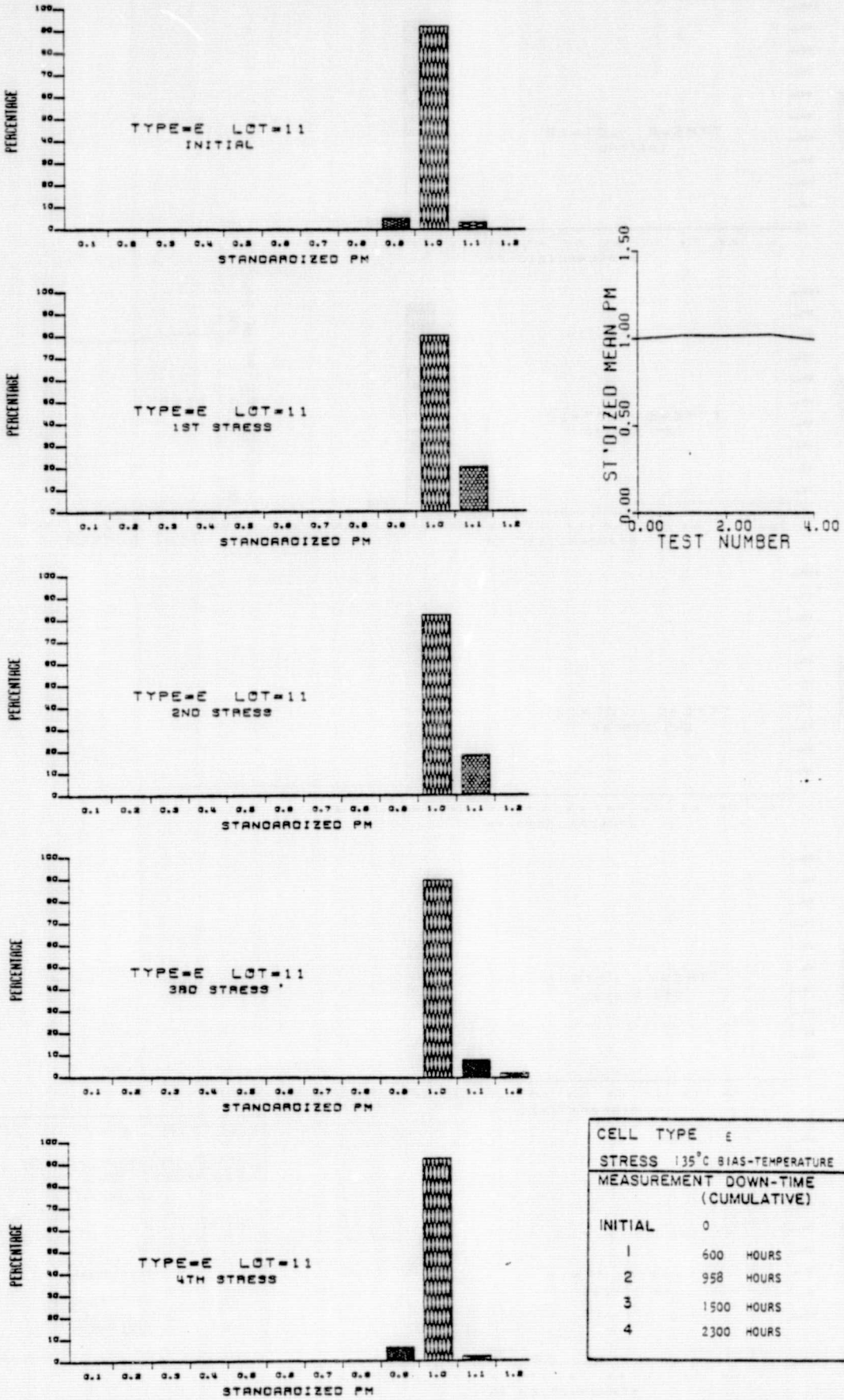

Figure 4.3.14. Behavior of P_m Distribution and Lot Mean P_m with 135°C Bias-Temperature Stress, Type E Cells.

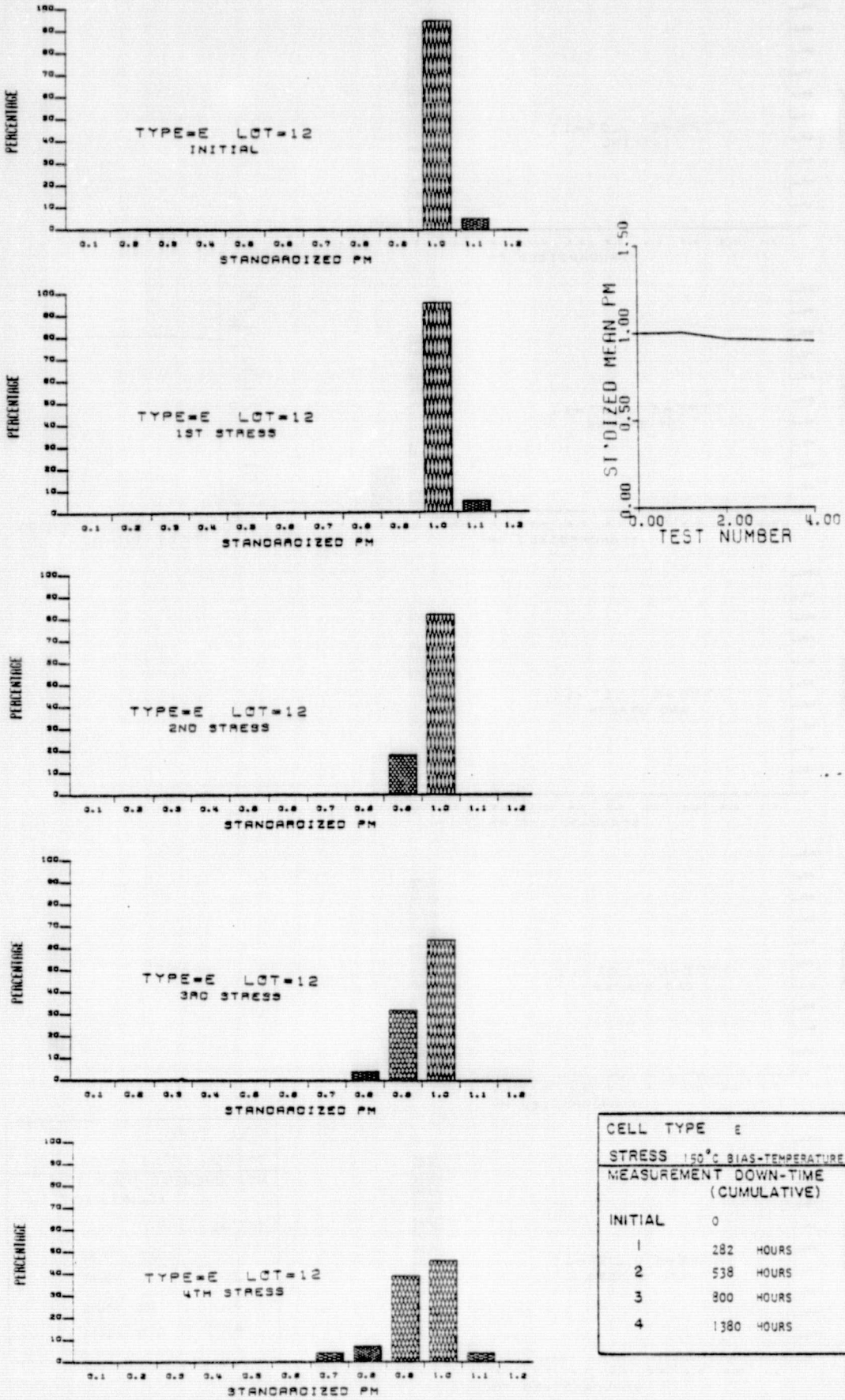

Figure 4.3.15. Behavior of P_m Distribution and Lot Mean P_m with 150°C Bias-Temperature Stress, Type E Cells.

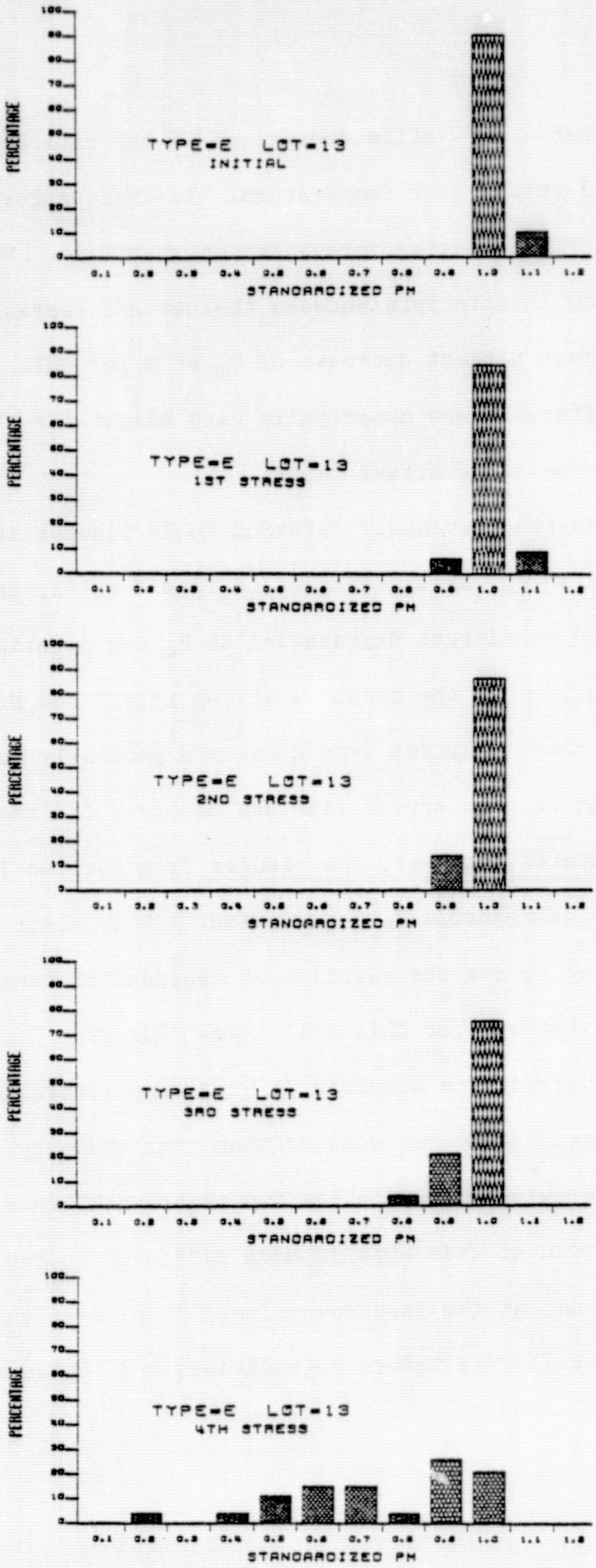

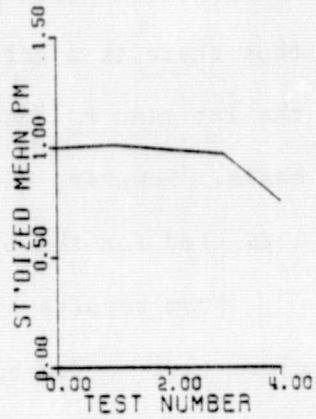

CELL TYPE	E	
STRESS	165°C BIAS-TEMPERATURE	
MEASUREMENT	DOWN-TIME (CUMULATIVE)	
INITIAL	0	
1	148	HOURS
2	362	HOURS
3	600	HOURS
4	1180	HOURS

Figure 4.3.16. Behavior of P_m Distribution and Lot Mean P_m with 165°C Bias-Temperature Stress, Type E Cells.

Figures 4.3.17 through 4.3.24 allow comparison of the cell P_m response by cell type and stress test temperature. In these figures the mean percent decrease in P_m is plotted versus stress test time. Note that there is a difference in principle between the percent decrease of the lot mean P_m and the mean percent decrease of P_m on a per cell basis. However, this difference was numerically very slight for the large lots used for the bias-temperature stress tests.

From results shown in the previously referred to 24 figures it is clear that no degradation in P_m was experienced by type B cells, and that relatively severe and consistent degradation in P_m was experienced by type A cells. Less obvious is the response of the type C and E cells. From Figure 4.3.23 it is clear that for type C cells a generally monotonic (though small) decrease in P_m with stress time was observed for the higher two stress temperatures; however, the results from the two lower temperature tests show no discernable P_m degradation. It is clear that additional data is required before the question of degradation, and degradation rate, can be resolved for this cell type. For type E cells it is somewhat clearer that degradation occurred in bias-temperature testing. However, the amount of degradation was smaller than that shown by the type A cells and again was evident only in the two higher temperature stress tests. Interpretation of this data is made difficult by the large incremental degradation shown at the last down-time. Thus additional data is also required for this cell type before degradation, and degradation rate, can be quantified.

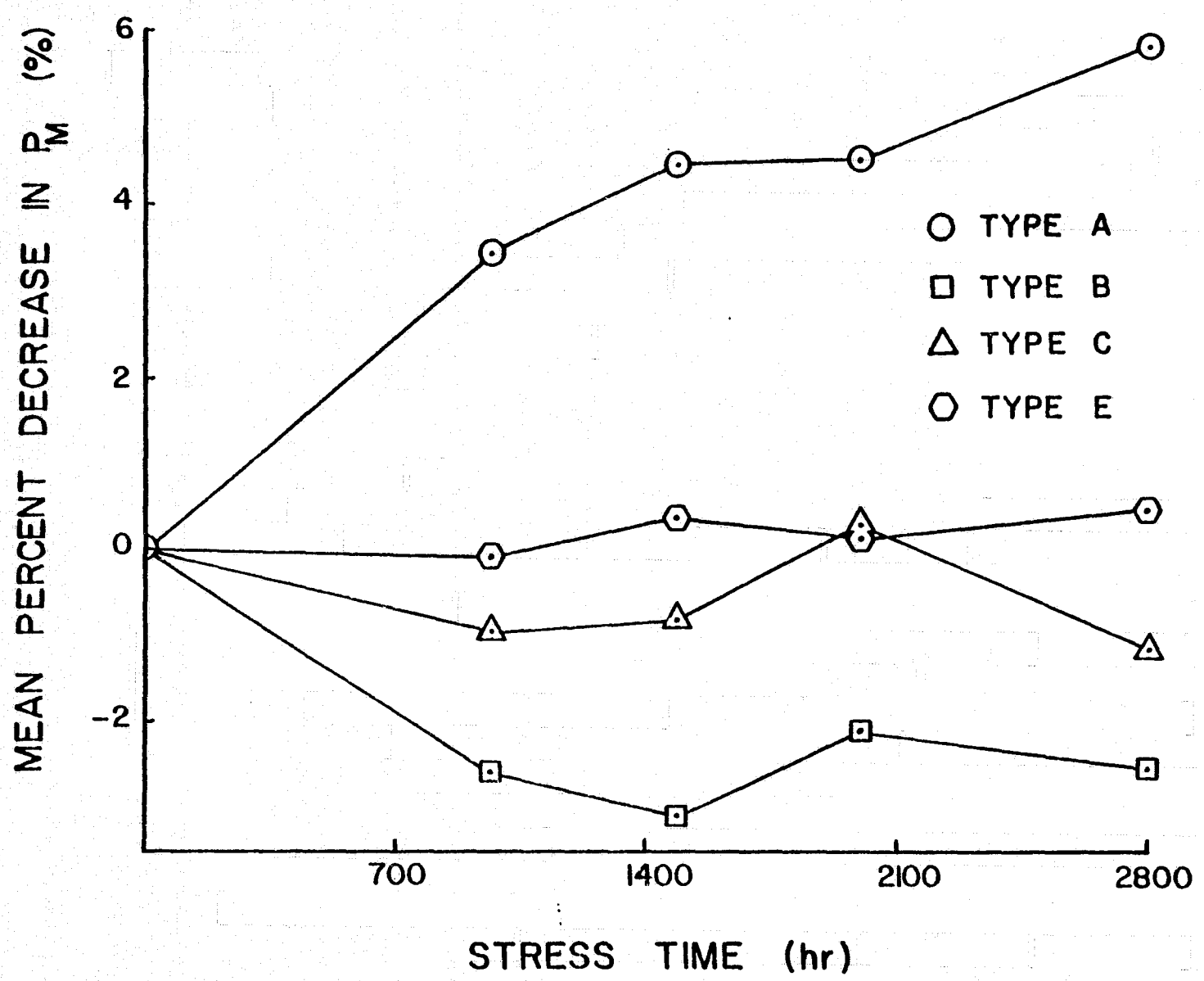

Figure 4.3.17. Mean Percent Decrease in P_m for 75°C Bias-Temperature Stress Test, All Cell Types.

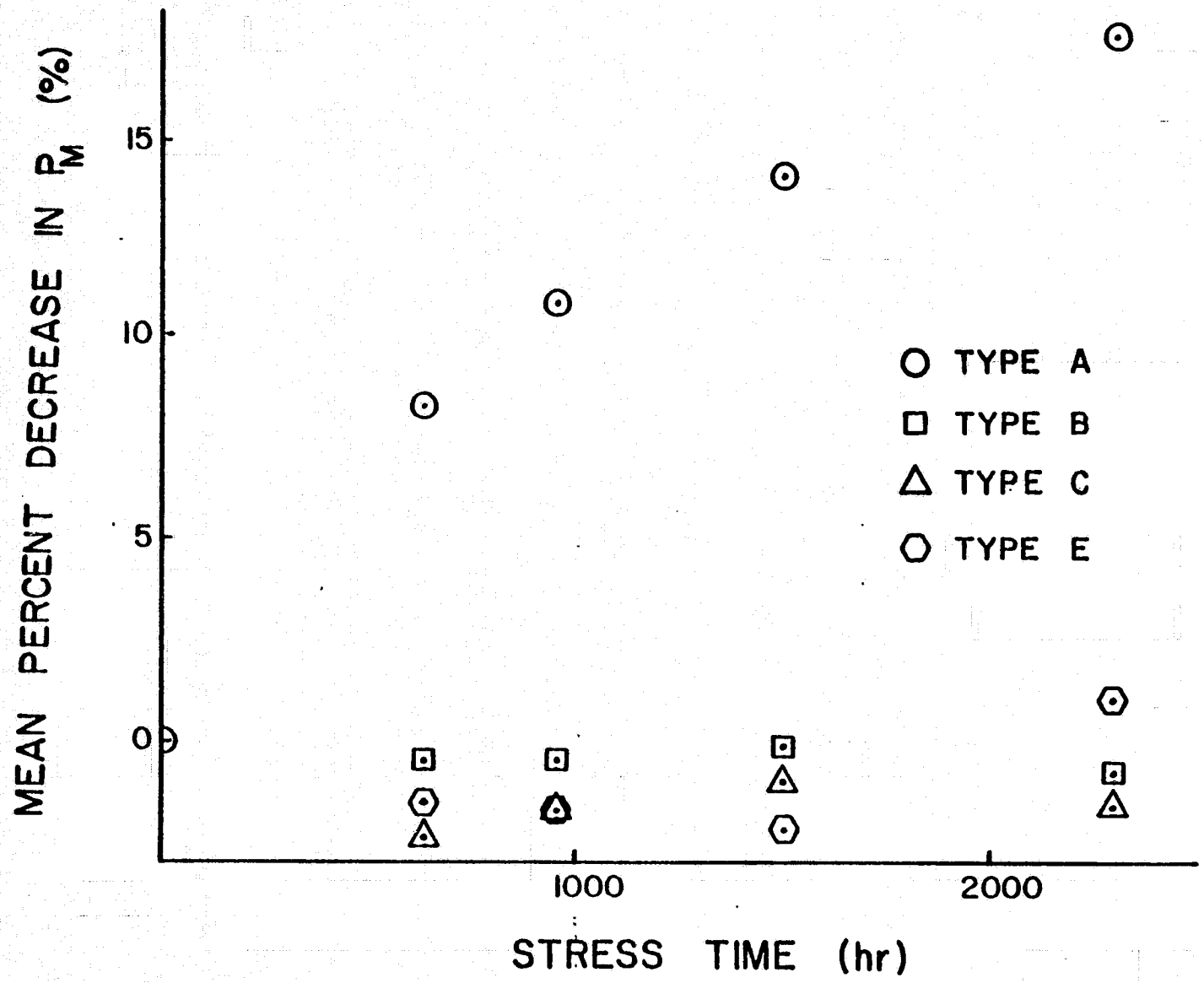

Figure 4.3.18. Mean Percent Decrease in P_m for 135°C Bias-Temperature Stress Test, All Cell Types.

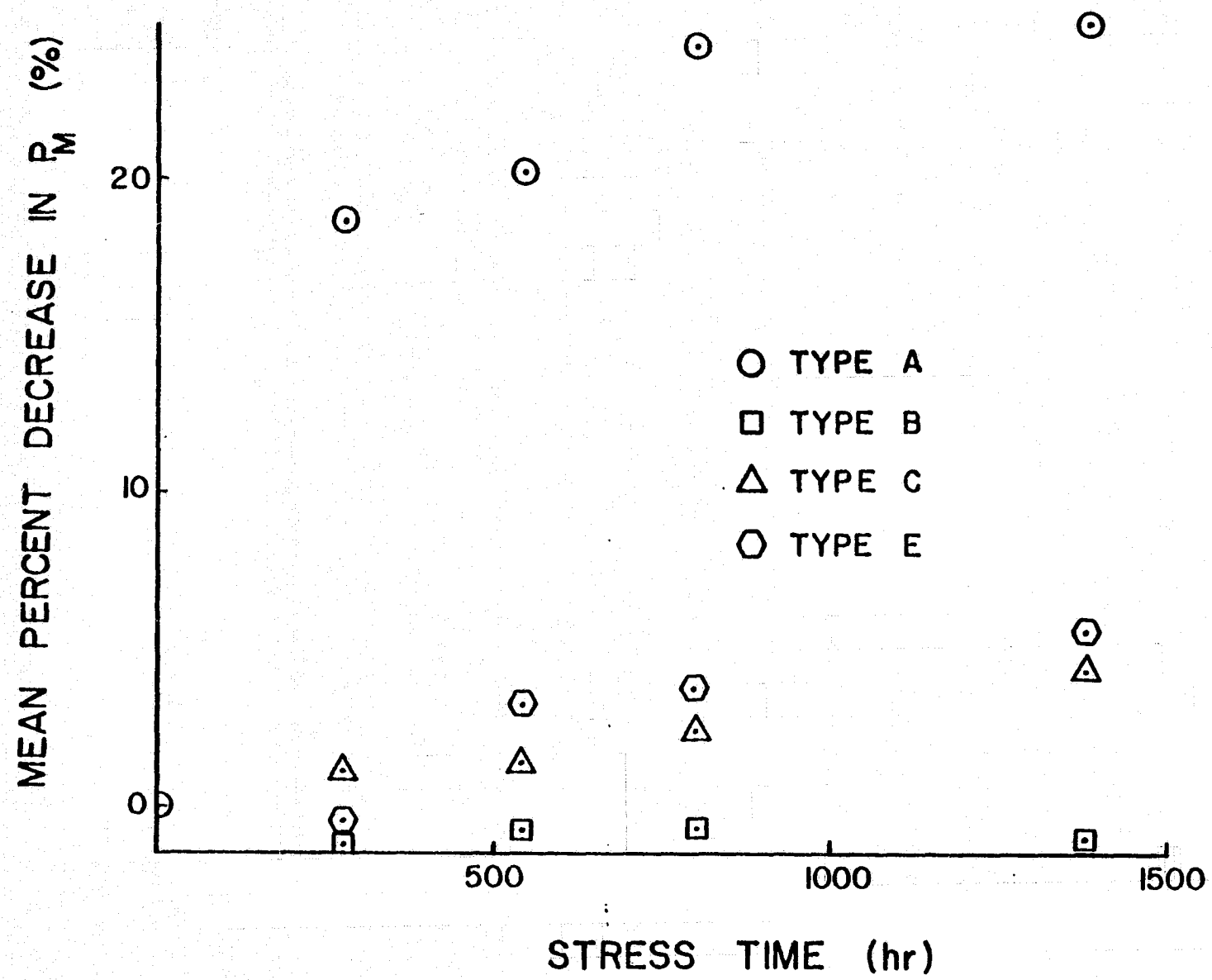

Figure 4.3.19. Mean Percent Decrease in P_m for 150°C Bias-Temperature Stress Test, All Cell Types.

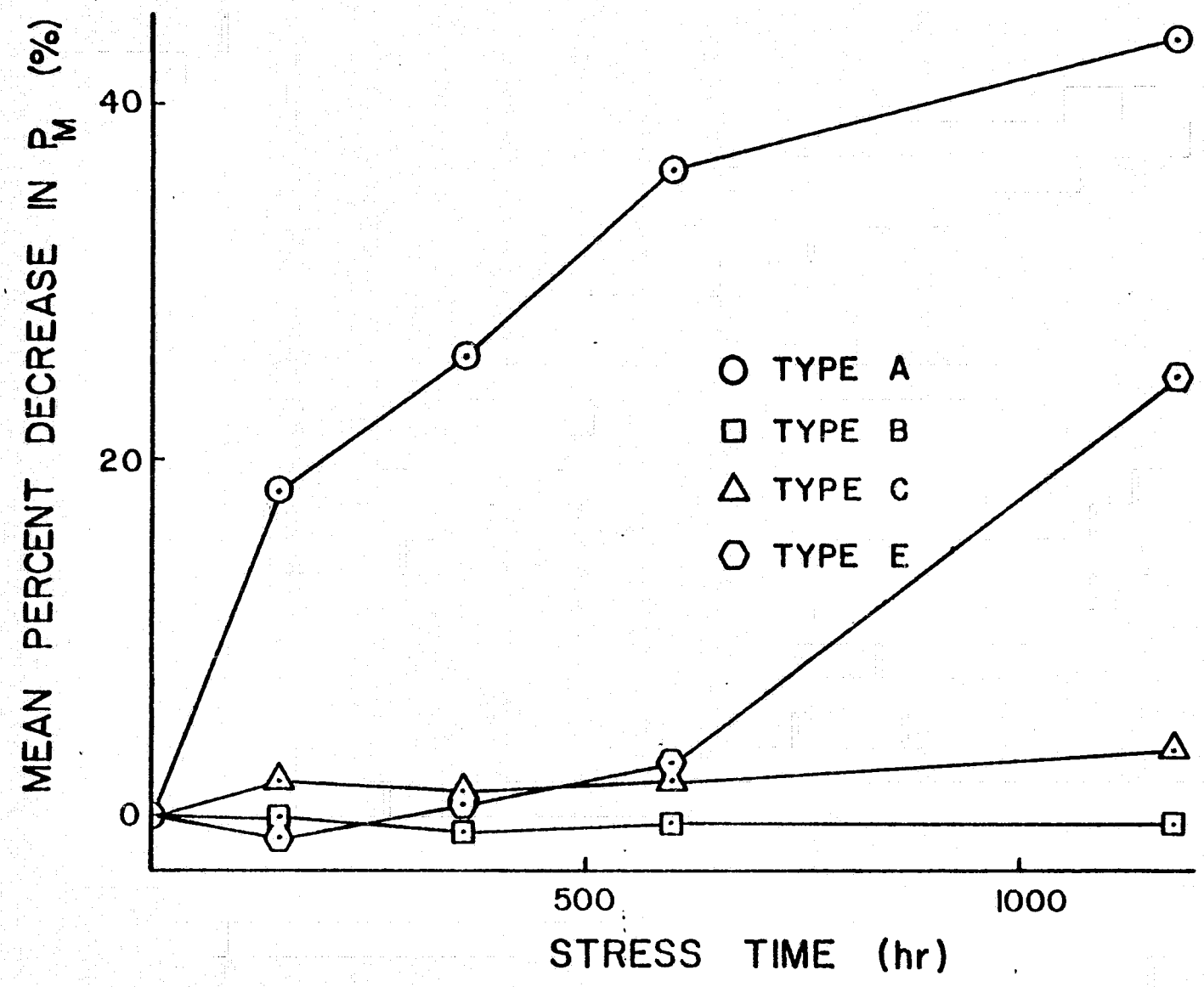

Figure 4.3.20. Mean Percent Decrease in P_m for 165°C Bias-Temperature Stress Test, All Cell Types.

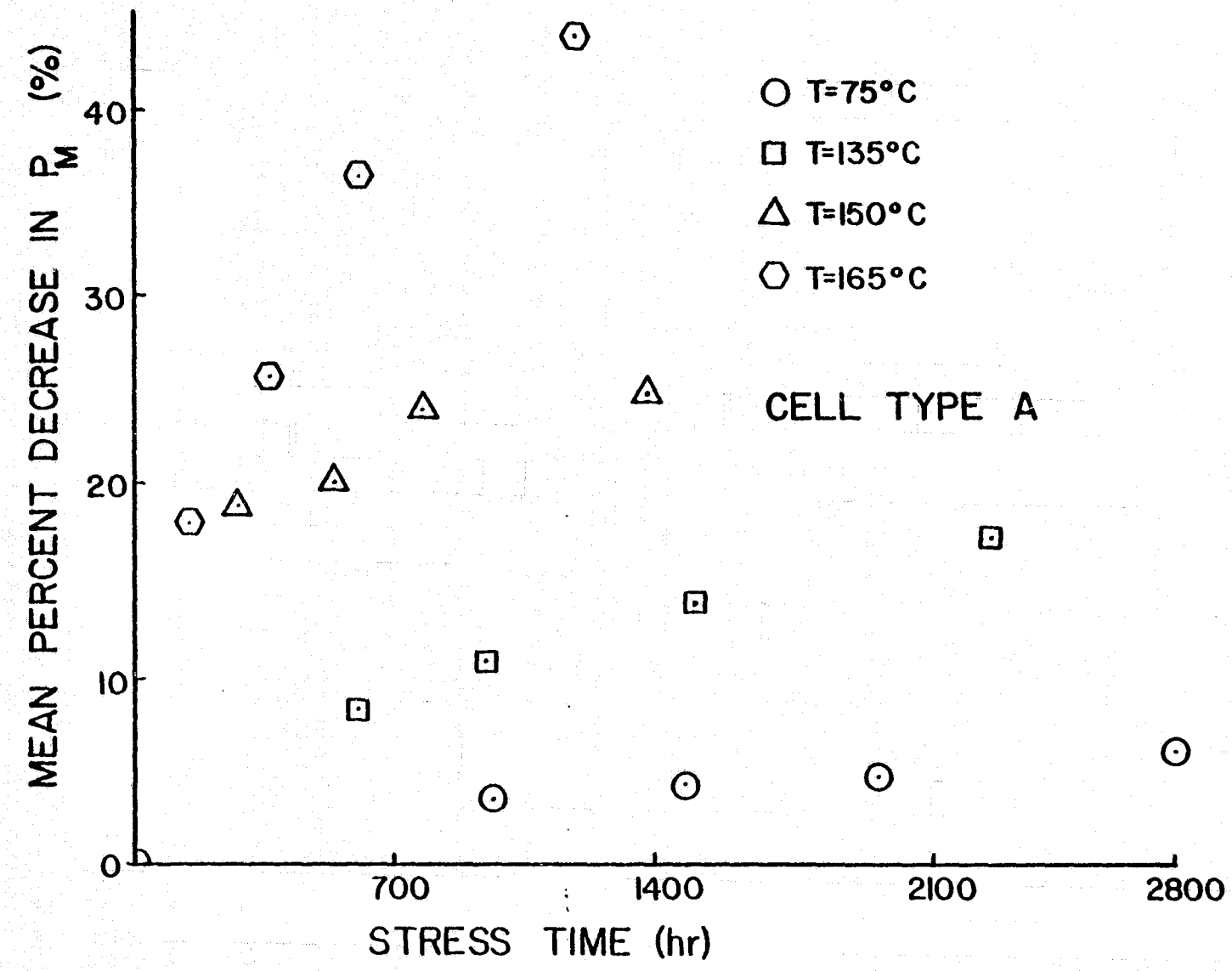

Figure 4.3.21. Mean Percent Decrease in P_m for Bias-Temperature Stress Test, Type A Cells.

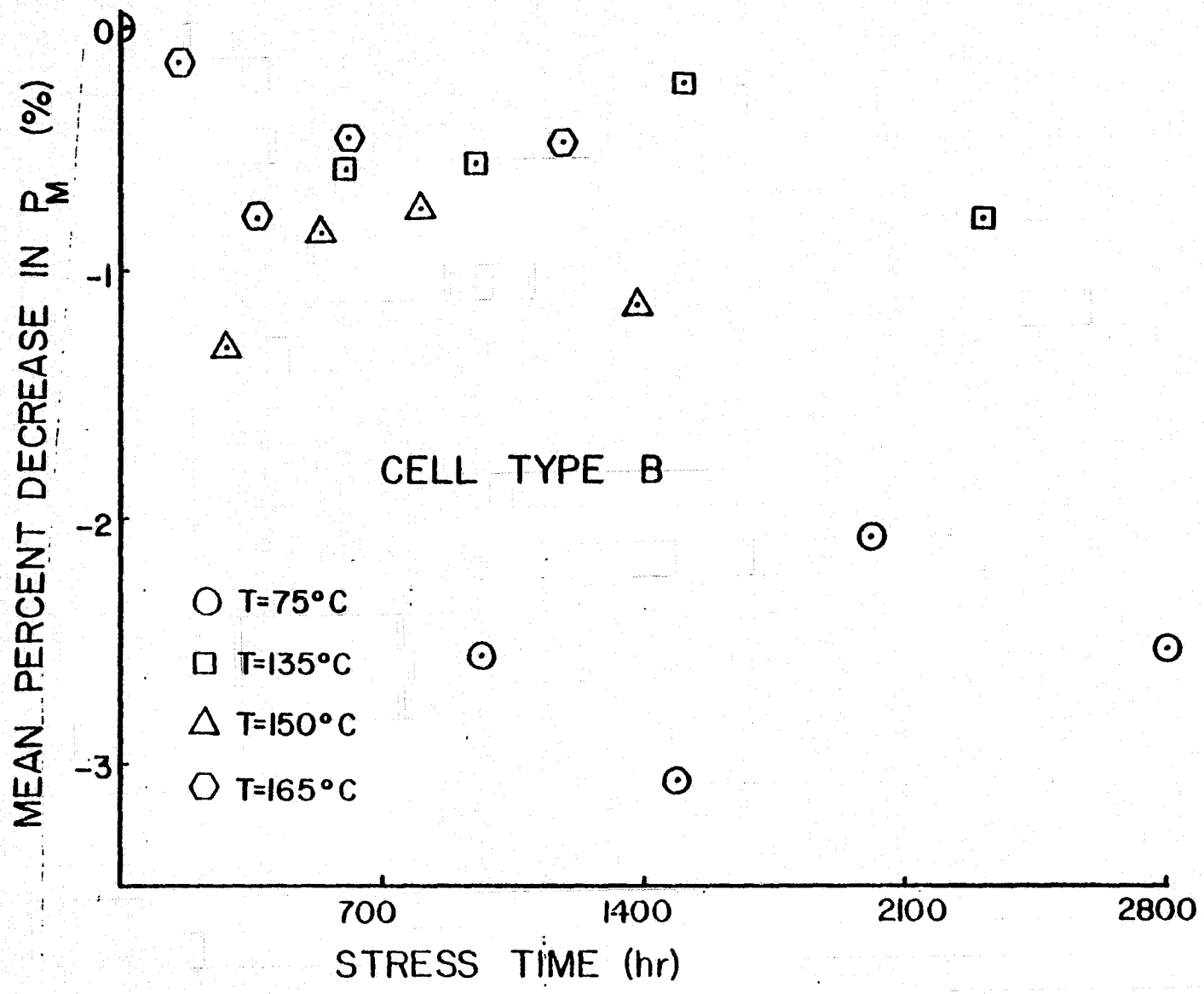

Figure 4.3.22. Mean Percent Decrease in P_m for Bias-Temperature Stress Test, Type B Cells.

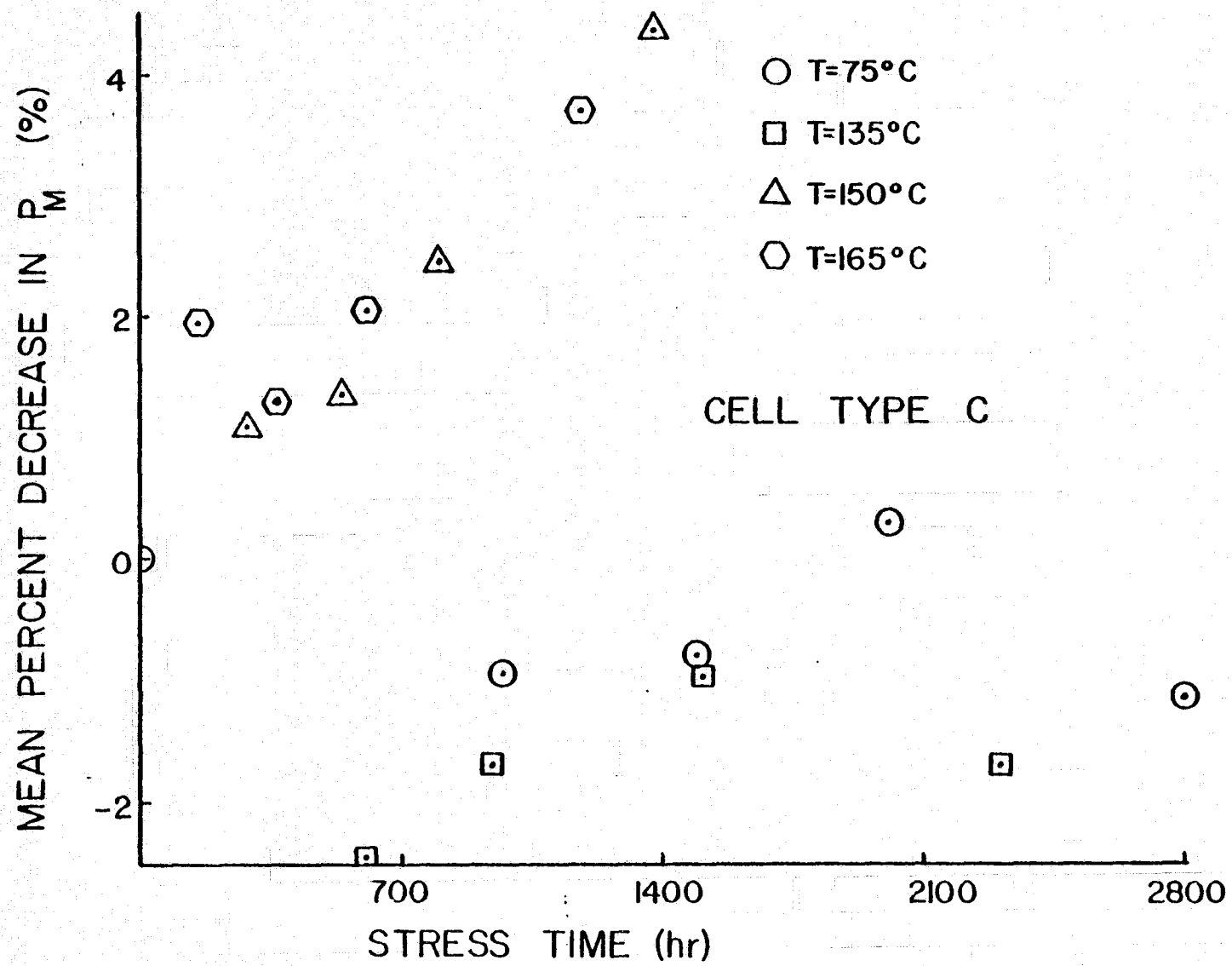

Figure 4.3.23. Mean Percent Decrease in P_m for Bias-Temperature Stress Test, Type C Cells.

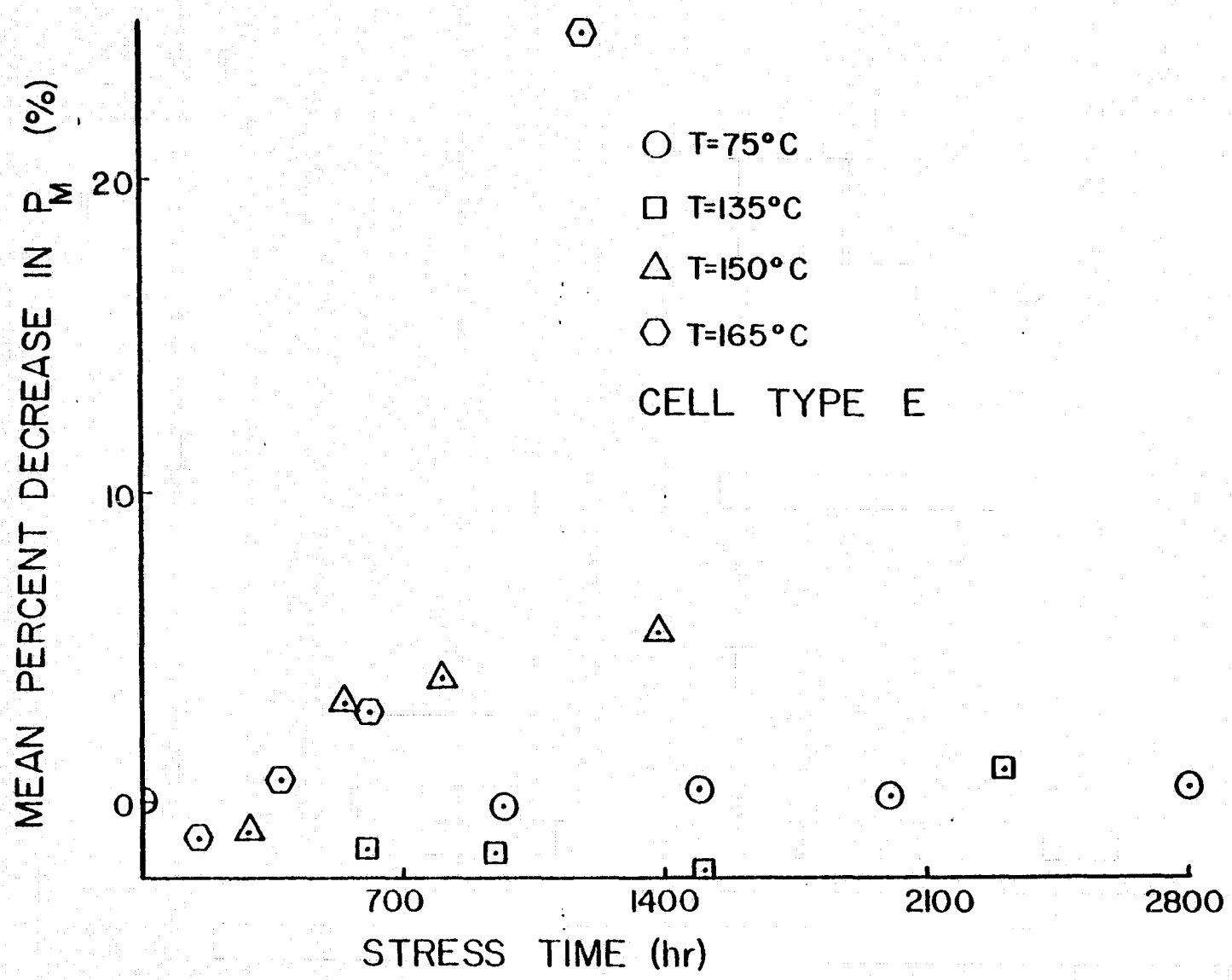

Figure 4.3.24. Mean Percent Decrease in P_m for Bias-Temperature Stress Test, Type E Cells.

For the type A cells, analysis of I-V far-forward data showed that the observed degradation in P_m was due at least partially to an increase in R_s. As an example of the influence of increasing R_s on the cell I-V characteristics, Figure 4.3.25 through 4.3.27 show I-V data for a typical cell subjected to the 165°C bias-temperature stress and for a best-case and a worst-case cell. The increase in R_s with increasing stress test time is evident in all three figures. Figure 4.3.28 shows the behavior of R_s with bias-temperature stress time for a typical cell from each stress test lot. Although increase in R_s certainly accounts in large part for the observed decrease in P_m for these cells, the specific mechanism responsible for the increase has not been identified.

From earlier discussion it is clear that projections to use conditions of degradation rate due strictly to bias and temperature are not warranted by the data for three cell types. In fact, the type B cells investigated did not degrade under this stress to any detectable degree. However, data for type A cells does permit a crude extrapolation to use conditions. In order to do this it is necessary to somehow extrapolate (or interpolate) the P_m degradation data for the various tests to a common degradation level. It was noted that a plot of the cumulative mean percent degradation versus time on lognormal paper results in acceptable straight lines for three stress test temperatures, 75°C, 135°C, and 165°C. Such a plot of the data is shown in Figure 4.3.29. Note from this figure that the 75°C, 135°C, and 165°C, data is fitted by roughly parallel straight lines, while the 150°C test data appears to be anomalous. Other types of plots of the raw data were made and in every case the 150°C data did not fit the pattern exhibited by the data from the other three tests. The 150°C stress

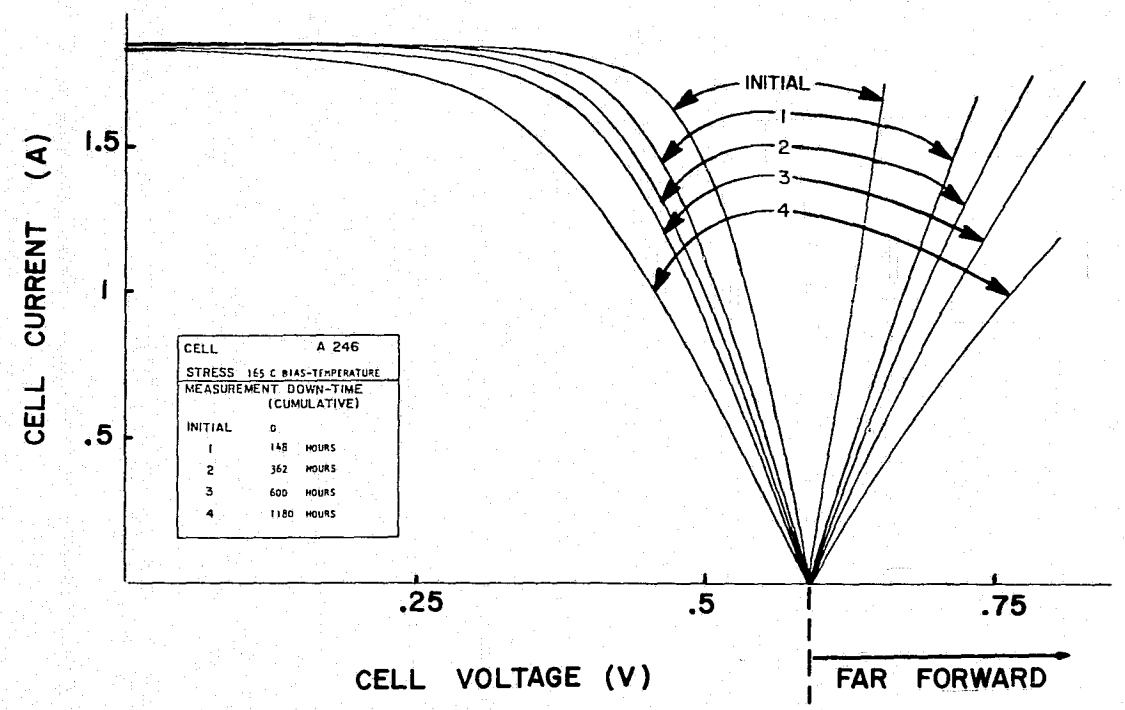

Figure 4.3.25. Type A Cell I-V Characteristics After 165°C B-T Stress, Typical Case.

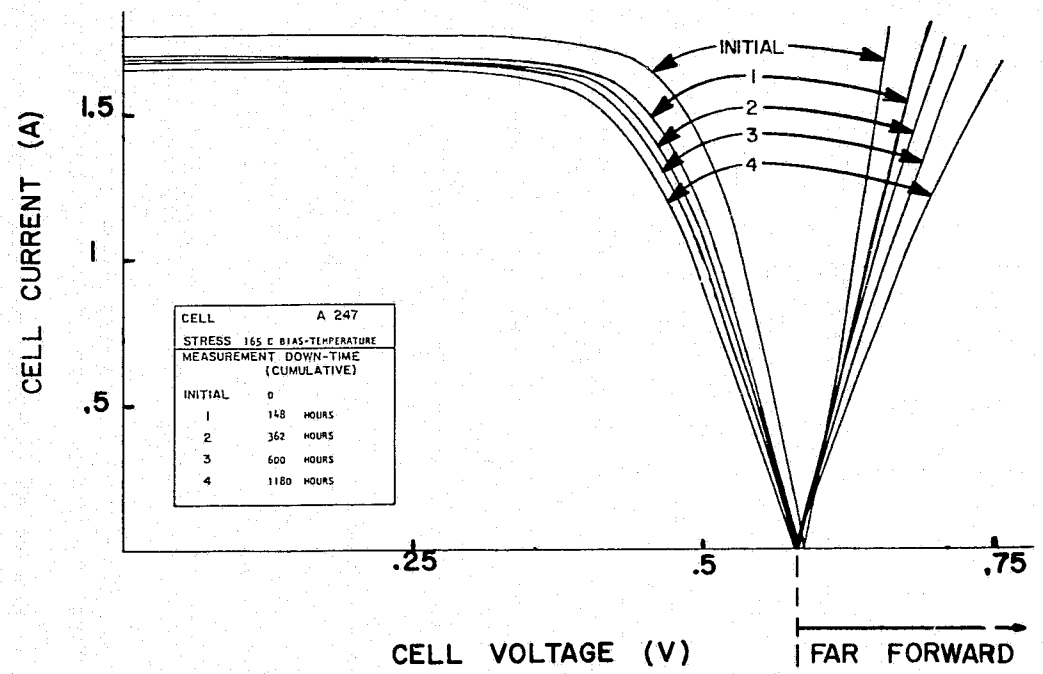

Figure 4.3.26. Type A Cell I-V Characteristics After 165°C B-T Stress, Best Case.

REPRODUCIBILITY OF THE ORIGINAL PAGE IS POOR

144 INTENTIONALLY BLANK

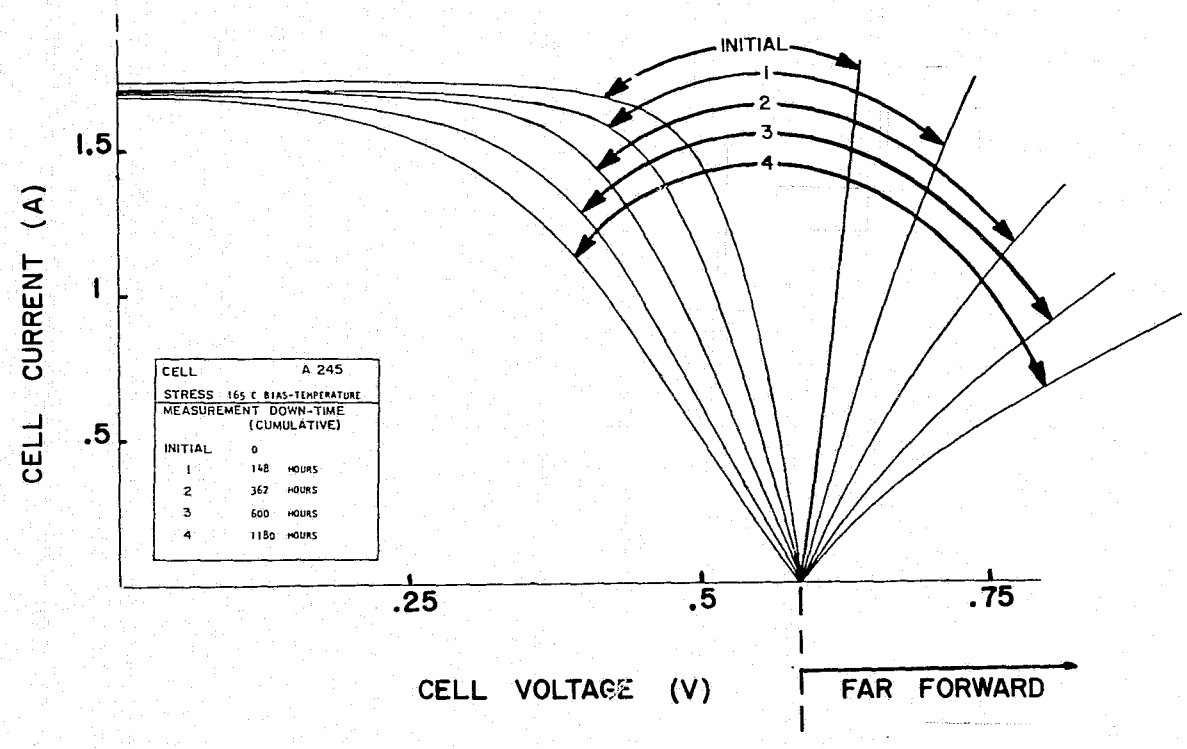

Figure 4.3.27. Type A Cell I-V Characteristics After 165°C B-T Stress, Worst Case.

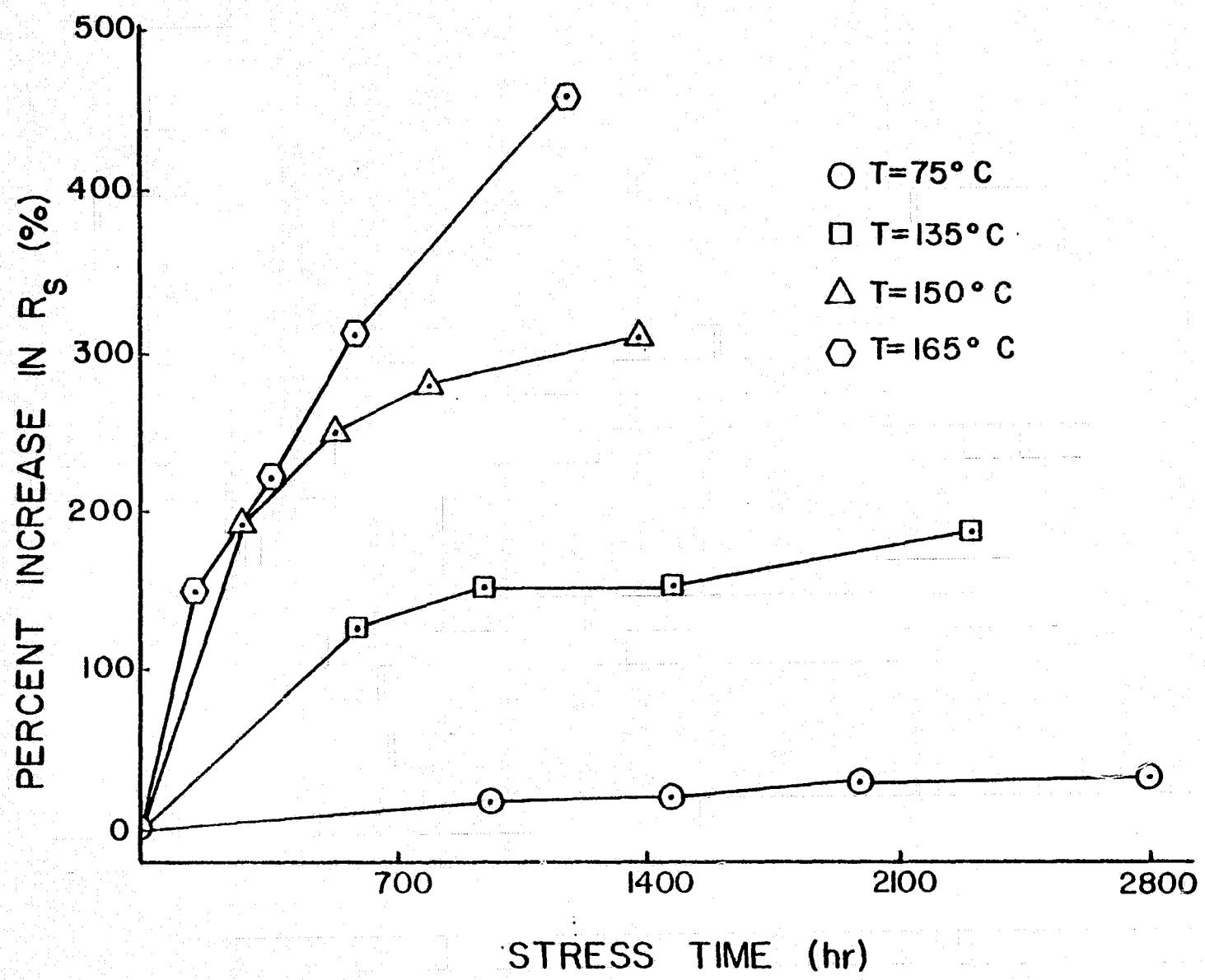

Figure 4.3.28. Behavior of R_s with B-T Stress Time, Typical Type A Cells.

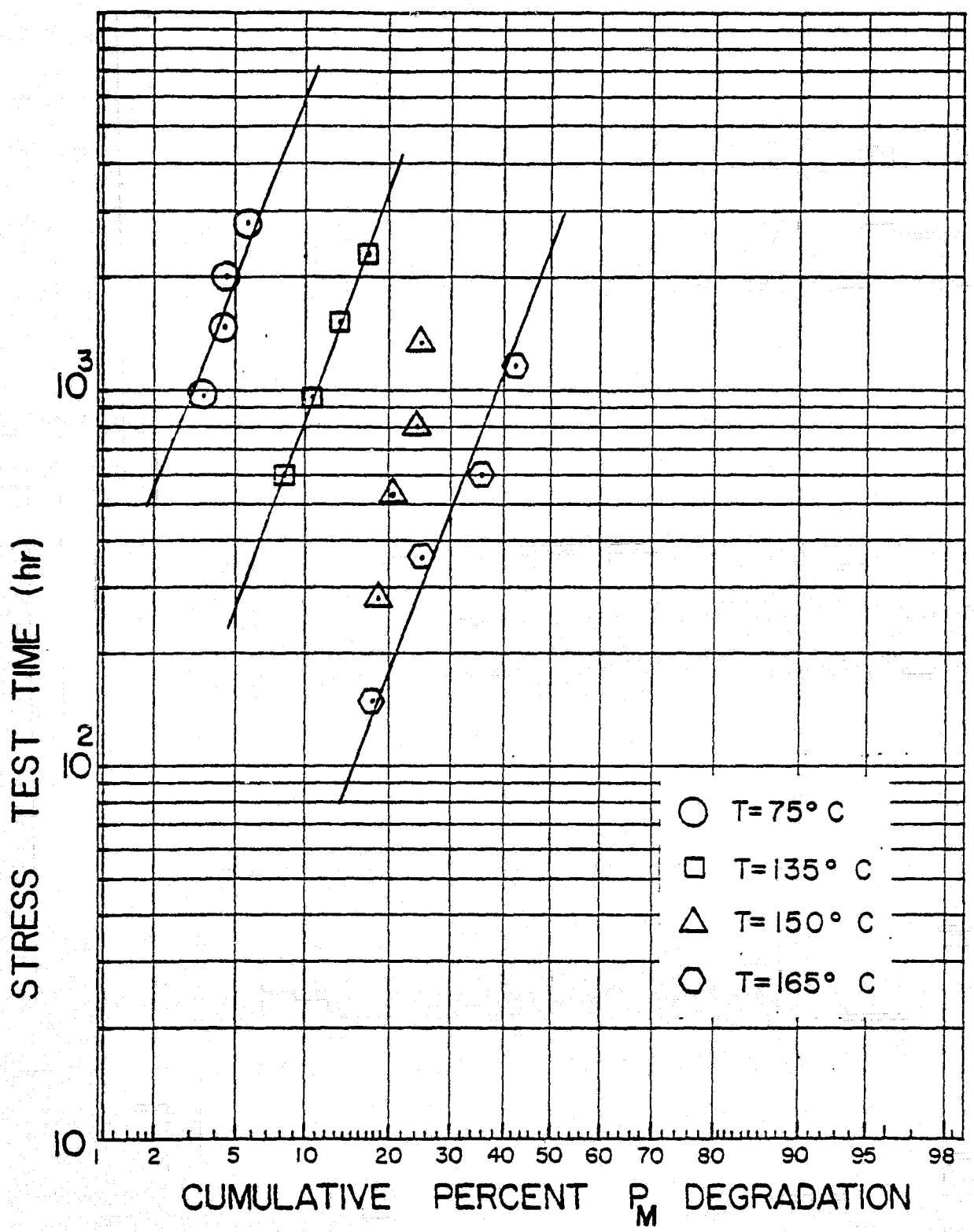

Figure 4.3.29. Cummulative Mean Percent P_m Degradation Versus Bias-Temperature Stress Time, Lognormal Scale.

test data was thus ignored in subsequent analyses. Figure 4.3.30 shows the behavior of the time to 10% P_m degradation versus inverse absolute stress test temperature, for type A cells. In this figure are shown two straight line fits to the three data points. Line A was obtained ignoring the 165°C stress test data altogether, and is attributable to a mechanism having an activation energy of slightly greater than 0.4 eV. Line B was obtained taking into account all three data points. Although "fitting" a straight line to three data points such as shown in the figure might seem presumptuous, it is of course commonly done in reliability work. Line B is describable by a mechanism having activation energy in the neighborhood of 0.6 eV. Extrapolation of the two lines to 50°C results in a range of 2×10^4 hr to 7×10^4 hr (2 to 10 years) as an estimate of the time to 10% degradation for type A cells at that temperature.

Although the analysis above was done in order to obtain some information on use-condition degradation rates due strictly to current and temperature, the data clearly does not warrant a literal interpretation of the results of the extrapolation. Far more data will be required before definite "life" prediction can be done for these or any other cell types. What the data absolutely does show is that the cells do exhibit definite P_m degradation under the stress test conditions even at relatively low temperatures, and that this degradation is associated with an increase in R_s. The analysis performed to date does not give insight into the responsible mechanisms.

A physical effect common to all cell types was discoloration of collector and grid metalization and back metalization. The degree of discoloration observed varied between cell types, as of course did the

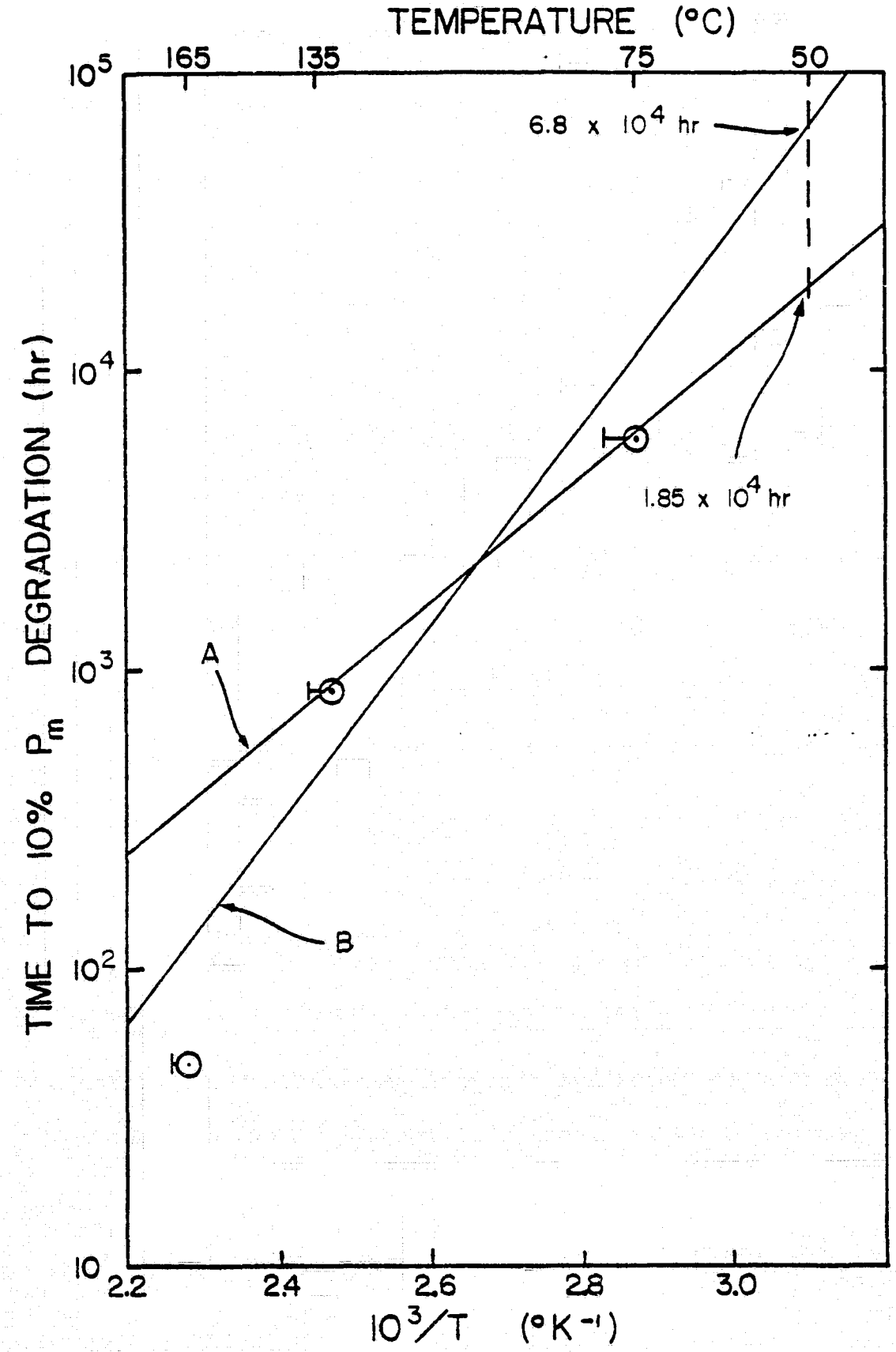

Figure 4.3.30. Behavior of Time to 10% Degradation versus Inverse Temperature, Type A Bias-Temperature Stress Test Lots.

metalization type, but appeared to be most severe on type B and E (silver-metalized) cells. Colors observed ranged from dull gold to brownish-green and reddish-brown, with many shades in between. Interestingly, definite patterns were observed on the back metal of the types B and E cells. The backs of type B cells showed a rectangular grid of circles approximately 3/16" in diameter at the second and subsequent down-times, while the type E cells showed discoloration in the pattern of the collector metalization at the last down-time (but not before). The "circle pattern" was also observed on type B units subjected to power cycle stress.

Other physical effects, such as minor bubbling of the collector metalization and partial failure of the AR coating for type B cells, were noted for various cell types at various points in the tests. However, the solder-metalized cells showed a common effect, that of hollow bubble formation in both front and back metal. The bubbles observed were common, occurring either on front metal or back metal or both in practically every cell of these two types tested, and in many cases were fairly large (1/16" diameter). Type A cells exhibited collector and grid bubbles to a larger extent than did type C cells. These bubbles occurred least frequently (30% of the stress tested cells) in the 75°C test lot. In most cases the bubbles for both cell types had appeared at the second down-time and little increase in the number of cells affected was noted between the second and fourth down-times. An exception to this was the occurrence of bubbles on the backs of type A cells. The mechanism responsible for bubble formation, and the significance of their occurrence, is not clear. However, collector bubbles may be connected with the increase of R_s observed for type A cells.

4.4 Bias-Temperature-Humidity Stress Testing

PAGE 152 INTENTIONALLY BLANK

PRECEDING PAGE BLANK NOT FILMED

4.4.1 Stress Test Conditions and Experiment Design

Bias-Temperature-Humidity (B-T-H) stress tests were performed in order to determine the sensitivity of solar cells to degradation which is accelerated by combinations of electrical bias, high humidity, and temperature. Degradation mechanisms which could be accelerated by these factors include corrosion of the metalization system, with resultant increase in R_s or decrease of metal adherence strength, and electroplating of one or more components of the metalization system, with resultant decrease of R_{SH} and/or increase in R_s. This type of stress test was considered a key test in that cells in field deployment will almost certainly eventually be subjected to the presence of moisture. The use of most encapsulation techniques currently under consideration for terrestrial modules will simply delay rather than prevent the ingress of moisture.

In considering alternatives for stress test conditions it was soon realized that some key conditions which exist in modules could not be properly imposed during the stress tests. For example, the "contaminants" which will be given off by, and trapped within the module by, some organic encapsulants could not be easily included in the stress testing of unencapsulated cells. The nature of the "contaminants" will also change with time if the modules are eventually required to meet U.L. flammability requirements. Also, the lateral voltage gradients which can exist between adjacent cells in modules could not adequately be simulated in the tests. This lateral voltage could be of critical importance since electroplating and some corrosion mechanisms require the presence of a voltage in excess of a threshold in order to be activated.

The temperature and humidity conditions selected for the stress tests were 85°C/85% Relative Humidity, and 121°C/15 Psig steam. Bias

PAGE 154 INTENTIONALLY BLANK

conditions were approximately 0.45 V forward bias. This was chosen to simulate the cell potential for operation near the maximum power point. Minimizing cell power dissipation is very important in the conduct of both B-T-H stress tests since excessive power dissipation will lower the local relative humidity, at the cell surface. Current flow with 0.45 V forward bias was in the range 0.3A to 1A, depending on cell type.

The 85/85 test condition is as near to a semiconductor industry standard for potentially moisture sensitive devices as exists. It is not included in MIL-STD-883A. The presssure cooker test condition is one which has semiconductor industry proponents, on the basis of even higher acceleration factor than that for the 85/85 test. Note that neither test involves cycling the test units through the dew point. Dew point operation is certainly encountered in the field, and is a possibility for inclusion in future work. The acceleration rate for the two stress tests, relative to field conditions, is an inexact factor. It depends, of course, on the failure mechanism which is accelerated. For aluminum-metalized integrated circuits the primary failure mechanism under biased 85/85 conditions is aluminum corrosion, and the acceleration factor is estimated to be in the range 10^4 to 10^5 for most normal use conditions. The pressure cooker accleration factor is usually taken to be more than an order of magnitude greater than that of the 85/85 test. Note that if an acceleration factor is to be firmly established for terrestrial solar cells, stress tests using combinations of humidity and temperature different from the 85/85 test should be performed.

Both Phase I experiments and large-quantity stress tests were designed assuming an acceleration factor of 10^4 for 85/85 tests, and 10^5 for pressure cooker stress tests. A median-time-to-failure of 10^7hr was also

assumed. Sample sizes were chosen for the large-quantity testing keeping in mind test chamber capacity. Tables 4.4.1 and 4.4.2 show the resulting stress test schedules. Results from the Phase I experiments were of course intended for use in choosing initial down-times for the larger quantity tests, and to assure that no unexpectedly rapid degradation would be encountered.

4.4.2 Bias-Temperature-Humidity Stress Tests Results

Initial bias-temperature-humidity stress test experimentation was performed using the schedules discussed in Section 4.4.1. Table 4.4.3 and 4.4.4 show the resulting decrease in P_m observed for the biased 85/85 test and the biased pressure cooker experiments respectively. In addition to the effects of stress on P_m, some physical effects were also noticed. These included the formation of bubbles in the solder of the collectors and, rarely, grids of type A cells and color changes in the AR coating of type C cells, particularly for the pressure cooker experiments. Analysis showed that for type C cells the 6% decrease in P_m shown in Table 4.4.2 was accompanied by a 6% decrease in I_{sc}, presumably caused by the degradation of the AR coating.

From results of this experimentation initial electrical measurement and inspection down times were chosen. Subsequent down-times were selected considering both the results obtained at earlier down-times and electrical measurement capacity. Table 4.4.5 shows actual down-times for the biased 85/85 and pressure cooker stress tests. Figures 4.4.1 through 4.4.8 show observed behavior of the stress test lot P_m distribution and the lot mean P_m (relative to the prestress P_m value; called "Standardized P_m") for all cell types and all B-T-H stress tests. The distribution plots shown in these figures coupled with the lot mean P_m graphs allow estimates of the behavior of both the mean and the dispersion of the stress tests lots with

Stress Test	Sample Size per Type	Down Time (hr)
85/85	5	3,30,100
Pressure Cooker	5	1,3,10,20,50,100

Table 4.4.1 Sample Size and Down-Time for Phase I Experiments, B-T-H Stress

Stress Test	Initial Sample Size per type	Test Duration (hr)
85/85	25	1000
Pressure Cooker	20	300

Table 4.4.2 Sample Size and Test Duration, Large-Quantity Tests, B-T-H Stress

Cell Type	P_m Initial	P_m 3 hr	P_m 20 hr	P_m 100 hr
A	0.678	0.689	0.683	-
B	0.545	0.545	0.555	0.553
C	0.258	0.251	0.248	0.242
E	0.440	0.449	0.447	0.433

Table 4.4.3. Mean Values of P_m (W) for Biased Pressure cooker Experiments.

Cell Type	P_m Initial	P_m 3 hr	P_m 20 hr	P_m 100 hr
A	0.690	0.707	0.703	0.699
B	0.527	0.529	0.528	0.535
C	0.259	0.257	0.250	0.252
E	0.435	0.440	0.436	0.434

Table 4.4.4. Mean Values of P_m (W) for Biased 85°C/85% Relative Humidity Experiments.

Stress Test	First Down-Time (hr)	Second Down-Time (hr)	Third Down-Time (hr)
Biased 85/85	215	525	1025
Pressure Cooker, Type A	96	288	
Pressure Cooker, Type B	132	337	
Pressure Cooker, Type C	76	286	
Pressure Cooker, Type E	100	306	

Table 4.4.5. Down-Times for Bias-Temperature-Humidity Stress Tests.

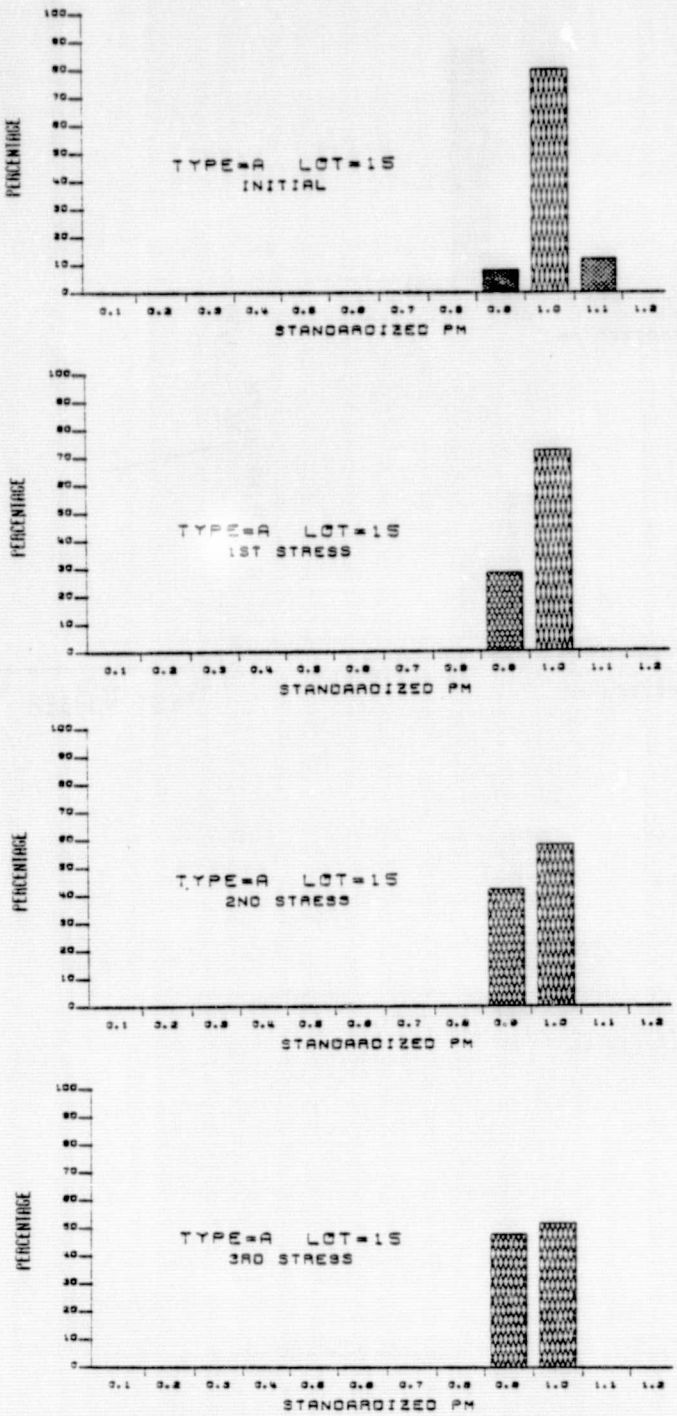

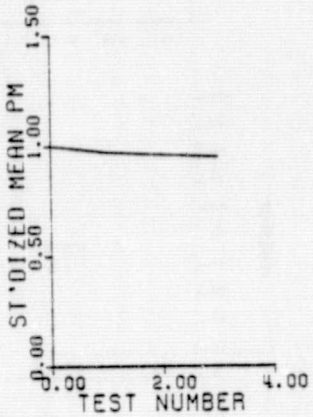

CELL TYPE	A	
STRESS	BIAS-TEMP-HUMIDITY 85/85	
MEASUREMENT	DOWN-TIME (CUMULATIVE)	
INITIAL	0	
1	215	HOURS
2	525	HOURS
3	1025	HOURS

Figure 4.4.1. Behavior of P_m Distribution and Lot Mean P_m with Biased 85°C/85% R.H. Stress, Type A Cells.

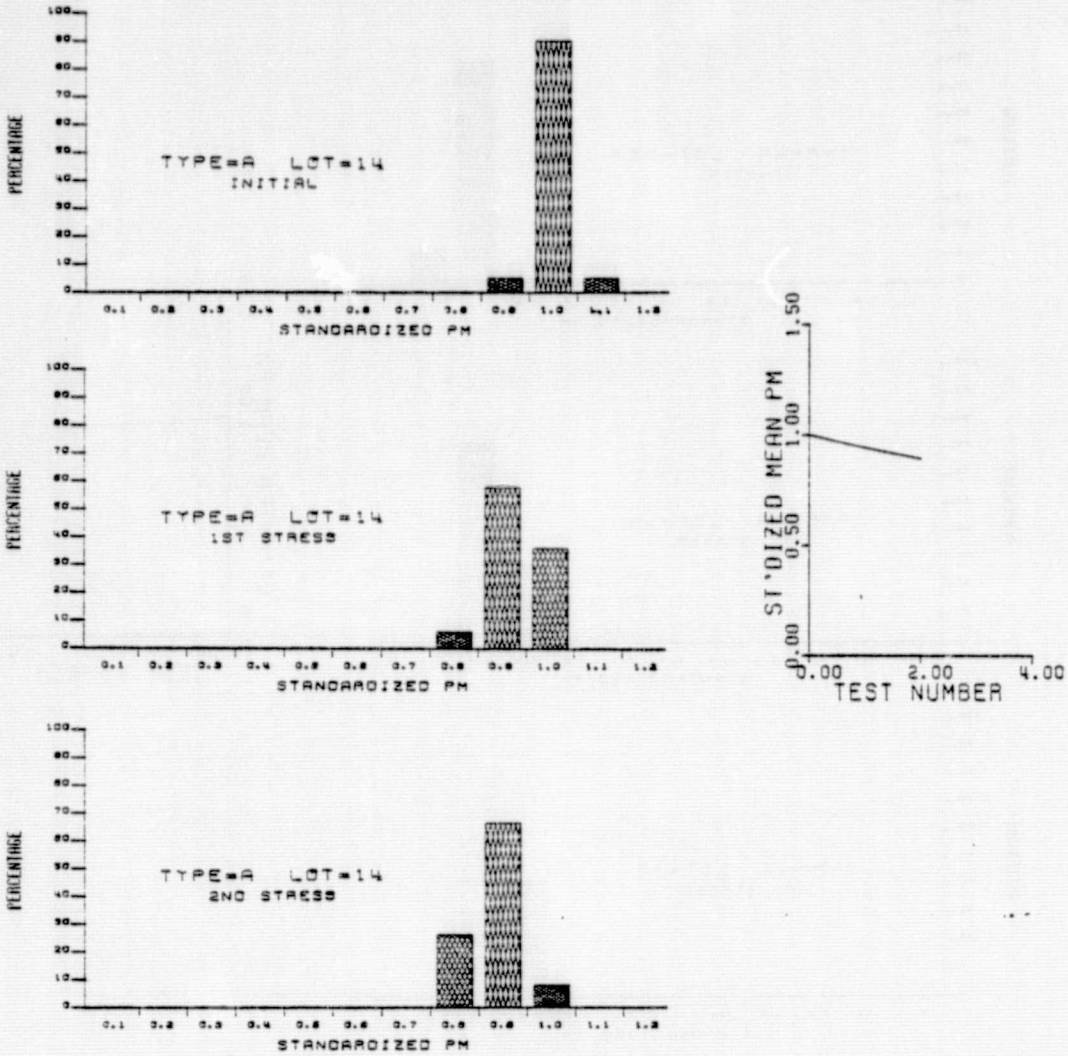

CELL TYPE	A	
STRESS	B-T-H PRESSURE COOKER	
MEASUREMENT	DOWN-TIME (CUMULATIVE)	
INITIAL	0	
1	96	HOURS
2	288	HOURS

Figure 4.4.2. Behavior of P_m Distribution and Lot Mean P_m with Biased 121°C/15 Psig Steam Stress, Type A Cells.

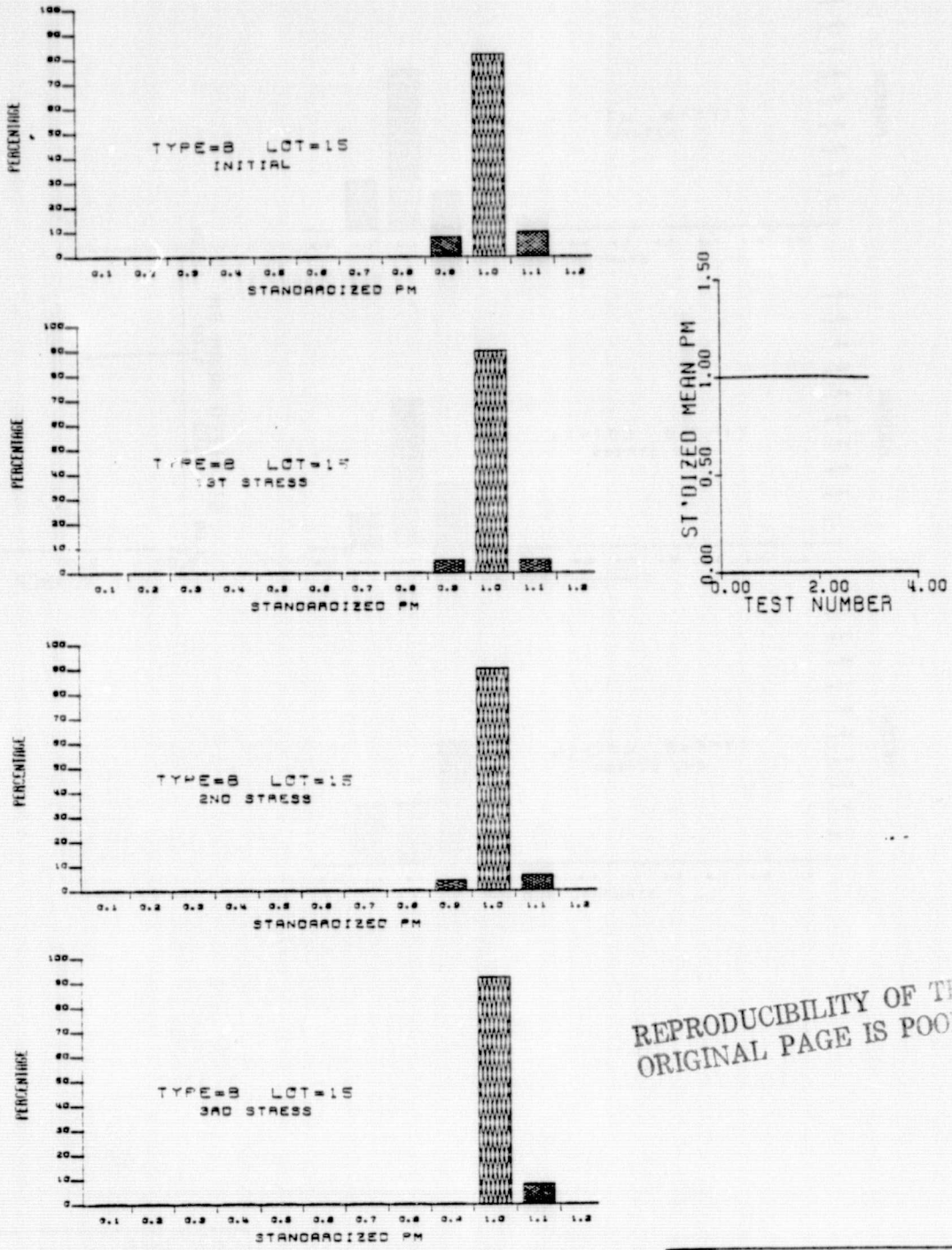

REPRODUCIBILITY OF THE ORIGINAL PAGE IS POOR

CELL TYPE	B
STRESS	BIAS-TEMP-HUMIDITY 85/85
MEASUREMENT	DOWN-TIME (CUMULATIVE)
INITIAL	0
1	215 HOURS
2	525 HOURS
3	1025 HOURS

Figure 4.4.3. Behavior of P_m Distribution and Lot Mean P_m with Biased 85°C/85% R.H. Stress, Type B Cells.

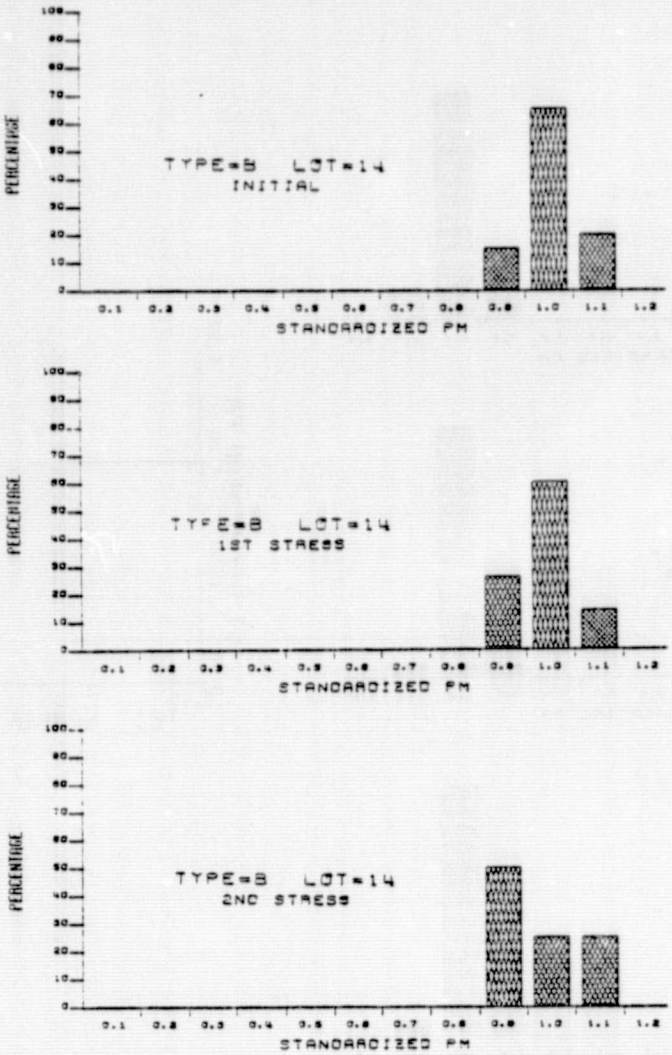

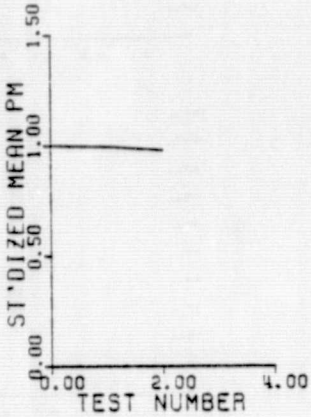

CELL TYPE	B	
STRESS	8-T-H PRESSURE COOKER	
MEASUREMENT	DOWN-TIME (CUMULATIVE)	
INITIAL	0	
1	132	HOURS
2	337	HOURS

Figure 4.4.4. Behavior of P_m Distribution and Lot Mean P_m with Biased 121°C/15 Psig Steam Stress, Type B Cells.

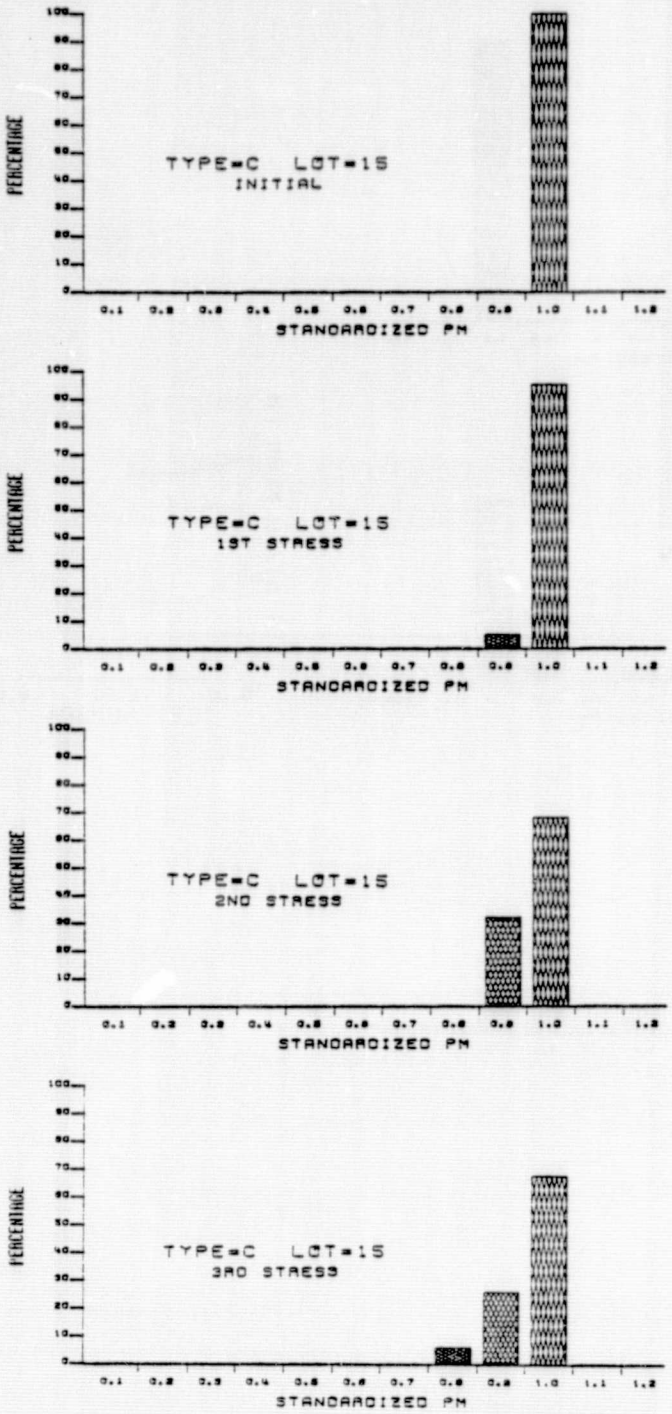

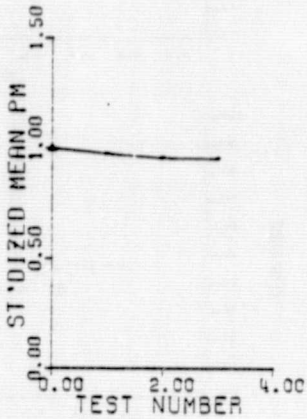

REPRODUCIBILITY OF THE
ORIGINAL PAGE IS POOR

CELL TYPE	C	
STRESS	BIAS-TEMP-HUMIDITY 85/85	
MEASUREMENT	DOWN-TIME (CUMULATIVE)	
INITIAL	0	
1	215	HOURS
2	525	HOURS
3	1025	HOURS

Figure 4.4.5. Behavior of P_m Distribution and Lot Mean P_m with Biased 85°C/85% R.H. Stress, Type C Cells.

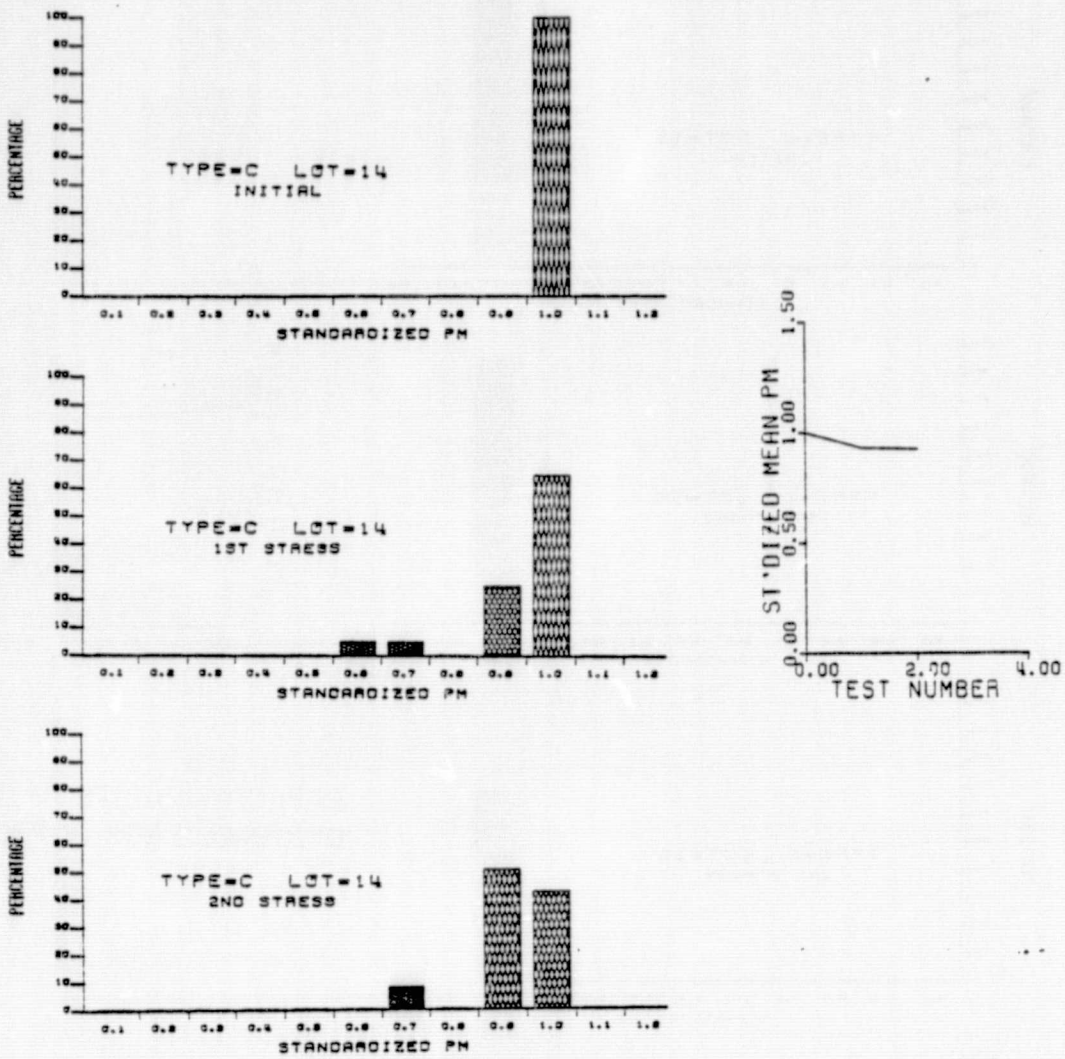

CELL TYPE	C	
STRESS	B-T-H PRESSURE COOKER	
MEASUREMENT	DOWN-TIME (CUMULATIVE)	
INITIAL	0	
1	96	HOURS
2	286	HOURS

Figure 4.4.6. Behavior of P_m Distribution and Lot Mean P_m with Biased 121°C/15 Psig Steam Stress, Type C Cells.

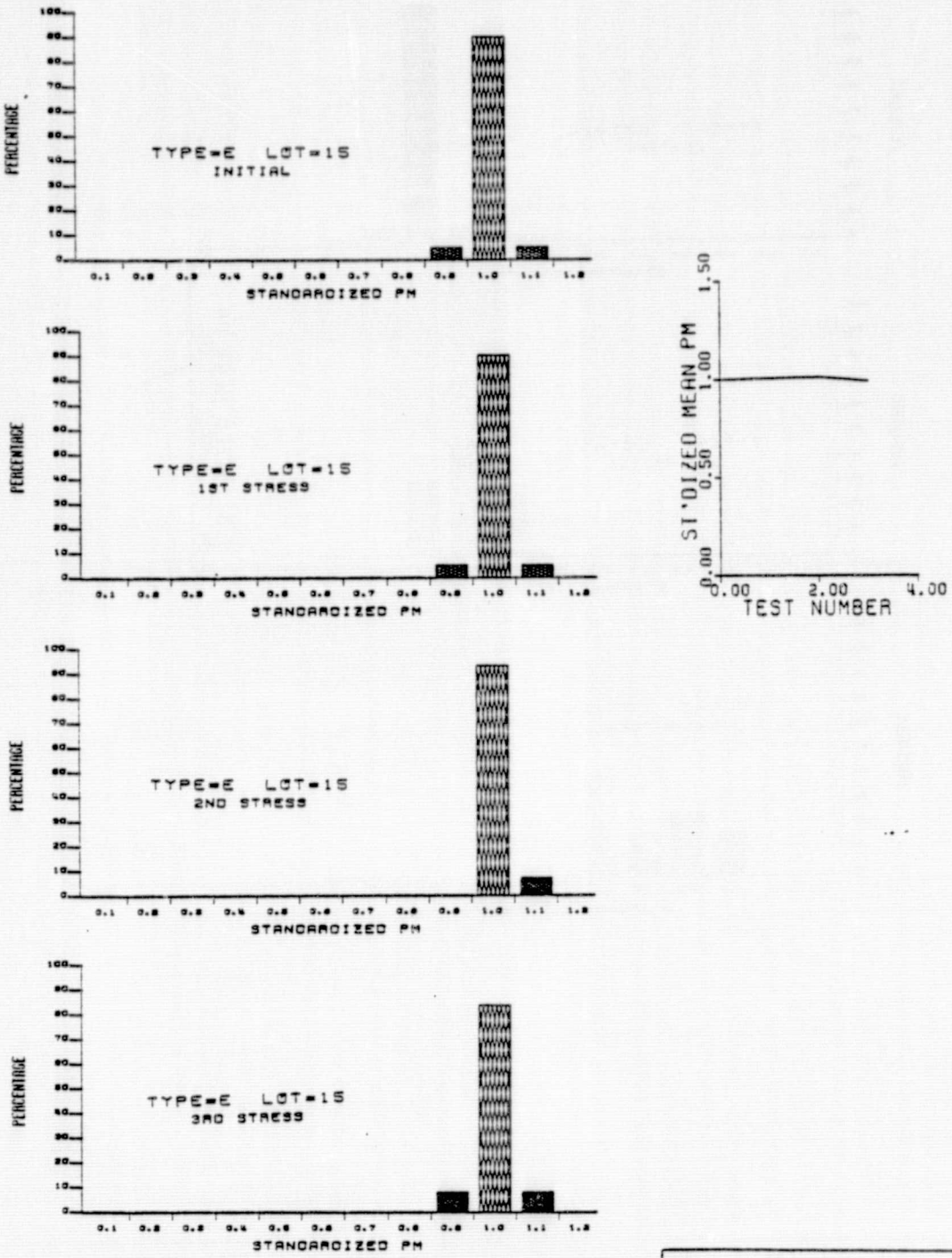

CELL TYPE	E
STRESS	BIAS-TEMP-HUMIDITY 85/85
MEASUREMENT DOWN-TIME (CUMULATIVE)	
INITIAL	0
1	215 HOURS
2	525 HOURS
3	1025 HOURS

Figure 4.4.7. Behavior of P_m Distribution and Lot Mean P_m with Biased 85°C/85% R.H. Stress, Type E Cells.

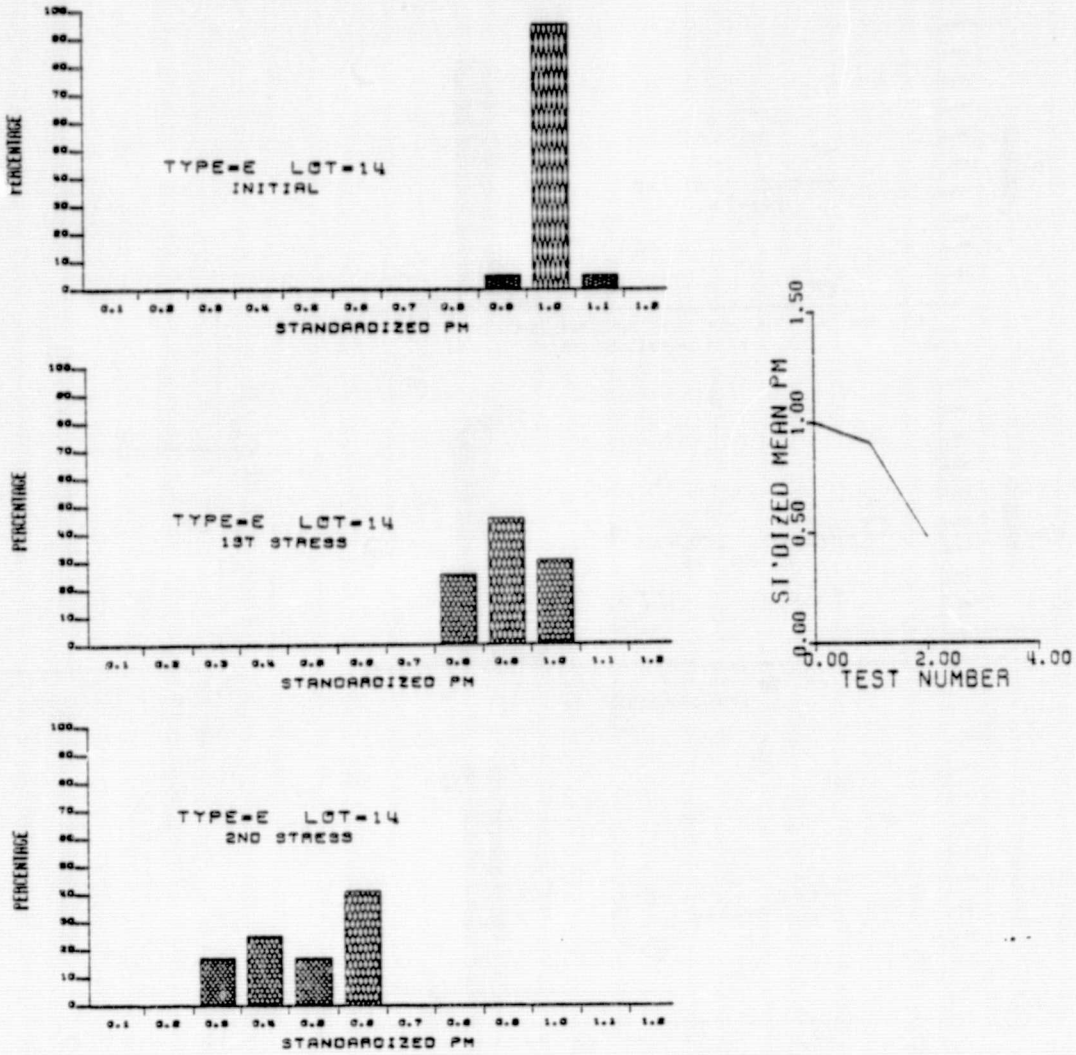

CELL TYPE	E	
STRESS	B-T-H PRESSURE COOKER	
MEASUREMENT	DOWN-TIME (CUMULATIVE)	
INITIAL	0	
1	100	HOURS
2	306	HOURS

Figure 4.4.8. Behavior of P_m Distribution and Lot Mean P_m with Biased 121°C/15 Psig Steam Stress, Type E Cells.

stress. Figure 4.4.9 and 4.4.10 show the cell P_m response in somewhat more detail. In these figures the mean percent decrease in P_m for the test population is plotted versus stress test time. Note that after the first down-time eight cells per type were removed for each stress test for contact integrity testing.

From data presented in the preceding ten figures it is clear that type B cells showed the least degradation in P_m under both types of B-T-H stress testing (approximately zero effect for 85/85 stress and only minor effect for pressure cooker stress) and that type E cells showed relatively severe P_m degradation in the pressure cooker stress test. However, type E cells did not show significant P_m degradation in the 85/85 stress test. The source of this difference in response of type E cells is not clear. Difficulty was experienced with the bias cabling inside the pressure cable during the first stress period for type E cells (only one cell type was stressed at a time in the pressure vessel.) The insulation on the cabling was attacked by steam. The wiring was replaced and other cell types were subsequently stressed in the same pressure vessel. Since rapid decrease in P_m was noted at the second down-time and not at the first down-time for type E cells, it is assumed that deleterious contamination of the type E test lot did not occur due to the wiring problem. Distortion of the I-V plot was so severe for the pressure cooker-stressed type E cells at the second down-time that straightforward interpretation of the results to determine the source of the degradation was not possible. By analogy to the I-V plots of the type A cells which showed similarly severe P_m degradation under B-T stress, due to R_s increase, it would appear that R_{sh} of the type E cells decreased thereby causing the decrease in P_m. However, firm conclusions in this regard must be delayed until further analysis is performed. Type A and type C cells

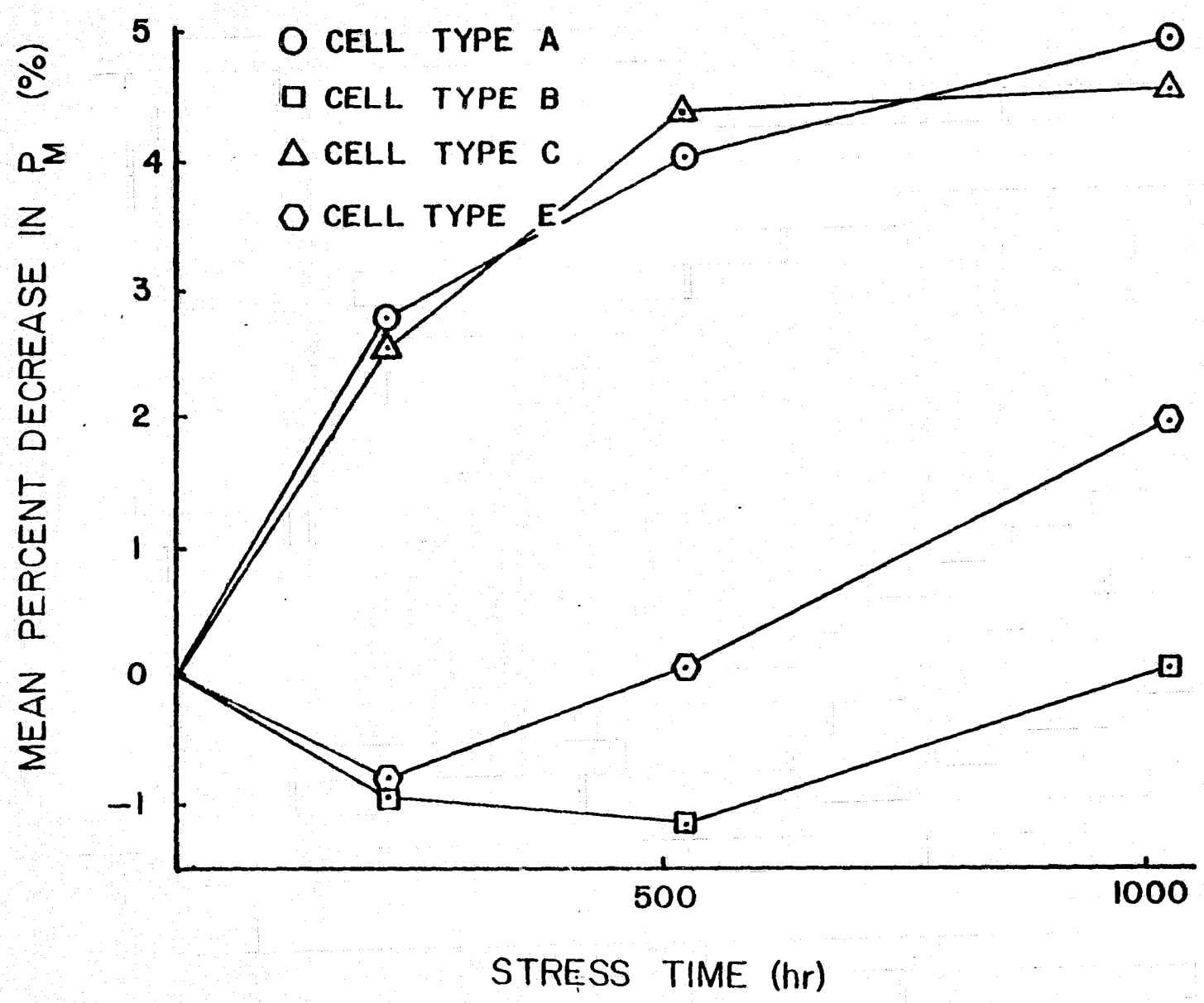

Figure 4.4.9. Mean Percent Decrease in P_m versus Stress Time, 85°C/85% R.H. Test.

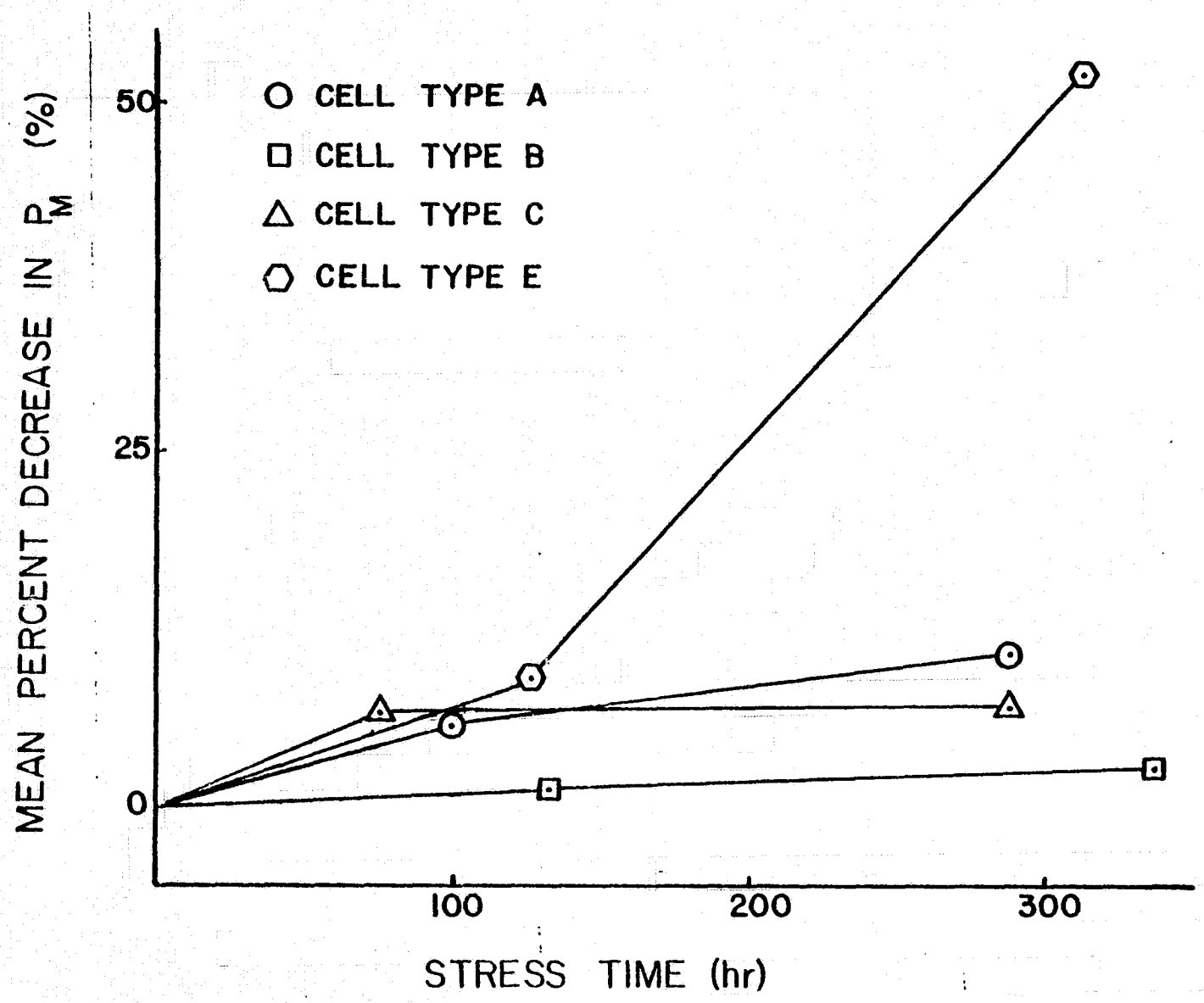

Figure 4.4.10. Mean Percent Decrease in P_m versus Stress Time, 121°C/15 Psig Steam Test

showed definite, but less severe P_m degradation in the pressure cooker stress test. The P_m degradation for these two types was more severe than for the type E cells in the 85/85 test. For type C cells the source of the P_m degradation in both stress test lots can be traced to decrease in I_{sc} due to degradation of the AR coating. This same effect was noted during the phase I experiments for type C cells. Table 4.4.6 shows the mean percent decrease in P_m and in I_{sc} for the two type C B-T-H test lots. The correlatio in degradation of the two parameters is obvious, and the nature of the deg dation correlates with the physical appearance of the cells after stress testing. The source of the decrease in P_m of the type A cells has not y been identified positively, but is probably an increase in series resistan similar to that which was discussed in Section 4.3.2 for type A cells subjected to bias-temperature stress testing. This is plausible since the temperatures were similar, the degree of degradation in P_m was similar, solder bubbles were manifested in both B-T and pressure cooker B-T-H stres tested units. Thus the degradation in P_m for type A cells resulting fro B-T-H stress may well be due strictly to temperature effects, and possibly bias effects, and not to humidity stress.

Two of the more striking physical effects observed, attack of the typ cell AR coating and solder bubbles in the collector and grid metalization the pressure cooker-stressed type A cells, have been mentioned. Bubbles w also observed in the back of type A cells in both B-T-H tests, and in both front and back metal of type C cells in both B-T-H tets. Bubbles on the backs of type A cells and on the fronts of type C cells were similar in size, barely visible to the naked eye. Bubbles on the fronts of type A cells and on the backs of type C cells were similar in size, as large as 1/16" in diameter. Since metalization bubbles were observed during B-T stress testing

	85°C/85% R.H.			121°C/15 Psig	
	215 hr	525 hr	1025 hr	76 hr	286 hr
Mean Percent Decrease in P_m (%)	2.55	4.35	4.55	7.02	7.37
Mean Percent Decrease in I_{sc} (%)	2.74	3.59	3.57	6.19	6.62

Table 4.4.6. Mean Percent Decrease in P_m and I_{sc}, versus B-T-H Stress Test Time, Type C Cells.

for both cell types, the influence of humidity on bubble formation may be negligible. Type B cells also showed evidence of some AR coating degradation in the course of pressure cooker stress testing. The degradation was severe, but was isolated to only a few units in the test lot. Type B cells also showed peeling of the back metal around the rim of the cell similar to the peeling noted in the units subjected to power cycle stress. They also showed blistering of the back metal after both B-T-H stress tests, similar to blistering noted in the case of the power cycled units. The B-T-H stressed units also exhibited clear evidence of silver electroplating around the cell rim. Type E cells showed no physical effects except discoloration. The discoloration was most severe at the second down-time of the pressure cooker stress test, when gross black deposits were observed on two of the cells in the test lot. The source and the significance of the deposits are not clear.

It is clear that the biased pressure cooker stress test produces degradation more rapidly than the biased 85/85 stress test. This tends to support the assumption that the pressure cooker test is simply an accelerated version of the 85/85 test. However, insufficient information is available at this point to say with certainty that extraneous degradation modes are not excited by the pressure cooker test. The 85/85 test is to some a more reasonable test, and it is certain that the amount of industry experience with it is much greater than for the pressure cooker test. For the foreseeable future (until sufficient data has been obtained and analyzed) it would appear that in order to obtain results in acceptable time, as a realiability monitor, for example, the biased pressure cooker stress test would be the preferred B-T-H test. For more definitive results, where test duration is not a consideration, the longer biased 85/85 test would be preferred due to its pedigree.

4.5 Power Cycle Stress Testing

Cell Type	ON Current (A)	Thermocouple Location	ON Temperature (C)	Time Constant (sec)
A	3.5	edge	39	23
A	3.5	center	41	24
B	3.5	edge	44	17
B	3.5	center	43	20
B	2.0	edge	40	17

Table 4.5.1. Thermal Time Constant of Type A and type B Cells, Ambient Temperature 35°C.

Cell Diameter (in.)	ON Current (A)
2	1.2
3	2.8
4	3.6

Table 4.5.2. ON Current for Power Cycle Stress Test.

Large-quantity stress tests used the forward current levels shown in Table 4.5.2. Other experiment conditions were the same as for the Phase I experiments. Quantities of 25 cells per type were used in the large-scale testing. Power was applied to one-half the stress test population while the other half was in the OFF half-cycle, in order to minimize temperature excursions and reduce requirements on the power source.

4.5.2 Power Cycle Stress Test Results

Phase I experiments using 5 cells per type were conducted with one down-time, at 1470 cycles. Both electrical and physical effects of this test were minor. In fact, type A cells were observed to show an increase in lot mean P_m under the stress. This increase was small (2%) but unexpected. In spite of the small effects observed during these experiments, it was decided to proceed with the large-quantity stress testing with plans to continue it well beyond 1500 cycles. The reasons for this were a desire to see if the observed "improvement" in type A cells was repeatable, and the feeling that 1470 power cycles were perhaps too few cycles to show significant electrical or physical effects. Large-quantity stress testing was performed using 25 cells per type, with down-time at 1000, 5000, 10,000, and 25,000 cycles. Figure 4.5.1 through 4.5.4 show the observed behavior of the P_m distribution and the lot mean P_m with power cycle stress. From the data shown in these figures it is clear that no large effects on either the P_m distribution or on the lot mean P_m occurred for any cell type. Figure 4.5.5 shows the behavior of the mean percent decrease in P_m versus the number of power cycles. From this figure it is clear that the maximum mean percent change in P_m was approximately 2%, with two cell types showing improvement and two types

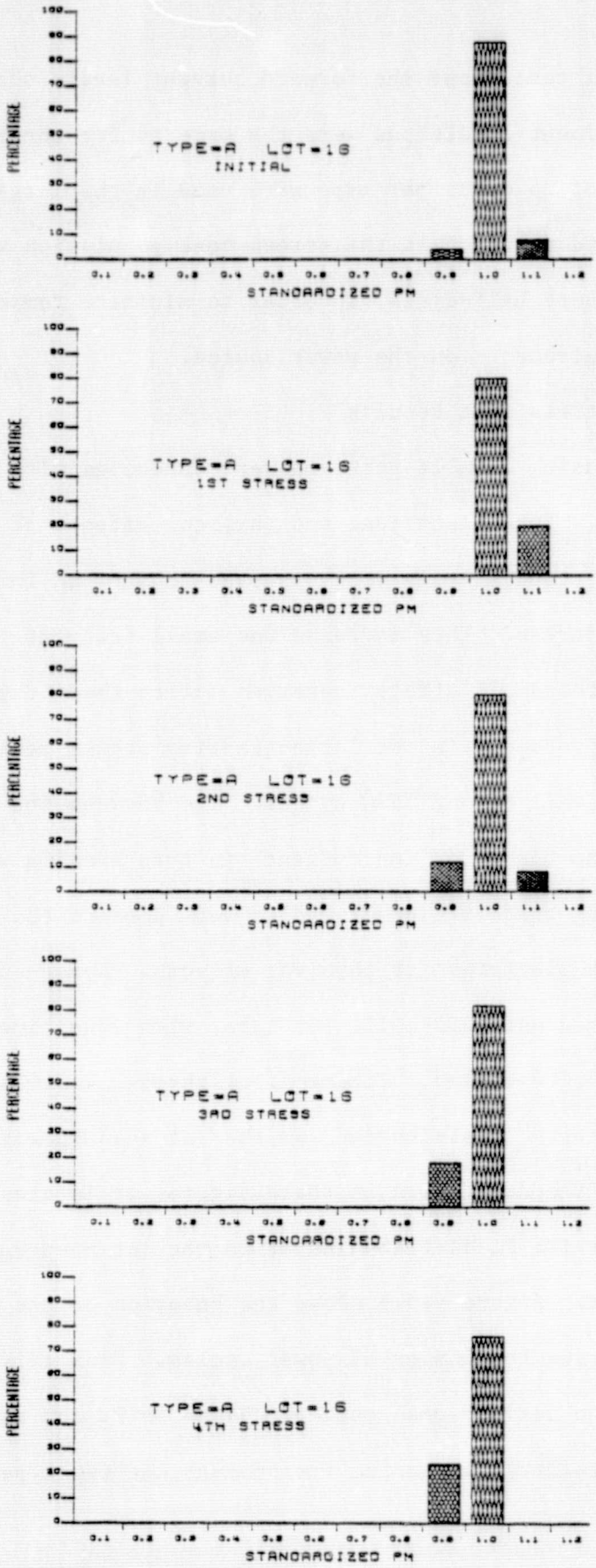

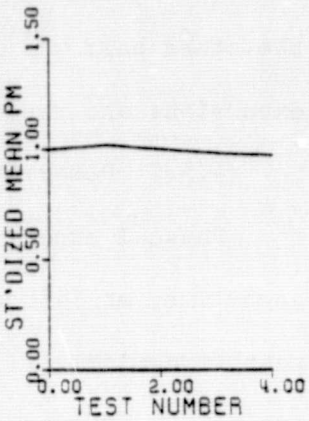

CELL TYPE	A
STRESS	POWER CYCLE
MEASUREMENT	DOWN-TIME (CUMULATIVE)
INITIAL	0
1	1034 CYCLES
2	5000 CYCLES
3	10000 CYCLES
4	26560 CYCLES

Figure 4.5.1. Behavior of P_m Distribution and Lot Mean P_m with Power Cycle Stress, Type A Cells.

REPRODUCIBILITY OF THE
ORIGINAL PAGE IS POOR

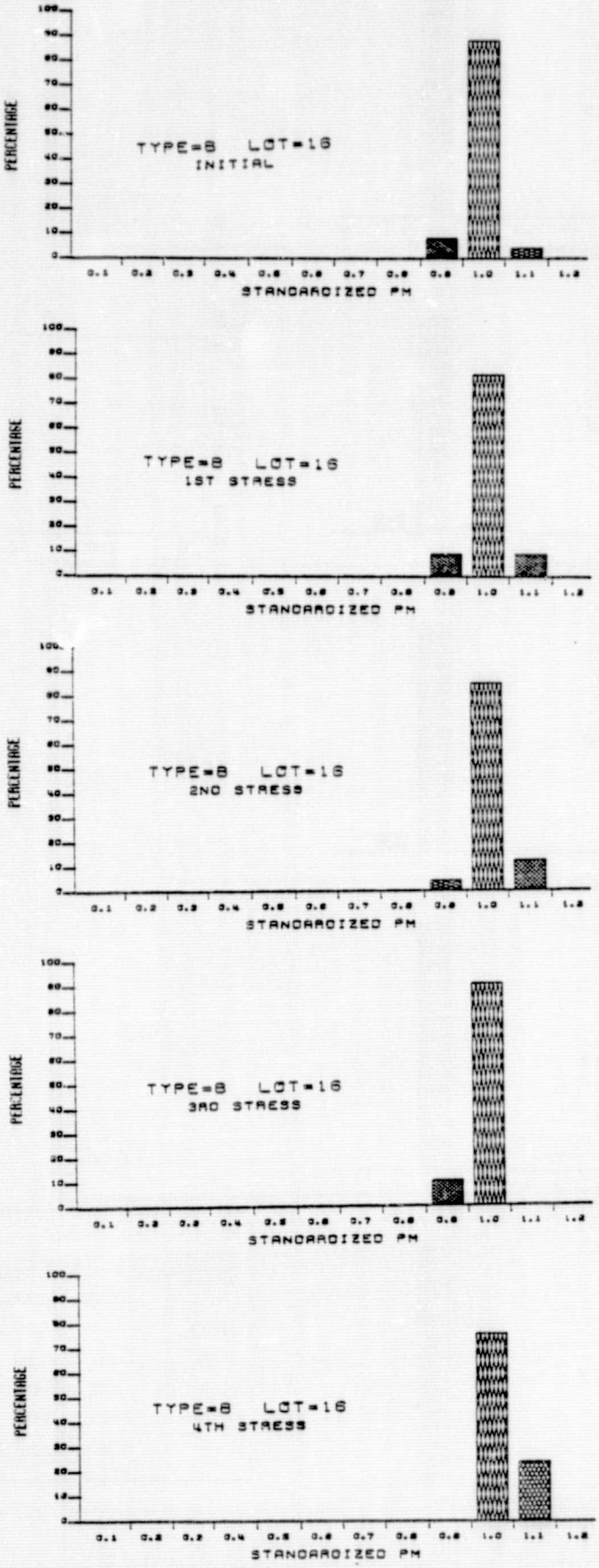

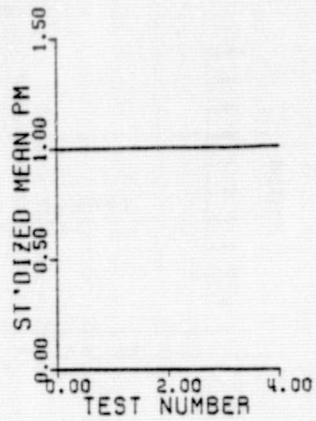

CELL TYPE	B
STRESS	POWER CYCLE
MEASUREMENT	DOWN-TIME (CUMULATIVE)
INITIAL	0
1	1034 CYCLES
2	5000 CYCLES
3	10000 CYCLES
4	26560 CYCLES

Figure 4.5.2. Behavior of P_m Distribution and Lot Mean P_m with Power Cycle Stress, Type B Cells.

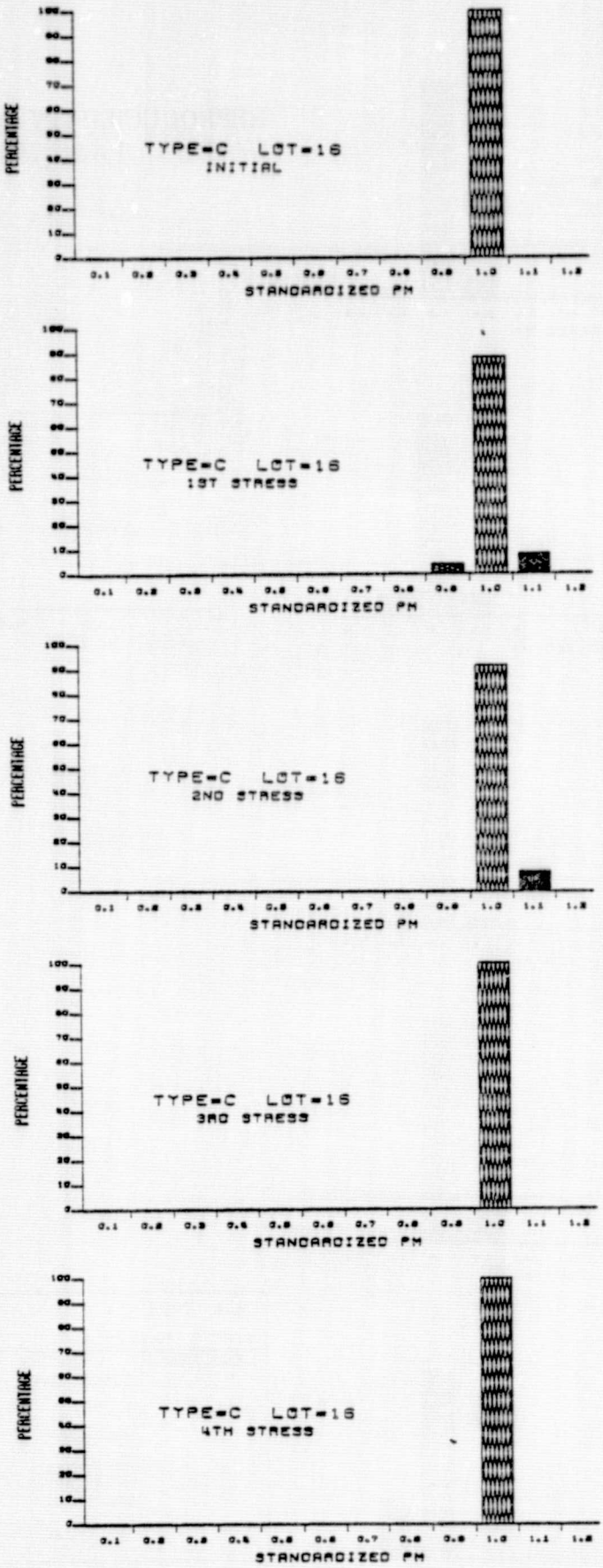

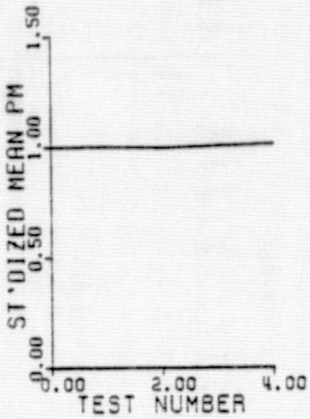

CELL TYPE	C
STRESS	POWER CYCLE
MEASUREMENT	DOWN-TIME (CUMULATIVE)
INITIAL	0
1	1034 CYCLES
2	5000 CYCLES
3	10000 CYCLES
4	26560 CYCLES

Figure 4.5.3. Behavior of P_m Distribution and Lot Mean P_m with Power Cycle Stress, Type C Cells.

REPRODUCIBILITY OF THE
ORIGINAL PAGE IS POOR

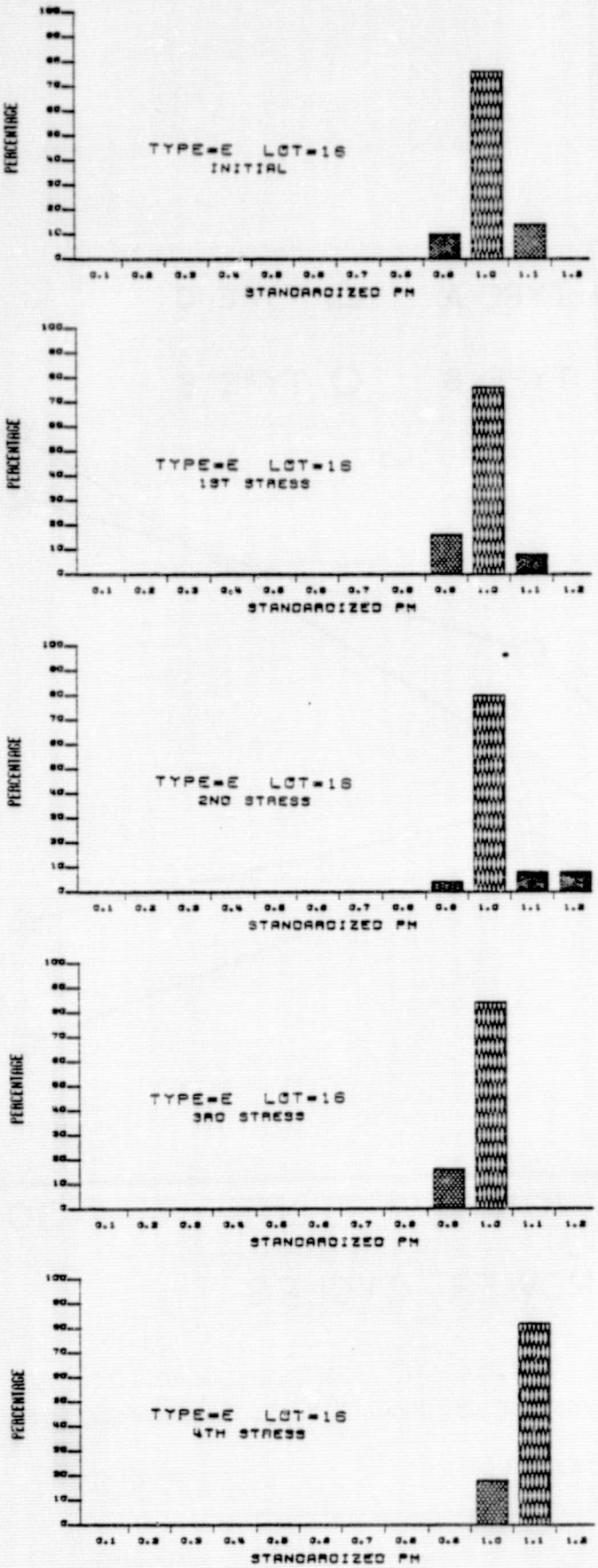

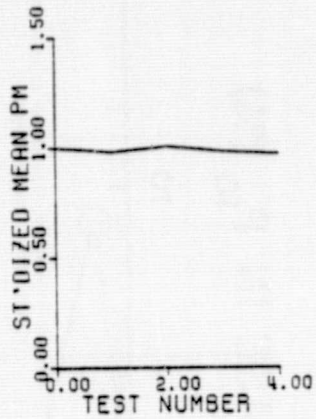

CELL TYPE	E
STRESS	POWER CYCLE
MEASUREMENT	DOWN-TIME (CUMULATIVE)
INITIAL	0
1	1034 CYCLES
2	5000 CYCLES
3	10000 CYCLES
4	26560 CYCLES

Figure 4.5.4. Behavior of P_m Distribution and Lot Mean P_m with Power Cycle Stress, Type E Cells.

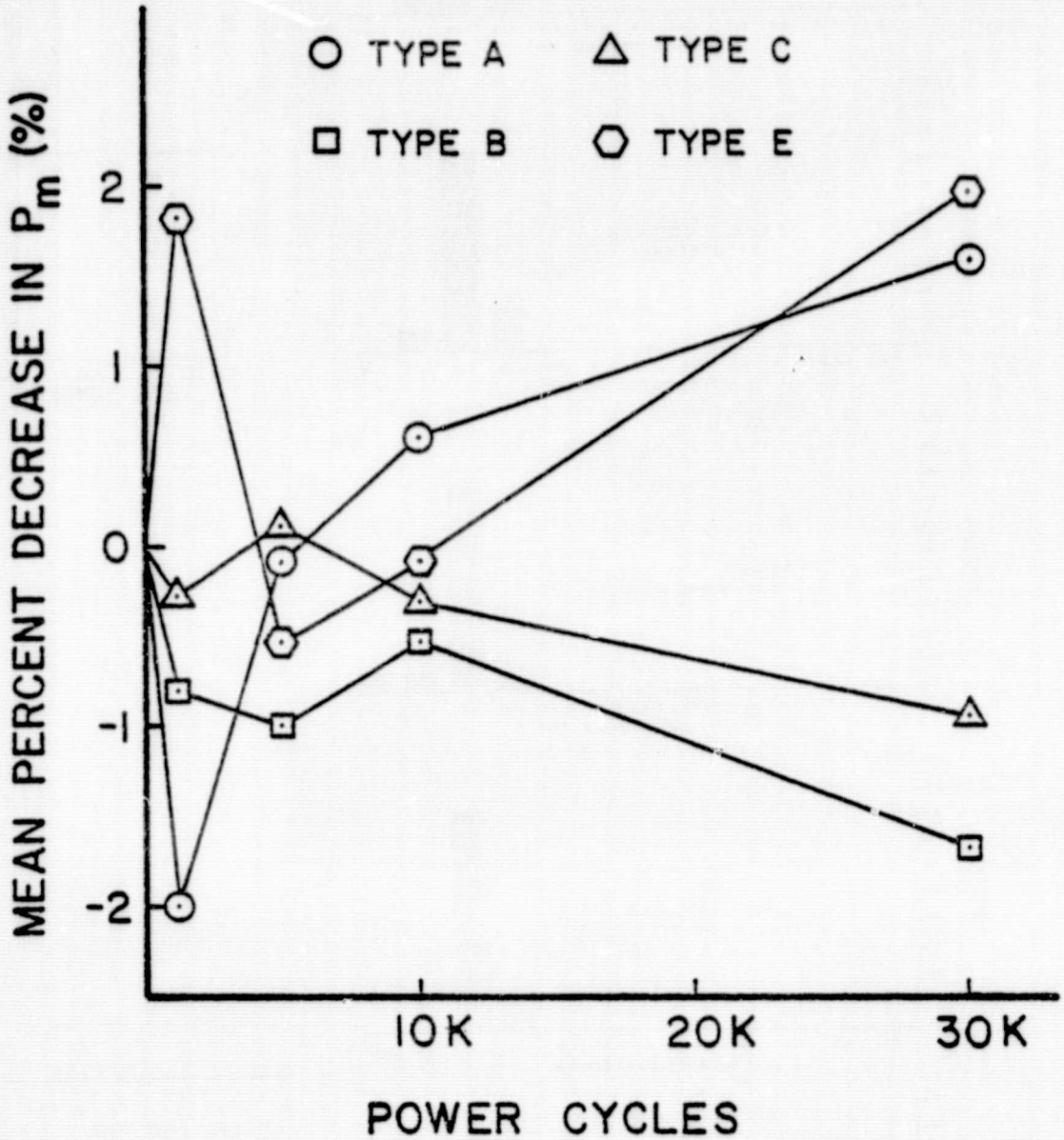

Figure 4.5.5. Behavior of Lot Mean P_m with Power Cycle Stress, All Cell Types.

showing degradation at the test termination point. The improvement of P_m (negative mean percent decrease) noted for type A cells in the Phase I experiments was in fact repeated very exactly at the first down-time in the large-quantity testing. However, subsequent power cycling clearly resulted in a reversal of the improvement.

Generally, relatively minor physical effects were observed in the course of the large-quantity tests. Type B cells showed the most striking effects. For these cells the back-side metal discolored from a grayish-silver color to brown, and it showed evidence of peeling around the rim of the cells. Similar sorts of changes were observed in some B-T stress tests, but at higher temperatures.

Considering both the electrical and physical results obtained from the power cycle testing, it can be concluded that the stress test was inefficient and probably should not be included in qualification test schedules or future solar cell accelerated stress testing, at least as a large-quantity test. In the future the test should be done on small cell quantities only unless significant effects are observed.

4.6 Metal-Silicon Contact Integrity of Stress-Tested Cells

PRECEDING PAGE BLANK NOT FILMED

4.6.1 Contact Integrity Test Development

In order to determine the effect of accelerated stress testing on the metal-silicon contact integrity (i.e., metalization adherence strength) or solar cells a contact integrity test procedure was developed. Quantities of cells of all four manufacturer's types were subjected to the contact integrity test after having been stressed by one or the other of the accelerated tests discussed earlier. The contact integrity test procedure was developed and applied to stressed cells by Mr. G.W. Witter and others of Optical Coating Laboratory, Inc., under subcontract to Clemson University and in consultation with Clemson University personnel.

Contact integrity testing was performed in the course of the overall accelerated stress testing program in order to obtain at least a first-order estimate of the degradation rate of the adherence of the cell front-side metal (grid and collectors) with various accelerated stresses. With sufficient experimental and theoretical work this degradation rate can then be related to a degradation rate under use conditions. No effort was devoted to back-contact metal adherence. In order to perform meaningful measurements on terrestrial solar cells, and to establish a standard procedure for these cells which will hopefully stand the test of use and time, it was necessary to develop a contact integrity test procedure or method. Central to testing the integrity of terrestrial solar cell contacts are the method of test lead attachment and type of test lead. In the contact integrity test, a test lead is attached to the surface of the contact and pulled normal to the surface or at a specified angle to the point at which contact adherence failure, lead failure, or lead-metal

adherence failure occurs. Two key areas were thus addressed; 1) What type of test lead should be used? and 2) What method should be employed in test lead attachment? In addition, the mechanics of the actual pull-testing procedure and the classification of experimental observations during testing were considered.

Various methods of test lead attachment are utilized today in contact integrity testing of space and terrestrial solar cells. Some of these are:

- soldering a tinned Kovar tab or 26 AWG wire to the contact with a soldering iron;
- soldering a tinned copper interconnect to the contact by the reflow method;
- soldering a tinned Kovar tab to the contact with a resistance soldering machine; and
- welding a Kovar tab to the contact with a parallel gap resistance welder.

Of course, an alternative to the use of test tabs or leads is the use of the electrical contact tab attached by the manufacturers (MAT). All of the above methods simulate conditions that are encountered during the actual assembly and have the latent function of screening for solderability or weldability problems because no surface treatment or activated flux is permitted. However, the purpose of the contact integrity testing described here was not to uncover solderability or weldability problems after accelerated stress testing. All of the methods shown above (except the use of the MAT) have one aspect which was considered undesirable for our purposes; they all involve application of considerable heat in the

area in which contact adherence is to be determined, after stress testing. The possibility thus exists that in the act of attaching the test lead, the physical/chemical status of the metal-silicon interface could be altered and an artifact could be introduced into the data. The artifact could either result in artificially high values of contact adherence, or artificially low values. Thus it was decided to investigate low-temperature means of attaching test leads and, if no satisfactory low temperature method was found, then to investigate solder and various lead material combinations.

After consultation with manufacturers, three types of epoxy adhesives were chosen for evaluation for test lead attachment. Several tests with each adhesive type were conducted using two types of test lead, copper ribbon .085" x .005" and 26 AWG tinned copper wire. All pulls were performed at a 90° angle to the cell surface. The sequence of the tests were as follows:

1. Using a Pink Pearl eraser abrade the cell contact and test lead. Then rinse with solvent and blot dry with paper towel.
2. Mix adhesive in accordance with the manufacturer's directions.
3. Apply adhesive to the area of the contact to be tested.
4. Place the test lead into the adhesive and position for curing.
5. Place in oven to cure in accordance with the manufacturer's instructions to full strength condition.
6. Remove from the oven and allow to set overnight.
7. Test using the Unitek Micropull Pull Strength Tester with Chatillion Force Gage. Pull the test lead normal to the cell surface until destruction.
8. Record the pull strength value.
9. Examine the cell to determine the failure mode and record.

Epoxies used were Hysol 907, Furane Furalane 5738A/B, and Hysol 1105. Test leads were .085" wide Cu ribbon, attached by epoxying to the cell a .050" section at the end of the ribbon, and 26 AWG wire. Both the epoxy experiments and the subsequent solder-attachment experiments were performed using OCLI cells with contact adherence strengths in the several thousand gram range.

None of the adhesives gave satisfactory results with the 26 AWG wire test lead, and the Hysol 907 and Furane Furalane 5738 A/B did not give satisfactory results with the Cu ribbon tests lead. For example, Hysol 907 used with Cu ribbon test leads provides a uniform tensile strength of about 1,600 grams. This value is very low when compared to the large interface area. In each case the epoxy ruptured without damage to the cell contact. Results obtained with Hysol 907 and 26 AWG wire were even less acceptable, with mean tensile strength of about 850 grams for the combination. Furane Uralane 5738 A/B in combination with Cu ribbon showed a mean tensile strength of about 2,300 grams. This seemingly high strength is marred by the fact that in each case the test lead peeled from the epoxy without damage to the cell. The failure mode exhibited (ribbon peeling from epoxy) resulted in rejection of this combination of adhesive and test lead material. The combination of Hysol 1105 and 26 AWG wire yielded variable results from 275 grams to > 3,500 grams, with "wire pulled from epoxy" as the only failure mode. The mean tensile strength was about 1,500 grams. The variability of the results eliminated this combination from serious consideration.

The combination of Hysol 1105 and Cu ribbon provided the strongest epoxy-test lead combination, with ten of eleven samples exhibiting failure

levels in excess of 3,500 grams. The strength of this combination approached that of the tensile strength of silicon, as shown by the fact that silicon failed, rather than the lead, adhesive, or metal, in two cases. The high tensile strength shown by Hysol 1105 and Cu ribbon makes that combination the best suited for contact integrity testing of the low temperature methods for test lead attachment that were evaluated. However, wide variability in rupture strength of the epoxy-ribbon bond was observed in subsequent larger-scale testing, as discussed in the following section. It is concluded at this point that the epoxy technique is provisionally acceptable as an alternative to solder attachment, for cases where high temperature must be avoided, and that further experimentation with and use of the technique is required before it can be unhesitatingly recommended.

In light of the marginally satisfactory results shown by the epoxy attachment methods, both flat-soldering and butt-soldering of copper ribbon and 26 AWG wire were evaluated for contact integrity testing. The only soldering method used involved uniform heating of the cell. This was felt to be preferable to the use of a soldering iron method since thermally-induced stresses are minimized and since the maximum temperature of the cell is more easily controlled. The sequence for testing was:

1. Using a Pink Pearl Eraser, abrade the cell contact area to be soldered and the test lead.

2. Tin the test lead.

3. Apply a small amount of Alpha Sn 62 Solder Cream to the area to be soldered, as close to the edge of the contact as possible.

4. Place the tinned end of the test lead into the solder cream, supported at 90° to the cell surface.

5. Place the cell onto a hot plate pre-heated to 200°C until solder cream melts and a solder joint is formed, then remove and allow to cool. This usually takes about 15 seconds on the hot plate.

6. Test using the Unitek Micropull Pull Strength Tester with Chatillion Force Gage. Pull the test lead normal to the cell surface until destruction.

7. Record the pull strength value.

8. Examine the cell to determine the failure mode.

The above technique used with flat-soldered Cu ribbon, pulled at 90° to the cell, gave variable results. In this case the test lead-solder interface was .085" x .060". Eight of the eleven test cells failed at forces > 3,500 grams. However, only three of the eight left the cell damaged; the other test leads peeled from the solder. Peeling of the test lead is clearly not an acceptable failure mode. Note that this method of lead attachment also provides a large surface area thereby reducing stress on the contact, for a given pull force level. It is for these reasons that this method is considered marginal and is not recommended. Flat-soldered Cu ribbon pulled at 135° to the cell surface also gave unacceptable results. The mean value for failure was about 650 grams, and in five of six cases the ribbon or solder peeled from the contact without damage to the cell. Thus this technique is also not recommended. Similarly, butt-soldered 26 AWG wire gave a mean tensile strength of about 1,500 grams. In each case the wire pulled out of the solder. This method is also unacceptable.

Butt-soldered copper ribbon, pulled at 90° to the cell, gave the most consistent results in the evaluation experiments. In this case the test lead-cell metal interface area is also small, allowing high stress to be applied with acceptable force levels. Seventeen of 25 cells tested with this technique showed damage to silicon after testing. This is the expected failure mode for the test cell type. Of the other eight cells, six failed due to the ribbon pulling out of the solder. However, the

force levels for five of these six were in excess of 3500 g, and therefore were greater than the 3500 g measurement capability of the force gage in use at that time. Considering the small interface area inherent in this method, failure of the test lead - solder bond at force levels greater than 3500 g is not unacceptable. The mean force at failure for the lot was in excess of 2900 g. Since eight of the 25 cells failed at force levels greater than 3500 g, and in the judgment of the machine operator failed at levels considerably greater than 3500 g, the true mean failure force could well have been several hundred grams greater than 2900 g. Considering the experimental results discussed above, butt-soldered copper ribbon applied to a uniformly heated cell is the recommended combination for contact integrity testing if the high temperatures involved can be accepted.

The contact integrity test procedure, which is based on the two recommended test lead-attachment methods discussed earlier, is shown in Appendix E. Note that the use of the MAT is not included in the test procedure; only techniques using the solder-attached tab (SAT) and the epoxy-attached tab (EAT) are specified. This omission of the MAT is not meant to exclude it from use in contact integrity testing. It even has certain unique advantages for this testing, since the MAT and the metal underneath it has undergone all the stress-testing to which the other cell metal has been exposed. However, if the MAT is to be used in contact integrity testing then whatever disadvantages it may have (e.g., large or variable interface area, lead material with insufficient strength to adequately stress the cell metal, etc.) must be considered in evaluating test results. Note also that if quantitative comparision is to be made of different cell types, variations in MAT between manufacturers is a complicating factor.

4.6.2 Contact Integrity Testing Results

Contact integrity testing was performed, using the procedure contained in Appendix E, on both stress-tested cells and control units as shown in Table 4.6.1. Each cell was tested using the two MAT's and one SAT, except in the case of the type B cell which was supplied with only one front-side tab. In addition, all type A cells (104 total) and twenty of the type C cells were tested using an EAT in order to obtain a comparison with the SAT results. Figures 4.6.1 through 4.6.4 show test lead placement for the four cell types. Table 4.6.2 summarizes the number of actual pull-tests performed. It is interesting to note that of the 728 MAT's that were used for pull testing, only eight of the leads themselves broke. Of these eight, which were distributed as two type A, one type B, three type C, and two type E, three were on virgin cells in the control populations. The virgin cells had been handled in order to measure their electrical characteristics, but had not been subjected to handling in the stress tests themselves.

In the large-scale testing, the pull force gage used was a Chatillion model DPP-5Kg. The unit was designed to measure from 0 to 5 kilograms with over-range capability of approximately +2 kilograms allowing measurement of values ranging near 7 kilograms. The measurements were taken to the nearest 50 grams. This limitation in precision is the result of a trade off between precision and measurement range. The gage was calibrated against reference standards traceable to the National Bureau of Standards before testing was started and upon completion. Accuracy was $\pm$ 50 grams.

Results from pull-testing the control units are shown below in Table 4.6.3. Two points can be made regarding the information in this table.

Stress Test	Number of Hours/Cycles	Number of Cells Tested per Type
75°C Bias-Temperature	968 Hr.	10
135°C Bias-Temperature	600 Hr.	10
150°C Bias-Temperature	281.5 Hr.	10
165°C Bias-Temperature	148 Hr.	10
121°C/15 Psig Bias-Temperature-Humidity	100 Hr.	8
85°C/85% R.H. Bias-Temperature-Humidity	215 Hr.	8
Power Cycle	1034 Cycles	8
Thermal Cycle	10 Cycles, 0°C to +150°C; 10 Cycles, -25°C to +150°C	8
Thermal Shock	5 Cycles, -65°C to + 150°C	7
Control Units	0	25

Table 4.6.1. Number of Cells from Stress Test Lots and Control Cell Population Subjected to Contact Integrity Testing.

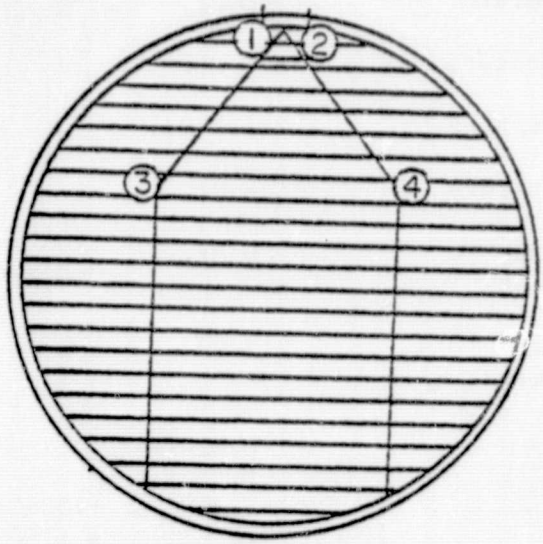

1. MAT
2. MAT
3. EAT
4. SAT

Figure 4.6.1

CELL A TEST LEAD PLACEMENT

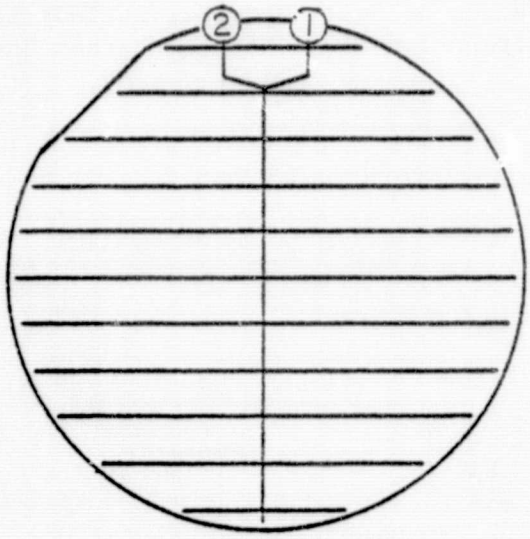

1. MAT
2. SAT

Figure 4.6.2

CELL B TEST LEAD PLACEMENT

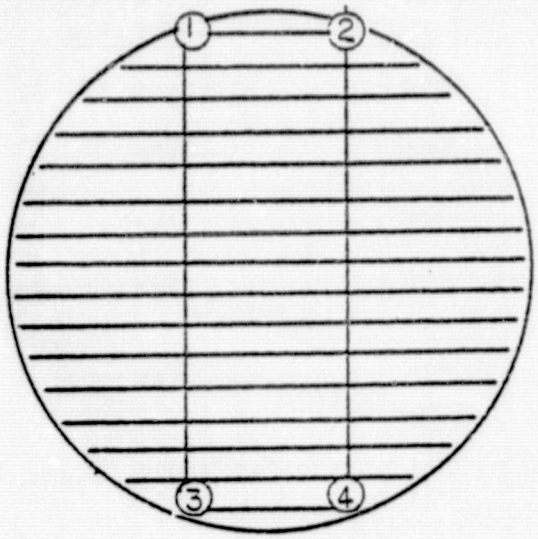

1. MAT
2. MAT
3. SAT
4. EAT

Figure 4.6.3

CELL C TEST LEAD PLACEMENT

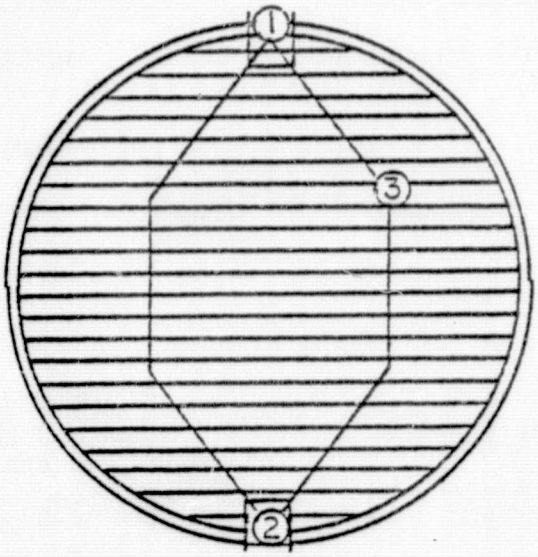

1. MAT
2. MAT
3. SAT

Figure 4.6.4

CELL E TEST LEAD PLACEMENT

Cell Type	Number of MAT Pulls	Number of SAT Pulls	Number of EAT Pulls
A	208	104	94
B	104	104	
C	208	104	20
E	208	104	
Total	728	416	114

Table 4.6.2. Pull-Tests Performed During Contact Integrity Testing.

	MAT		SAT		EAT	
Cell Type	Mean Pull Force (g)	Predominant Failure Mode	Mean Pull Force (g)	Predominant Failure Mode	Mean Pull Force (g)	Predominant Failure Mode
A	2078	77%A	4954	72%B/C	2868	88%F
B	304	100%A	2163	96%B/C	N/A	N/A
C	1345	59%A	4140	92%B/C	2890	100%F
E	170	100%A	1735	88%B/C	N/A	N/A

Table 4.6.3. Mean Pull Force and Predominant Failure Mode, Contact Integrity Test Control Units.

First, note the low values of mean pull force shown for the EAT's, compared to the values for the geometrically identical SAT's, and the characteristic F failure mode. As described in Appendix E, failure mode F is due to failure of the attachment material. Thus the mean EAT pull force values shown are definitely lower bounds to the true contact adherence strength of the control unit population. Some stress test lots showed predominantly type F failures using EAT, while others showed primarily failure modes B and C which are due to silicon failure rather than contact or attachment material failure. The spectrum of mean pull force values for cell Type A lots showing predominantly type F EAT failures ranged from 1300g to 5100g, while other lots which had predominantly type B and C EAT failures exhibited mean pull force values in the range 3000 to 4000. In light of the variability of results obtained using EAT's, especially the results showing type F failure modes, it was concluded that the EAT technique needs further development and that no useful analysis could be done on the EAT results. Note particularly that since abnormally low value, Type F failures occurred with the control units, there was not a useful zero-stress value with which to compare the mean failure force values of the stressed cells.

The second point concerning the data in Table 4.6.3 revolves around the relative sizes of the values obtained using the MAT and SAT, and the types of failure modes observed. Since the pull test lead configuration was different for the MAT and SAT tests, no direct comparison is possible between the mean values obtained (for a given cell type) using the two lead types. Also, since the actual MAT's for the various cell types were all different, no direct comparision can be made between cell types using

C-3

the numerical MAT results. Thus all data was analyzed by comparing the mean pull force for a given cell and pull lead type to the mean pull force observed for the control population of that cell type, using the same pull test lead. There is even a difficulty in this analysis method, since several of the SAT and MAT control lots and stress test lots showed an appreciable percentage of type B, C, or D (i.e., silicon fracture) failures. For these "silicon" types of failures it is only possible to say that the contact adherence strength was greater than the failure force value observed. Thus in Table 4.6.3 the mean pull force values shown for cell types A and C, MAT, are measures of the minimum value of contact adherence strength. Likewise, the mean pull force values shown for all cell types, SAT are measures of the lower bounds to the true contact adherence strength.

In the results described below the failure force data for a given cell, test lead type, and stress test lot were examined and the mean failure force value for type A failures computed. Data associated with any type B, C, or D failures in the lot which showed failure force levels below the lot mean of the type A failures were discarded. Any values corresponding to anomalous (i.e., types E, F, and G) failure modes were also discarded. Then, the mean of all failure forces (excluding values discarded as described above) for that lot was computed and the ratio of the stress test lot mean failure force to the control lot mean failure force was determined. If both the stress test lot and the control lot, for that cell and test lead type, had primarily type A failures then the above ratio is the contact adherence strength of the stressed units relative to virgin units. If on the other hand, the stress test lot had

primarily type A failures and the control lot had primarily B, C, or D failures then the ratio of the lot mean failure forces is an upper limit on the true contact adherence strength of the stressed units relative to virgin units. The converse is of course true if the stress test lot had primarily type B, C, or D failures and the control population had primarily type A failures. In the cases where both the stress test lot and the control population had primarily type B, C, or D failures, the ratio of mean failure forces is indeterminate as far as the true relative contact adherence strength of the stressed units is concerned since the ratio is really that of two inequalities. Such cases are denoted below by a question mark preceding the value of the ratio.

Results of the contact integrity testing are shown below in Tables 4.6.4 and 4.6.5 for the two test lead types. In comparing the data in these two tables it is remarkable that so many stress test lots showed silicon fracture failure modes using SAT, compared to the predominant metal peeling failure mode shown in the MAT tests. This same pattern is present to an extent in the control unit data shown in Table 4.6.3. Although it could be supposed that the predominance of A failures in the MAT results in Table 4.6.4 was an artifact caused by mechanical stress on the leads during accelerated stress testing, the fact that the same sort of pattern appears in the data of Table 4.6.3 does not support this supposition. The source of the difference in the failure mode distributions observed using the two techniques is thus not clear, and should be a subject for further investigation.

Taking into account the absolute uncertainty in the ratio values denoted by question marks, there is no significant disagreement between data obtained using MAT's and that obtained using SAT's. There is some

Stress Test	Cell Type			
	A	B	C	E
75°C B-T	<.52	.52	<.72	.79
135°C B-T	<.37	1.24	<.56	.69
150°C B-T	<.56	.31	<.68	.79
165°C B-T	<.55	.97	<.57	.99
B-T-H Pressure Cooker	<.59	1.31	<.35	1.15
B-T-H 85/85	<.87	1.4	?1.0	1.06
Power Cycle	<1.0	1.0	?.84	1.06
Thermal Cycle	?.46		.94	>1.28
Thermal Shock	?.46	>.69	?1.14	>1.2

Table 4.6.4. Contact Adherence Strength of Stressed Cells Relative to Virgin Cells, Manufacturer-Attached Tab (MAT).

Stress Test	Cell Type			
	A	B	C	E
75°C B-T		?1.5	?.89	?.64
135°C B-T	<.43	?1.72	?.60	?.67
150°C B-T	<.36	?2.1	?.99	?.63
165°C B-T	<.43	?.94	?1.28	?.61
B-T-H Pressure Cooker	<.22	?1.62	?.32	<1.05
B-T-H 85/85	?1.0	?1.44	?1.1	?1.18
Power Cycle	?1.0	?1.18	?.89	?1.09
Thermal Cycle	?1.0	?1.33	?.97	?1.54
Thermal Shock	?.69	?1.56	?1.1	?1.59

Table 4.6.5. Contact Adherence Strength of Stressed Cells Relative to Virgin Cells, Solder-Attached Tab (SAT).

internal inconsistency, however, in the data in Table 4.6.4. For example, the 135°C B-T mean contact adherence strength for type B cells was greater than that of the other type B B-T test lots, whereas the 135°C B-T mean strength was lower than that of the other B-T test lots for the other three cell types. Ignoring minor discrepancies, it is clear from Table 4.6.4 that under B-T stress, even for relatively short times, significant contact adherence strength degradation occurred with the solder-metalized cell types, and somewhat less degradation occurred with the silver-metalized cell types. Under B-T-H stress the solder-metalized cell types also showed significant contact adherence strength degradation, while the silver-metalized types showed no degradation under this stress. Power Cycle stress had no significant effect on any of the cell types. Thermal Cycle and Thermal Shock stress had no definite effect on any of the cell types except type A. In that case the mean failure force decreased by 50%, and the predominant failure mode was type B and C. This is undoubtedly simply an indication of thermo-mechanically induced cracking of the silicon substrate. This type of cracking was visually observed after additional stressing of the remaining cells in the stress test lots, during the course of the normal accelerated stress testing. To the extent that firm comparisons can be made, data in Table 4.6.5 confirms the above conclusions. Some additional confirmation was given by EAT test results for type A B-T-H pressure cooker-stressed cells. These results cannot be expressed in terms of a relative contact adherence strength for reasons discussed earlier, but the raw data showed remarkably low failure force values, and all failure modes were type A rather than the type B, C, or D, or type F failure modes most commonly observed in the EAT contact integrity testing.

5.0 RELIABILITY QUALIFICATION TEST SCHEDULES - PRELIMINARY RECOMMENDATIONS

Two distinct areas of application exist for a solar cell reliability qualification test schedule: testing for the purpose of monitoring a previously "qualified" cell technology, and testing for the purposes of establishing initial "qualification" of a cell technology.

The first application is one of continually verifying reliability for cells manufactured by a technology which has no fundamental weaknesses which could lead to poor parameter stability over life.

The second application is one of establishing ab initio that a cell technology is free from built-in failure mechanisms. In the first case a reliability testing history is presumed to exist, to which on-going test results can be compared; in the second case by definiton no directly relevant testing results exist. For these two quite different situations, two different reliability qualification tests schedules have been proposed.

The suggested test schedule for technology qualification is shown in Table 5.1. Test conditions and methods are those discussed in the pertinent parts of Section 4.* Measurements and observations to be made are: I_{sc}, V_{oc}, and P_m prestress and poststress; contact integrity, using the method of Appendix E, on a sample of 25 virgin units and on all stress test units (poststress) using both MAT's and one SAT; and visual inspection of thermally cycled tests units at 4 X magnification over the entire cell, and 10 X magnification in the vicinity of the tab attachment points. Proposed electrical degradation limits for lot mean P_m are: Test A1, 5%; Test A2, 10%; Test A3, 20%; Test A4, 10%. The proposed limit for lot mean contact integrity degradation is 50%. The proposed limit for frequency of occurrence of cell fractures

*The thermal cycle method thus will not permit the use of two temperature chambers with manual work transfer.

PAGE 208 INTENTIONALLY BLANK

	Test	Quantity	Duration
A1.	Bias-Temperature, 75°C	25	2000 hr
A2.	Bias-Temperature, 150°C	25	1000 hr
A3.	Bias-Temperature-Humidity, 121°C/15 Psig	10	240 hr
A4.	Thermal Cycle or Thermal Shock, -65°C to +150°C	10	10 cycles

Table 5.1 Reliability Qualification Test Schedule for Cell Technology Qualification.

	Test	Quantity	Duration
B1.	Bias-Temperature, 150°C	25	500 hr
B2.	Bias-Temperature-Humidity, 121°C/15 Psig	10	100 hr
B3.	Thermal Cycle or Thermal Shock, -65°C to +150°C	10	10 cycles

Table 5.2 Reliability Qualification Test Schedule for Reliability Monitoring.

is 50% including especially conchoidal fractures at tab attachment points. Gross delamination of metal (delamination extending over greater than 1" length) of any cell should be cause for disqualification.

Table 5.2 shows the suggested test schedule for cell reliability monitoring. Tests conditions and methods are those discussed in the pertinent parts of Section 4. Measurements and observations to be made are those discussed in the previous paragraph except that contact integrity testing of virgin units should not be required, since results of previous testing should exist for comparison purposes. The criteria for acceptance should ideally be based on qualification test performance relative to previous test performance. At this point, quantification of acceptable deviation from previous results is difficult and more history must be obtained before the reasonableness of such quantification can be verified. However, based on the criteria for the technology qualification test some absolute limits can be suggested. Proposed electrical degradation limits for lot mean P_m are: Test B1, 5%; Test B2, 10%; Test B3, 10%. The proposed limit for lot mean contact integrity degradation is 25%. The proposed limit for frequency of occurrence of cell fractures and gross delamination is the same as for the cell technology qualification schedule.

6.0 CONCLUSIONS

PAGE 212 INTENTIONALLY BLANK

In this program the general ability of accelerated stress tests to discriminate between cell types and technologies was demonstrated. This discrimination was observed on the basis of P_m degradation, visual observation, and metalization adherence degradation. Thus it is clear that taken as a whole the results of the accelerated stress tests can be used to rank-order cell types with respect to potential field reliability. On the basis of results the technique should be usable as a reliability or quality monitor if systematically applied to production run samples.

Figures 6.1 and 6.2 summarize the relative effects of P_m and contact integrity degradation for the various stress tests for the four cell types investigated. In these figures, the darkest squares signify a degradation which was progressive with stress test duration, and significantly above the "noise" of the measurement technique. The lightest squares signify no discernable effect after stressing. "Medium" squares denote cases between the two extremes. Obviously subjective judgement was required in formulating the figures.

It can be seen from an examination of the columns in these figures that A cells show appreciable degradation on being subjected to accelerated stress testing whereas B cells show very little degradation. C and E cells lie between these extremes. While these conclusions demonstrate the applicability and potential usefulness of the technique, they should not be interpreted at this time as a quantitative measure of field degradation rates. It is felt that the technique is capable of such prediction, but considerable additional stress testing and field degradation analysis will be required before conclusive evidence can be demonstrated.

PAGE 214 INTENTIONALLY BLANK

RELATIVE STRESS TEST EFFECTIVENESS

STRESS TEST	CELL TYPE			
	A	B	C	E
B-T				
PRESSURE COOKER				
85°C/85% R.H.				
POWER CYCLE				
THERMAL CYCLE				
THERMAL SHOCK				

Figure 6.1. Relative Effects of Accelerated Stress Tests on P_m.

RELATIVE STRESS TEST EFFECTIVENESS

STRESS TEST	CELL TYPE			
	A	B	C	E
B-T				
PRESSURE COOKER				
85°C/85% R.H.				
POWER CYCLE				
THERMAL CYCLE				
THERMAL SHOCK				

Figure 6.2. Relative Effects of Accelerated Stress Tests on Contact Integrity.

From an examination of the rows in Figures 6.1 and 6.2 it can be seen that the various tests vary in their effectiveness. The power cycle and 85°C/85% RH tests show little effect regardless of the cell type. It is for this reason that they were omitted from the qualification test schedule of Section 5.0. Pressure cooker and thermal cycle tests show consistent degradation effects in most cell types, while B-T testing strongly affects only one type of construction.

In most instances the observed P_m degradation could be directly related to failure of the cell metalization, thus verifying the original assumption on which the stress testing was based. This metalization failure was evidenced physically by delamination of the contacts and electrically by an increase in the series resistance of the cells. On one cell type a leaching of the anti-reflective coating was observed after pressure cooker exposure. This caused P_m to decrease moderately and was the only failure mechanism, other than metalization failure, which resulted in electrical degradation. No unexplainable second order effects were observed.

All cell types were found to have difficulty, of varying degrees, with thermally induced mechanical stress. Because solar cells are so physically large and contain a variety of materials having different thermal expansion coefficients, they could be expected to experience difficulty when subjected to thermal cycle/thermal shock stress. Quantification of these problems was more difficult than with other tests because of the problems of relating P_m degradation to stress as discussed in Section 4.2. Cracking effects were most severe in large diameter cells having a thick solder coating and least severe in small diameter cells with other metalization. Cracking due to thermal changes may well be the limiting solar cell reliability failure mechanism.

The most useful electrical parameter for accelerated life testing analysis proved to be the cell's maximum power, P_m, and its usefulness was only as good as the measurement techniques used. Satisfactory measurement repeatability requires careful attention to detail with regard to both light intensity and cell temperature. Intensity should be set and frequently monitored using a reference cell or standard cell. This insures operation at constant irradiation level and avoids lamp drift problems.

Cell temperature should be monitored during measurement and should be held at fixed temperature, within $\pm$ 0.5°C. Such temperature control is difficult under equilibrium conditions for cells with irregular surfaces, such as caused by solder dipping. Under these conditions the only satisfactory method is a transient measurement technique whereby all data is taken so quickly that the cell's temperature does not rise. Instruments of this kind are not generally available and their development will require transient measurement standards to be set in the same way that equilibrium standards have been set.

Changes due to accelerated stress could be observed visually as well as measured electrically. Visual observations, however, are qualitative and largely subjective so their use should be restricted to understanding failure mechanisms rather than predicting reliability.

The results of the metal adherence testing were useful in differentiating between cell types and stress tests. The results of the metal adherence testing were, however, quite variable and thus served a largely qualitative purpose. Some of this lack of quantification, however, can be attributed to starting the contact integrity test effort late in the program and being restricted to less than ideal sample sizes.

7.0 RECOMMENDATIONS

PAGE 220 INTENTIONALLY BLANK

From the experiences of this first year's work, it is clear that if stress testing is to progress down the learning curve substantial additional baseline reliability testing experience and data is required. This point is particularly critical in view of the rate of change of cell technology. Thus it is recommended that additional accelerated stress testing be performed on as wide a spectrum of conventional and developmental cell technologies as possible. It is also recommended, in view of the successful use of accelerated stress to discriminate between cell types, that a systematic program to relate laboratory tests to field failures be undertaken. This is necessary to guide the development of accelerated stress tests, and to provide a basis for judging the relevance of current and future stress tests.

Implementation of extensive additional testing on a variety of cell types depends on the availability of sockets and test equipment. A highly repeatable electrical test set capable of measuring non-heat sunk cells under transient conditions should be developed for use with irregular cells. An inexpensive accelerated stress test jig to support the cells rigidly during stressing is also required.

Further work on thermal cycle/thermal shock induced cracking should be performed. The relationship between crack formation and cell construction needs further investigation. Also, the effect of cracks on P_m degradation is not understood.

It is recommended, in view of the weak effect of the 85/85 test on the cell degradation of unencapsulated cells, that a B-T-H accelerated test program be initiated for encapsulated cells. It is possible that the

ECEDING PAGE BLANK NOT FILMED

PAGE 222 INTENTIONALLY BLANK

results of such a program might reduce the environmental demands now placed on encapsulating coatings. It is also possible that interactions between cell and encapsulant might be uncovered.

Some work should be performed to determine the importance of bias during accelerated stress. All tests in the present program involve bias, based on an analogy with integrated circuit failure mechanisms. On the other hand, the current program has shown no failures definitely attributable to bias and its elimination as a stress would greatly simplify testing.

Additional work should be performed to develop better lead attachment techniques and test procedures for metal adherence testing. A carefully planned program, perhaps using specially constructed multiple lead cells and large sample sizes, should then be initiated to look at metal adherence problems.

8.0 NEW TECHNOLOGY

No reportable items of new technology have been identified during the reporting period.

PRECEDING PAGE BLANK NOT FILMED

PAGE 226 INTENTIONALLY BLANK

APPENDICES

Appendix A

Data Management and Analysis

This research project resulted in the collection of a massive amount of solar cell electrical parameter data. This bulk of information required the use of a large core computer to handle the data storage and statistical calculations. Because of the variety of analyses and manipulations which were performed, it was considered necessary to use a "canned" program to perform the data management and the necessary calculations. The use of the computer has resulted in accurate results and a data base that can be accurately transcribed onto magnetic tapes for further evaluation at other locations if appropriate.

The data base consists of electrical characteristics of solar cells from four different manufacturers exposed to a variety of stress tests for various amounts of time. At measurement and inspection down times during each accelerated stress test electrical parameter data was obtained for inclusion in the data base. There were a total of 4889 observations. Each observation in the data base contains the following information about a cell: the manufacturer type (a code letter of A, B, C, or E), the lot number (indicates the type of stress to which the cell was subjected), the test number (indicates the level or time of stress), the cell number (within manufacturer type) the open circuit voltage (V_{oc}), the short circuit current (I_{sc}), the voltage at maximum power (V_m), and the current at maximum power (I_m). Also for each cell the maximum power (P_m) was generated by the program as $V_m * I_m$. These data were stored on disk to allow for easy access for analysis and can be transcribed onto magnetic tapes.

By and large the manipulation of the data base was performed by SAS (Satistical Analysis System). SAS is an integrated system for data management and statistical analysis. By combining statistical versatility with

extensive capabilities for data manipulation and report writing, SAS yields a nearly complete system for managing data. It is a product of SAS Institute, Inc., of Raleigh, North Carolina. SAS is extremely well documented and has become over the last few years one of the most trusted and widely used statistical software packages. For statistical analyses, SAS has a rather extensive library of statistical procedures. Important to this research were the procedure for calculating summary statistics, plotting histograms, printing scatter plots, performing analysis of variance for several linear models, and performing Duncan's multiple range test.

To indicate how SAS was useful in our analysis, we use the following examples for illustration. Using SAS's print procedure and the labeling feature, a neatly formatted printout of the data is obtained as shown in Figure A-1. Notice that the observations 173-179, which have variables 'LOT' = 2 and 'TESTNO' = 1, have a complete explanation of the test run on those cells, namely, 'L 2 T 1 BT STEP STRESS FWD AFTER 135 C'. Notice also for cell number 8 (observation 188) there are no data values, only periods. These periods represent missing values. For this cell the lead broke off resulting in no electrical measurements on this cell at this stress level. These missing values present no problems for SAS in that the statistics are suitably adjusted for missing values.

Using SAS's chart procedure, the distribution of the sample values and an indication of the population distribution can be obtained. As an example, consider the histogram of the maximum power for B cells in lot 10 before any stress testing, shown in Figure A-2. Another procedure yields a scatter plot of the data. For example, in Figure A-3 are plotted the ordered pairs (I_{sc}, I_m) for A cells before stress testing. In this plot the letter A represents one observation with the coordinates indicated, B represents two such observations, C three observations, etc. As would hopefully be observed

TYPE=A DESC=L13 T 0 135C 0=T INITIAL

OBS	CELLNO	VOC	ISC	VM	IM	PM
165	164	0.561	1.733	0.443	1.57	0.69551
166	165	0.585	1.741	0.476	1.60	0.76640
167	166	0.570	1.779	0.455	1.58	0.71890
168	167	0.567	1.772	0.440	1.58	0.69520
169	168	0.569	1.749	0.450	1.57	0.70650
170	169	0.567	1.773	0.448	1.60	0.71680
171	170	0.583	1.733	0.435	1.58	0.75050
172	171	0.577	1.827	0.449	1.68	0.75432

TYPE=B DESC=L 2 T 1 B1 STEP STRESS FWD AFTER 135C

OBS	CELLNO	VOC	ISC	VM	IM	PM
173	7	0.540	1.383	0.420	1.27	0.53340
174	8	0.534	1.378	0.420	1.27	0.53340
175	9	0.572	1.375	0.445	1.22	0.54290
176	10	0.529	1.373	0.435	1.24	0.53940
177	11	0.532	1.391	0.420	1.28	0.53760
178	12	0.531	1.384	0.429	1.27	0.54483
179	13	0.545	1.358	0.440	1.25	0.55000

TYPE=B DESC=L 2 T 2 B1 STEP STRESS END AFTER 150C

OBS	CELLNO	VOC	ISC	VM	IM	PM
180	7	0.539	1.378	0.420	1.280	0.53760
181	8	0.532	1.374	0.422	1.255	0.52961
182	9	0.569	1.375	0.442	1.220	0.53624
183	10	0.527	1.372	0.435	1.240	0.53940
184	11	0.529	1.392	0.426	1.260	0.53676
185	12	0.527	1.385	0.425	1.280	0.54400
186	13	0.541	1.359	0.440	1.250	0.55000

TYPE=B DESC=L 2 T 3 B1 STEP STRESS END AFTER 165C

OBS	CELLNO	VOC	ISC	VM	IM	PM
187	7	0.538	1.380	0.424	1.265	0.53636
188	8	.	.	.	.	.
189	9	0.568	1.377	0.443	1.230	0.54489
190	10	0.526	1.371	0.435	1.250	0.54375
191	11	0.524	1.388	0.420	1.280	0.53760
192	12	0.526	1.378	0.424	1.270	0.53848
193	13	0.540	1.355	0.430	1.260	0.54180

Figure A-1. Data Printout from SAS Program

REPRODUCIBILITY OF THE
ORIGINAL PAGE IS POOR

TYPE=B GROUP=LOT 10 INITIAL

PERCENTAGE BAR CHART

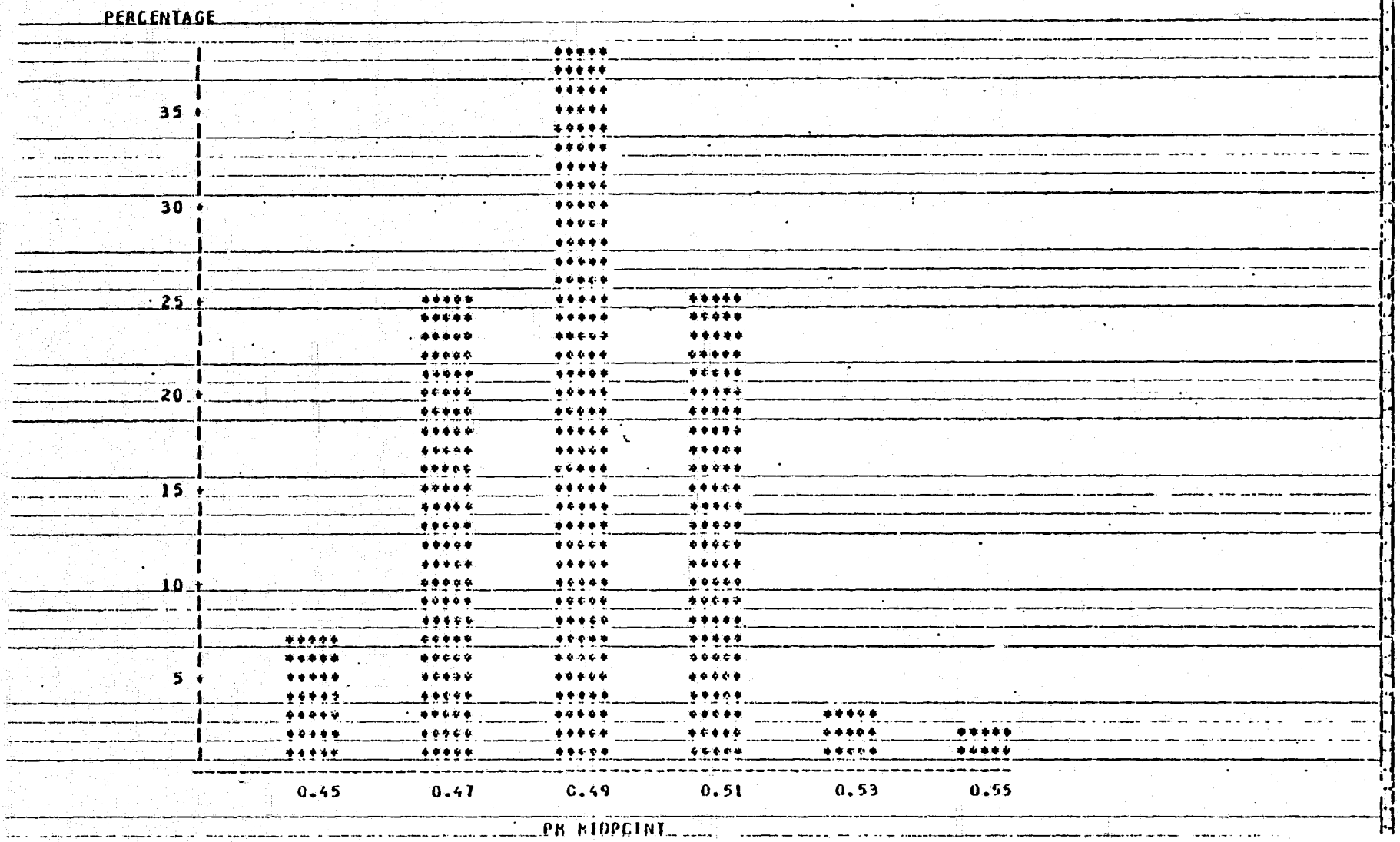

Figure A-2. Histogram of P_m Distribution for Type B Cells, Lot 10, Prestress. Lot Size = 60 Cells.

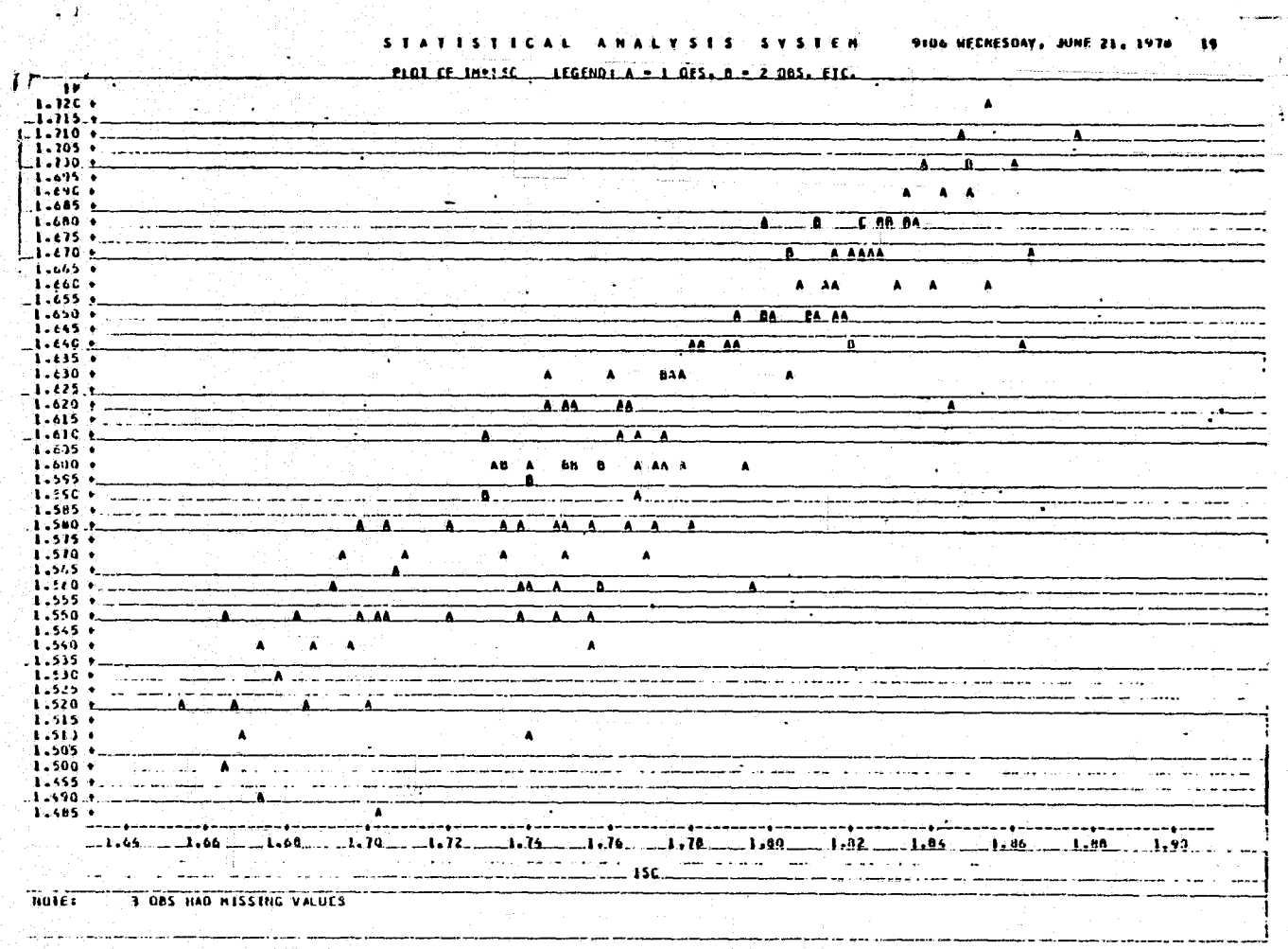

Figure A-3. Scatter Plot of I_{sc} vs. I_m, Type A Cells, Prestress.

REPRODUCIBILITY OF THE
ORIGINAL PAGE IS POOR

S T A T I S T I C A L A N A L Y S I S S Y S T E M

TYPE=B LOT=13

ANALYSIS OF VARIANCE PROCEDURE

DEPENDENT VARIABLE: PM

SOURCE	DF	SUM OF SQUARES	MEAN SQUARE	F VALUE	PR > F	R-SQUARE
MODEL	28	0.86801796	0.03100064	5.23	0.0001	0.737840
ERROR	52	0.30841273	0.00593101		STD DEV	
CORRECTED TOTAL	80	1.17643069			0.07701308	

SOURCE	DF	ANOVA SS	F VALUE	PR > F
TESTNO	2	0.53074539	44.74	0.0001
CELLNO	26	0.33727257	2.19	0.0082

DUNCAN'S MULTIPLE RANGE TEST FOR VARIABLE PM

MEANS WITH THE SAME LETTER ARE NOT SIGNIFICANTLY DIFFERENT.

ALPHA LEVEL=.05 DF=52 MS=0.005931

GROUPING	MEAN	N	TESTNO
A	0.759190	27	0
B	0.648444	27	1
C	0.561383	27	2

Figure A-4. Printout Showing Results of Analysis of Variance and Duncan's Multiple Range Test

there exists a high positive correlation between short circuit current and current at maximum power.

Two statistical tests that were of special interest for this research are the analysis of variance and Duncan's multiple range test. These two tests go hand in hand. Through an analysis of variance one tests the hypothesis that population means are equal versus the alternative hypothesis that at least one population mean is different from the others. If the alternative hypothesis is accepted, the Duncan's multiple range test is used to determine which means are different. The basic assumptions for these tests are that the populations are normal with equal variances. The data suggested that both of these assumptions were in general reasonable; however, the robustness of the F-statistic in this test insures that both tests are valid despite slight departures from normality and homogeneity of variance.

To illustrate the above tests of hypothesis consider testing the (statistical) hypothesis that the mean maximum power for cells of type A is the same initially as after 148 hours of B-T stress at 165°C, as after 362 hours of B-T stress at 165°C. In this case the experimental design is that of the complete block design where each cell represents a block and each stress level a treatment. Results of performing an analysis of variance are given in Figure A-4. The key results are the "F-VALUE" 44.74 and "PR > F" value of .0001 associated with "TESTNO". This implies that if indeed the parameters in question, i.e., the mean maximum power levels, are the same initially as after each stress level, then the probability of obtaining an F-statistic of 44.74 or greater is .0001. This is so unlikely we conclude that the stress has significantly affected the maximum power of these cells. The next question is which level(s) is (are) different. Duncan's multiple range test provides insight for the answer. In Figure A-4 are the results of Duncan's multiple range test with the stress test numbers and the means for P_m after the respective stresses. The fact that the means for each of the

stress levels have associated with them a different letter under the "GROUPING" column indicates that the means are significantly different from one another; in particular, the initial mean P_m is significantly greater than the mean P_m after one stress level which is significantly greater than the mean P_m after two stress levels.

The histograms that appear throughout the report were produced on a Calcomp plotter using special procedure written by Clemson's computer center personnel. The graphs of standardized mean P_m by stress test number were produced on the plotter by another SAS procedure. Note that in producing such plots, and in performing analyses such as those described above, it is not necessary to enter cell parametric data for each operation since the data is stored on disk and is retrieved as necessary by the various programs and subroutines.

Appendix B

Prestress Parameter Distributions of Stress Test Cell Populations

Prestress electrical data for both Phase I and Phase II test populations were analyzed statistically in order to determine whether the total cell populations were normally distributed, and whether the stress test lots formed from the total cell population were random samples. Stress test lots were formed by simply picking cells from shipping containers and scribing identification numbers in the backside metalization of each cell. No attempt was made by Clemson University workers to randomize the cells when forming stress test lots. Thus, some of the statistical tests, applied to the prestress data, test for bias in the individual stress test lot formation. A discussion of the nature and application of the statistical tests used is contained in Appendix A.

Tables B-1 through B-5 show the mean prestress electrical characteristics of the total Phase II cell populations, and the standard deviation of the parameters for the populations. Means of the prestress electrical parameters of the Phase I cell populations deviated by less than 10% from the means shown in Tables B-1 through B-5. Although the differences observed between Phase I and Phase II cell populations were found to be statistically significant for two of the cell types, the Phase I cell characteristics were considered to be close enough to the Phase II cell characteristics to permit valid stress testing experiments to be run with the Phase I units. Statistical tests applied to the Phase II cell populations indicated that the prestress parametric distributions were not perfectly gaussian in all cases. This can be seen for some parameters by casual inspection of the parametric distribution plots, Figures B-1 through B-20.

Cell Type	Total Units Measured	Mean P_m (W)	Standard Deviation (W)
A	337	0.757	0.030
B	343	0.502	0.023
C	341	0.262	0.007
E	354	0.452	0.016

Table B-1. Mean P_m and Standard Deviation, Phase II Cell Population Prestress

Cell Type	Total Units Measured	Mean I_{sc} (A)	Standard Deviation (A)
A	340	1.804	0.054
B	342	1.360	0.024
C	341	0.604	0.014
E	354	1.155	0.023

Table B-2. Mean I_{sc} and Standard Deviation, Phase II Cell Population Prestress

Cell Type	Total Units Measured	Mean V_{oc} (V)	Standard Deviation (V)
A	340	0.582	0.010
B	343	0.540	0.014
C	341	0.564	0.003
E	354	0.574	0.004

Table B-3. Mean V_{oc} and Standard Deviation, Phase II Cell Population Prestress

Cell Type	Total Units Measured	Mean I_m (A)	Standard Deviation (A)
A	337	1.646	0.050
B	343	1.201	0.035
C	341	0.560	0.013
E	354	0.986	0.016

Table B-4. Mean I_m and Standard Deviation, Phase II Cell Population Prestress

Cell Type	Total Units Measured	Mean V_m (V)	Standard Deviation (V)
A	337	0.460	0.012
B	343	0.418	0.015
C	341	0.468	0.006
E	354	0.458	0.005

Table B-5. Mean V_m and Standard Deviation, Phase II Cell Population Prestress

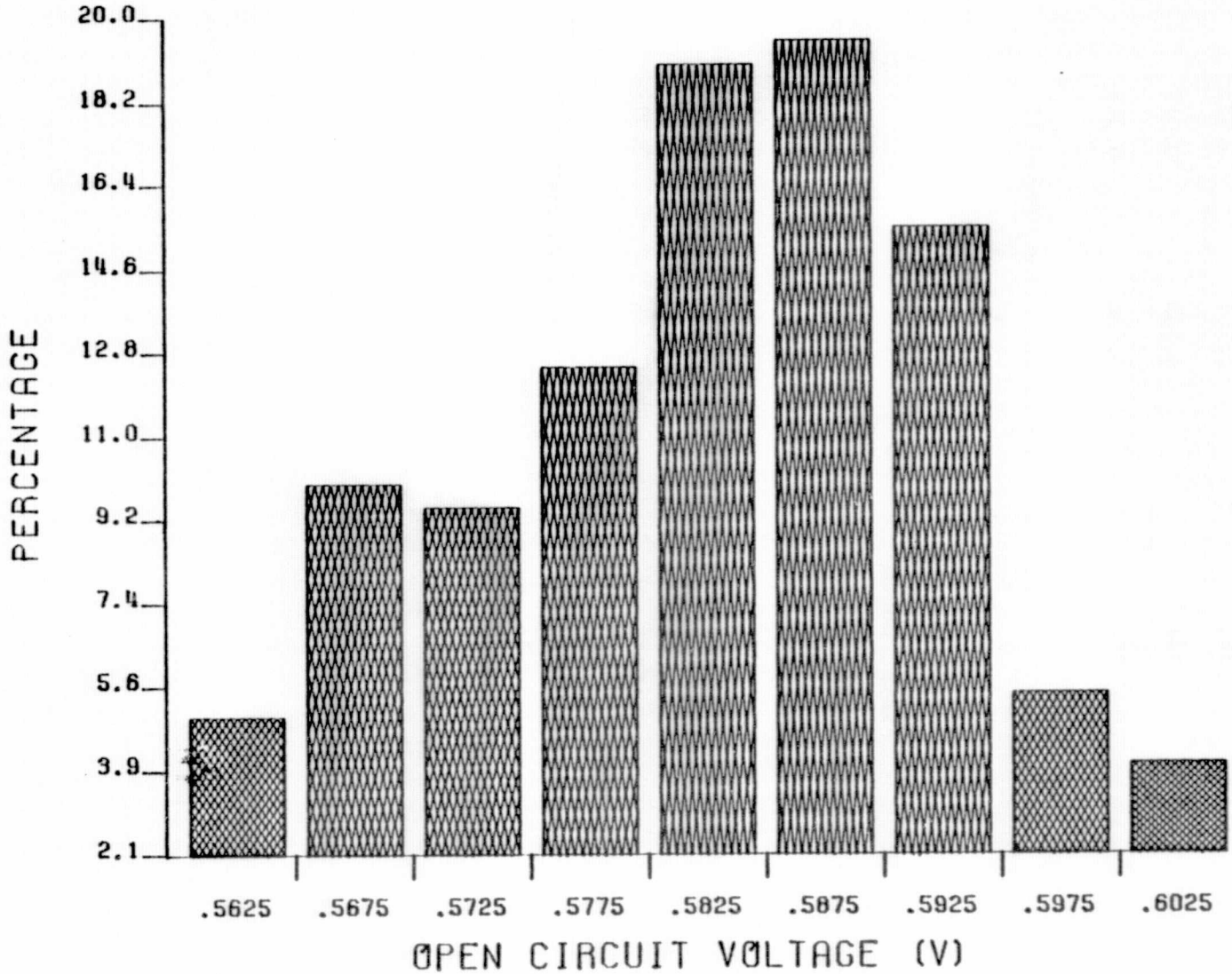

Figure B-1. Prestress Distribution of V_{oc}, Type A.

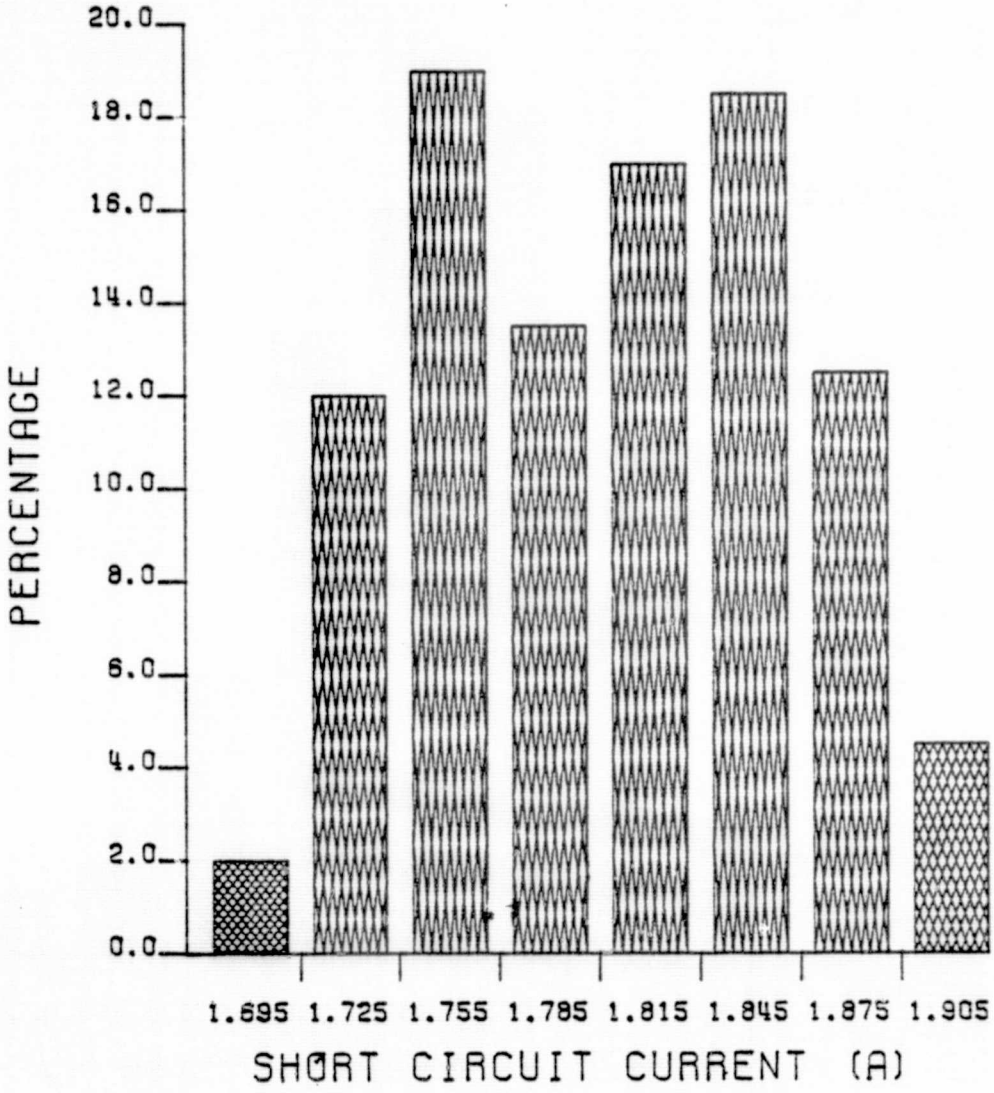

Figure B-2. Prestress Distribution of I_{sc}, Type A.

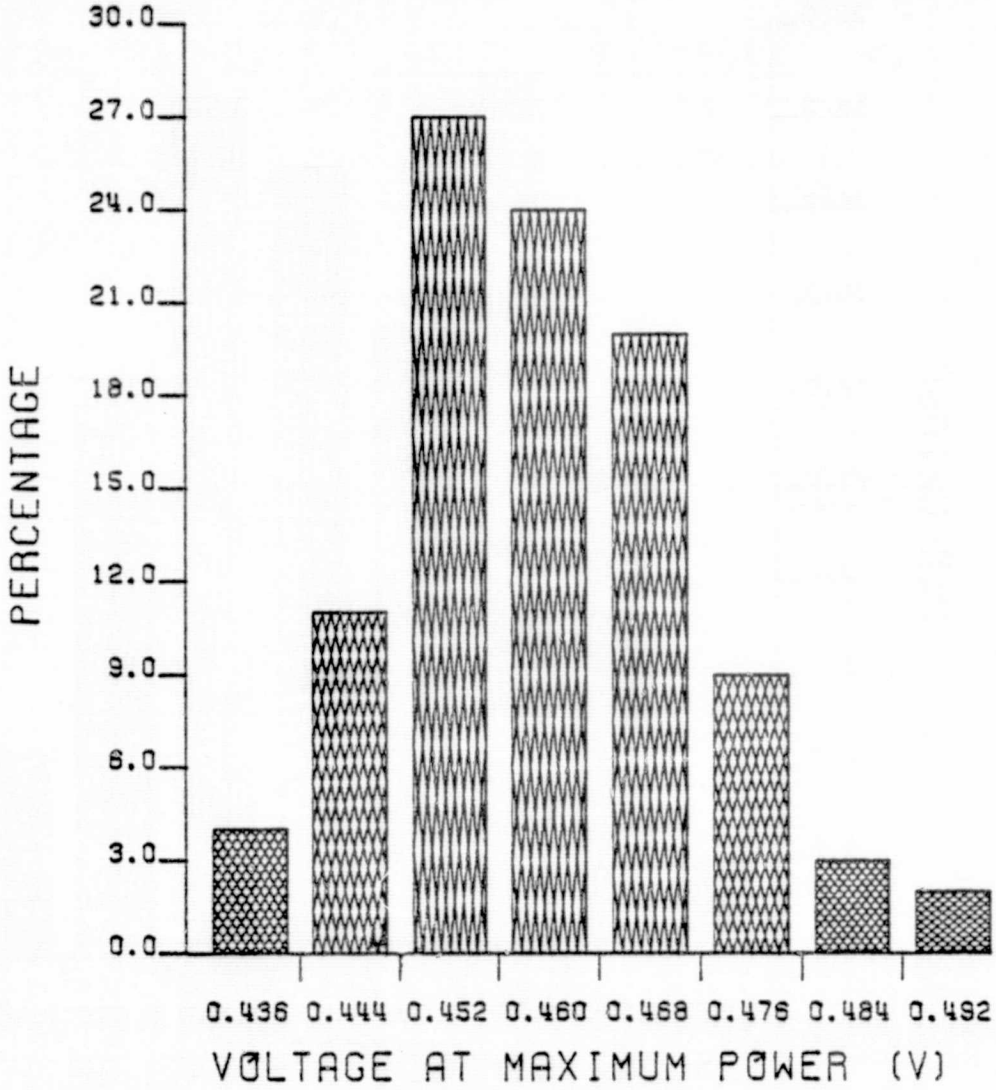

Figure B-3. Prestress Distribution of V_m, Type A.

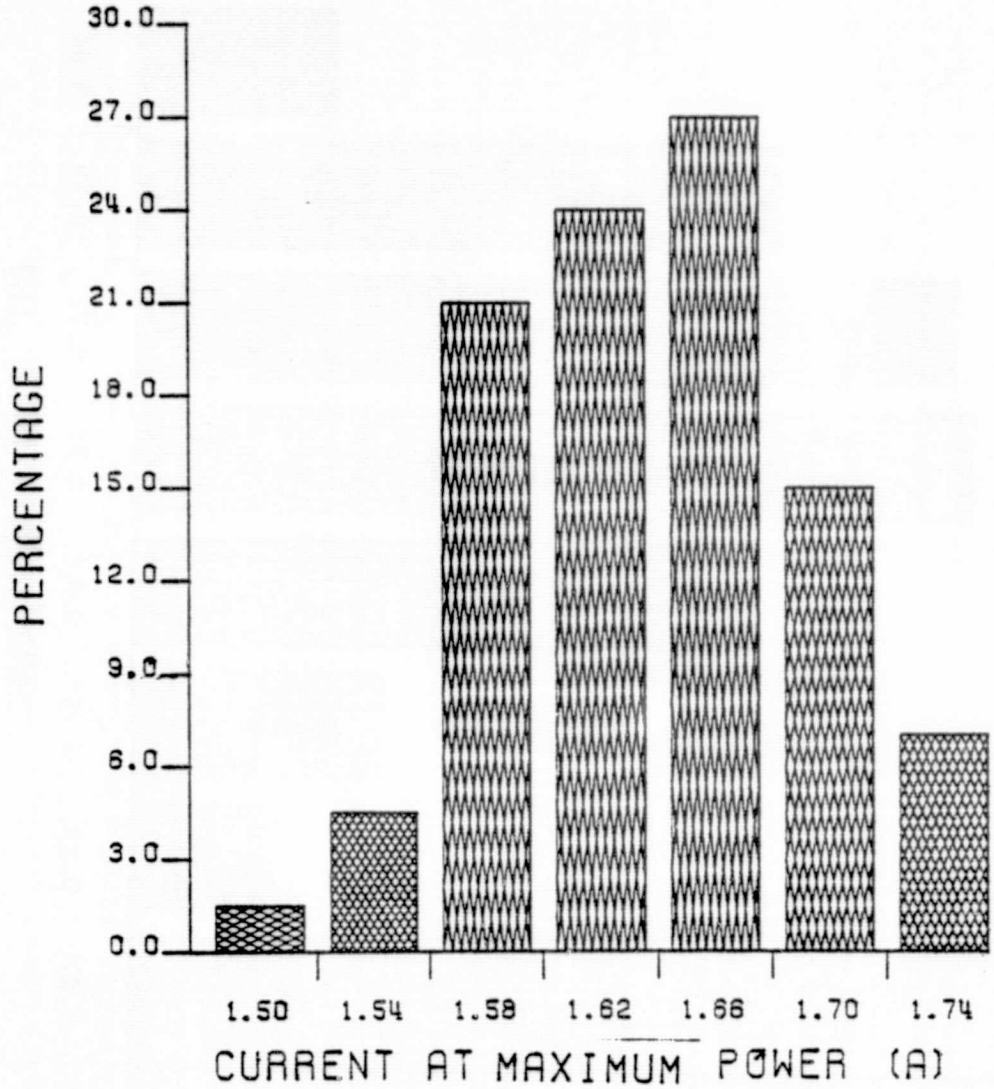

Figure B-4. Prestress Distribution of I_m, Type A.

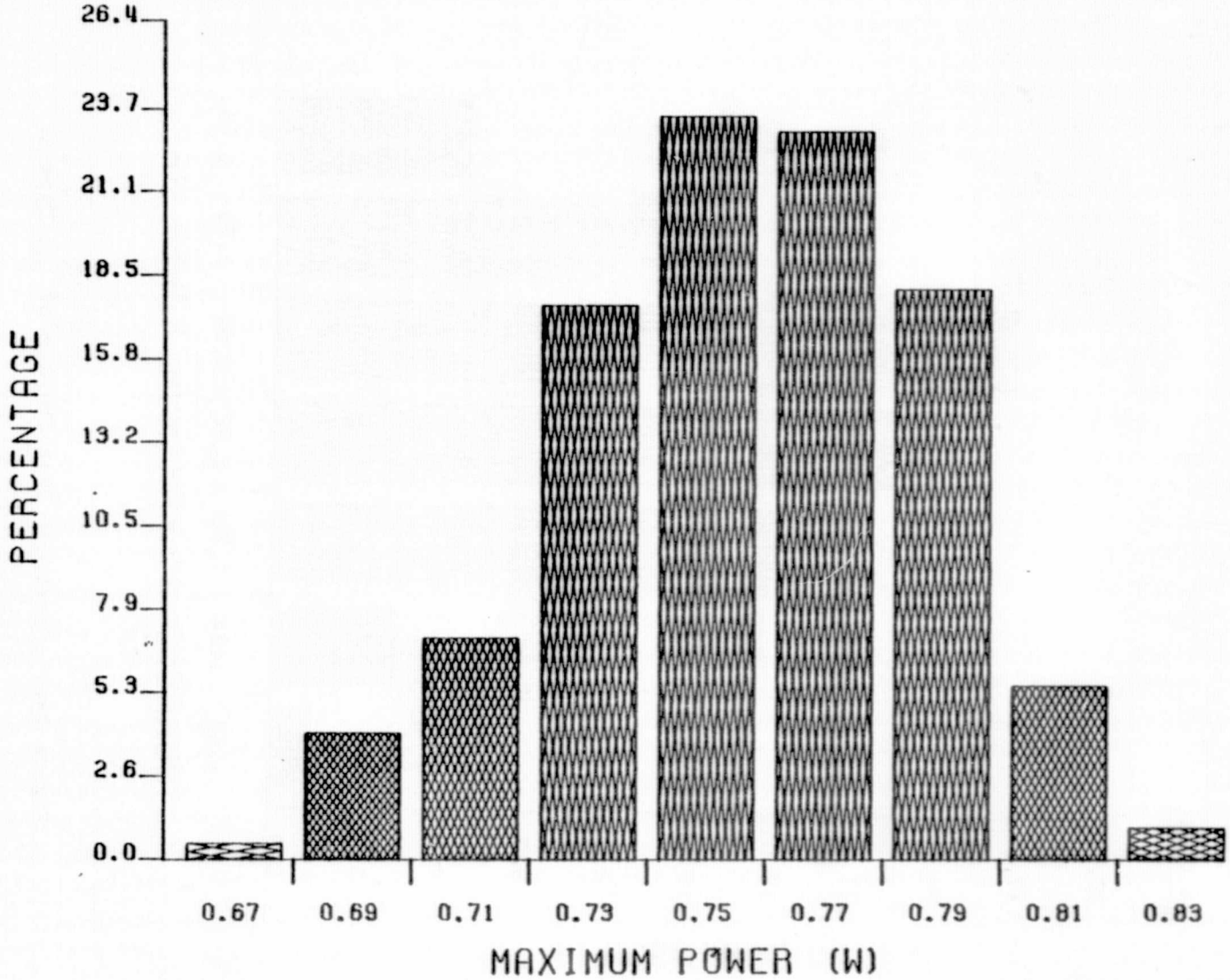

Figure B-5. Prestress Distribution of P_m, Type A.

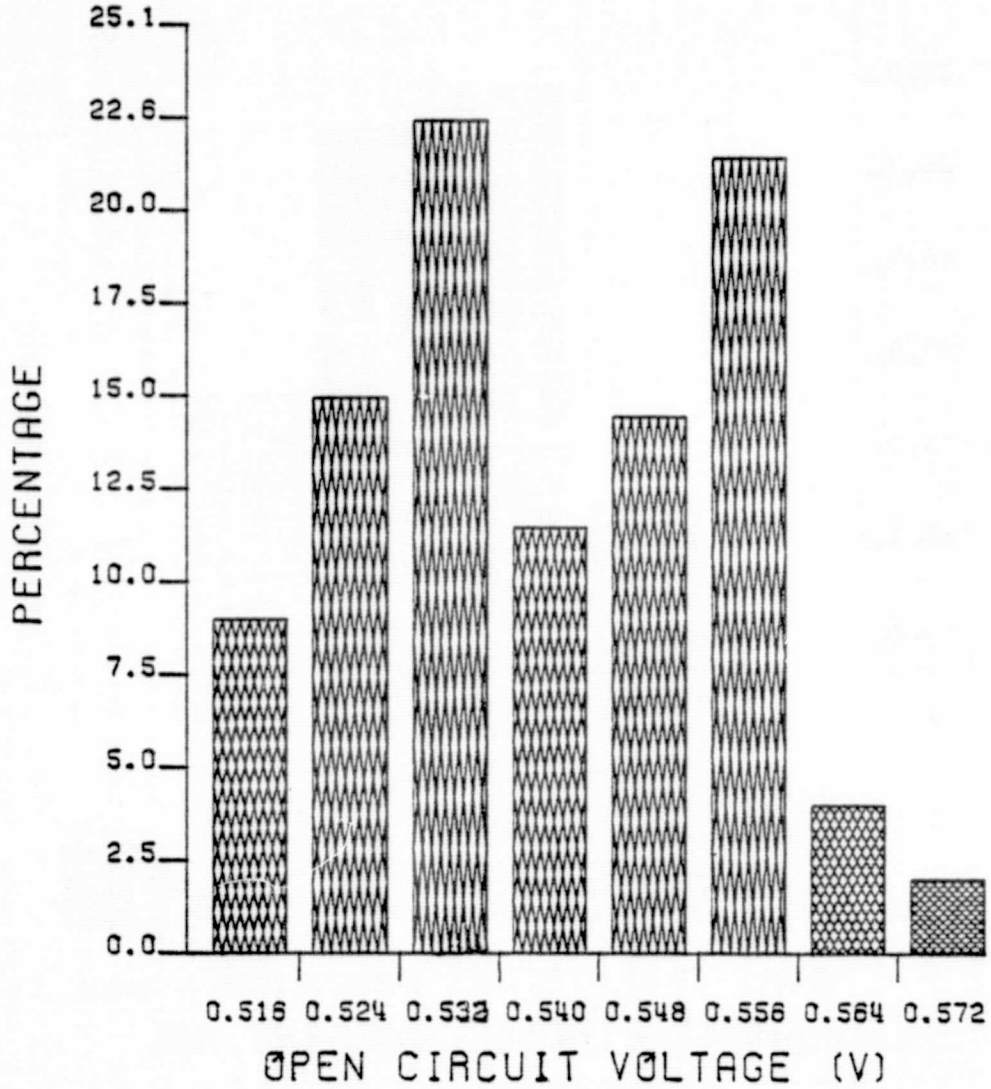

Figure B-6. Prestress Distribution of V_{oc}, Type B.

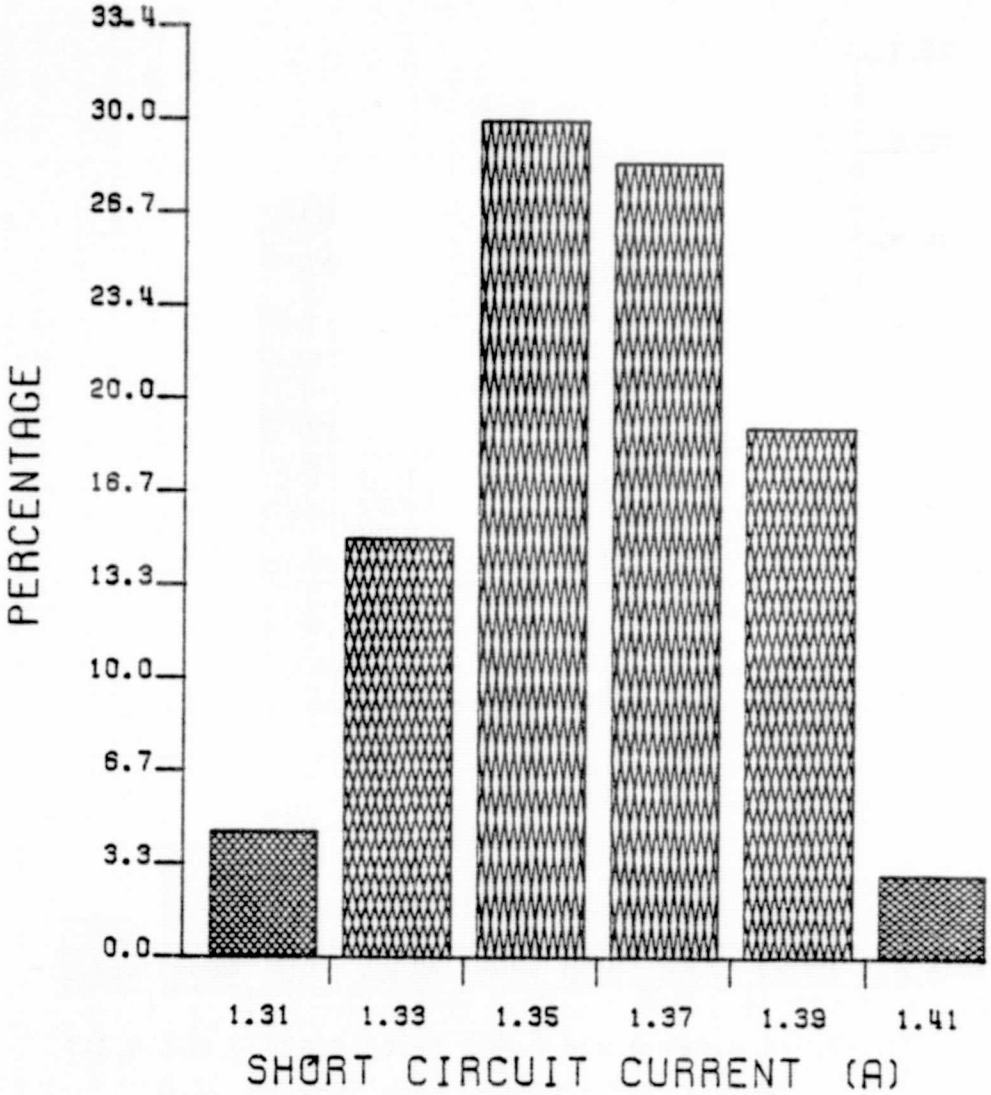

Figure B-7. Prestress Distribution of I_{sc}, Type B.

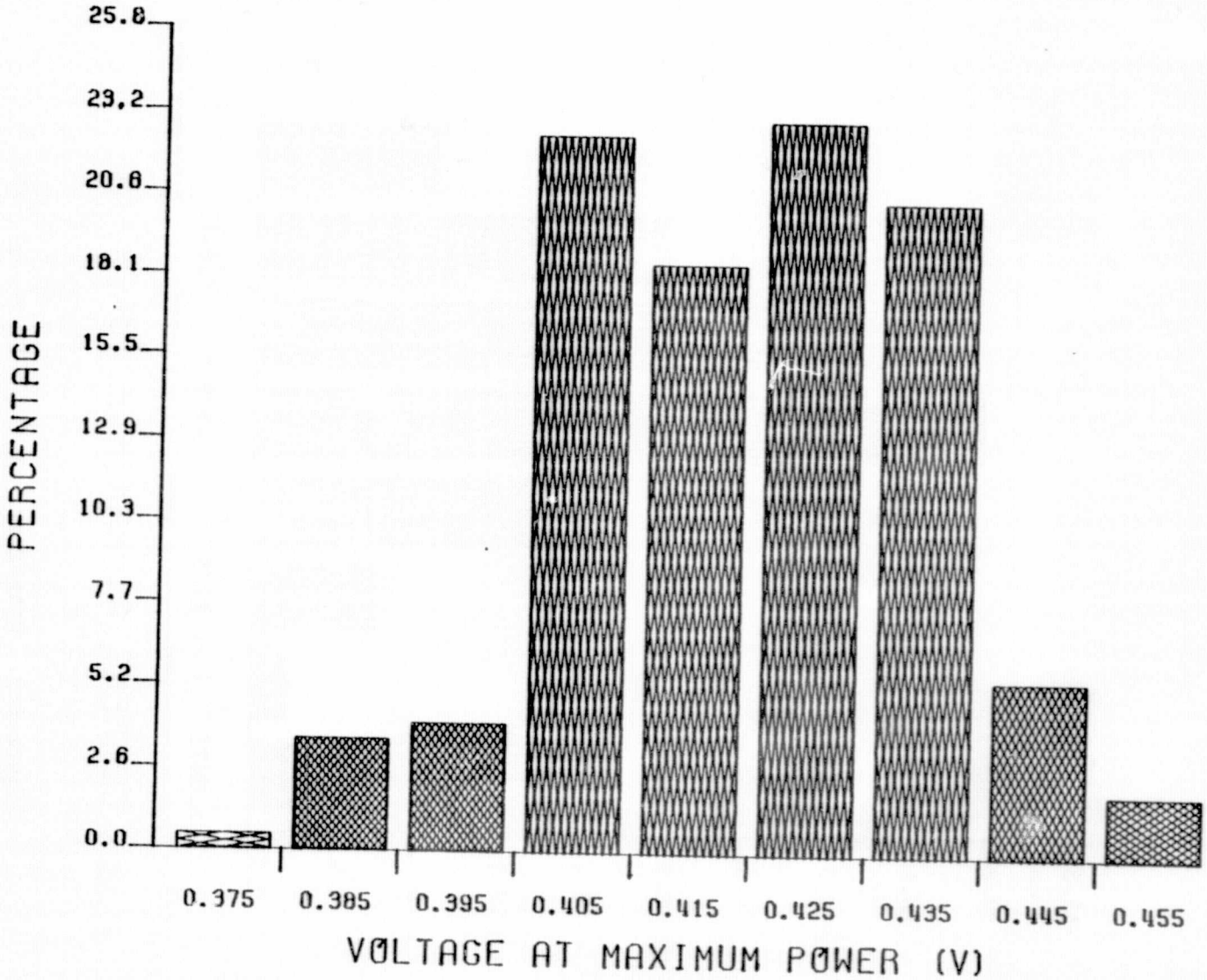

Figure B-8. Prestress Distribution of V_m, Type B.

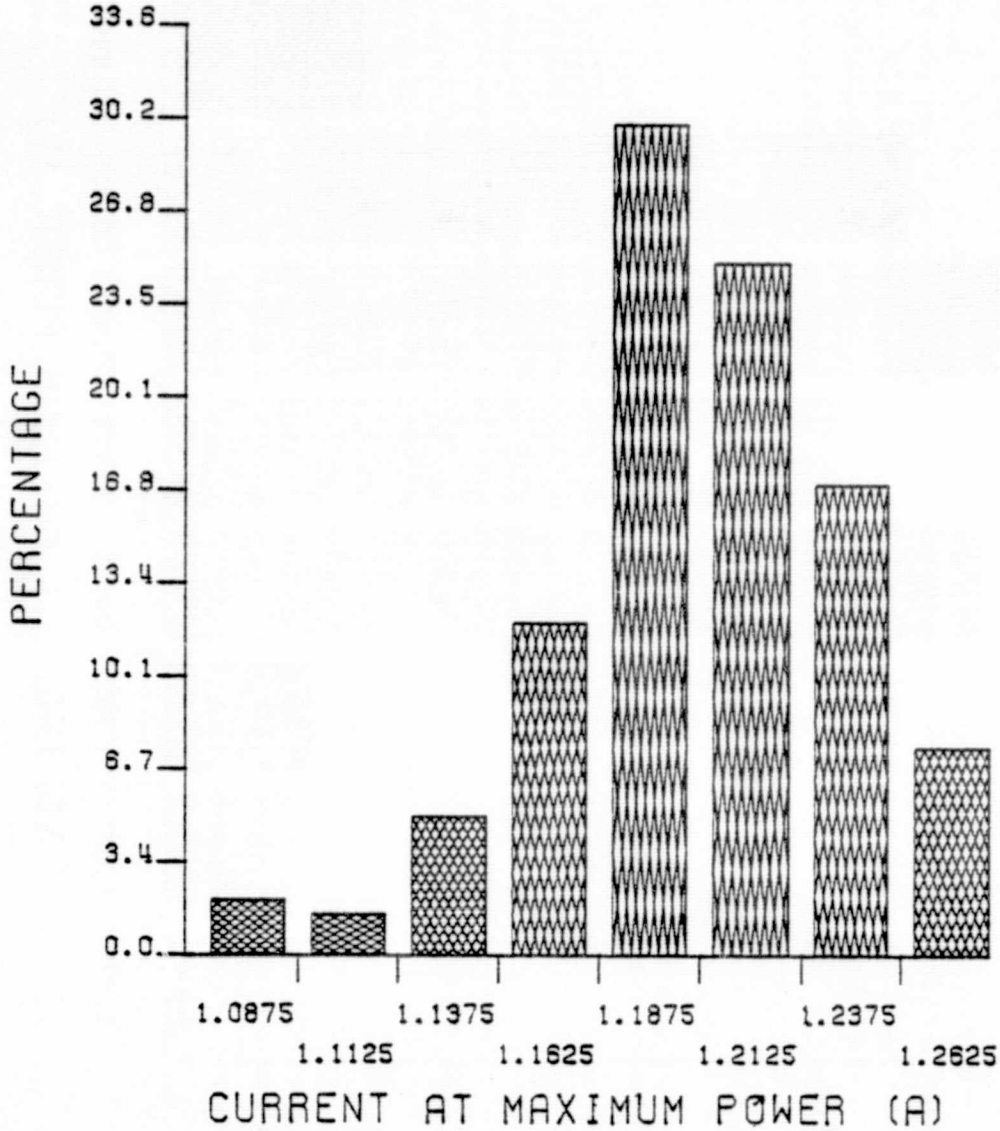

Figure B-9. Prestress Distribution of I_m, Type B.

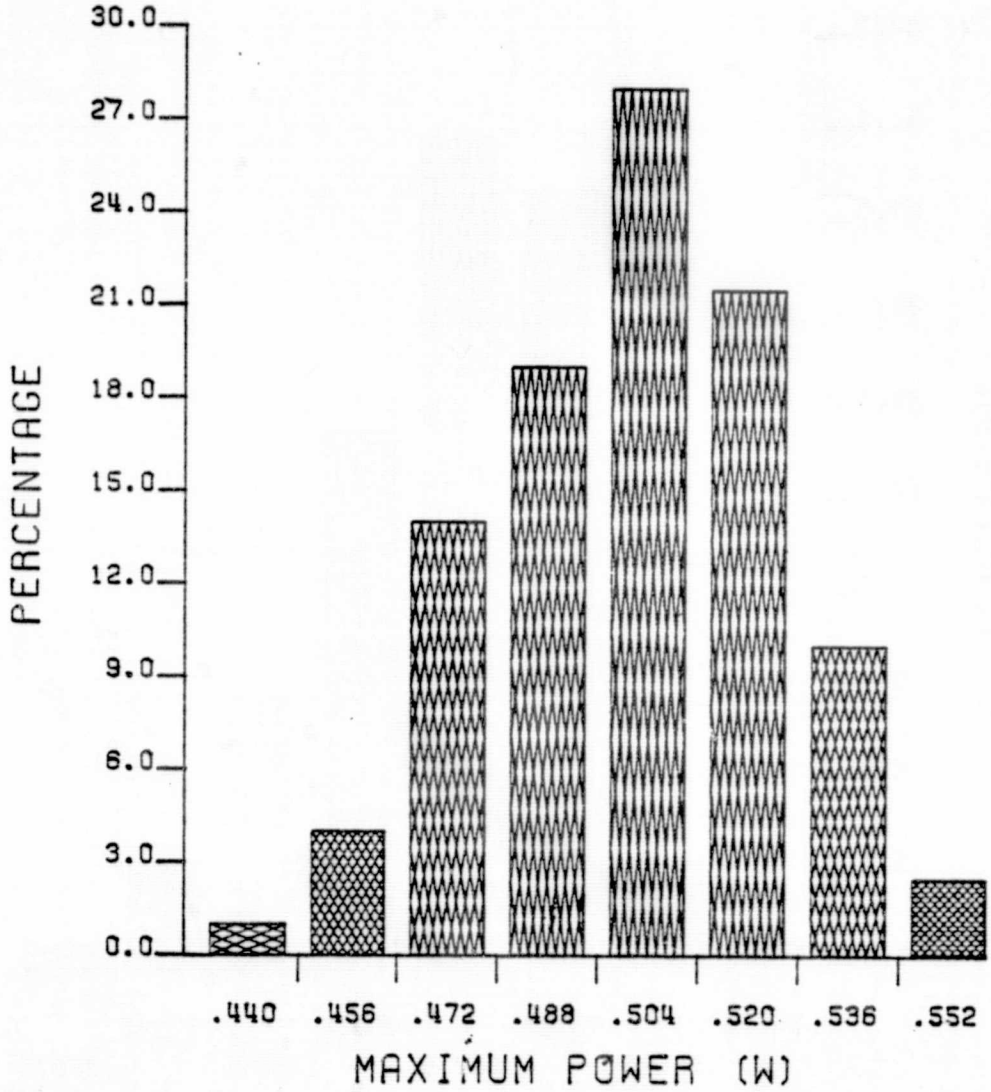

Figure B-10. Prestress Distribution of P_m, Type B.

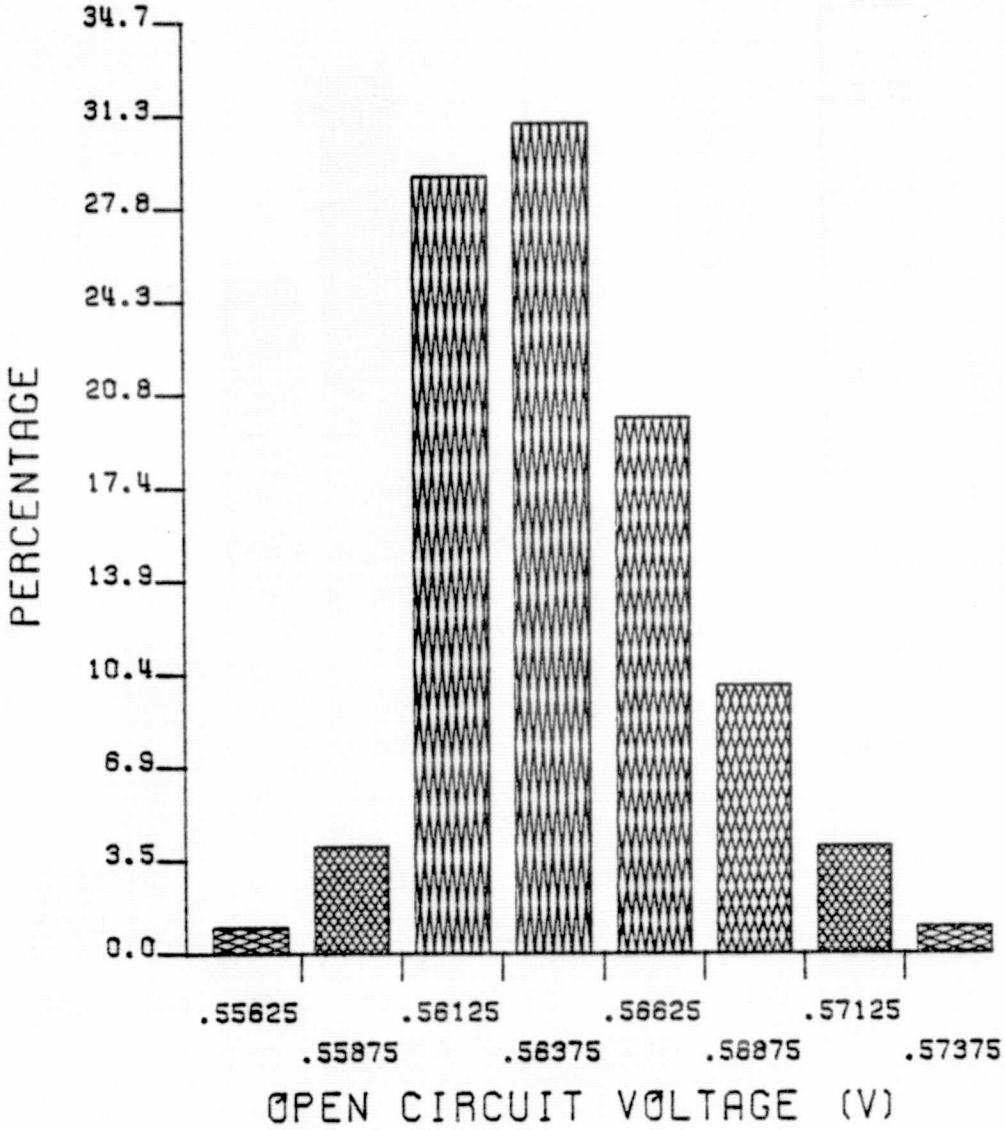

Figure B-11. Prestress Distribution of V_{oc}, Type C.

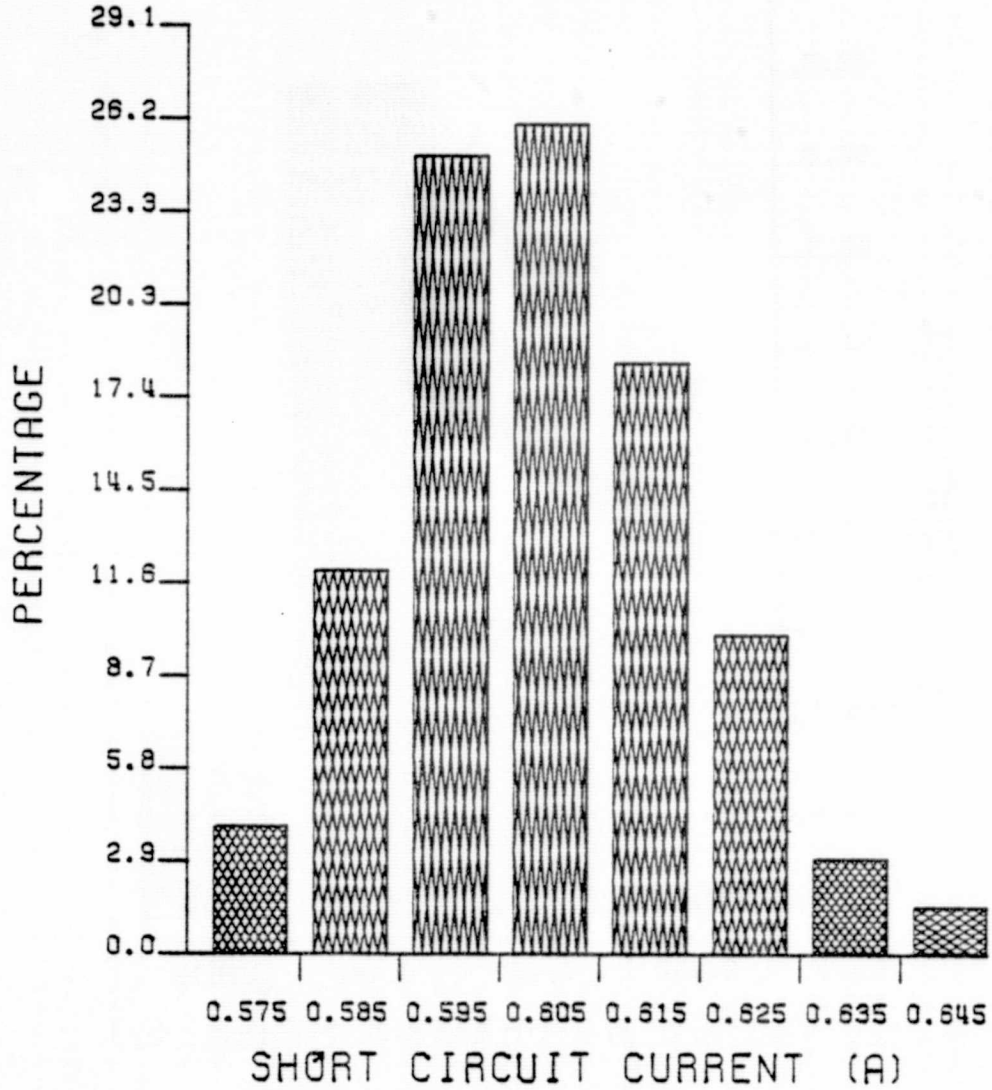

Figure B-12. Prestress Distribution of I_{sc}, Type C.

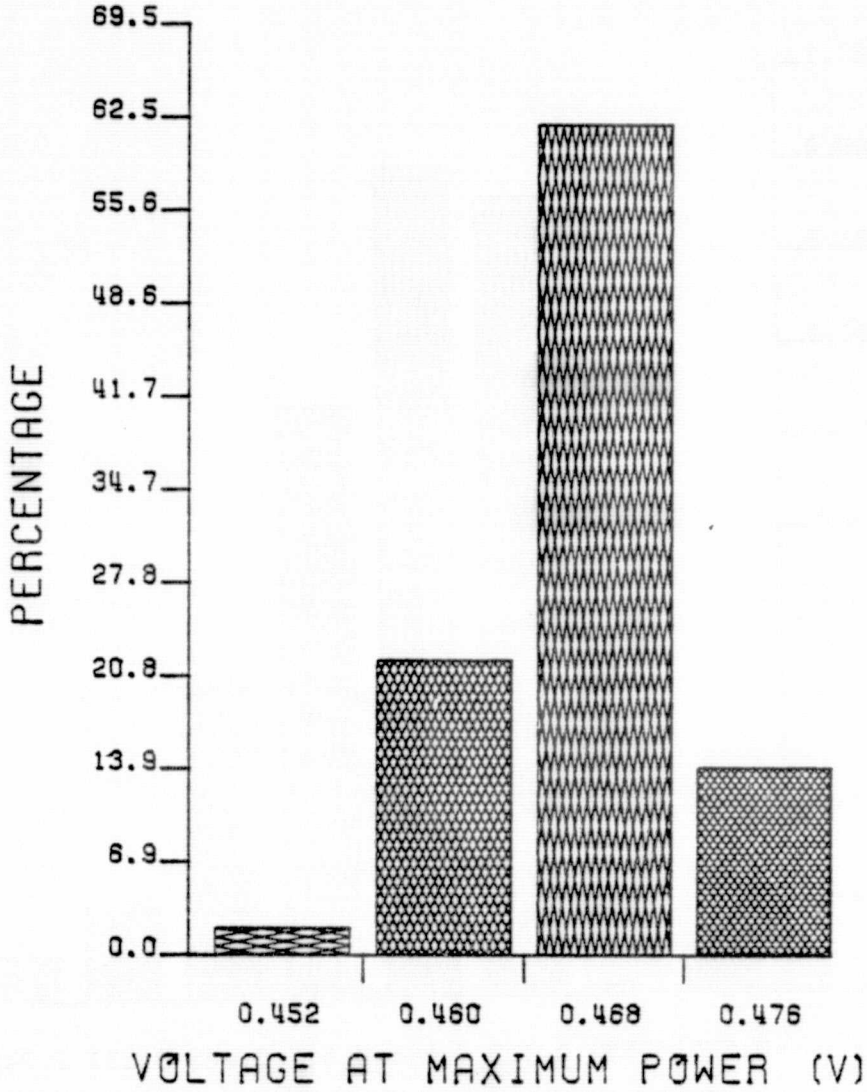

Figure B-13. Prestress Distribution of V_m, Type C.

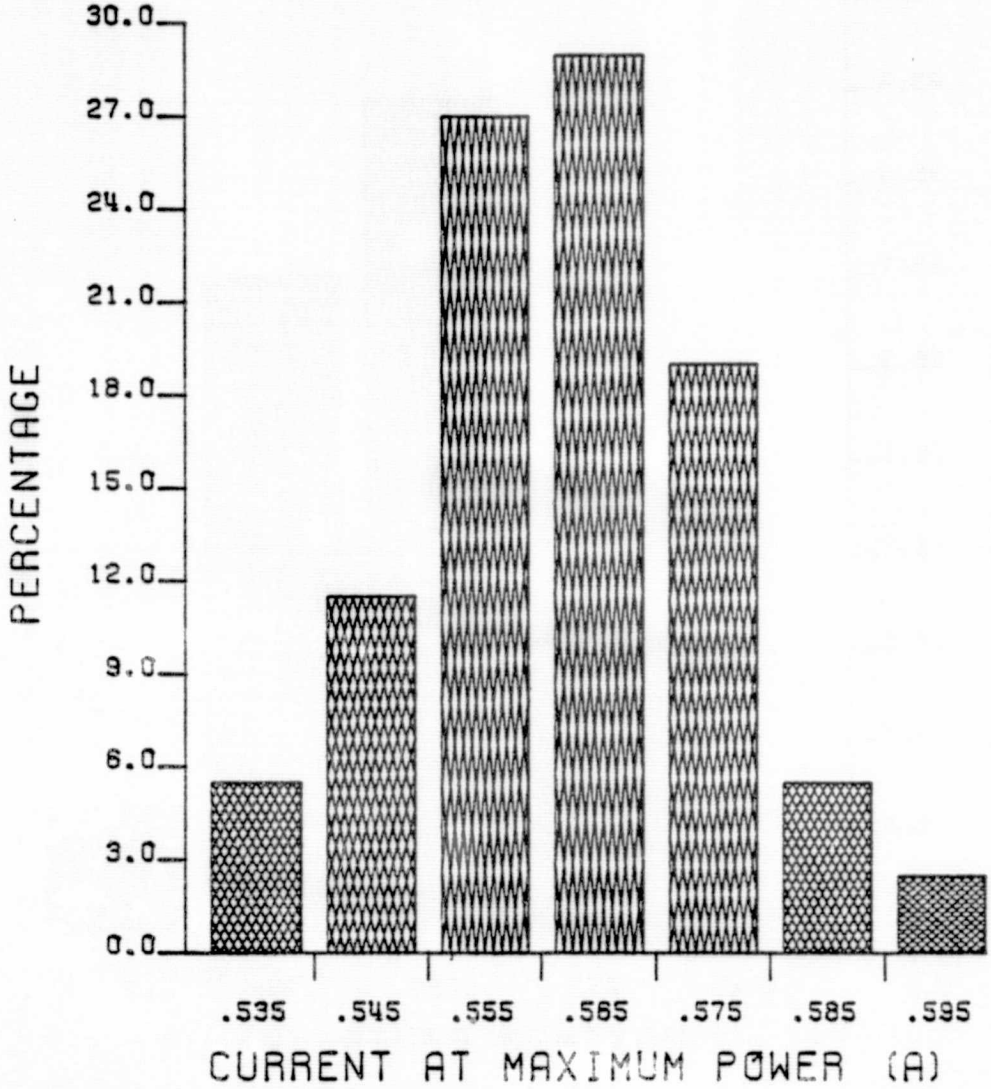

Figure B-14. Prestress Distribution of I_m, Type C.

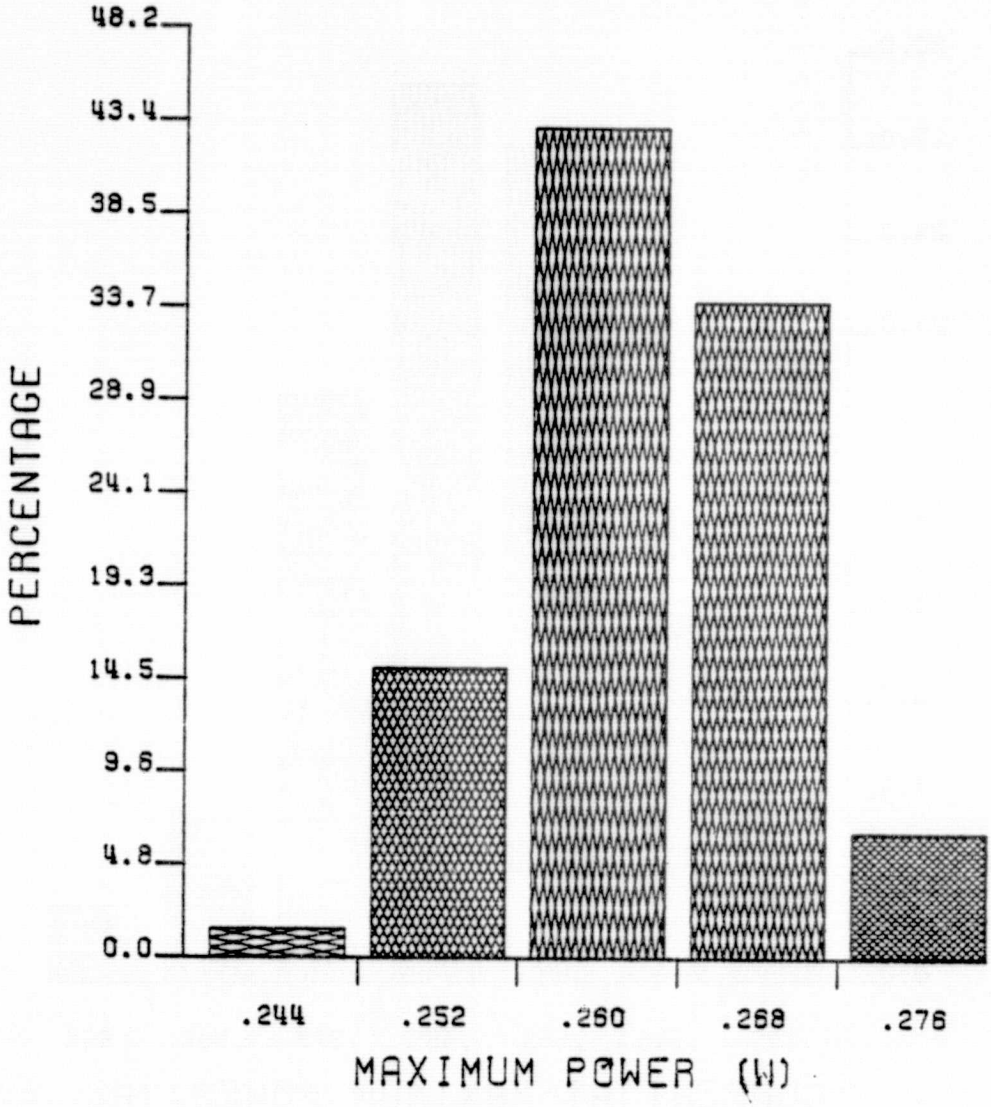

Figure B-15. Prestress Distribution of P_m, Type C.

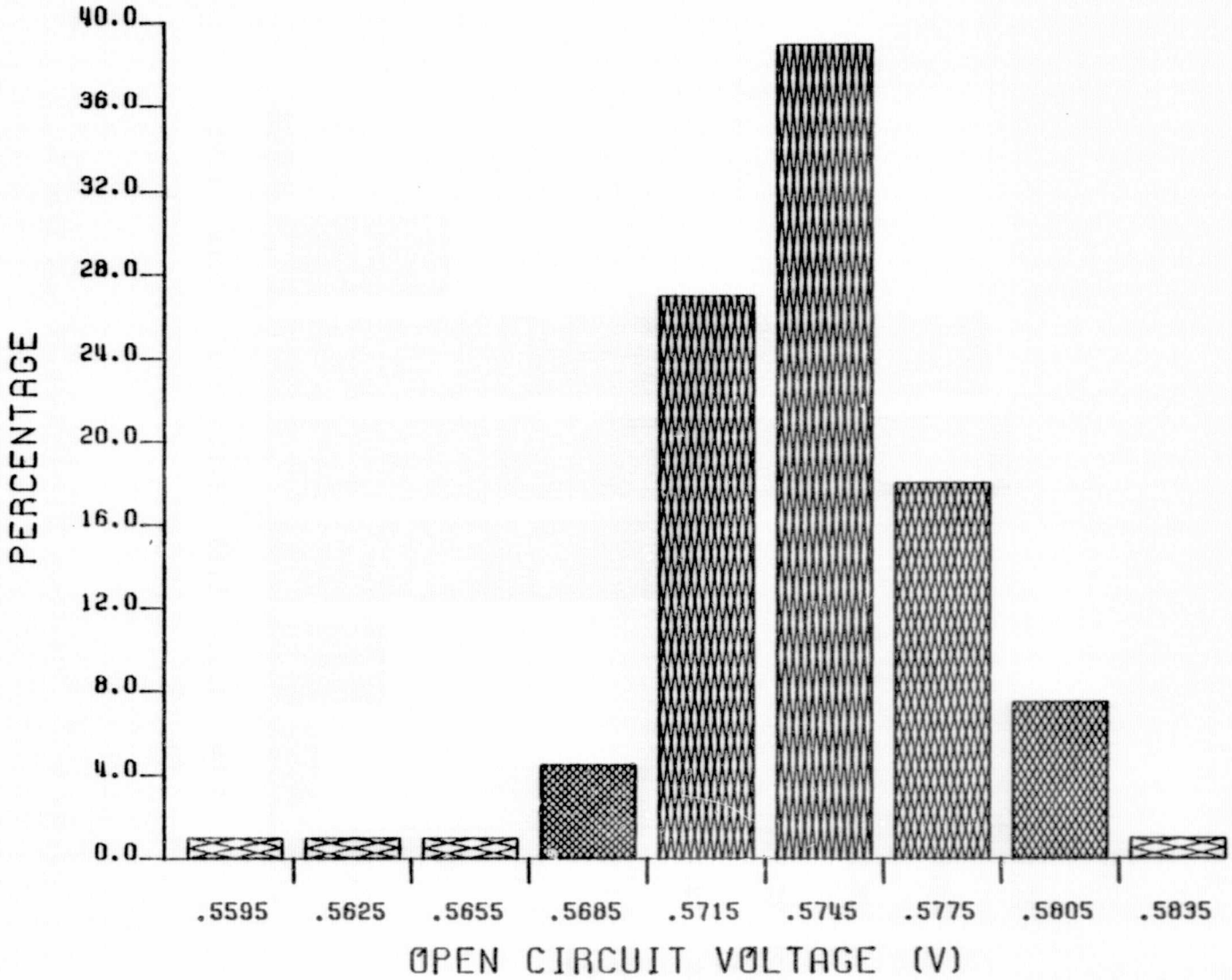

Figure B-16. Prestress Distribution of V_{oc}, Type E.

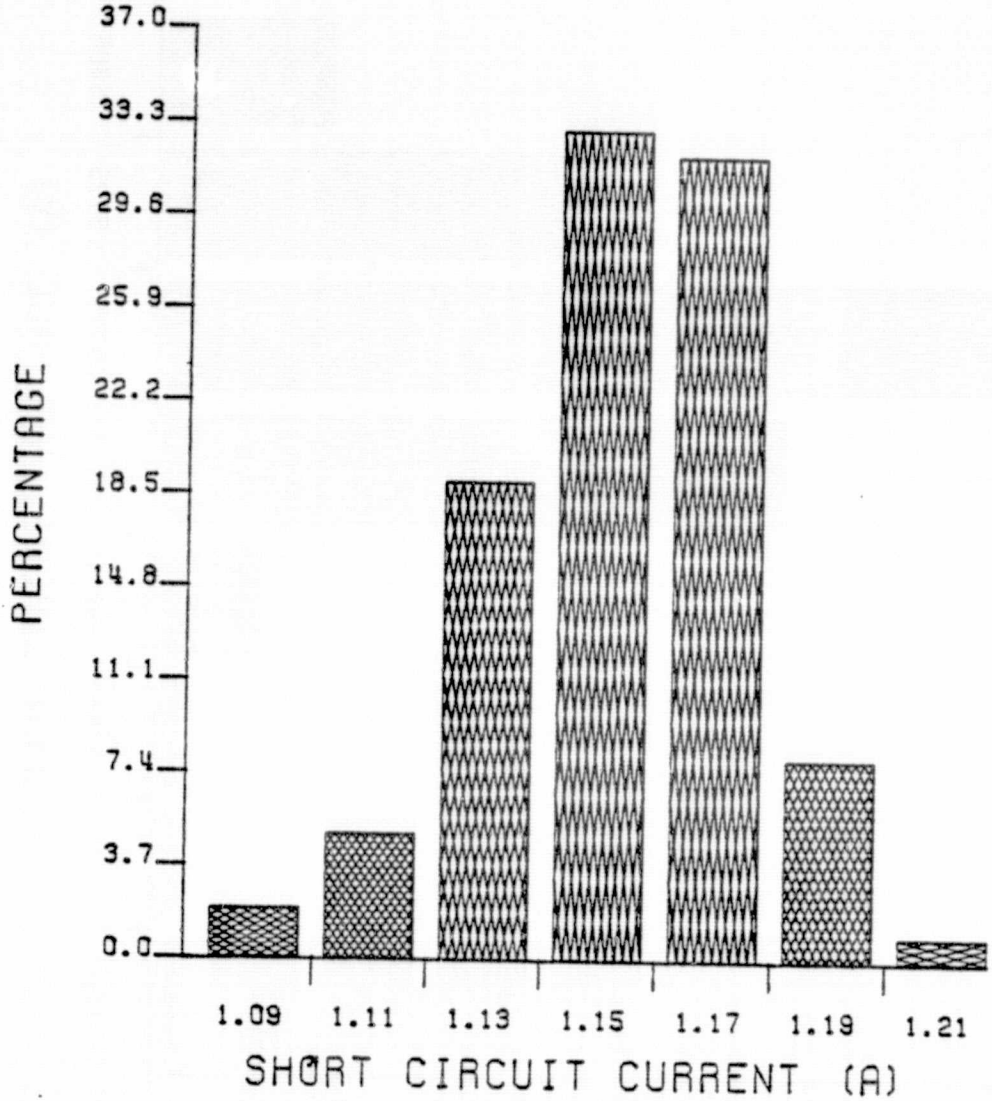

Figure B-17. Prestress Distribution of I_{sc}, Type E.

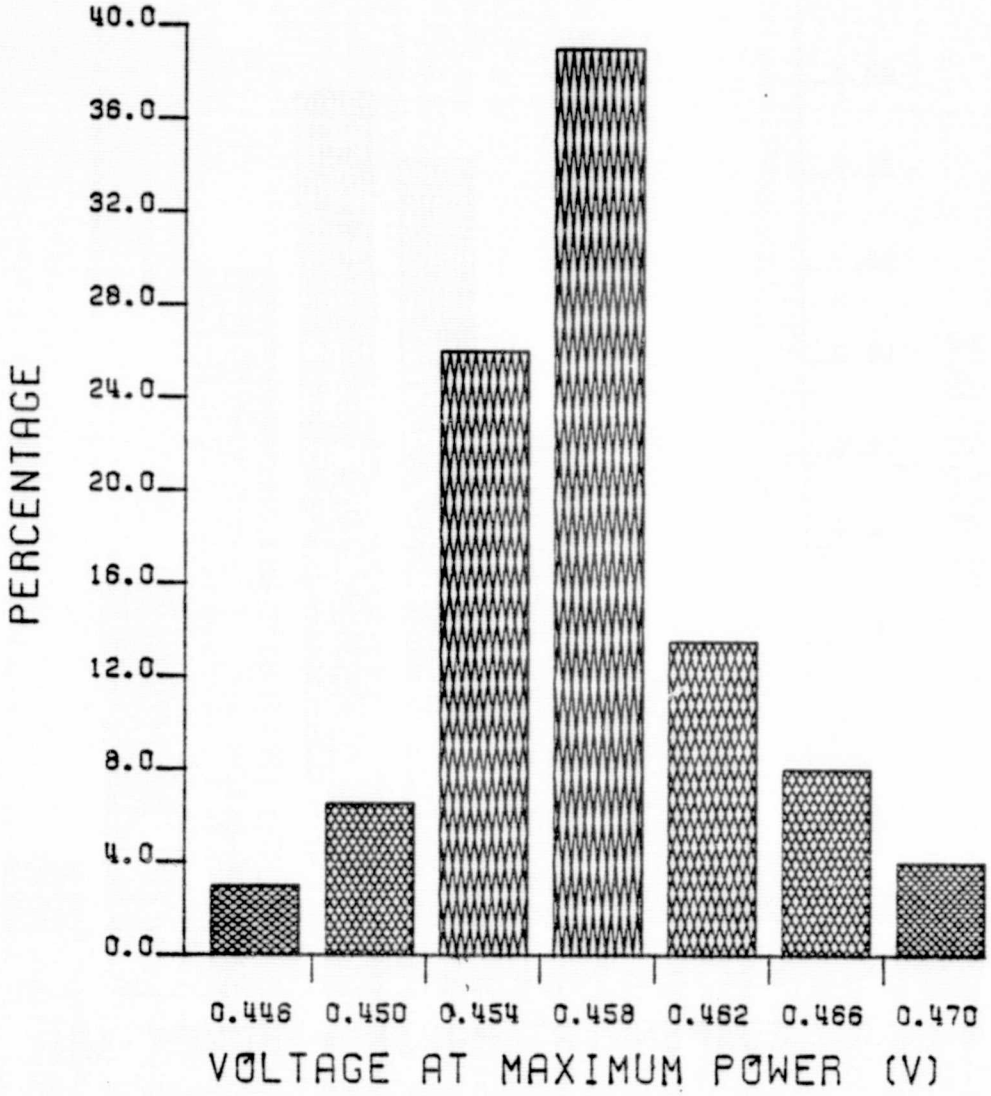

Figure B-18. Prestress Distribution of V_m, Type E.

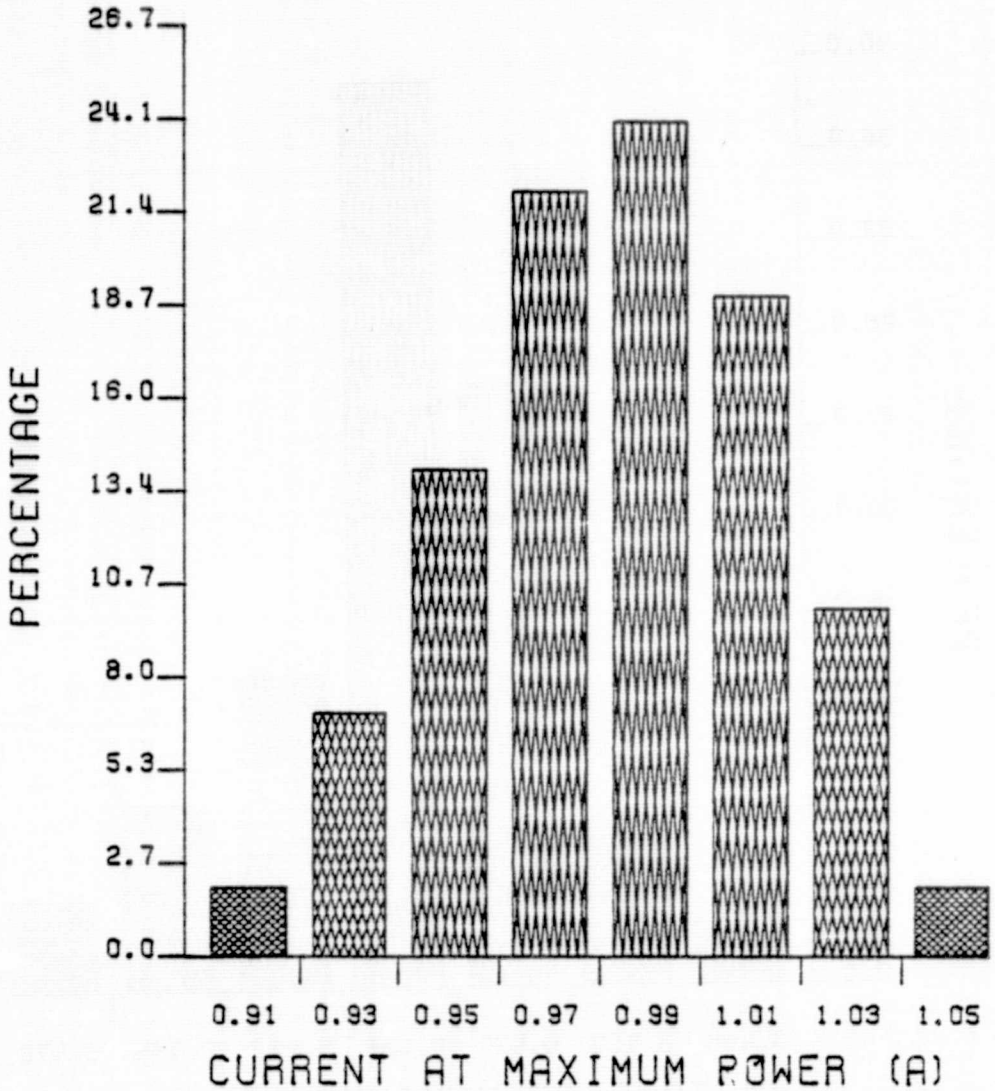

Figure B-19. Prestress Distribution of I_m, Type E.

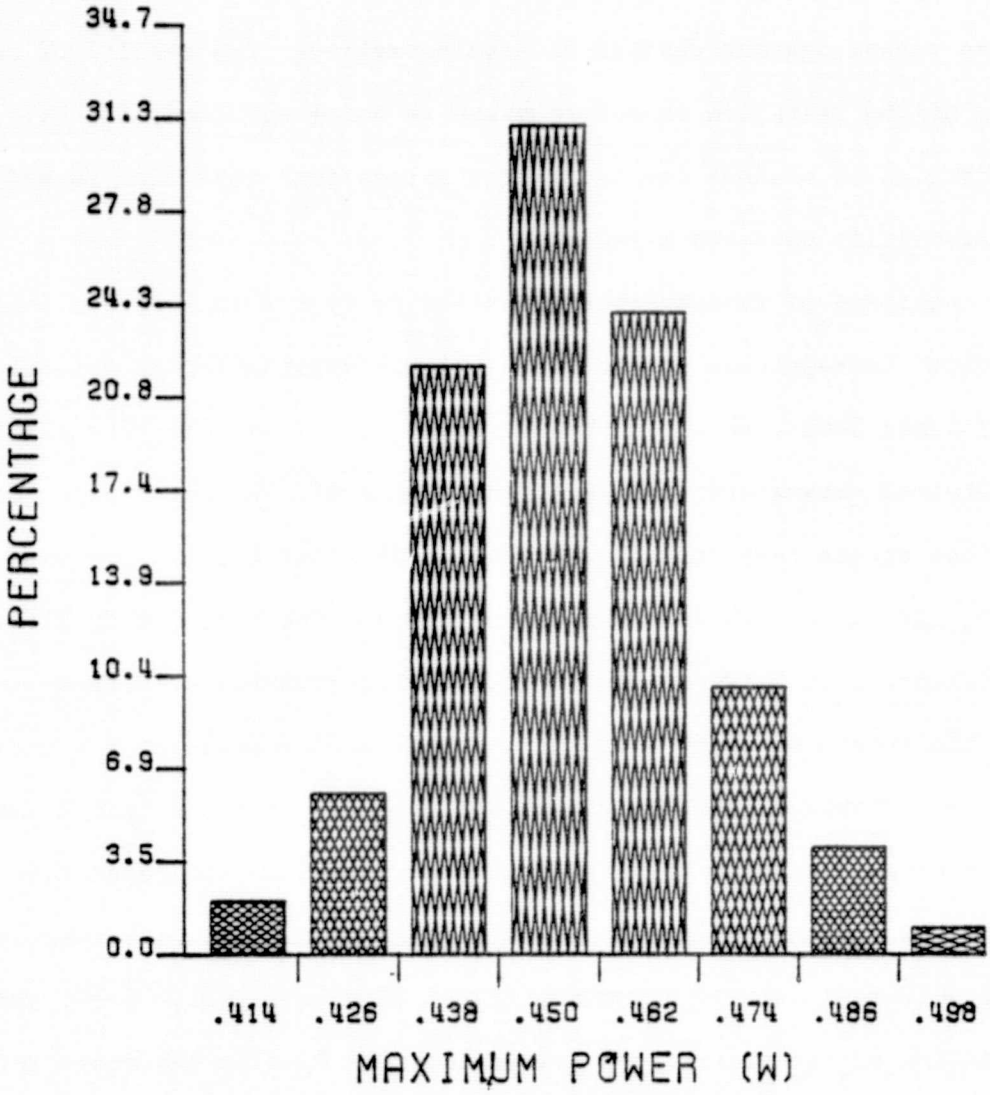

Figure B-20. Prestress Distribution of P_m, Type E.

Analysis of Variance (ANOVA) and Duncan's Multiple Range tests were applied to the prestress electrical parameters of the various Phase II stress lots in order to determine whether the parametric means of the lots were equal within expected statistical variability. Note that these tests assume a normal parametric distribution, an assumption which does not strictly hold as mentioned above. However, two tests are also known to be quite robust against deviations from normality. The results of application of the tests are therefore taken as being accurate, and give an indication of whether the individual stress test lots were formed in a statistically unbiased manner.

Analysis of variance tests applied to type A cell stress test lots resulted in rejection of the (statistical) hypothesis, at a fairly high confidence level, that all the lot means were identical, for all five electrical parameters. Application of Duncan's Multiple Range Test to the various stress test lots showed that in fact differentiation with respect to V_m and I_m between lots was not possible. However, fairly clear differentiation between lots 10 and 11 (bias-temperature stress test lots) and the remaining eight lots was possible with respect to V_{oc} and P_m. An example of the discrimination observed from the test is shown in Table B-6. It should be noted that even for these two parameters the lowest and highest of the lot mean P_m (lot 11 and lot 14 respectively) were different only by a maximum factor of approximatley 5.6%, and the deviation of the highest and lowest lot mean P_m from the total cell population mean P_m was less than $\pm$ 3.1%. Considering possible systematic measurement variability, the lots were judged to be sufficiently homogeneous for stress test purposes.

Grouping	P_m Mean (W)	N	Lot No.
A	0.781	20	14
B A	0.779	25	15
B A C	0.776	15	18
B D A C	0.769	36	19
B D C	0.765	40	13
B D C	0.762	20	17
D C	0.758	25	16
D	0.755	39	12
E	0.743	60	10

Table B-6. Results of Application of Duncan's Multiple Range Test to Phase II Lot Mean P_m, Type A Cells. Means With the Same Letter Are Not Significantly Different.

Grouping	P_m Mean (W)	N	Lot No.
A	0.517	19	17
A	0.516	25	15
B A	0.511	20	14
B A C	0.505	39	12
B A C	0.504	25	16
B C	0.503	43	19
B C	0.502	58	11
D C	0.497	41	13
D C	0.495	14	18
D	0.490	59	10

Table B-7. Results of Application of Duncan's Multiple Range Test to Phase II Lot Mean P_m, Type B Cells. Means With the Same Letter Are Not Significantly Different.

Analysis of variance tests applied to type B cell stress test lots resulted in rejection of the (statistical) hypothesis, at a fairly high confidence level, that all the lot means were identical, for V_m, I_{sc}, and P_m. However, application of Duncan's Multiple Range Test to the lot means showed that in fact clear discrimination between lots was not possible on the basis of any of the parameters. For example, Table B-7 shows results of the test for parameter P_m. From this table it is obvious that no clear difference exists between the various lots, with respect to P_m. The lots were judged to be sufficiently homogeneous for stress test purposes.

Analysis of variance tests applied to type C cell stress test lots resulted in rejection of the (statistical) hypothesis, at a fairly high confidence level, that the lot means were identical, for parameters V_{oc}, I_m, and P_m. However, application of Duncan's Multiple Range Test to the lot means showed that in fact clear discrimination between lots was not possible on the basis of any of the parameters. As an example, Table B-8 shows results of the test for parameter P_m. From this table it is obvious that no clear difference exists between the various lots, with respect to P_m. The lots were judged to be sufficiently homogeneous for stress test purposes.

Application of Analysis of Variance and Duncan's Multiple Range Tests to type E cell stress test lots showed results similar to those for type C cells. The statistical hypotheses that lot means were identical were rejected by the ANOVA tests; however, Duncan's Multiple Range Tests were unable to distinguish clear differences between lots. Table B-9 is an example of the testing of the P_m lot means by this test. Clearly no salient difference between lots was found in testing P_m. The lots were judged to be sufficiently homogeneous for stress test purposes.

Grouping		P_m Mean (W)	N	Lot No.
	A	0.266	38	12
	A	0.266	40	13
B	A	0.266	14	18
B	C	0.262	25	16
B	C	0.262	45	19
B	C	0.262	19	17
B	C	0.262	20	14
	C	0.260	40	10
	C	0.259	55	11
	C	0.259	25	15

Table B-8. Results of Application of Duncan's Multiple Range Test to Phase II Lot Mean P_m, Type C Cells. Means With the Same Letter Are Not Significantly Different.

Grouping		P_m Mean (W)	N	Lot No.
	A	0.461	25	15
	A	0.460	60	10
B	A	0.459	20	17
B	A	0.456	45	19
B	C	0.452	60	11
B	C	0.451	20	14
B	C	0.449	40	13
D	C	0.446	40	12
D	E	0.441	15	11
	E	0.434	29	16

Table B-9. Results of Application of Duncan's Multiple Range Test to Phase II Lot Mean P_m, Type E Cells. Means With the Same Letter Are Not Significantly Different.

Appendix C

Method 1010.1, MIL-STD-883A,

"Thermal Cycling"

1. PURPOSE. This test is conducted for the purpose of determining the resistance of a part to exposures at extremes of high and low temperatures, and to the effect of alternate exposures to these extremes, such as would be experienced when equipment or parts are transferred to and from heated shelters in arctic areas. These conditions may also be encountered in equipment operated noncontinuously in low-temperature areas or during transportations. Permanent changes in operating characteristics and physical damage produced during temperature cycling result principally from variations in dimensions and other physical properties. Effects of temperature cycling include cracking and delamination of finishes, cracking and crazing of embedding and encapsulating compounds, opening of thermal seals and case seams, leakage of filling materials, and changes in electrical characteristics due to mechanical displacement or rupture of conductors or of insulating materials.

2. APPARATUS. Suitable chamber(s) shall be used for the extreme temperature conditions of steps 1 and 3. The air temperature of the chamber(s) shall be held at each of the extreme temperatures by means of circulation and sufficient hot- or cold-chamber thermal capacity so that the ambient temperature measured downstream of the device under test, shall reach the specified temperature within 5 minutes after the specimens have been transferred to the appropriate chamber.

3. PROCEDURE. Specimens shall be placed in such a position with respect to the air-stream that there is substantially no obstruction to the flow of air across and around the specimen. When special mounting is required, it shall be specified. the specimen shall then be subjected to the specified condition for the specified number of cycles performed

PRECEDING PAGE BLANK NOT FILMED

continously. Unless otherwise specified, using test condition C, this test shall be conducted for a minimum 10 cycles. One cycle consists of steps 1 through 4 of the applicable test condition with the duration of exposure at each temperature as indicated in the table of test conditions. Whether single or multiple chambers are used, the effective total transfer time from the specified low temperature to the specified high temperature, or the reverse, shall not exceed 5 minutes. Direct heat conduction to the specimen should be minimized. In the case of multiple chambers, the transfer time shall be defined as the time between withdrawal from the low temperature chamber and introduction into the high temperature chamber.

3.1 Measurements. After completion of the final cycle, an external visual examination shall be performed for evidence of defects or damage to case, leads, or seals, or loss of marking legibility, resulting from testing. This examination and any additional specified measurements and examination shall be made after completion of the final cycle or upon completion of a group, sequence or subgroup of tests which include this test.

Temperature-cycling test conditions

Step	Minutes	Test condition					
		A Temperature	B Temperature	C Temperature	D Temperature	E Temperature	G Temperature
		°C	°C	°C	°C	°C	°C
1	10 min	-55^{+0}_{-5}	-55^{+0}_{-5}	-65^{+0}_{-5}	-65^{+0}_{-5}	-65^{+0}_{-5}	-65^{+0}_{-5}
2	5 max	25^{+10}_{-5}	25^{+10}_{-5}	25^{+10}_{-5}	25^{+10}_{-5}	25^{+10}_{-5}	25^{+10}_{-5}
3	10 min	85^{+3}_{-0}	125^{+3}_{-0}	150^{+5}_{-0}	200^{+5}_{-0}	300^{+5}_{-0}	175^{+5}_{-0}
4	5 max	25^{+10}_{-5}	25^{+10}_{-5}	25^{+10}_{-5}	25^{+10}_{-5}	25^{+10}_{-5}	25^{+10}_{-5}

NOTE: The time at the high and low temperatures shall be sufficient to allow the total mass of each device under test to reach the specified temperature. If carriers or holders employed or other factors make 10 minutes inadequate to allow the mass of each device under test to reach the specified temperature, the time at the temperature extremes shall be increased to meet this requirement. Temperature of worst case loads shall be established with a calibrated thermocouple(s) or other suitable temperature measuring device(s) appropriately placed within the chamber load area.

4. SUMMARY. The following details shall be specified in the applicable procurement document:

(a) Special mounting, if applicable (see 3).

(b) Test condition letter if other than test condition C (see 3).

(c) Number of test cycles, if other than 10 cycles (see 3).

(d) End point measurements and examination (see 3.1) (e.g., end point electrical measurements, seal test (Method 1014) or other acceptance criteria).

Appendix D

Method 1011.1, MIL-STD-883A,

"Thermal Shock"

1. PURPOSE. The purpose of this test is to determine the resistance of the device to sudden exposure to extreme changes in temperature. These conditions may be encountered in equipment operated intermittently in low temperature areas. Permanent changes in operating characteristics and physical damage produced during temperature shock result principally from variations in dimensions and other physical properties. Effects of thermal shock include cracking and delamination of substrates or wafers, opening of terminal seals and case seams, and changes in electrical characteristics due to moisture effects or to mechanical displacement of conductors or insulating materials.

2. APPARATUS. Suitable temperature controlled baths containing liquids shall be chosen to obtain the temperature excursion specified in the table of test conditions (see 3) and within the indicated tolerances.

3. PROCEDURE. The device shall be preconditioned by being immersed and in intimate contact with a suitable liquid at the temperature specified in step 1 of the specified test condition for a minimum of 5 minutes. Immediately upon conclusion of the preconditioning time, the device shall be transferred to a liquid at the temperature specified in step 2 of the specified test condition. The device shall remain at the low temperature for a minimum of 5 minutes and then be transferred to a liquid at the step 1 temperature. The device shall remain at the high temperature for a minimum of 5 minutes. Transfer time from high temperature to low temperature and from low temperature to high temperature shall be less than 10 seconds. Unless otherwise specified, using test condition A, the duration of the test shall be 15 complete cycles, where one cycle consists of proceeding from step 1 to step 2 and back to the beginning of step 1.

3.1 Measurements. After completion of the final cycle, an external visual examination shall be performed for evidence of defects or damage to case, leads, or seals, or loss of marking legibility resulting from testing. This examination and any additional specified measurements and examination shall be made after completion of the final cycle or upon completion of a group, sequence or subgroup of test which include this test.

Thermal shock test conditions

Test condition	A Temperature °C	B Temperature °C	C Temperature °C	D Temperature °C	E Temperature °C	F Temperature °C
Step 1	100^{+5}_{-0}	125^{+5}_{-0}	150^{+5}_{-0}	200^{+5}_{-0}	150^{+5}_{-0}	200^{+5}_{-0}
Step 2	-0^{+0}_{-5}	-55^{+0}_{-5}	-65^{+0}_{-5}	-65^{+0}_{-5}	-195^{+5}_{-5}	-195^{+5}_{-5}

Suggested thermal shock fluids

Test condition	A Fluid	B Fluids	C Fluids	D Fluids	E Fluids	F Fluids
Step 1	Water 1/	FC40	FC40	Silicon oil or UCON 100	FC40	Silicon oil or UCON 100
Step 2	Water 1/	FC77	FC77	FC77	Liquid nitrogen	Liquid nitrogen

NOTES:

1/ Water is indicated as an acceptable fluid for this temperature range; its suitability chemically shall be established prior to use.

2. Ethylene glycol shall not be used as a thermal shock test fluid.

4. SUMMARY. The following details shall be specified in the applicable procurement document:

(a) Special mounting, if applicable.

(b) Test condition if other than test condition A (see 3).

(c) Number of test cycles if other than 15 cycles (see 3).

(d) End point measurements and examination (see 3.1) (e.g., end point electrical measurements, seal test (Method 1014) or other acceptance criteria).

Appendix E

Contact Integrity Test Procedure for Terrestrial Solar Cells

1.0 SCOPE AND PURPOSE

1.1 Scope: This procedure is applicable to the destructive testing of terrestrial solar cell metal-silicon contact integrity.

1.2 The purpose of this procedure is to evaluate the adhesion between the contact metal and the silicon substrate. It is desirable that a means by which the effects of cell aging, either under use conditions or under accelerated conditions, can be determined. The procedure will also be useful for assessment of manufacturing process stability.

2.0 REQUIRED EQUIPMENT AND MATERIALS

2.1 Pull strength tester, Unitek, Micropull, Model 1092 or equivalent with force gage, range 0 to 5 Kg.

2.2 Hot plate, Thermolyne, Model HP-A8805B, or equivalent.

2.3 Pyrex cover, 4" dia.

2.4 Pink Pearl Eraser, or equivalent.

2.5 Cu ribbon .085" x .005".

2.6 Alpha Sn 62 Solder Cream, mildly activated, or equivalent.

2.7 Cell holding fixture

2.8 1 Liter container, or equivalent.

2.9 Isopropyl alcohol.

2.10 Surface thermometer 150°C to 300°C range or equivalent.

2.11 Orange stick, or tooth pick.

2.12 5X magnifier

2.13 Epoxy, Hysol 1105, or equivalent (for alternate method per paragraph 3.2).

2.14 Utility-wipes, Scott, #05320, or equivalent.

3.0 TEST PROCEDURE

3.1 Solder Method of Test Lead Attachment

3.1.1 Turn on hot plate and heat to 225°C ± 10°C.

3.1.2 Place Pyrex cover over hot plate.

3.1.3 Cut Cu ribbon to approximate 2" length to use as test leads.

3.1.4 Pour isopropyl alcohol into container jar.

3.1.5 Using the Pink Pearl Eraser, abrade the test lead and the cell surfaces in the area to be soldered.

3.1.6 Rinse cell and test leads in isopropyl alcohol and blot dry with Utility-wipe.

3.1.7 Tin the test lead and bend to the approximate configuration shown by Figure E-1.

3.1.8 Apply solder cream to the cell in the area that the test lead is to be attached as shown by Figure E-2.

3.1.9 Place the test lead in the position for soldering as shown by Figure E-3.

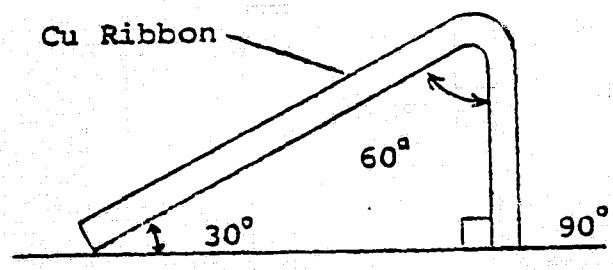

Figure E-1.

TEST LEAD BEND

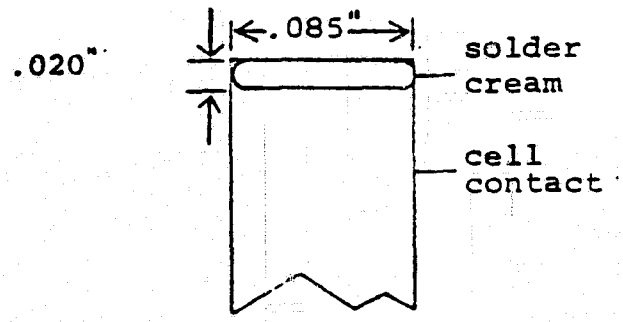

Figure E-2.

SOLDER CREAM PLACEMENT

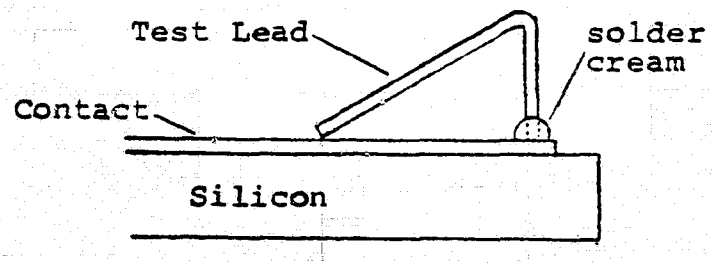

Figure E-3.

TEST LEAD PLACEMENT

3.1.10 Place cell on the Pyrex Glass on top of the hot plate and carefully watch for the solder to melt. When a solder joint has been formed, remove the Pyrex cover from the hot plate and set aside to cool.

3.1.11 When the cell has been cooled, examine under 5X magnification to verify that an acceptable solder joint has been formed in accordance with the criteria shown in Figure E-4.

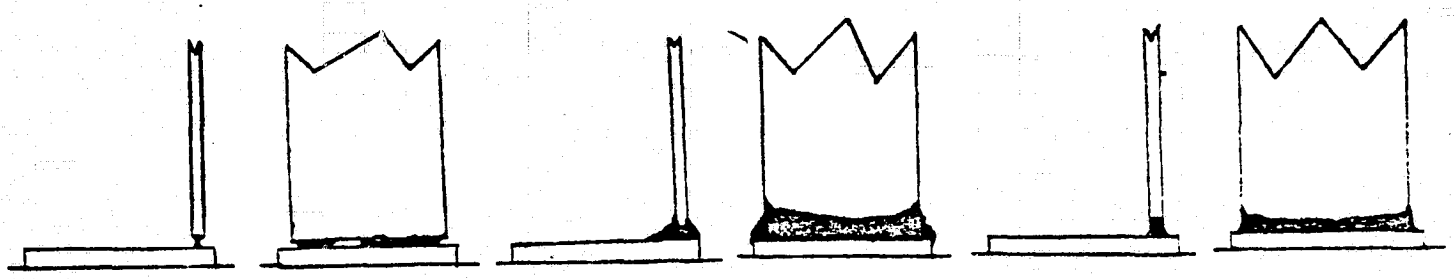

TOO LITTLE SOLDER
NOT ACCEPTABLE

TOO MUCH SOLDER
NOT ACCEPTABLE

RECOMMENDED

Figure E-4

TEST LEAD SOLDER

3.1.12 When it has been verified that the solder joint is acceptable, proceed with the contact pull test in accordance with paragraph 3.3.

3.2 Alternate Lead Attachment Method, "Adhesive Method"

3.2.1 Prepare cell and Cu ribbon in accordance with paragraph 3.1.3 through 3.1.6.

3.2.2 Mix epoxy, Hysol 1105 or equivalent in accordance with manufacturer's instructions.

3.2.3 Apply a very small amount of epoxy to the cell contact area to be tested. The epoxy should cover an area approximately .050" in diameter.

3.2.4 Bend the Cu ribbon as shown by Figure E-5 and position on the cell as shown by Figure E-6.

NOTE: Pot life restriction must be complied with.

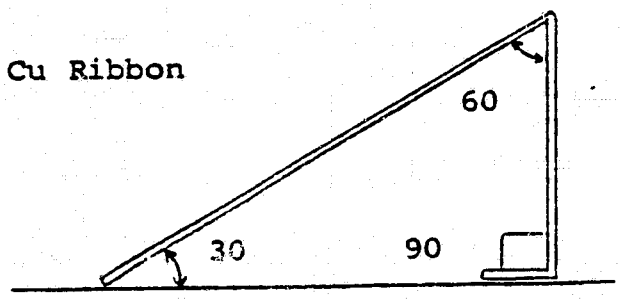

Figure E-5

TEST LEAD BEND FOR EPOXY METHOD

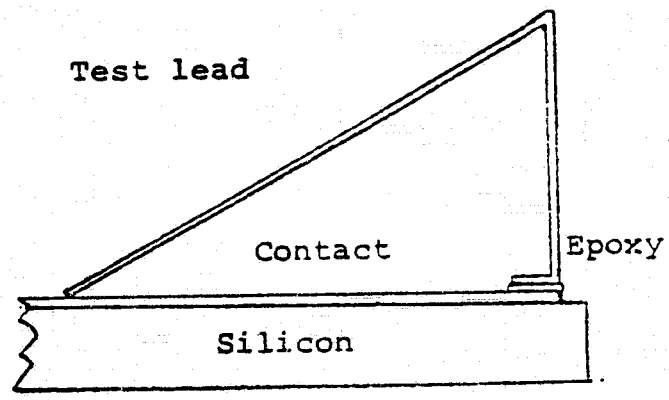

Figure E-6

TEST LEAD PLACEMENT, EPOXY METHOD

3.2.5 Cure epoxy in accordance with manufacturer's directions.

3.2.6 Upon completion of the epoxy cure, the cells are ready for the contact pull test in accordance with paragraph 3.3.

3.3 Contact Pull Test

3.3.1 Place the cell into the cell holding fixture on the pull tester.

3.3.2 Align the holding fixture with the pull force gage jaws so that the direction on the pull will be normal to the cell surface.

3.3.3 Close the pull force gage jaws securely on the test lead and activate the pull tester drive mechanism.

3.3.4 Record the ultimate tensil strength from the pull force gage.

3.3.5 Examine the cell and test lead to determine the failure mode and record the appropriate failure mode code as shown by Table E-1.

Code	Failure Mode Description
A	Contact metal peeled from silicon
B	Silicon "cratered" equal or greater than 1/3 the solder joint interface area
C	Silicon fractured, pulling a hole through the cell
D	Cell broken
E*	Test lead broken; cell not damaged
F*	Test lead pulled from solder; cell not damaged
G*	Solder and Test Lead pulled from cell; cell not damaged

*Retest on another cell or retest the same cell in an alternate location.

TABLE E-1. PULL TEST FAILURE MODE CODES

3.4 Safety

3.4.1 Eye protection should be worn during soldering and pull test procedures.

3.4.2 Care must be exercised when handling broken silicon solar cells. The pieces are sharp enough to cut the skin.